SECURITY CLASSIFICATION OF THIS PAGE (When Data Entered)

REPORT DOCUMENTATION PAGE

READ INSTRUCTIONS BEFORE COMPLETING FORM

1. REPORT NUMBER: AR 4 (16)
2. GOVT ACCESSION NO.: AD-A105 789 (8)
3. RECIPIENT'S CATALOG NUMBER:
4. TITLE (and Subtitle): Theoretical Studies Relating to the Interaction of Radiation with Matter: Atomic Collision Processes Occurring in the Presence of Radiation Fields
5. TYPE OF REPORT & PERIOD COVERED: Interim 8/1/80-7/31/81
6. PERFORMING ORG. REPORT NUMBER:
7. AUTHOR(s): (10) P. R. Berman
8. CONTRACT OR GRANT NUMBER(s): (15) N00014-77-C-0553
9. PERFORMING ORGANIZATION NAME AND ADDRESS: Prof. P.R. Berman, Physics Dept. - New York University, 4 Washington Place., New York, NY 10003 406850
10. PROGRAM ELEMENT, PROJECT, TASK AREA & WORK UNIT NUMBERS: (11) 45 Sep 84
11. CONTROLLING OFFICE NAME AND ADDRESS: Office of Naval Research - Code 613C: MAK, 800 N. Quincy Street, Arlington, Virginia 22217
12. REPORT DATE: September 15, 1981
13. NUMBER OF PAGES: 140 (12) 147
14. MONITORING AGENCY NAME & ADDRESS (if different from Controlling Office): Office of Naval Research Resident Representative New York, 715 Broadway - 5th Floor, New York, NY 10003
15. SECURITY CLASS. (of this report): Unclassified
15a. DECLASSIFICATION/DOWNGRADING SCHEDULE:

LEVEL II

16. DISTRIBUTION STATEMENT (of this Report)

Approved for public release; distribution unlimited

17. DISTRIBUTION STATEMENT (of the abstract entered in Block 20, if different from Report)

(9) Annual rept. no. 4, 1 Aug 80-31 Jul 81,

DTIC ELECTE OCT 19 1981 D H

18. SUPPLEMENTARY NOTES

19. KEY WORDS (Continue on reverse side if necessary and identify by block number)

Laser Spectroscopy, Optical Collisions, Radiative Collisions. Velocity-Changing Collisions, Two-Level System, Atomic Coherence, Zeeman Coherence, Dressed-Atom Picture, Degenerate Four-Wave Mixing.

20. ABSTRACT (Continue on reverse side if necessary and identify by block number)

Work is reported in the areas of:-
(1) Two-Level Atom & Radiation Pulse;
(2) Effects of Collisions on Atomic Coherences;
(3) Effects of Collisions on Zeeman Coherences;
(4) Collision Effects in Degenerate-Four-Wave-Mixing;
(5) Dressed-Atom Picture in Laser Spectroscopy.

DD FORM 1 JAN 73 1473 EDITION OF 1 NOV 65 IS OBSOLETE
S/N 0102-LF-014-6601

406850

SECURITY CLASSIFICATION OF THIS PAGE (When Data Entered)

81 10 14

AD A105789

DTIC FILE COPY

Annual Report (AR4)

Title: "Theoretical Studies Relating to the Interaction of Radiation with Matter: Atomic Collision Processes Occurring in the Presence of Radiation Fields"

Supported by the U.S. Office of Naval Research

Contract No.: N00014-77-C-0553

Report Period: August 1, 1980 - July 31, 1981

Date of Report: September 15, 1981

Approved for public release; distribution unlimited.

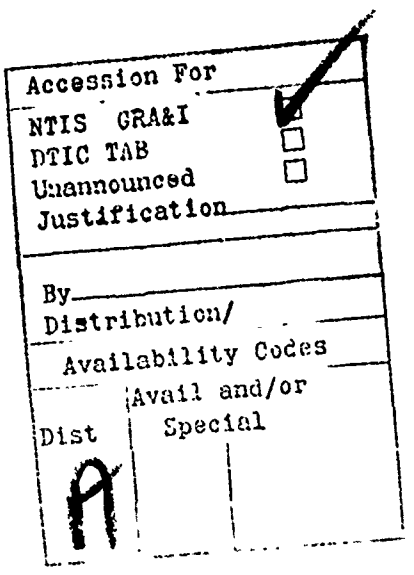

Research has been carried out in the areas of (1) Two-level atom and radiation pulse, (2) Effects of collisions on atomic coherences, (3) Effects of collisions on Zeeman coherences, (4) Colision effects in degenerate-four-wave-mixing, and (5) Dressed-atom picture in laser spectroscopy.

1. Two-level Atom and Radiation Pulse (P. Berman, E. Robinson)

The work reported in last year's Annual Report[1] has been completed. In collaboration with Dr. A. Bambini (Quantum Electronics Institute, Florence, Italy), we have found an analytic solution to the problem of determining the atomic state probability amplitudes when a two-level atom interacts with a radiation pulse.[2]* Until this work, the only analytic solution that had been obtained for smooth pulses (assuming non-zero detuning of the field from the atomic resonance) was that for a hyperbolic secant coupling pulse. The class of pulse functions for which we have found a solution contains the hyperbolic secant pulse as a special case. All other pulses in the class, however, are not symmetric about any time during the pulse. For these asymmetric pulses, a qualitatively new feature arises. In contrast to the situation for symmetric pulses, there are no pulse intensities for which the system returns to its initial conditions. Robinson[3]* has given a general proof of this result by relating the atom-pulse equations to an eigenvalue problem.

* Asterisks on references indicate that the reference is appended to this report.

The pulses for which we have obtained analytic solutons can have very long leading or trailing edges. We have given a physical explanation[2] to the response of the atoms to such pulses. The availability of an analytic solution for asymmetric pulses may prove useful in problems where pulses are shaped to provide a given response of the atomic system (e.g. laser-pellet interactions in laser fusion).

2. Effects of Collisions on Atomic Coherences (P. Berman)

In collaboration with T.W. Mossberg and S.R. Hartmann (Columbia University), significant progress has been made in understanding collisional processes in atomic and molecular vapors. In an atomic vapor, a quantity of physical interest is the collision kernel $W_{ii}(\vec{v}' \to \vec{v})$ giving the probability density per unit time that an atom in state i undergoes a change of velocity from $\vec{v}'$ to $\vec{v}$, owing to collisions with perturber atoms. For atoms in a superposition of states i and j there is an analogous "kernel" $W_{ij}(\vec{v}' \to \vec{v})$ (it need not be positive) which describes the effects of collisions on atomic state coherences. The coherence kernel is important in problems relating to atomic spectroscopy where an external radiation field creates a linear superposition of atomic states. The coherence kernel specifies the manner in which collisions modify superposition states; in turn the collision-induced modification alters the absorptive and dispersive properties of the vapor. A complete analysis of the line shapes associated with laser spectroscopy can be achieved only with an understanding of the collision kernels.

Conversely, the line shapes can be used to provide inforamtion on collisional processes occurring within the vapor.

Formal expressions for the collision kernels exist[4], but limited progress has been achieved in gaining physical insight into those expressions for the case when the collisional interactions for states i and j differ appreciably (as they will for most electronic transition). Classically, the i and j state populations would follow different trajectories during a collision, and it is not obvious that a collision trajectory can be assigned to the atomic coherence (superposition state).

Using arguments based on the uncertainty principle, we have shown[5]*, [6]* that collisions can be divided roughly into two regions. Let b_o be some characteristic impact parameter in the scattering process. For collisions having impact parameters $b<b_o$, collisions may be treated classically leading to classical population kernels and vanishing coherence kernels. The coherence kernel vanishes owing to a spatial separation of the state i and j collision trajectories. On the other hand, collisions having $b>b_o$ must be treated quantum-mechanically. These collisions give rise to diffractive scattering contributions to both the population and coherence kernels. An extensive theoretical article on this subject is in preparation.

Experimentally,[5],[6],[7] the various conclusions mentioned above have been verified using coherent transient techniques. It seems that a comprehensive understanding of the effects of collisions on atoms prepared in a linear superposition of electronic states has been achieved.

3. Effects of Collisions on Zeeman Coherences (P. Berman)

Another area where collisions can play an important role is in experiments in which a magnetic state (Zeeman) coherence is generated. With laser spectroscopic methods, such coherences are generally created by the action of two fields as shown below.

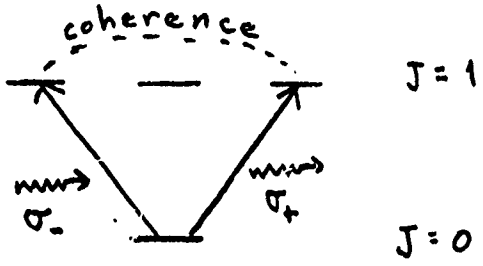

The action of the two fields leaves the atom in a linear superposition of magnetic substates. Collisions modify this magnetic state coherence. There has been significant renewed experimental interest in the effects of collisions on Zeeman coherences[7],[8].

While formal expressions for the collision kernels exist[4], it has been difficult to give a physical interpretation to these results. In contrast to the electronic state case (Sec. Z), it is not meaningful to distinguish populations from coherences in the magnetic sublevel case, since these definitions will depend on the axis of quantization. Thus, it becomes an interesting problem to understand collision trajectory effects. Can polarization or population be transferred from one velocity class to another?

With J.L. LeGouet (Laboratoire Aime Cotton, Orsay, France), we have given the first physical picture of collisional effects on

Zeeman coherences.[9]* A collision can be divided into two regions, $r < r_o$ and $r > r_o$, where r_o is some characteristic atom-perturber separation. For $r > r_o$, the common trajectory approximation is valid and the collision mixes the magnetic substates. For $r < r_o$, the collision interaction is strong enough so that there exist adiabatic states which are not mixed by the collision. Each of these adiabatic states follows a distinct trajectory for $r < r_o$. The general theory and method of calculation has been given[9]; specific evaluations of the collision parameters are in progress.

4. Collision Effects in Degenerate-Four-Wave-Mixing (P. Berman)

In collaboration with L.M. Humphrey and P. Liao (Bell Laboratories), we have tried to explain an experiment in which collisions enhance certain Degenerate-Four-Wave-Mixing (D4WM) signals.[10]* This is another area that is receiving a great deal of experimental and theoretical interest.[11] The collision effects are basically related to those discussed in Sec. 3.

There remains an unexplained feature in Humphrey and Liao's data. It appears as if foreign gas collisions are depolarizing the ground state of Na with cross-sections on the order of 100Å^2, whereas it is well-known that such cross sections should be a factor of 10^{-7} smaller. Work on the theory of collision effects in D4WM is continuing in collaboration with J. Lam (Hughes Research).

5. Dressed-Atom Picture in Laser Spectroscopy (R. Salomaa, P. Berman)

A rigorous comparison between the Dressed-Atom Picture (DAP) and Bare-Atom Picture (BAP) as applied to laser spectroscopy has been

carried out.[12] An article representing our work in this area will be submitted for publication in the near future.

In the BAP, the basis states are those of the free atom and free field whereas, in the DAP, the basis states encompass some part of the atom-field interaction. Whereas calculations are usually more easily done using the BAP, one can gian useful insight into the underlying physical processes using the DAP. Moreover, when the radiation field strengths (in frequency units) are larger than the relaxation rates in the problem, the DAP equations simplify considerably and lead to line shape expressions which may be given a simple interpretation.

We have sued the DAP to obtain resonance conditions for (1) traveling-wave fields interacting with three and four-level atoms and (2) a standing-wave saturator and traveling-wave probe interacting with three-level atoms. Moreover, we have analyzed a number of coherent transient processes in which the DAP can be put to effective use. An interesting duality between the DAP and BAP approaches has been discovered (e.g., optical notation in the BAP corresponds to free-induction decay in the DAP). A detailed comparison of the various advantages and disadvantages of the DAP is contained in our work.[12]

6. Previous Work

Articles related to our past work on coherences produced by radiative collisions,[13]*,[14]* strong-field effects in radiative collisions using a model potential,[15]* collisionally aided radiative

excitation in three-level systems,[16]* resonance fluorescence in three-level systems,[17]* as well as two review articles[18]*,[19]* have either appeared or are awaiting publication.

References

1. Annual Report AR3.
2. A. Bambini and P.R. Berman, Phys. Rev. A23, 2496 (1981).
3. E.J. Robinson, Phys. Rev. A24, to appear, (1981).
4. See P.R. Berman, Phys. Reps. 43, 101 (1978).
5. R. Kachru, T.J. Chen, T.W. Mossberg, S.R. Hartmann and P.R. Berman, Phys. Rev. Letters, to appear, (1981).
6. T.W. Mossberg, R. Kachru, T.J. Chen, S.R. Hartmann and P.R. Berman, to appear in Laser Spectroscopy V edited by T. Oka and B. Stoicheff (Springer-Verlag, Berlin, 1981).
7. M. Gorlicki, A. Peuriot, and M. Dumont, J. de Physique Lett. 41 L275 (1980).
8. Private communications with F. Laloe, C. Aminoff and T. Hansch. Also see ref. 11.
9. J.L. LeGouet and P.R. Berman, Phys. Rev. A24, September (1981).
10. L.M. Humphrey, P.F. Liao and P.R. Berman, J. Opt. Soc. Amer. 70 1612 (1980).
11. See, for example, J.F. Lam, D.G. Steel, R.A. McFarlane and R.C. Lind, App. Phys. Lett. 38, 977 (1981); D. Bloch and M. Ducloy, J. Phys. B14, L471 (1981); G. Grynberg, J. Phys. B14, 2089 (1981); G. Grynberg, to appear in Opt. Comm.; M. Ducloy and D. Bloch, to appear in J. de Physique; Y. Prior, A.R. Bogdan, M. Dagenais and N. Bloembergen, Phys. Rev. Letts. 46, 111 (1981).

12. R. Salomaa and P.R. Berman (to be submitted to Phys. Rev. A).

13. P.R. Berman, Phys. Rev. A22, 1838 (1980).

14. P.R. Berman, Phys. Rev. A22, 1848 (1980).

15. E.J. Robinson, submitted to J. Phys. B.

16. S.Yeh and P.R. Berman, Phys. Rev. A22, 1403 (1980).

17. S. Yeh and P. Stehle, to appear in J. Phys. B.

18. P.R. Berman, Annales de Physique 5, 199 (1980).

19. R. Vetter and P.R. Berman, Comm. on Atom. Mol. Phys. 10, 69 (1981).

PHYSICAL REVIEW A VOLUME 23, NUMBER 5 MAY 1981

Analytic solutions to the two-state problem for a class of coupling potentials

A. Bambini

*Research Institute for Theoretical Physics, University of Helsinki, Siltavuorenpenger 20C, SF 00170 Helsinki 17, Finland and Istituto di Elettronica Quantistica del Consiglio Nazionale delle Ricerche, via Panciatichi 56/30, I-50127 Florence, Italy**

P. R. Berman

Physics Department, New York University, 4 Washington Place, New York, New York 10003

(Received 22 December 1980)

A class of pulse functions is found for which analytic solutions to the problem of two levels coupled by these pulse functions is obtained. The hyperbolic-secant coupling pulse is included in this class of functions leading to the Rosen-Zener solution, but all other pulses belonging to the class function are asymmetric. The asymmetric pulses lead to qualitatively new features in the solutions; in general, it is impossible to have a zero-transition probability with such asymmetric pulses.

I. INTRODUCTION

A problem of considerable interest in physics is to determine the time evolution of a two-level system whose levels are coupled by a time-dependent potential. The probability amplitudes for the two levels in the interaction representation denoted by $a_1(t)$ and $a_2(t)$, obey the coupled differential equations

$$da_1/dt = -i\chi(t)e^{-i\omega t}a_2 , \tag{1a}$$

$$da_2/dt = -i\chi(t)e^{i\omega t}a_1 , \tag{1b}$$

where ω is the frequency separation of levels 2 and 1 and $\chi(t)$ is the coupling parameter (assumed real). By introducing a characteristic time scale T and defining dimensionless parameters

$$\tau = t/T , \tag{2a}$$

$$\alpha = \omega T , \tag{2b}$$

$$\beta = S/\pi , \quad S = \int_{-\infty}^{\infty} \chi(t)\,dt , \tag{2c}$$

$$f(\tau) = \chi(\tau T)T/\beta , \tag{2d}$$

one can transform Eqs. (1) into

$$\dot{a}_1 = -i\beta f(\tau)e^{-i\alpha\tau}a_2 , \tag{3a}$$

$$\dot{a}_2 = -i\beta f(\tau)e^{i\alpha\tau}a_1 , \tag{3b}$$

where a dot indicates $d/d\tau$. Owing to Eqs. (2c) and (2d), the function $f(\tau)$ is normalized as

$$\int_{-\infty}^{\infty} f(\tau)\,d\tau = \pi \tag{4}$$

and the parameter S is the pulse area.

Equations (3) arise in any semiclassical two-state calculation in which the two levels, separated in energy by $\hbar\alpha/T$, are coupled by a potential $\hbar\beta f(\tau)/T$. These equations also arise in two-state problems in which the levels are coupled by a nearly resonant oscillating field. In that case, assuming the "antiresonant" component of the field can be neglected, the quantity $\hbar\beta f(\tau)/T$ takes on the role of an envelope function for the field while α/T represents the atom-field detuning. Since Eqs. (3) are of such fundamental importance in many branches of physics, it is useful to have analytic solutions of these equations for various envelope functions $f(\tau)$. Of course, one can numerically integrate Eqs. (3), but such procedures can be costly (especially for large α) and do not necessarily yield the more general qualitative features of the solutions.

If $\alpha = 0$, a simple solution can be found for arbitrary $f(\tau)$. The probability amplitude a_1 or a_2 is given by

$$a_i = A_i\cos\theta(\tau) + B_i\sin\theta(\tau) , \tag{5a}$$

$$\theta(\tau) = \beta\int_{-\infty}^{\tau} f(\tau')\,d\tau' , \tag{5b}$$

where A_i and B_i are constants. For $\alpha \neq 0$, however, there are, to our knowledge, only two *smooth* envelope functions $f(\tau)$ for which an analytic solution of Eqs. (3) has been obtained. One such function is $f(\tau) = \text{const} = 1$ for which the solution[1] is

$$a_{1,2} = A_{1,2}\cos\sigma_{1,2}\tau + B_{1,2}\sin\sigma_{2,1}\tau , \tag{6a}$$

$$\sigma_{1,2} = \tfrac{1}{2}\left[-\alpha \pm (\alpha^2 + 4\beta^2)^{1/2}\right] . \tag{6b}$$

It should be noted, however, that this envelope function does not vanish at $\tau = \pm\infty$ implying that it cannot represent a physical pulse of finite duration. The other function for which an analytic solution of Eqs. (3) is known is $f(\tau) = \operatorname{sech}\tau$. By employing the change of variable

$$z = \tfrac{1}{2}\int_{-\infty}^{\tau} \operatorname{sech}^2\tau'\,d\tau' , \tag{7}$$

Rosen and Zener[2] were able to show that the gen-

Supported by the U.S. Office of Naval Research under Contract No. N00014-77-C-0553.

eral solution in this case could be given in terms of hypergeometric functions.

It is the purpose of this note to indicate that analytic solutions to Eqs. (3) may be found for an entire class of positive definite functions $f(\tau)$. The hyperbolic secant is included in this class of functions as a special case, but the rest of the functions are *not* symmetric about any given τ. This asymmetry leads to new features in the solutions.

II. SOLUTION FOR A CLASS OF FUNCTIONS

Equations (3a) and (3b) may be combined to yield the following second-order linear differential equation for $a_1(\tau)$:

$$\ddot{a}_1 + (i\alpha - \dot{f}/f)\dot{a}_1 + \beta^2 f^2 a_1 = 0 . \tag{8}$$

The amplitude a_2 obeys a similar equation with $-\alpha$ replacing α. In order to determine a class of functions $f(\tau)$ for which analytic solutions of Eq. (8) exist, we introduce the change of variable

$$z = z(\tau) \geq 0 , \tag{9a}$$

subject to the restriction that z is real and that

$$z(-\infty) = 0 , \tag{9b}$$

$$z(\infty) = 1 ;$$

the transformation $z(\tau)$ changes the range of the independent variable from $(-\infty, \infty)$ to $[0,1]$.

In terms of the variable z, one may write Eq. (8) in the form

$$a_1'' + \frac{\frac{d}{d\tau}(\ln \dot{z}) + (i\alpha - \dot{f}/f)}{\dot{z}} a_1' + \frac{\beta^2 f^2}{[\dot{z}]^2} a_1 = 0 , \tag{10}$$

where a prime indicates differentiation with respect to z. The general idea is to see whether or not Eq. (10) can be cast into the form of a standard equation of mathematical physics. In this paper, we determine the conditions under which Eq. (10) becomes the hypergeometric equation[3]

$$z(1-z)a_1'' + (Az + B)a_1' + Da_1 = 0 , \tag{11}$$

where

$$A = -(a + b + 1) , \tag{12a}$$

$$B = c , \tag{12b}$$

$$D = -ab , \tag{12c}$$

and a, b, c are the constants appearing in the hypergeometric equation of standard form.[3] We could determine equally well those conditions under which Eq. (10) becomes a generalized hypergeometric equation (equation of gauss); however, the hypergeometric equation is the only equation of gauss that yields physical solutions which are nonidentically zero at $z = 0$ and 1.

By equating Eqs. (10) and (11), one may obtain

$$\beta^2 f^2/(\dot{z})^2 = D/z(1-z) \tag{13}$$

and

$$\dot{z} = i\alpha z(1-z)/[(1+A)z + (B - \tfrac{1}{2})] . \tag{14}$$

In order to have a one to one mapping of τ onto z, we require that $z(\tau)$ is a monotonically increasing function, implying that $\dot{z}$ is real and positive. This requirement used in conjunction with Eqs. (13) and (14) implies the following restrictions:

$$A + 1 = i\alpha\lambda, \quad \lambda \text{ real} \tag{15a}$$

$$B - \tfrac{1}{2} = i\alpha\mu, \quad \mu \text{ real} \tag{15b}$$

$$\mu > 0, \quad \lambda/\mu > -1 , \tag{16}$$

$$D \text{ real}, \quad D > 0 . \tag{17}$$

In terms of these new variables, Eqs. (3) take the form

$$a_1' = -i\left(\frac{D}{z(1-z)}\right)^{1/2} e^{-i\alpha\tau(z)} a_2 , \tag{18a}$$

$$a_2' = -i\left(\frac{D}{z(1-z)}\right)^{1/2} e^{i\alpha\tau(z)} a_1 . \tag{18b}$$

Equation (10) becomes

$$z(1-z)a_1'' + [c - (a + b + 1)z]a_1' - aba_1 = 0 \tag{19}$$

with

$$a = i\alpha\lambda[-1 + (1 - 4D/\alpha^2\lambda^2)^{1/2}]/2 , \tag{20a}$$

$$b = i\alpha\lambda[-1 - (1 - 4D/\alpha^2\lambda^2)^{1/2}]/2 , \tag{20b}$$

$$c = \tfrac{1}{2} + i\alpha\mu , \tag{20c}$$

and Eq. (14) may be rewritten

$$\dot{z} = z(1-z)/(\mu + \lambda z) . \tag{21}$$

The general solution of Eq. (19) is[3]

$$a_1 = A_1 F(a, b, c; z) + A_2 z^{1-c} F(a - c + 1, b - c + 1, 2 - c; z) , \tag{22}$$

where $F(a, b, c; z)$ is the hypergeometric function, and A_1 and A_2 are integration constants. The time variable τ as a function of z may be obtained by integrating Eq. (21); one finds

$$\tau = \ln[z^{\mu}/(1-z)^{\mu+\lambda}] . \tag{23}$$

The upper-state amplitude may now be calculated by combining Eqs. (23), (18), (20), and (12c) to give

$$a_2 = i(-ab)^{-1/2} z^{c} (1-z)^{1-c+a+b} a_1' . \tag{24}$$

By differentiating Eq. (22) and using some simple properties of F functions,[3] one finds

$$a_2 = i(-ab)^{-1/2}[(ab/c)z^c F(c-a, c-b, 1+c; z)A_1 + (1-c)(1-z)^{1-c+a+b}F(a-c+1, b-c+1, 1-c; z)A_2]. \quad (25)$$

The constant A_1 and A_2 appearing in Eqs. (22) and (25) may be evaluated by imposing initial conditions $a_1(z=0)$ and $a_2(z=0)$. In terms of $a_1(0)$ and $a_2(0)$, Eqs. (22) and (25) become

$$a_1(z) = F(a, b, c; z)a_1(0) - \frac{i(-ab)^{1/2}z^{1-c}}{1-c}F(a-c+1, b-c+1, 2-c; z)a_2(0), \quad (26a)$$

$$a_2(z) = -\frac{i(-ab)^{1/2}z^c}{c}F(c-a, c-b, 1+c; z)a_1(0) + (1-z)^{1-c+a+b}F(a-c+1, b-c+1, 1-c; z)a_2(0), \quad (26b)$$

which together with Eqs. (20), (12c), (13), and (21) provide a complete solution to the problem.

III. NATURE OF THE PULSE

In this section, we describe the pulse shapes for which the solution (26) is valid and in Sec. IV, we present an analysis of the solution in light of these pulse shapes. The pulse shape $P(t)$, as defined by

$$P(t) = (\beta/T)f(\tau), \quad \tau = t/T, \quad (27)$$

is obtained from Eqs. (13), (21), (4), (23), and (2c) to be

$$P(t) = \frac{S}{\pi T}\frac{[z(1-z)]^{1/2}}{1+\lambda z}, \quad (28a)$$

$$t = T\ln[z/(1-z)^{1+\lambda}], \quad (28b)$$

where S is the pulse area defined in Eq. (2c). In arriving at Eq. (28), we used the normalization condition (4) to obtain

$$D = \beta^2 = S^2/\pi^2 \quad (29)$$

and set

$$\mu = 1 \quad (30)$$

without loss of generality.

The pulse is characterized by its area S, its time-scale parameter T, and the parameter $\lambda(-1 < \lambda < \infty)$. Various properties of the pulse may now be listed as follows:

Pulse amplitude. The pulse maximum A_0 occurring at

$$z_{max} = 1/(2+\lambda), \quad (31a)$$

$$t_{max} = T[\lambda\ln(2+\lambda) - (1+\lambda)\ln(1+\lambda)], \quad (31b)$$

is given by

$$A_0 = \frac{S}{\pi T}\frac{1}{2(1+\lambda)^{1/2}}. \quad (32)$$

Pulse area. The pulse area is $\int_{-\infty}^{\infty}P(t)dt = S$.

Pulse asymmetry. For any value $\lambda \neq 0$, the pulse is not symmetric. Defining

$$P_- = \int_{-\infty}^{t_{max}}P(t)dt, \quad P_+ = \int_{t_{max}}^{\infty}P(t)dt, \quad (33)$$

and an asymmetry parameter

$$A = \frac{P_+ - P_-}{P_+ + P_-}, \quad (34)$$

one can use Eqs. (28a), (21), and (31a) to obtain

$$A = 1 - (4/\pi)\tan^{-1}[1/(1+\lambda)^{1/2}]. \quad (35)$$

As λ varies from -1 to 0 to ∞, A varies from -1 to 0 to 1.

If $\lambda = 0$, $A = 0$ and the pulse is symmetric. In this limit one obtains from Eqs. (28) and (21)

$$P(t) = (S/2\pi T)\,\mathrm{sech}(t/2T), \quad (36)$$

$$\dot{z} = dz/d\tau = \tfrac{1}{4}\,\mathrm{sech}^2(t/2T), \quad (37)$$

which corresponds to both the pulse and transformation [Eq. (7)] used to arrive at the Rosen-Zener solution.

Pulse width. To find the full width at half maximum (FWHM) of the pulse, we seek those values of z, labeled $z_{1/2}$, for which $P(z) = \frac{1}{2}A_0$ and then calculate the corresponding $t_{1/2}$ values using Eq. (28b). From Eqs. (32) and (28a), it follows that $z_{1/2}$ may be obtained as a solution to

$$\frac{1}{4(1+\lambda)^{1/2}} = \frac{[z_{1/2}(1-z_{1/2})]^{1/2}}{1+\lambda z_{1/2}},$$

which yields values

$$z_{1/2} = \frac{7\lambda + 8 \pm 4\sqrt{3}(1+\lambda)}{\lambda^2 + 16\lambda + 16}. \quad (38)$$

Using Eqs. (38) and (28b) one can evaluate the FWHM in t space as

$$\Delta t_{FWHM} = T\left[\ln\left(\frac{7\lambda+8+4\sqrt{3}(1+\lambda)}{7\lambda+8-4\sqrt{3}(1+\lambda)}\right) - (1+\lambda)\ln\left(\frac{\lambda+8-4\sqrt{3}}{\lambda+8+4\sqrt{3}}\right)\right]. \quad (39)$$

TABLE I. Pulse characteristics.

	Amplitude[a] A_0	t_{max}/T	Asymmetry A	FWHM	HAW	Comments
$\lambda=-1+\epsilon$ $(0<\epsilon\ll 1)$	$\frac{1}{2\sqrt{\epsilon}}$	$-\epsilon(1+\ln\epsilon)$	$-1+\frac{4\sqrt{\epsilon}}{\pi}$	$19.1\epsilon T$	$T\ln 2$	Most pulse area for $t<t_{max}$
$\lambda=0$	$\frac{1}{2}$	0	0	$5.27T$	∞	Symmetric, hyperbolic-secant pulse
$\lambda\gg 1$	$\frac{1}{2\sqrt{\lambda}}$	$1-\ln\lambda$	$1-\frac{4}{\pi\sqrt{\lambda}}$	$19.1T$	$\lambda T\ln 2$	Most pulse area for $t>t_{max}$

[a] In units of $(S/\pi T)$.

Half-area width (HAW). Another useful parameter is the HAW defined as

$$\Delta t_{HAW}=|t_H-t_{max}|,$$

where t_H is the time defined such that half the pulse area lies between t_H and t_{max}. Setting

$$\tfrac{1}{2}S=\pm\int_{t_H}^{t_{max}}P(t)dt$$

and using Eqs. (28a), (21), (31a), (28b), and (31b), one may obtain

$$\Delta t_{HAW}=T\left|\ln[g^2(1+g^2)^\lambda]-\ln\frac{(2+\lambda)^\lambda}{(1+\lambda)^{1+\lambda}}\right|, \tag{40a}$$

where

$$g=\frac{1-(1+\lambda)^{1/2}}{1+(1+\lambda)^{1/2}}. \tag{40b}$$

For symmetric pulses the HAW is infinite since half of the pulse area lies between $t=-\infty$ and $t=t_{max}$. However, for very asymmetric pulses ($A\approx -1$ or 1), the HAW is a characteristic long-time scale pulse width.

The pulse properties are summarized in Table I for $\lambda=-1+\epsilon(0<\epsilon\ll 1)$, $\lambda=0$, and $\lambda\gg 1$. For $\lambda=-1+\epsilon$ or $\lambda\gg 1$ the pulses are very asymmetric, containing narrow central peaks and long tails extending out toward $t=-\infty$ and $t=+\infty$, respectively. The case $\lambda=0$ represents the symmetric hyperbolic secant pulse. Less extreme pulse asymmetries are represented in Fig. 1 where pulse shapes $P(t)(\pi T/S)$ are drawn for $\lambda=-0.8$, $\lambda=0$, and $\lambda=5$.

IV. NATURE OF THE SOLUTION

The general solution for the state amplitudes is given by Eqs. (26) along with Eqs. (20), (12c), (13), and (21); the class of pulse envelope functions $f(\tau)$ for which this solution is valid has been described in the previous section. Although Eqs. (26) could be used to determine the transient response to a pulse, we consider only the transition probability induced by the pulse. That is, we take as initial conditions

$$a_1(t=-\infty)=a_1(z=0)=1,$$
$$a_2(t=-\infty)=a_2(z=0)=0, \tag{41}$$

and calculate the probability

$$P_2=|a_2(t=\infty)|^2=|a_2(z=1)|^2 \tag{42}$$

that the atom has been excited by the pulse. Setting $z=1$ on the rhs of Eq. (26b) and using Eq. (41), we find

$$P_2=\frac{|ab|}{|c|^2}|F(c-a,c-b,1+c;1)|^2$$
$$=\frac{|ab|}{|c|^2}\left|\frac{\Gamma(1+c)\Gamma(1-c+a+b)}{\Gamma(1+a)\Gamma(1+b)}\right|^2, \tag{43}$$

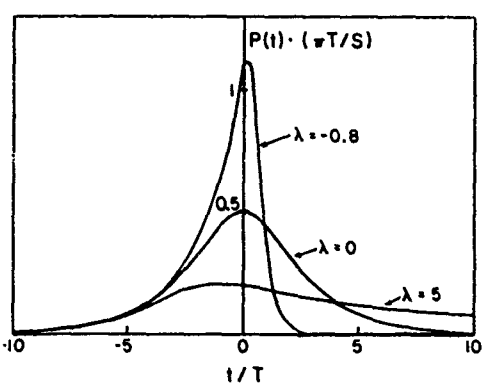

FIG. 1. Graphs of the pulse function $P(t)(\pi T/S)$ versus t/T for $\lambda=-0.8$, $\lambda=0$ (hyperbolic secant), and $\lambda=5$.

where Γ is the gamma function.[3] By substituting the values for a,b,c from Eqs. (20) into Eq. (43) and using some elementary properties of the gamma functions,[3] one may obtain the transition probability

$$P_2=[\sinh^2\delta+\sin^2(S^2-\delta^2)^{1/2}]\,\mathrm{sech}(\pi\alpha)\,\mathrm{sech}(\pi\alpha+2\delta)\,, \tag{44}$$

where S is the pulse area (2c) and

$$\delta=\pi\alpha\lambda/2 \quad (-\pi\alpha/2<\delta<\infty). \tag{45}$$

As a function of S, P_2 increases until $S=|\delta|$ and then oscillates between $\mathrm{sech}(\pi\alpha)\,\mathrm{sech}(\pi\alpha+2\delta)$ $(\sinh^2\delta)$ and $\mathrm{sech}(\pi\alpha)\,\mathrm{sech}(\pi\alpha+2\delta)$ $(\cosh^2\delta)$.

Whereas the pulse was characterized by the parameters T, S, and λ, the transition probability is a function of the detuning parameter $\alpha=\omega T$, the pulse area S, and the quantity $\delta=\pi\alpha\lambda/2$ which reflects the pulse asymmetry through Eq. (35). We now examine the nature of the solution (44) for several specific cases in light of the pulse structure described in the previous section.

$\alpha=0$. For zero detuning, the solution (44) reduces to the well-known solution [see Eq. (5)]

$$P_2=\sin^2 S\,. \tag{46}$$

$\delta=0$. For α arbitrary and $\delta=0$, one must have $\lambda=0$. The pulse is the hyperbolic secant given in Eq. (36) and Eq. (44) becomes

$$P_2=\sin^2 S\,\mathrm{sech}^2\pi\alpha\,, \tag{47}$$

which is the Rosen-Zener solution.[2]

Both solutions (46) and (47) are of the form $P_2=|\mathcal{F}(\alpha,S)\sin S/S|^2$, where $\mathcal{F}(\alpha,S)$ is the Fourier transform of the pulse evaluated at frequency α/T. Rosen and Zener conjectured that this result will be valid for arbitrary smooth pulses. For asymmetric pulses, the general solution (44) clearly violates this conjecture. Moreover, even for symmetric smooth pulses, one can show that the conjecture is false by numerically integrating Eqs. (1). However, numerical calculations using Lorentzian and Gaussian pulses do seem to indicate that, for symmetric pulses, there is an oscillatory behavior of P_2 as a function of S, and there are values of the pulse area S for which $P_2=0$. In contrast to this result, the result for asymmetric pulses and nonzero detuning $\delta\neq 0$ always yields $P_2>0$ regardless of the value of S.

$\pi\alpha\ll 1$, $\delta\gtrsim 1$. This limit implies that

$$\lambda=2\delta/\pi\alpha\gg 1$$

which is an asymmetric pulse of amplitude $1/2\sqrt{\lambda}$, FWHM $19.1T$, and HAW $\lambda T\ln 2$ (Table I). The corresponding transition probability (44) is given by

$$P_2=[\sinh^2\delta+\sin^2(S^2-\delta^2)^{1/2}]\,\mathrm{sech}2\delta\,. \tag{48}$$

The solution is graphed as a function of S for $\alpha=0.001$ and two non-zero values of δ in Fig. 2 along with the corresponding $\delta=0$ solution [Eq. (47)] for the hyperbolic-secant pulse. One notes that P_2 oscillates as a function of S about its saturation value of $\frac{1}{2}$ and that the oscillation amplitude decreases with increasing δ (increasing λ). With increasing δ, it is the central peak region that is providing the major contribution to the transition probability since the pulse wing is becoming increasingly adiabatic [i.e., $\Delta\nu_{\mathrm{HAW}}(\alpha/T)>1$—see Table I]. The sharply asymmetric nature of the central peak *cannot* give rise to the zero-transition probability effect (i.e., $P_2=0$ for $S\neq 0$) that occurs with symmetric pulses. Even though the peak amplitude decreases as $\lambda^{-1/2}$, the transition probability from the central peak region still leads to saturation behavior for $S>\delta$.

$\pi\alpha\approx 1$, $\delta=(\pi\alpha/2)(-1+\epsilon)(0<\epsilon\pi\alpha\ll 1)$. This limit implies $\lambda=-1+\epsilon(\epsilon\ll 1)$ which is an asymmetric pulse of amplitude $1/2\sqrt{\epsilon}$, FWHM $19.1\epsilon T$, and HAW $T\ln 2$. The transition probability is given by

$$P=[\sinh^2(\pi\alpha/2)+\sin^2(S^2-\pi^2\alpha^2/4)^{1/2}]\,\mathrm{sech}\pi\alpha\,. \tag{49}$$

and is plotted in Fig. 3 for $\alpha=\frac{1}{3}$, $\epsilon=0.001$ along with the corresponding P_2 for the $\delta=0$ hyperbolic-

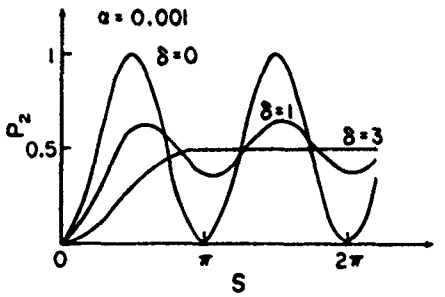

FIG. 2. Graph of the transition probability P_2 as a function of pulse area S for $\alpha=0.001$ and $\delta=0$ $(\lambda=0)$, $\delta=1$ $(\lambda=637)$, and $\delta=3$ $(\lambda=1910)$.

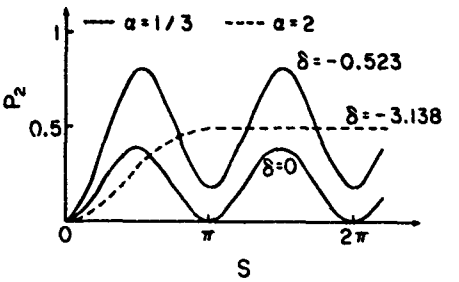

FIG. 3. Graph of P_2 versus S for $\alpha=\frac{1}{3}$, $\delta=0$ $(\lambda=0)$, $\alpha=\frac{1}{3}$, $\delta=-0.523$ $(\lambda=-1+0.001)$, and $\alpha=2$, $\delta=-3.138$ $(\lambda=-1+0.0011)$.

secant pulse. A graph of P_2 versus S for $\alpha = 2$, $\epsilon = 0.0011$ is also drawn (the corresponding hyperbolic-secant solution has amplitude 1.4×10^{-3}) showing its similarity to the $\delta = 3$ curve of Fig. 2.

These graphs are explained by the fact that the hyperbolic-secant pulse is "semiadiabatic" ($\alpha \approx 1$), and becomes increasingly adiabatic with increasing α (with a corresponding decrease of P_2). In contrast, the central peak region of the asymmetric pulse is always sudden with respect to $1/\alpha$. It is true that the long-tail region of the asymmetric pulse is also "semiadiabatic" $[\Delta f_{\mathrm{HAW}}(\alpha/T) \approx 1]$ and this tail gives rise to the oscillations in P_2. However, for $\alpha \gtrsim 2$ the central asymmetric region dominates the contribution to P_2 and a saturation behavior similar to the $\delta = 3$ curve of Fig. 1 results.

$\pi\alpha \approx 1$, $\delta \gg 1$. This limit corresponds to the asymmetric pulse with $\lambda \gg 1$, amplitude $1/2\sqrt{\lambda}$, FWHM $19.1T$, and HAW $\lambda T \ln 2$. The transition probability is given by

$$\begin{aligned} P_2 &= \tfrac{1}{2}(S^2/\delta)\,\mathrm{sech}\pi\alpha\, e^{-\pi\alpha}, \quad S^2 \ll \delta \\ &= \tfrac{1}{2}\,\mathrm{sech}\pi\alpha\, e^{-\pi\alpha}, \quad S^2 \gtrsim \delta^2. \end{aligned} \tag{50}$$

Only the central peak contributes to P_2 since the HAW wing is adiabatic for a detuning $\pi\alpha \approx 1$ [i.e., $\pi(\alpha/T) \cdot \Delta f_{\mathrm{HAW}} \gg 1$]. Thus, the probability is much less than that in the corresponding hyperbolic-secant case (47), except when the pulse area S is strong enough to have the central peak region of the $\lambda \gg 1$ pulse saturate P_2.

$\pi\alpha \gg 1$, $\delta = (\pi\alpha/2)(-1+\epsilon)$, $\epsilon\pi\alpha \approx 1$. This limit corresponds to the asymmetric pulse $\lambda = -1 + \epsilon$ $(0 < \epsilon \ll 1)$ having amplitude $1/2\sqrt{\epsilon}$, FWHM $19.1\epsilon T$, and HAW $T \ln 2$. The transition probability is given by

$$\begin{aligned} P_2 &= \frac{S^2}{\pi\alpha} e^{-\pi\alpha\epsilon}\,\mathrm{sech}(\pi\alpha\epsilon), \quad S^2 \ll |\delta| \\ &= \tfrac{1}{2} e^{-\pi\alpha\epsilon}\,\mathrm{sech}(\pi\alpha\epsilon), \quad S^2 \gtrsim \delta^2. \end{aligned} \tag{51}$$

The central peak of the pulse is "semisudden" ($\epsilon\pi\alpha \approx 1$) and gives rise to the major contribution to P_2. As in the previous case, for large enough S, the pulse is strong enough to lead to saturation behavior. The transition probability for this case is larger than that for the corresponding hyperbolic-secant pulse since the hyperbolic-secant pulse is adiabatic for a detuning $\pi\alpha \gg 1$.

$\pi\alpha \gg 1$, $2\delta + \pi\alpha \gg 1$, $|\delta| \gg 1$. This adiabatic limit can apply to a wide variety of pulses. The transition probability is given by

$$\begin{aligned} P_2 &= (S^2/|\delta|)e^{-2\pi\alpha} e^{2(|\delta|-\delta)}, \quad S^2 \ll |\delta| \\ &= e^{-2\pi\alpha} e^{2(|\delta|-\delta)}, \quad S^2 \gtrsim \delta^2 \quad (\lambda \neq 0) \end{aligned} \tag{52}$$

and

$$P = 4\sin^2 S\, e^{-2\pi\alpha} \quad (\lambda = 0). \tag{53}$$

The entire pulse is adiabatic for the conditions given, but the central portions of the asymmetric pulse can still provide the major contribution to the transition probability. The transition probability for the asymmetric pulse does not oscillate as a function of S in contrast to that for the $\lambda = 0$ (hyperbolic-secant pulse). (Actually there is an oscillatory term in P_2 even for the asymmetric case, but its amplitude relative to the background term is negligible.)

To summarize, we have found a new class of functions for which analytic solutions of the two-state problem may be obtained. These positive definite pulses vanish at $t = \pm\infty$. With the exception of the hyperbolic-secant pulse which is a member of this class of functions, the pulses are asymmetric. For the asymmetric pulses, the transition probability does not vanish for any pulse area $S > 0$ (provided $\alpha \neq 0$), a result that differs from the corresponding calculation for symmetric pulses.

ACKNOWLEDGMENTS

One of the authors (P.R.B.) would like to thank his hosts at the Istituto di Elettronica Quantistica for the hospitality shown to him during his stay when part of this research was carried out. He is also grateful to Professor E. Robinson and Dr. S. Yeh for helpful discussions. The research of P. R. B. is supported by the Office of Naval Research.

---

*Permanent address.

[1]The normalization (4) cannot be maintained for a constant pulse amplitude. In this work we shall consider only pulses which vanish at $t = \pm\infty$ for which Eq. (4) may be satisfied.

[2]N. Rosen and C. Zener, Phys. Rev. 40, 502 (1932).

[3]M. Abramowitz and I. A. Stegun, *Handbook of Mathematical Functions* (U. S. Government Printing Office, Washington, D. C., 1965).

PHYSICAL REVIEW A VOLUME 24, NUMBER 4 OCTOBER 1981

Two-level transition probabilities for asymmetric coupling pulses

E. J. Robinson
Physics Department, New York University, 4 Washington Place, New York, New York 10003
(Received 2 March 1981)

In a recent paper, Bambini and Berman [A. Bambini and P. R. Berman, Phys. Rev. A 23, 2496 (1981)] presented analytic solutions to a certain family of coherent-coupling pulses for a two-level system. They show, for nonresonant temporally asymmetric members of the class, that there are no solutions corresponding to vanishing transition probabilities. In this Comment, we examine the problem in greater generality, and demonstrate that this property is the norm for asymmetric pulses, and that a vanishing transition probability is possible only if severely overdetermined conditions are satisfied.
1977 PACS numbers: 32.70.Jz, 32.80.Kf, 42.65.Gv ACK201

The problem of a two-level system coupled by an external field has a long history in physics, dating back to the 1930's.[1,2] Originally motivated by investigations on atoms in magnetic fields, theories of such systems have more recently been applied to laser-related problems.[3]

Let a_1, a_2 be the amplitudes of the two states. We assume that the coupling potential connecting the two states is of variable amplitude and central frequency Ω, so that, in the rotating wave approximation, the time-dependent Schrödinger equation becomes a pair of coupled equations for a_1, a_2:

$$i\dot{a}_1 = V(t)e^{i\Delta t}a_2 , \tag{1a}$$

$$i\dot{a}_2 = V(t)e^{-i\Delta t}a_1 . \tag{1b}$$

Here Δ is the detuning of Ω from the atomic frequency. We work in a system of units where $\hbar = 1$.

For the case where V is a constant in time, the solution for initial conditions $a_1 = 0$, $a_2 = 1$ at $t = 0$ is

$$a_1 = \frac{-iV}{(\Delta^2/4 + V^2)^{1/2}} e^{i\Delta t/2} \sin[(\Delta^2/4 + V^2)^{1/2} t] .$$

This is the Rabi problem. For this to be relevant, the approximation that the rise time of the field is much shorter than other characteristic times should be a good one. In their paper, Rosen and Zener[2] considered a case where this sudden approximation was not valid. They were motivated by a serious discrepancy between results of the sudden-approximation theory and experiment. They analyzed the effect of a smoothly varying pulse, choosing a hyperbolic secant because of the exactly solvable nature of the equations that result from such a time dependence. For the hyperbolic secant pulse, one may make a change of variable that transforms the equation of motion into the hypergeometric equation. Robiscoe[4] has shown how to generalize this to the case of decaying states.

Recently, Bambini and Berman[5] have gone beyond the Rosen-Zener problem. They show that there is an entire class of envelope functions that may be mapped into the hypergeometric equation, of which the hyperbolic secant pulse is merely one member. All $V(t)$ in the family, other than the hyperbolic secant, are asymmetric in time, i.e., $V(t) \neq V(-t)$. Bambini and Berman show that for these asymmetric pulses, there is no case, apart from exact resonance, where there is a nonvanishing transition probability, a striking and surprising result.

In the case of the Rabi problem, on the other hand, for any given detuning, there are always values of the pulse area for which the amplitude a_1 returns to zero. In the Rosen-Zener case, the amplitude $a_1(+\infty)$ goes like $(\sin A)/A$, where A is the pulse area, so that here too, once the hyperbolic secant envelope function is specified, one can find values of the area of the pulse for which $a_1(+\infty)$ vanishes. Similar remarks hold for other symmetric potentials, where solutions have been obtained with computers.[6,7] It is a most remarkable feature of the Bambini-Berman problem that it admits no asymmetric envelopes for $\Delta \neq 0$ with a nonvanishing transition probability. That is, it asserts that for asymmetric pulses of the form studied, if the amplitudes $a_2 = 1$ and $a_1 = 0$ at $t = -\infty$, then at time $t = +\infty$, the probability for finding the system in state 1 is nonvanishing, i.e., there will always be some population in state 1 for this class of off-resonant asymmetric pulse. No

Supported by the U.S. Office of Naval Research under Contract No. N00014-77-C-0553.

previous prediction of this kind of behavior seems extant in the literature. It should be understood that only envelopes of a single algebraic sign are being considered, so that, for example, pulses that are completely antisymmetric in time are excluded from this discussion.

Bambini and Berman[5] reach their conclusion by obtaining a complete analytic solution to their problem. Since most pulse shapes do not admit of closed form solutions, it is of interest to inquire whether the nonvanishing of transtion probabilities holds for other smooth, asymmetric pulses and whether this property can be demonstrated in a general way, i.e., through the structure of the equations of motion. It is to this question that we address the present work.

Equations (1) may be put in the form of uncoupled second-order equations,

$$\ddot{a}_1-(\dot{V}/V+i\Delta)\dot{a}_1+V^2a_1=0\,, \tag{2a}$$

$$\ddot{a}_2-(\dot{V}/V-i\Delta)\dot{a}_2+V^2a_2=0\,. \tag{2b}$$

Defining $z=\int_{-\infty}^{t}f(t')dt'-\frac{1}{2}$, with $A=\int_{-\infty}^{\infty}V\,dt$ and $f=V/A$, Eqs. (2) become, in the z plane,

$$\ddot{a}_1-i\frac{\Delta}{f}\dot{a}_1'+A^2a_1=0\,, \tag{3a}$$

$$\ddot{a}_2+i\frac{\Delta}{f}a_2'+A^2a_2=0\,. \tag{3b}$$

We assume, with Bambini and Berman,[5] that $f(t)$ does not change sign, so that the transformation, which differs from theirs, is single valued. If one transforms Eq. (3a) via the substitution

$$b=a_1\exp[(-i\Delta/2)\textstyle\int_0^z dz'/f(z')]=a_1e^{-i\Delta z/2f}\,,$$

into an equation with the first derivative missing, we have

$$\ddot{b}+\left[\frac{\Delta^2}{4f^2}+\frac{i\Delta f'}{2f^2}+A^2\right]b=0\,, \tag{3a'}$$

$$-\ddot{b}+\left[\frac{-\Delta^2}{4f^2}-\frac{i\Delta f'}{2f^2}\right]b=A^2b\,. \tag{3b'}$$

Eq. (3b') resembles a one-dimensional, time-independent Schrödinger equation for a particle of mass $\frac{1}{2}$ moving in the complex "potential"

$$V=-\left[\frac{\Delta^2}{4}+\frac{i\Delta f'}{2}\right]\frac{1}{f^2}\,,$$

where $\hbar$ has been set $=1$.

This equation is to be solved subject to the initial conditions that $b=0$ at $z=-\frac{1}{2}$. If the dynamics of the problem permit a transition probability of zero for certain pulse areas, this means $b(z=+\frac{1}{2})$ also vanishes for those values of A. In short, we must solve an eigenvalue problem and find those values of A^2 for which the solutions of Eq. (3b') vanish at $z=\pm\frac{1}{2}$. Now for physical pulses, only real envelopes exist. For these, A^2 is real and positive. If none of the eigenvalues A^2 meets this criterion, A will have an imaginary part for all the eigenfunctions of Eq. (3b'), and none will correspond to a system driven by an actual pulse, i.e., there will be no physically meaningful pulse areas for which the system undergoes a transition probability of zero. In the following, we shall assume a nonvanishing detuning. Note that the case of exact resonance is entirely equivalent to the elementary quantum mechanical problem of a particle in a box, whose eigenvalues A^2 are $n^2\pi^2$. In this way, we confirm the simple result that the transition probability vanishes for pulse areas that are integral multiples of π, if $\Delta=0$.

We should comment that if one constructs an asymmetric potential from two temporally distinct symmetric pulses, one can, by making each of the component pulses produce a net transition amplitude of zero, cause the overall probability to vanish. To force the components to be exactly nonoverlapping in time requires that they be sharply cut off. Thus, these pulses do not conform to the smoothness criterion of Bambini and Berman.[5]

We consider now pulses where the imaginary term is present. We examine first the case of symmetric pulses. Let A^2 be a typical eigenvalue. If we replace the imaginary term by its negative, then the resulting equation will have A^{2*} for its eigenvalue. Now, since $f(z)$ is symmetric in z, $f'(z)$ will be antisymmetric. Therefore, the transformation $z\rightarrow -z$ reverses the sign of the imaginary term on the left-hand side of Eq. (3b'), but leaves the eigenvalue unchanged. Immediately, $A^2=A^{2*}$, i.e., all the eigenvalues are real, although not necessarily larger than zero. For asymmetric pulses, the transformation $z\rightarrow -z$ does not reproduce the complex-conjugate equation, and A^2 will not, in general, be the same as A^{2*}. This does not absolutely rule out the possibility that for particular $f(t)$ and detuning, one might have one or more real and positive eigenvalues, but demonstrates that it could occur only by accident. We shall show in the following that the conditions that must necessarily be fulfilled for A^2 to be real for asymmetric pulses are severely overdetermined.

To proceed, we will analyze the problem from a

perturbative viewpoint, and assume that the entire perturbation expansion can be summed. We do not restrict ourselves to the first few terms, but study the parity-related properties of the full series. We take the zero-order problem to be

$$-\ddot{b}_0 - \left[\frac{\Delta^2}{4f^2}\right] b_0 = \Lambda_0^2 b_0 . \tag{4}$$

This is Hermitian and identical to a time-independent Schrödinger equation, which has only real eigenvalues. The imaginary term $-i\Delta f'/2f^2$ is to be considered as a perturbation.

We wish to contrast the case of symmetric and asymmetric pulse envelopes. Assume $f(t)$ to be symmetric—$f(z)$ is also symmetric. (If $f(t)$ were not symmetric about $t=0$, $f(z)$ would lack symmetry about its origin.) For this case, the unperturbed eigenfunction b_0 has definite parity, and the perturbation $-i\Delta f'/f^2$ is odd under reflection. It follows directly that if one writes a perturbation series for Λ^2 as an expansion in the usual way, contributions from odd powers of the "strength" of the "interaction" will be absent. Since only the even orders survive, and the strength parameter is purely imaginary, the resulting eigenvalues will be real.

If the potential $V(t)$ is not symmetric neither $1/f^2$ nor f'/f^2 will be operators of definite parity, nor will unperturbed solutions b_0 possess well-defined inversion properties. Hence, both even and odd terms in the perturbation expansion will be present, and the eigenvalues Λ^2 will all be complex, unless there is a case where, for a specific detuning, the odd powers of the expansion sum to zero.

The latter is an extremely unlikely circumstance. Equations (3b') is of the form

$$-\ddot{b} - \left[\frac{\mu}{f^2} + i\frac{\lambda f'}{f^2}\right] b = \Lambda^2 b . \tag{5}$$

We require not only that the odd powers sum to zero, but that they do so for a value of λ that is exactly the square root of μ. We cannot quite exclude this possibility, but it is evidently highly overdetermined.

To summarize, we have shown that the result obtained for particular asymmetric pulses by Bambini and Berman,[5] namely that there are no non-resonant cases for which the transition probability vanishes, is the normal consequence of the general structure of the equations of motion, and applies, apart from some remotely possible accidental cases, to all smoothly varying, asymmetric pulses which possess envelopes of a single algebraic sign.

The author is grateful to Professor P. R. Berman for valuable discussions of this problem, and for a copy of the Bambini-Berman manuscript prior to publication. He also wishes to thank Dr. R. Salomaa for useful comments. This work was supported by the Office of Naval Research.

[1]I. I. Rabi, Phys. Rev. 51, 652 (1937).
[2]N. Rosen and C. Zener, Phys. Rev. 40, 502 (1932).
[3]An extensive compilation of references is given by L. Allen and J. H. Eberly, *Optical Resonance and Two-Level Atoms*, (Wiley, New York, 1975).
[4]R. T. Robiscoe, Phys. Rev. A 17, 247 (1978).
[5]A. Bambini and P. R. Berman, Phys. Rev. A 23, 2496 (1981).
[6]S. Yeh and P. R. Berman, private communication.
[7]E. J. Robinson (unpublished).

To Appear in Physical Review Letters 8/28/81 submitted

Measurement of a total (atomic-radiator)-perturber scattering cross section.

R. Kachru,+ T. J. Chen, and S. R. Hartmann
Columbia Radiation Laboratory, Department of Physics
Columbia University, New York, N. Y. 10027

T. W. Mossberg
Department of Physics, Harvard University
Cambridge, Massachusetts 02138

P. R. Berman
Department of Physics, New York University
4 Washington Place, New York, N. Y. 10003

Working on the $2S\text{-}2P_{1/2}$ transition of atomic ^7Li, perturbed by noble gases, and using the photon echo technique, we report the first measurement of a "total" (atomic radiator)-perturber scattering cross section. The phase-changing, inelastic, and velocity-changing aspects of collisions contribute to this cross section, which is significantly larger than the corresponding pressure broadening cross section. Typical velocity changes are found to be roughly one percent of the mean thermal speed.

Supported by the U.S. Office of Naval Research under Contract No. N00014-77-C-0553.

In most spectroscopy experiments, one monitors the dipole moment of the system under investigation. The collisional perturbation of optical dipoles or "optical radiators" represents an interesting problem, since it requires one to understand the way in which collisions affect a superposition state. At first glance, it might seem that any collision destroys the superposition state since the states a and b involved in the optical transition generally follow different collision trajectories.[1,2] The notion of distinct trajectories, however, is a classical one which is known to fail for large impact parameter collisions. Thus the dipole moment or optical coherence is not necessarily destroyed in such large impact parameter collisions.[3] Despite the fact that state-dependent trajectory effects seem to play a crucial role in determining the fate of the optical dipoles, for reasons to be discussed below, steady-state spectroscopy experiments are not overly sensitive[4] to such effects. As a result traditional theories of pressure broadening,[5] in which collisions are assumed to affect only the phases of the optical dipoles, have been successful in explaining these experiments. Only recently has the effect of velocity-changing collisions been put in better perspective.[6] To clearly identify the effects of velocity-changing collisions on optical dipoles experimentally, coherent transient techniques offer unique possibilities.[7]

We present here results of a photon-echo study of $2S\text{-}2P_{1/2}$ Li radiators perturbed by noble-gas atoms which provide the first comprehensive picture ~~(for any collision partners)~~ of the quant

mechanical-velocity-changing aspect of collisions.[3,7] We measure a total radiator-perturber scattering cross section σ_t (representing the combined effect of the inelastic, phase-changing, and velocity-changing aspects of collisions), and find that it is significantly larger than the broadening cross sections deduced from spectral line measurements. Fitting our data to a phenomenological collision kernel allows us to estimate the average velocity change experienced by a radiator in those collisions which produce identifiable velocity changes.

Assume that the two photon-echo-excitation pulses propagate along $\hat{z}$ and occur at the times t=0 and t=τ. The phase of a radiator residing at a particular location $\vec{r}$ in the sample is given[8] (for t>τ) by $\exp[-i(\phi-\vec{k}\cdot\vec{r})]$, where

$$\phi(t) = -\int_0^\tau [\omega(t') + \vec{k}\cdot\vec{v}(t')]dt' + \int_\tau^t [\omega(t') + \vec{k}\cdot\vec{v}(t')]dt, \qquad (1)$$

$\omega(t')$ $[\vec{v}(t')]$ is the instantaneous oscillation frequency [velocity] of the radiator, and $\vec{k}$ is the common wavevector of the excitation pulses. In the absence of collisions, $\omega(t')$ and $\vec{v}(t')$ are time-independent so that $\phi(t_e=2\tau) = 0$ (i. e. Doppler dephasing is eliminated) and an echo is emitted along $\hat{z}$.

In the presence of collisions, the echo intensity I_e is degraded by the factor $\langle\exp[-i\phi(2\tau)]\rangle^2$, where the angled brackets indicate an ensemble average. While a more detailed calculation of the collisionally induced modification of the echo amplitude will be given elsewhere, we can roughly speaking, evaluate this factor by considering collisions to be divided into two groups, i. e. those having impact parameters, b, less than or greater than the

Weisskopf radius b_w.[5] For $b<b_w$, classical trajectory notions are valid and owing to the separation of trajectories argument, one is led to the conclusion that the dipole moment is destroyed in a collision. In traditional pressure broadening theories, phase changes in this region are large enough to destroy the optical coherence. A broadening cross section σ_B can be calculated using either theoretical picture (loss of dipoles because of phase changes or distinct trajectories) and interestingly, both approaches lead to the same value. For collisions with $b>b_w$, the distinct trajectory argument fails and one must perform a quantum-mechanical calculation. Collisions for which $b>b_w$ give rise to all velocity-changing effects in which the dipole moment may be preserved and the small phase changes which occur in these collisions (which for simplicity we neglect) contribute to the pressure-induced shifts in spectral profiles. We can understand the success of traditional theories of pressure broadening despite their neglect of velocity-changing effects by noting that $b>b_w$ collisions generally give rise only to small angle [$\theta \lesssim \lambda_B/b_w \ll 1$, where λ_B = DeBroglie wavelength of Li] diffractive scattering. The small velocity changes associated with diffractive scattering do not significantly modify the output of most steady-state spectroscopic experiments. For large τ, however, photon echo experiments can be sensitive to the velocity changes resulting from even diffractive scattering.

Thus collisions with $b<b_w$ can be viewed as "inelastic-like" and accordingly lead to a decrease in echo intensity by the factor

$$\exp(-4nv_r\sigma_B\tau), \qquad (2)$$

where n is the perturber number density, $v_r=(8k_bT/\pi\mu)^{1/2}$ is the mean perturber-radiator relative speed, k_b is Boltzman's constant, T is the absolute temperature, μ is the radiator-perturber reduced mass, and σ_B is the τ-independent broadening cross section. Velocity-changing collisions decrease the echo intensity by the factor[9]

$$\exp[-4nv_r\tau\sigma_v(\tau)], \tag{3a}$$

where

$$\sigma_v(\tau) = \sigma_v^o[1 - \frac{1}{\tau}\int_0^\tau d\tau' \int_{-\infty}^{\infty} e^{ik\tau'(\Delta v_z)} g(\Delta v_z) d(\Delta v_z)], \tag{3b}$$

σ_v^o is the total cross section for velocity-changing collisions, $k = |\vec{k}|$, and the collision kernel $g(\Delta v_z)$ gives the probability of a particular change in the z-component of velocity Δv_z. Overall, the echo intensity varies as

$$I_e(n,\tau) = I_e^o \exp[-4nv_r\tau\sigma_{eff}(\tau)], \tag{4a}$$

where

$$\sigma_{eff}(\tau) = \sigma_B + \sigma_v(\tau), \tag{4b}$$

and I_e^o is the n=0 echo intensity.
Since the root-mean-square change in Δv_z is finite for any realistic $g(\Delta v_z)$, $\sigma_v(\tau) = \alpha\tau^2$ for sufficiently small τ and

$$\sigma_{eff}(\tau) = \sigma_B + \alpha\tau^2 \quad \text{(short } \tau\text{)}. \tag{5}$$

Here α depends on the details of $g(\Delta v_z)$. Therefore, $\sigma_{eff}(\tau=0) \equiv \sigma_B$. On the other hand, $\sigma_v(\tau \to \infty) = \sigma_v^o$ which

implies that $\sigma_{eff}(\tau \to \infty) = \sigma_t \equiv \sigma_B + \sigma_v^o$.

The excitation pulses used in our experiment on the 6708 Å $2S$-$2P_{1/2}$ transition of ^{7}Li have a 6 Ghz spectral width, a 4.5 nsec temporal width, and a peak power of a few watts. The two pulses, optically split from the single output pulse of an N_2-laser-pumped dye laser, were collimated to a 4 mm diameter, and directed through a stainless steel heat-pipe-type cell containing Li of natural isotopic concentrations. The cell, maintained at 525± 15 K (implying a Li pressure of $\approx 10^{-6}$ torr), had a vapor region approximately 10 cm in length. For reasons described elsewhere,[3] we used excitation pulses of orthogonal linear polarization in short-τ measurements. Excitation pulses of parallel polarization, which depending on τ produce echo signals 10 to 100 times larger than pulses of orthogonal polarization, were used for long-τ measurements, where radiative decay of the $2P_{1/2}$ state weakened the echo signal (by ≈1600 times for τ ≈100 nsec). Measurements in the intermediate-τ regime revealed no polarization dependence of observed cross sections.

We have measured I_e versus n (maximum n ≈ 10^{16} cm^{-3}) for various fixed τ, and used Eq. 4a to calculate $\sigma_{eff}(\tau)$. In Fig. 1, we plot $\sigma_{eff}(\tau)$ versus τ for each noble gas perturber. We obtained values of σ_B by using our two shortest-τ measurements of $\sigma_{eff}(\tau)$ for each perturber and extrapolating, according to Eq. 5, back to $\sigma_{eff}(\tau=0) = \sigma_B$. These values of σ_B are presented in Table I along with the values of σ_B obtained in traditional line-broadening experiments.[10] Except in the case of He, we find that the measurements are in good agreement.

We attempt to reproduce $\sigma_v(\tau)$ (computed using our value of σ_B and Eq. 4b) and hence $\sigma_{eff}(\tau)$ by inserting various $g(\Delta v_z)$ in Eq. 3b. For $g(\Delta v_z) = (\pi u_o)^{-1/2}\exp(-\Delta v_z^2/u_o^2)$, we obtain the solid lines shown in Fig. 1. The least-squares-fit values of the free parameters σ_v^o and u_o are shown in Table I. The quality of the fits is quite good. A Lorentzian kernel of the form $g(\Delta v_z) = (u_o/\pi)/(u_o^2 + \Delta v_z^2)$ (but with $g(\Delta v_z) = 0$ for $\Delta v_z >> u_o$) produces a better fit to $\sigma_v(\tau)$ for Li-He collisions, but a poorer fit for the other perturbers. These results, as well as the ratio $\sigma_B/\sigma_v^o \approx 1.0$ observed in our experiment, are in qualitative agreement with a theory based on a quantum mechanical hard sphere model of collisions.

The derived values of u_o and σ_v^o depend somewhat on our choice for $g(\Delta v_z)$. We note, however, that our measurements are sensitive to all velocity changes $\Delta v_z > \Delta v_z^{min} \equiv 1/k\tau_{max}$ (τ_{max} is our maximum pulse separation). Our value for Δv_z^{min} is less than the characteristic diffractive velocity change $v_D \equiv v_r\lambda_B/\sqrt{\sigma_t}$. The fact that the scattering is diffractive in nature restricts

our choice of $g(\Delta v_z)$ to functions which are relatively flat in the region $\Delta v_z \lesssim v_D$. With this restriction, we do not expect our derived value of σ_v^o to differ greatly from those shown in Table I. If a heavier radiator is used, the corresponding value of $u_o \approx v_D$ could be smaller and the region in which velocity changes are seen (i. e. $ku_o\tau \gtrsim 1$) might no longer be accessible. It is perhaps for this reason that velocity-changing effects were not seen in a coherent-transient experiment with I_2 as the radiator.[11]

Recent treatments of radiator-perturber scattering have shown that the net polarization in a medium obeys a quantum-mechanical transport equation.[12,13] This equation contains a loss term whose real part, which corresponds to the time rate of change of the polarization's magnitude, is given by $nv_r(\sigma_a+\sigma_b)$, where σ_a (σ_b) corresponds to the cross section for ground-state (excited-state) radiator-perturber scattering. Since this is the only term important to the long-time behavior of the photon echo, we equate our σ_t with $(\sigma_a+\sigma_b)/2$.

The cross section σ_a has been measured by atomic beam techniques.[14] In Table I, we list, for each perturber, the velocity-selected value of σ_a obtained at the velocity v_r. Our values of $\sigma_t = \sigma_B + \sigma_v^o$, based on both Lorentzian and Gaussian kernels, are also presented. Since the long-range part of the potential should reasonable approximation, determine the magnitude of the scatterin

section, we expect (at least for Ar, Kr, and Xe) that $\sigma_b/\sigma_a \approx (C_6^b/C_6^a)^{2/5}$, where C_6^b (C_6^a) is the coefficient of the Van der Waals

portion of the potential. Assuming that $C_6 = 2\varepsilon r_m^6$, where ε is the potential well depth and r_m is the internuclear separation at which the potential is minimum, (as is true of a Lennard-Jones (6,12) potential), we can use the potential calculation of Ref. 15 to find that $(C_6^b/C_6^a)^{2/5}$ falls between 1 and 1.6 depending on the perturber and which of the possible excited-state potentials is considered. This implies that σ_t should be between 1 and 1.3 times σ_a. Our data are reasonably consistent with this result.

Our results clearly demonstrate the role played by velocity-changing collisions. Their contribution to the echo signal underlines the importance of quantum-mechanical scattering effects in collisions undergone by an optical dipole.

Supported financially by the U. S. Office of Naval Research (Contracts N00014-78-C-517 and N00014-77-C-0553) and by the U. S Joint Services Electronics Program (Contract DAAG29-79-C-0079).

References

+ Present Address: Molecular Physics Lab., SRI International, Menlo Park, CA. 94025.

1. In the case of transitions between similar levels (e. g. the vibrational-rotational levels of a single molecular electron state) collisional phase changes do not occur, and collisional velocity changes produce marked effects. See R. H. Dicke, Phys. Rev. 89, 472 (1953) and C. J. Borde in Laser Spectroscopy III, Springer-Verlag, Berlin, 1977, p 121.

2. P. R. Berman, Phys. Rep. 43, 101 (1978); Adv. At. Molecular Phys. 13, 57 (1977) and references therein.

3. The first evidence of collisional velocity changes affecting an optical radiator involving dissimilar states was reported by: T. W. Mossberg, R. Kachru, and S. R. Hartmann, Phys. Rev. Lett. 44, 73 (1980).

4. A method of observing the effect of velocity-changing collisions on the lineshape of optical transitions involving three coupled energy levels has recently been proposed [J. L. LeGouët and P. R. Berman, Phys. Rev. A 17, 52 (1978)]; however, experiments have thus far failed to detect the effect [P. Cahuzac, J. L. LeGouët, P. E. Toschek, and R. Vetter, Appl. Phys. (Ger) 20, 83 (1979)].

5. Two recent reviews with additional references are: W. R. Hindmarsh and J. M. Farr, Prog. Quantum Electron. 2, 139 (1972) and E. L. Lewis, Phys. Rep. 58, 1 (1980).

6. S. Avrillier, C. J. Borde, J. Picart, and N. Tran Minh, Spectral Line Shapes, B. Wende, Ed., Walter de Gruyter Co., Berlin, 1981.

7. The power of the photon echo technique in the study of collisional velocity-changes (in the absence of phase-changing effects) was demonstrated by P. R. Berman, J. M. Levy, and R. G. Brewer, Phys. Rev. A 11, 1668 (1975). See also B. Comaskey, R. E. Scotti, and R. L. Shoemaker, Opt. Lett. 6, 45 (1981).

8. R. Kachru, T. W. Mossberg, and S. R. Hartmann, J. Phys. B 13, L363 (1980).

9. A. Flusberg, Opt. Commun. 29, 123 (1979).

10. N. Lwin, Thesis (University of Newcastle upon Tyne) 1976, as reported by E. L. Lewis in Ref. 5.

11. R. G. Brewer and A. Z. Genack, Phys. Rev. Lett. 36, 959 (1976); R. G. Brewer and S.S. Kano, Nonlinear Behavior of Molecules, Atoms and Ions in Electric, Magnetic or Electromagnetic Fields, L. Neal, Ed., Elsevier, Amsterdam, 1979, p 45.

12. P. R. Berman, Phys. Rev. A 5, 927 (1972).

13. G. Nienhuis, J. Quant. Spectrosc. Radiat. Transfer 20, 275 (1978).

14. P. Dehmer and L. Wharton, J. Chem. Phys. 57, 4821 (1972).

15. W. E. Baylis, J. Chem. Phys. 51, 2665 (1969).

TABLE I

The G and L in parentheses indicate results obtained with a Gaussian and Lorentzian collision kernel, respectively.

Perturber	σ_B (this work)	v_B^* (Ref. 10)	$\sigma_v^o(G)$	$\sigma_v^o(L)$	$u_o(G)$	$u_o(L)$	σ_α (Ref. 14)	$\sigma_t(G)$	$\sigma_t(L)$
He	99 Å^2	86(3) Å^2	34 Å^2	49 Å^2	1060 $\frac{cm}{sec}$	247 $\frac{cm}{sec}$	130 Å^2	133 Å^2	148 Å^2
Ne	101	104(4)	47	90	1140	187	150	149	191
Ar	181	164(8)	145	207	1400	340	400	326	388
Kr	206	211(9)	170	236	1320	335	440	376	442
Xe	233	265(10)	200	289	1320	315	510	433	522

* Scaled from 628K to 525K according to $(1/T)^{1/5}$.

Figure Caption

Figure 1. Plot of $\sigma_{eff}(\tau)$ versus τ. Error bars represent statistical uncertainty. At right we show σ_t.

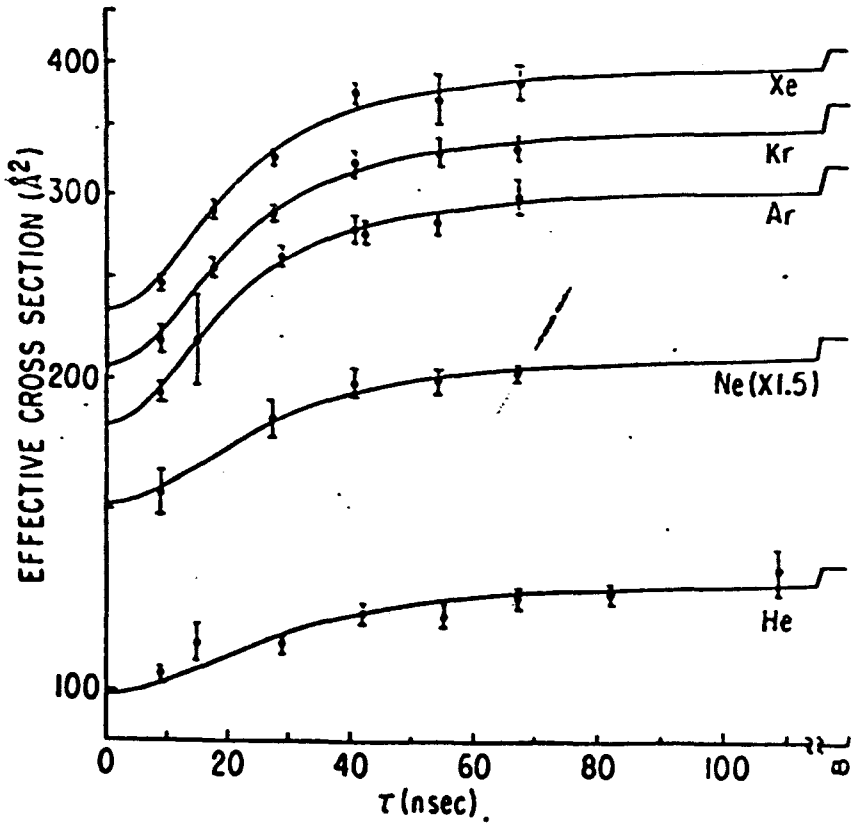

Figure 1

NOBLE GAS INDUCED RELAXATION OF THE Li 3S-3P TRANSITION SPANNING THE SHORT TERM IMPACT REGIME TO THE LONG TERM ASSYMPTOTIC REGIME

T. W. Mossberg,* R. Kachru,+ T. J. Chen, S. R. Hartmann
Columbia Radiation Laboratory, Dept. of Physics
Columbia University, New York, NY 10027
and
P. R. Berman
Department of Physics, New York University
4 Washington Place, New York, NY 10003

Photon echoes have a doppler free character which allows one to study relaxation processes which would otherwise be hidden in the inhomogenously broadened spectral profile. It has recently been shown, for example, that contrary to expection, a radiating atom in a linear superposition of dissimilar electronic states can undergo identifiable velocity changing collisions [1]. Studies of this nature require an examination of the sub-doppler region of the spectral line shape. The effect manifests itself, in the case of photon echoes, in a dependence of the effective relaxation cross section σ_{eff} on the excitation pulse separation τ. In this paper we report measurements in Li vapor where τ can be increased into the regime where σ_{eff} once again becomes independent of τ. In the limit $\tau = 0$ we measure σ_0 which is the phase changing cross section as calculated by Baranger [2] while in the large τ limit we measure σ_∞ the average total scattering cross section of the ground and the excited states. Our data at intermediate values of τ is used to determine the form of the scattering kernel and the average velocity change per collision. These measurements are for the 2S-2P superposition states in atomic Li perturbed by each of the noble gases. For He perturbers the scattering kernel is found to be Lorentzian, for the other perturbers it is Gaussian.

We use a N_2 laser pumped dye laser to generate a 4.5 nsec light pulse at the 6708 Å $2S-2P_{1/2}$ transition of ^7Li. The pulse which has a 6 GHz spectral width is attenuated, split, delayed an amount τ, recombined, and directed into a cell, whose effective length is 10 cm, at 525 ± 15^oK containing the Li vapor (at $\sim 10^{-6}$ torr). For short values of τ the polarizations of the photon echo excitation pulses were orthogonal in order to reduce the effects of detector saturation which arose because of the non instantaneous response the Pockels cell shutters used for their protection.

For a superposition state relaxing at an effective rate $\Gamma_{eff} = nv\,\sigma_{eff}$ where n is the perturber density, v is the average relative velocity of the collision partners and σ_{eff} is an effective cross section, the corresponding echo intensity will decay according to

$$I = I_0 \exp(-4\Gamma_{eff}\tau) \qquad (1)$$

and since Γ_{eff} varies linearly with perturber pressure P

$$I(P) = I(0)\exp(-\beta P) \qquad (2)$$

where the constant β, which we measure directly, is characteristic of the perturber and the collision process. We determine β at several discrete

Supported by the U.S. Office of Naval Research under Contract No. N00014-77-C-0553.

values of τ by measuring the echo intensity as a function of the perturber gas pressure. The value of σ_{eff} is obtained from

$$\sigma_{eff} = \Gamma_{eff}/nv = \beta P/4nv\tau. \qquad (3)$$

Fig. 1 Plot of $\sigma_{eff}(\tau)$ versus τ. Error bars represent statistical uncertainty.

In fig. (1) we summerize our work by plotting all measured values of σ_{eff} as a function of τ. A dependence on τ arises because each collision of the Li atom with a perturber gives rise to a velocity change in addition to a phase change of the Li superposition state. If only phase changing collisions occured σ_{eff} would be independent of τ. Velocity changing collisions have a delayed effect which manifests itself in a dependence of σ_{eff} on τ. Our data indicates that at the shortest values of τ σ_{eff} increases at a large and relatively constant rate while at higher τ it levels off considerably.

Echoes in the optical regime (photon echoes) are generally formed in a volume large compared to the wavelength of the optical transition. Thus any atom experiencing a velocity change sufficient to displace it an appreciable fraction of a wavelength from the position it would otherwise have taken in the phased array which radiates the echo will not necessarily reinforce the echo signal. As τ is increased the resulting displacement increases and the effect of a particular velocity change is enhanced. This proceeds up to a point that being when τ is so large that all atoms experiencing a velocity change are effectively eliminated from the echo formation processes. The data of fig. (1) at large τ shows this effect clearly in the weakening dependence of σ_{eff} on τ.

In what may be called the collision kernel approximation Flusberg [3] has shown that σ_{eff} may be expressed as

$$\sigma_{eff} = \sigma_0 + \sigma_v \left[1-(1/\tau) \int_0^\tau dt\, \tilde{g}(kt)\right] \tag{4}$$

where $\sigma_0(\sigma_v)$ is the phase changing (velocity changing) cross section and

$$g(kt) = \int_{-\infty}^{\infty} \exp(ikt\Delta v)\, g(\Delta v)\, d(\Delta v). \tag{5}$$

The collision kernel $g(\Delta v)$ gives the probability of a particular change Δv in the component of the velocity along the laser pulse direction. For $k\tau << 1$

$$\sigma_{eff} = \sigma_0 + \sigma_v \frac{1}{6} k^2\tau^2 \langle\Delta v^2\rangle \tag{6}$$

where $\langle\Delta v^2\rangle$ is the second moment of the collision kernel. For $k\tau >> 1$

$$\sigma_{eff} = \sigma_0 + \sigma_v \left[1 - \pi g(0)/2k\tau\right] \tag{7}$$

where $g(0)$ is the amplitude of the collision kernel at $\Delta v = 0$.

Our data at short τ does not fit (6) well, shorter excitation pulses would have been required to enter the regime where this approximation is valid. Our data does suffice however to use (6) to estimate σ_0 and we find that except for He we agree to within a few percent with measurements of σ_0 made from line broadening experiments [4]. Our estimate of σ_0 for He runs ~10% high.

The solid line curves of fig. (1) were obtained using an explicit form of the collision kernel. For all perturbers except He we have used a gaussian kernel

$$g(\Delta v) = (1/\sqrt{\pi}\, u_0)\exp(-\Delta v^2/u_0^2) \tag{8}$$

while for He we have used the Lorentzian kernel

$$g(\Delta v) = (u_0/\pi)/(u_0^2 + \Delta v^2). \tag{9}$$

We vary u_0 and σ_v to obtain the best fit. All relevant parameters are tabulated in table I.

Table 1

Perturber	σ_0	σ_v	$\sigma_\infty = \sigma_0+\sigma_v$	u_0	$\sigma_\infty = \sigma_0+\sigma_v$ (from fig.2)
He	99 Å^2	49 Å^2	148 Å^2	247 cm/sec	146
Ne	101	47	148	1140	146
Ar	181	145	326	1400	338
Kr	206	170	376	1320	356
Xe	233	200	434	1320	434

An alternative proceedure for presenting our data is to plot $\sigma_{eff}\tau$ as a function of τ, see fig. (2), in which case we expect that from (7)

$$\sigma_{eff} = (\sigma_0 + \sigma_v)\tau - \sigma_v \pi g(0)/2k \qquad (10)$$

Fig. 2 $\sigma_{eff}\tau$ plotted versus τ.

and we should obtain an assumptotic fit to a straight line whose slope yields $\sigma_0 + \sigma_v = \sigma_\infty$ and whose negative intercept yields the product of σ_v with g(0). The values of $\sigma_0 + \sigma_v = \sigma_\infty$ so obtained are compared with that calculated from the data of table I.

Supported financially by the U.S. Office of Naval Research (Contracts N00014-78-C-517 and N00014-77-C-0553) and by the U.S. Joint Services Electronics Program (Contract DAAG29-79-C-0079).

REFERENCE

*Present Address: Dept. of Physics, Harvard University, Cambridge, Mass. 02138.
+Present Address: Molecular Physics Lab., SRI International, Menlo Park, Ca. 94025.

1. T.W. MOSSBERG, R. KACHRU, and S.R.HARTMANN, Phys. Rev. Lett. 44, 73 (1980).
2. MICHEL BARANGER, Physics Rev. 111, 481 (1958).
3. A. Flusberg, Opt. Commun. 29, 123 (1979).
4. N. LWIN, Thesis (University of Newcastle upon Tyne) 1976, as reported by E. L. Lewis, Phys. Rep. 58, 1 (1980).

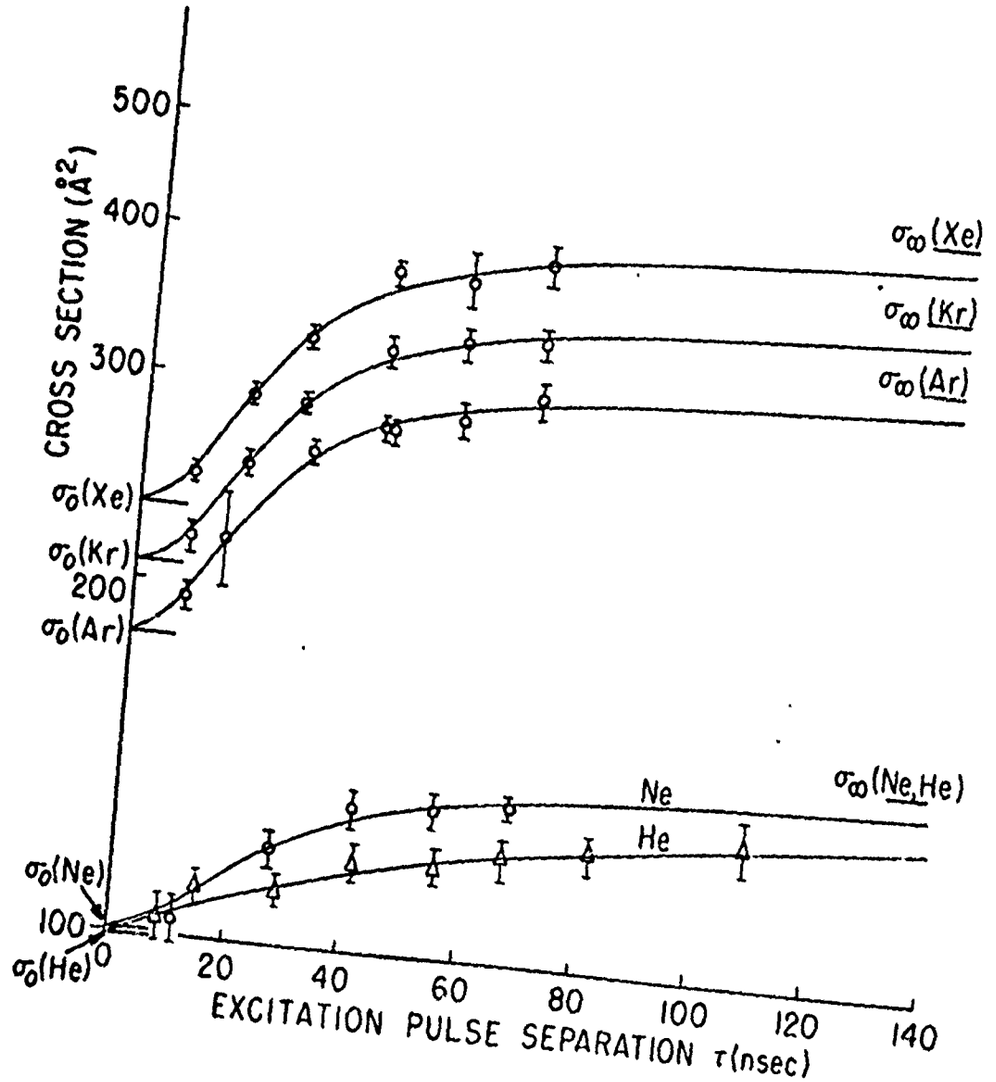
500
400
300
200
100
0
CROSS SECTION (Å²)
σ∞(Xe)
σ∞(Kr)
σ∞(Ar)
σ₀(Xe)
σ₀(Kr)
σ₀(Ar)
σ∞(Ne,He)
Ne
He
σ₀(Ne)
σ₀(He)
20
40
60
80
100
120
140
EXCITATION PULSE SEPARATION τ(nsec)

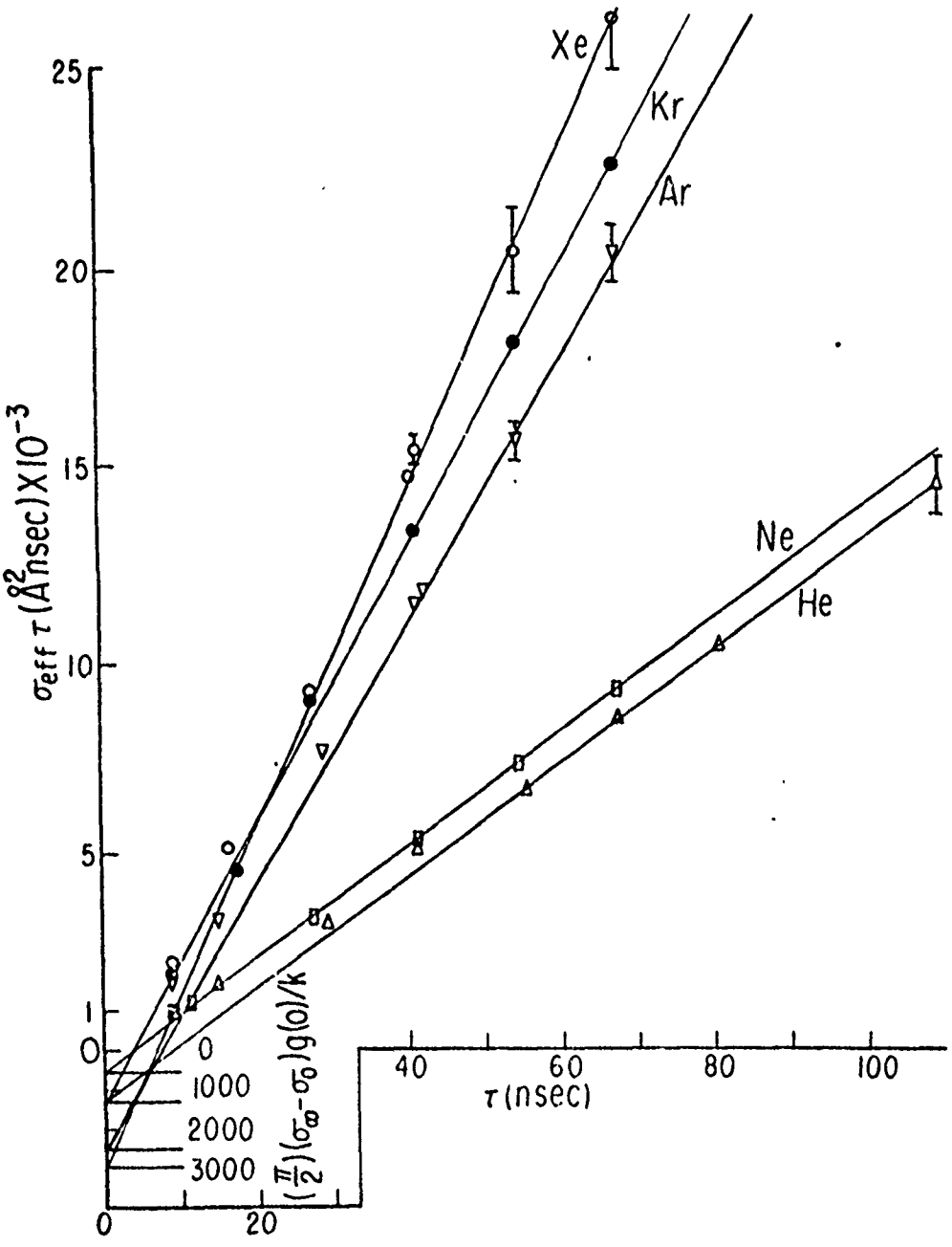
Xe
Kr
Ar
Ne
He
25
20
15
10
5
1
0
$\sigma_{eff}\tau$ (Å^{2}nsec) X10^{-3}
0
1000
2000
3000
$(\frac{\pi}{2})(\sigma_\infty - \sigma_0)g(0)/k$
0
20
40
60
80
100
τ (nsec)

Sched. issue Sect.
Code Vol.
Galleys thru
Estimated no. of pages

PRA09000 PLRAA.810900Ad2002.2

Semiclassical picture of depolarizing collisions: Application to collisional studies using laser spectroscopy

J.-L. Le Gouët

Laboratoire Aimé Cotton, Centre National de la Recherche Scientifique, Bât. 505, 91405 Orsay-Cedex, France*

P. R. Berman

Physics Department, New York University, 4 Washington Place, New York, New York 10003

(Received 2 April 1981)

An extension of the Jeffreys-Wentzel-Kramers-Brillouin approximation to inelastic processes is used to obtain the scattering amplitude which describes the collisionally induced depolarization of magnetic substate coherences. It is found that the scattering amplitudes contain contributions from two overlapping regions. For large interatomic separations, the different Zeeman sublevels are shifted and mixed by collisions but follow a common collision trajectory. For small interatomic separations, it is possible to find adiabatic eigenstates which follow distinct collision trajectories. The theory is used to investigate the nature of the depolarizing collision kernels and rates which enter into the analysis of laser spectroscopy experiments.

PACS numbers: 34.70.+n, 32.70.Jz, 42.62.Gv

I. INTRODUCTION

Laser saturation spectroscopy experiments are beginning to provide an important probe of collisional processes occuring in low pressure gases.[1] The elimination of the broad Doppler background encountered in standard spectroscopy permits a more sensitive measure of the manner in which collisions perturb the energy levels and alter the velocity of atoms.

A particularly interesting process that may be studied in such experiments is the way in which collisions perturb *superposition* states in atoms that have been created by an atom-field interaction. Since the various internal states comprising the superposition state are generally shifted and scattered *differently* in a collision, one is led to a somewhat complicated description of the entire scattering process for the superposition state, especially if collisions can also couple the superposition levels. Formal theories[2,3] have been developed to describe the scattering and time evolution of atomic superposition states via a quantum-mechanical transport equation, but little progress has been made in obtaining solutions or physical interpretations of the results. It is the purpose of this paper to provide a simplification of the transport equation and some additional physical insight into the scattering process. Methods of semiclassical scattering theory are used to achieve these goals.

The specific problem we choose to study involves the scattering of atoms prepared in a linear superposition of magnetic substates of a level characterized by internal-angular-momentum quantum number j. The way in which collisions couple, shift, and scatter the various magnetic substates is investigated. Coherent superpositions of magnetic substates (magnetic moments, Zeeman coherences) are conveniently created and probed using the "three-level" system of Fig. 1. The 1-2 transition is excited with a nearly monochromatic laser beam and the 2-3 transition is probed with another colinear laser beam. Level 2 (shown for $j=1$) is $(2j+1)$ fold degenerate; Zeeman coherences within level 2 may be produced and detected using a proper choice of the laser beam polarizations. Owing to the Doppler effect, the excitation-detection scheme excites or probes only those atoms having a specific velocity component along the laser beam direction. Thus, any collision-induced modification of the Zeeman coherences for atoms having a specific longitudinal velocity can be monitored in such a system. The Zeeman coherences tend to be destroyed by inseparable contributions from collisional effects on the internal (shifting and mixing of magnetic sublevels) and external (state-dependent scattering for the different magnetic sublevels) atomic degrees of freedom. In such experiments, the collisional relaxation is determined by the number of collisions per lifetime of the level under con-

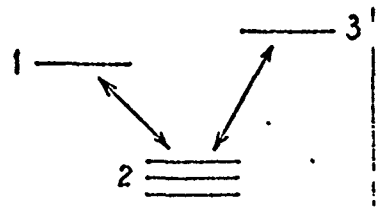

FIG. 1. "Three-level" scheme for depolarizing collision studies. Levels 1 and 3 are nondegenerate. Level 2 has three substates which, though separately indicated in the figure, are assumed to be energy degenerate.

Supported by the U.S. Office of Naval Research under Contract No. N00014-77-C-0553.

sideration and the specific interatomic potential.

It should be noted that collisional depolarization studies are not new. Optical pumping techniques have been used to investigate depolarizing collisions between optically oriented excited state atoms and ground-state perturbers.[4] However the general nature of such optical pumping work (broadband sources, total cross-section measurements) does not lead to results that are overly sensitive to velocity-changing effects. Recent laser saturation experiments[5] based on schemes similar to that shown in Fig. 1 provide a more sensitive measure of such effects.

In attempting to analyze the scattering process for an atom in a linear superposition of magnetic substates one is naturally led to examine the applicability of the classical pictures shown in Fig. 2. The first drawing represents the single-trajectory limit. The dependence of the deflection on internal state is negligible so that the internal and the translational motions are decoupled. The second scheme depicts the situation where a diagonal representation has been found. Then each sublevel obeys the rules of elastic scattering along a substate-labeled trajectory. When none of these extreme situations holds, is a classical picture still possible? Answering this question would help to complete the blanks in the third drawing of Fig. 2. It should be noticed that the existence of a classical picture is questionable since depolarizing collisions imply a coupling between the internal motion, which is highly quantumlike due to the smallness of the electronic angular momentum, and the translational motion which can be quasiclassical. We shall discuss applicability of the various limits and approximations in terms of standard treatments of collision problems.

In Sec. II various methods available for treating inelastic scattering, when the de Broglie wavelength of the colliding particle is much smaller than the characteristic dimension of the interaction region, are reviewed. In Sec. III exact equations for the scattering amplitudes are obtained

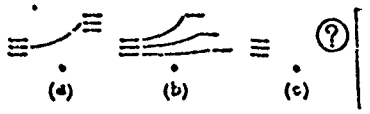

FIG. 2. Schematic representation of atomic trajectories during a depolarizing collision. In (a) an atom in a superposition state is scattered along a trajectory common to the three substates which are mixed by the collision. In (b) a distinct trajectory is associated with each substate and no transition between substates is induced by the collision. In (c) the single-trajectory approximation is not valid and transitions are induced between substates: What trajectory does the atom follow?

and those expressions are evaluated in the various semiclassical limits discussed in Sec. II. In Sec. IV we return to the problem encountered in laser spectroscopy and examine the semiclassical limit of the transport equation for atomic multipoles of a degenerate level. A summary is given in Sec. V.

II. APPROXIMATIONS IN INELASTIC SCATTERING THEORY

A few years ago, the development of research in the fields of collisional rotational and vibrational excitation of molecules,[7,8] and of electronic excitation and charge transfer in atoms[9] stimulated efforts for obtaining a semiclassical description of inelastic collisions,[10-16] which should be, by far, more tractable than a purely quantum approach. Since certain procedures in these theories are similar to those encountered in obtaining semiclassical limits of elastic scattering, it is useful to recall that two semiclassical approximation schemes[17] may be used to calculate the elastic scattering amplitude

$$f(\theta)=\frac{1}{2iK}\sum_l (2l+1)(e^{2i\eta_l}-1)P_l(\cos\theta), \qquad (1)$$

(where K is the magnitude of the atomic wave vector and η_l is the phase shift of the l-labeled partial wave).

(i) The first method is the semiclassical phase shift approximation, which is valid when the de Broglie wavelength λ is much smaller than the distance of closest approach r_c. In this form of the JWKB approximation, each η_l is calculated along a classical path which is characterized by the initial velocity and the impact parameter $(l+\frac{1}{2})/K$. Although the η_l are calculated along classical trajectories, the classical correspondence between scattering angle θ and impact parameter is lost in Eq. (1) since a large range of l values contribute to scattering at angle θ.

(ii) The second method, valid under the more stringent condition $\sqrt{\lambda} \ll \sqrt{r_c}$, is the classical trajectory limit. The condition $\sqrt{\lambda} \ll \sqrt{r_c}$ permits one to retain in Eq. (1) only those l values such that the impact parameter $(l+\frac{1}{2})/K$ corresponds to classical scattering at angle θ.

A number of papers have explored the conditions for generalizing the JWKB approximation to inelastic processes[13-15] using an approach which was initiated by Kemble.[18] They have concluded that such an extension is possible only when the atomic translational motion is nearly independent of the internal states. In the case when the additional condition $\sqrt{\lambda} \ll \sqrt{r_c}$ is fulfilled, the JWKB extension is thus possible only when atoms follow

the same common spatial trajectory in any of the coupled internal states as in Fig. 1(a). A completely different approach has been developed under the name of classical S-matrix theory by Miller and Marcus.[10,11] They treat the internal degrees of freedom quasiclassically, retaining only the interference properties of quantum mechanics, since they calculate scattering amplitudes. In these papers there is no apparent condition of common trajectory. A special mention must be made to the work of Pechukas[16] which bypasses the common trajectory condition at the expense of complications with a noncausal interaction.

In light of these general methods let us examine the depolarizing collision problem. A ground-state spinless particle, the perturber, collides with an atom having internal angular momentum $\vec{j}$. The magnitude of $\vec{j}$ is on the order of a few $\hbar$ and is supposed to be much smaller than that of the translational angular momentum. Since the collision is assumed to result only in a change of direction of $\vec{j}$, the other numbers which characterize the internal state of the active atom are implicit. The effective interatomic potential is a function of the internuclear distance $\vec{r}$ and of the angle $(\vec{r},\vec{j})$.

A classical S-matrix method[10,11] seems very tempting for solving the problem formulated in this manner. With this approach, for given initial and final values for the variables describing the system (internal and interparticle angular momentum, energy), one calculates S-matrix elements classically along the trajectory connecting these initial- and final-state values. A phase $\varphi_c = \int \vec{p}\cdot d\vec{r}/\hbar$ evaluated along the trajectory is associated with each S-matrix element, enabling one to account for any quantum interference effect arising from contribution of several trajectories to a given S-matrix element. The classical S matrix has the advantage of eliminating the discussion about common trajectory for the various magnetic substates since it is only the initial- and final-state variables that determine the scattering process. However the solution of the problem in the frame of classical mechanics is rather difficult: the couple of colliding particles in the center-of-mass system has 8 degrees of freedom and after taking account of the conservation of $|\vec{j}|$ of the total angular momentum $\vec{J}$, of total energy E, one is left with three differential equations, two of which are coupled. In general these equations must be solved numerically.

If instead, we adopt a quantum-mechanical formulation of the problem, certain simplifications are possible. Since the interatomic potential depends only on the quantum variable $\vec{r}$ and on the operator $\vec{j}\cdot\vec{r}$, one immediately notes that, if the "instantaneous" axis of quantization is taken along $\vec{r}$, then the Hamiltonian is a function of $\vec{r}$ and j_z and commutes with j_z (recall that $[\vec{r},\vec{j}]=0$ since $\vec{r}$ is the interatomic separation and $\vec{j}$ acts in the active-atom subspace). Thus using this basis, known as the helicity representation after Jacob and Wick,[19] one concludes that the various magnetic sublevels in this representation are coupled only by the rotation of the internuclear axis during a collision. Two limiting cases may be envisioned:

(i) If the various instantaneous magnetic substates experience approximatively the same collisional interaction (the explicit condition is prescribed in the next section), then the notion of a common classical trajectory may be valid. The coupling between magnetic substates induced by the rotation of the internuclear axis can be significant in this case since the "instantaneous" eigenfrequencies differ by less than the inverse duration of a collision (i.e., the helicity representation is *not* an adiabatic one in this limit). The coupling and scattering of the levels can be calculated using a semiclassical phase-shift approach. One expects that the limit of nearly equal collisional interaction for the different substates is achieved for collisions with large impact parameters.

(ii) In the other extreme, one can imagine that the helicity representation is an adiabatic one. The various magnetic sublevels experience significantly different collisional interactions and are scattered independently according to the equations of classical scattering theory. Normally, one requires small internuclear separations to achieve this adiabatic limit.[20]

It is the classical trajectory limit of these two extreme situations which is illustrated in Figs. 2(a) and 2(b). One might expect that the range of validity of the semiclassical picture could be extended by combining these two approximations. For example, in a given collision, limits (i) and (ii) could be used for large and small internuclear separations, respectively. The precise conditions of validity of these different situations are examined in the next section.

III. CALCULATION OF THE SCATTERING AMPLITUDE

The calculation is performed using the helicity representation which has been defined in the preceding section. During a collision, the z component of the internal angular momentum changes from an initial value $\hbar M$ relative to a quantization axis directed *opposite* to the initial velocity (i.e., in the direction of the interparticle separation

$\vec{r}$) to a final value $\hbar M'$ relative to a quantization axis which is taken along the final direction $\theta\varphi$. The scattering amplitude takes the closed form[17]

$$f^{\rm tot}_{M'v'}(\theta,\varphi)=\frac{(-1)^{v-v'}}{2iK}\sum_J(2J+1)(S^J_{vv'}-\delta_{vv'})\times\mathfrak{D}^{J*}_{MM'}(\varphi,\theta,0), \quad (2)$$

where $S^J_{vv'}$ is an S-matrix element and $\mathfrak{D}^J_{MM'}(\varphi,\theta,0)$ is the rotation matrix of rank J. The internal angular momentum $\vec{j}$ and the relative orbital angular momentum $\vec{l}$ have been coupled into the total angular momentum $\vec{J}$ and the summation is over all allowed values of $\vec{J}=\vec{l}+\vec{j}$. The S-matrix elements can be obtained in terms of the asymptotic form of the radial wave functions $\Psi^{JM}_v(r)$ as (see Appendix A)[21]

$$\lim_{r\to\infty}\Psi^{JM}_v(r)=-\frac{2J+1}{2iK}(-1)^{v'-v+J+J}\times[\delta_{-M'M}e^{-iKr}-(-1)^{J+J}S^J_{M'M}e^{iKr}]. \quad (3)$$

This boundary condition selects appropriate solutions of the radial equation

$$\left(-\frac{\hbar^2}{2\mu}\frac{d^2}{dr^2}-\frac{\hbar^2K^2}{2\mu}+\langle M|V|M\rangle\right)\Psi^{JM}_v(r)=-\sum_{M'\neq M}\langle M|V|M'\rangle\Psi^{JM'}_v(r) \quad (4)$$

which is derived from the Schrödinger equation (see Appendix A). In this equation, μ is the reduced mass, and

$$\langle M|V|M'\rangle=\left(V_M(r)+\frac{J(J+1)}{2\mu r^2}\hbar^2\right)\delta_{MM'}-\frac{\hbar^2}{2\mu r^2}[\lambda_+(J,M)\lambda_+(j,M)\delta_{MM'+1}+\lambda_-(j,M)\lambda_-(J,M)\delta_{MM'-1}],$$

where $V_M(r)$ is the interatomic potential in substate M and

$$\lambda_\pm(J,M)=[J(J+1)-M(M'\pm1)]^{1/2}.$$

In the absence of coupling between the channels, Eq. (4) reduces to

$$\left(-\frac{\hbar^2}{2\mu}\frac{d^2}{dr^2}-\frac{\hbar^2K^2}{2\mu}+V_M(r)+\frac{J(J+1)}{2\mu r^2}\hbar^2\right)\Psi^{JM}_v(r)=0. \quad (5)$$

The general solution of this equation in the JWKB approximation is a linear combination of functions $e^{\pm iQ_{JM}}/\mathcal{P}^{1/2}_{JM}$ where

$$\mathcal{P}_{JM}=\left(\hbar^2K^2-\frac{J(J+1)}{r^2}\hbar^2-2\mu V_M(r)\right)^{1/2},$$

$$Q_{JM}=\int_{r_1}^{r}\frac{\mathcal{P}_{JM}(r')}{\hbar}dr'. \quad (6)$$

This suggests that one tries solutions to Eq. (4) of the form

$$\Psi^{JM}_v(r)=b^+_{JM}(r)\frac{e^{iQ_{JM}}}{\mathcal{P}^{1/2}_{JM}}+b^-_{JM}(r)\frac{e^{-iQ_{JM}}}{\mathcal{P}^{1/2}_{JM}} \quad (7)$$

The standard theory of second-order differential equations states that, in addition to the boundary conditions, a supplementary condition is needed to determine $b^\pm_{JM}(r)$.[14] We have chosen the following condition:

$$b^{+\prime}_{JM}e^{iQ_{JM}}+b^{-\prime}_{JM}e^{-iQ_{JM}}-\frac{1}{2}\frac{\mathcal{P}'_{JM}}{\mathcal{P}_{JM}}(b^+_{JM}e^{iQ_{JM}}+b^-_{JM}e^{-iQ_{JM}})=0 \quad (8)$$

which transforms Eq. (4) into the set of first-order differential equation

$$b^{\pm\prime}_{JM}(r)=\frac{\mathcal{P}'_{JM}}{2\mathcal{P}_{JM}}b^\pm_{JM}e^{\mp2iQ_{JM}}\pm\frac{\hbar X^+_{JM}}{2i(\mathcal{P}_{JM}\mathcal{P}_{JM+1})^{1/2}}(b^+_{JM+1}e^{i(Q_{JM+1}\mp Q_{JM})}+b^-_{JM+1}e^{-i(Q_{JM+1}\mp Q_{JM})})\pm\frac{\hbar X^-_{JM}}{2i(\mathcal{P}_{JM}\mathcal{P}_{JM-1})^{1/2}}(b^+_{JM-1}e^{i(Q_{JM-1}\mp Q_{JM})}+b^-_{JM-1}e^{-i(Q_{JM-1}\mp Q_{JM})}), \quad (9)$$

where $X^\pm_{JM}=\lambda_\pm(J,M)\lambda_\pm(j,M)/r^2$ and a prime indicates d/dr. (10)

Except within a distance of a few λ from the turning points where $\mathcal{P}_{JM}$ is close to zero, these "exact" equations may be simplified by using the conditions that we have imposed at the beginning. From $\lambda\ll r_c$, it follows that $\mathcal{P}'_{JM}\ll\mathcal{P}^2_{JM}/\hbar$ and since $j\ll J$, it follows that $\hbar X_{JM}/2(\mathcal{P}_{JM}\mathcal{P}_{JM\pm1})^{1/2}\ll\mathcal{P}_{JM}/\hbar$. Using these two inequalities one may neglect the terms having rapidly varying phase factors in Eq. (9) and obtain

$$b^{\pm\prime}_{JM}=\sum_{M'}A^\pm_{MM'}b^\pm_{JM'}, \quad (11)$$

where

$$A^\pm_{MM'}=\pm\frac{\hbar}{2i(\mathcal{P}_{JM}\mathcal{P}_{JM'})^{1/2}}(X^+_{JM}\delta_{M',M+1}+X^-_{JM}\delta_{M',M-1})e^{\pm i(Q_{JM'}-Q_{JM})}.$$

Thus, the inward wave (represented by b^-_{JM}) is decoupled from the outward wave (represented by b^+_{JM}). This is the essence of the semiclassical ap-

proximation and can be considered as an expression of microscopic causality. However, the semiclassical approximation requires, in addition, that a connection can be made between inward and outward waves at the classical turning point. This is accomplished provided one of the two following conditions is fulfilled[14]:

(i) $|\mathcal{P}_{JM}-\mathcal{P}_{JM+1}|\ll\mathcal{P}_{JM}+\mathcal{P}_{JM+1}$. This condition permits one to define a turning point, which is common to all the channels. When in addition $\sqrt{\chi}\ll\sqrt{r_c}$, a common trajectory is available.

(ii) $|\mathcal{P}_{JM}-\mathcal{P}_{JM+1}|\gg X^{\pm}_{JM}\hbar^2/2(\mathcal{P}_{JM}\mathcal{P}_{JM+1})^{1/2}$. In this case the $A_{MM'}$ in Eq. (11) are very rapidly varying functions of r. Thus the substates are not significantly mixed by collisions and the $b^{\pm}_{JM}$ are approximately constant. This decoupling corresponds to the adiabatic approximation.

These explicit requirements for a semiclassical description, correspond, as expected, to the limiting situations that we have evoked in the previous section. In terms of the potential difference between the internal states, the above conditions are, respectively, transformed into

$$|V_M(r)-V_{M+1}(r)|\ll(\mathcal{P}_{JM}+\mathcal{P}_{JM+1})^2/2\mu=E_1, \tag{12a}$$

$$|V_M(r)-V_{M+1}(r)|\gg X^{\pm}_{JM}\frac{\hbar^2}{4\mu}\frac{\mathcal{P}_{JM}+\mathcal{P}_{J(M+1)}}{(\mathcal{P}_{JM}\mathcal{P}_{JM+1})^{1/2}}=E_2. \tag{12b}$$

Condition (12a) requires that the difference between the scattering potentials for different magnetic substates be small enough to allow for a "single-trajectory" approach to the problem while condition (12b) requires that the potentials *differ* enough so that the collision is adiabatic with regard to the helicity eigenstates. Except in the vicinity of a classical turning point, E_1 is of the order of thermal energy and is much larger than E_2 which is of the order of $\hbar^2K/\mu r$. Therefore, throughout the classically accessible region, at least one of the inequalities (12) is satisfied by any potential difference. This guarantees the general validity of a semiclassical description of depolarizing collisions.

As an illustration, we consider a simple potential such that $|V_M(r)-V_{M+1}(r)|$ is a monotonic, decreasing function of r. Thus if r_0 is a distance such that $E_2\ll|V_M(r_0)-V_{M+1}(r_0)|\ll E_1$, the conditions (12a) and (12b) are fulfilled, respectively, when $r>r_0$ and $r<r_0$. This situation is represented in Fig. 3 which exhibits the overlap of the adiabatic and single-trajectory regions. In this situation one may transform Eq. (11) in order to examine the classical motion character of the problem. We define a set of classical trajectories using a time parameter t. The radial coordinate $r_{JM}(t)$ satisfies the equations

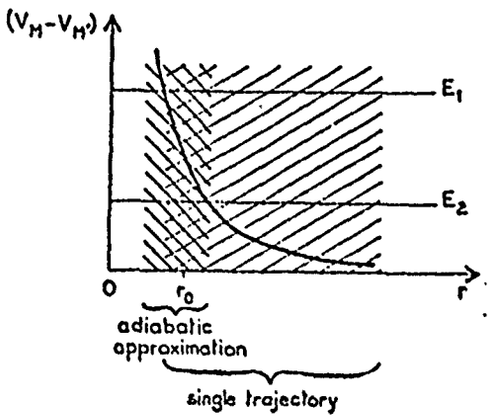

FIG. 3. The spatial domains for adiabatic and single-trajectory approximations are represented in the case of continuously decreasing $|V_M(r)-V_{M'}(r)|$. At r_0 both approximations are valid.

$$\frac{dr_{JM}}{dt}=\begin{cases}-v_{JM}(r_{JM}(t)) & \text{when } t<0,\\ v_{JM}(r_{JM}(t)) & \text{when } t>0,\end{cases} \tag{13}$$

$$r_{JM}(0)=r_{JM}^{(TP)},$$

where the radial speed $v_{JM}(r)$ is

$$v_{JM}(r)=\begin{cases}\mathcal{P}_{JM}(r)/\mu & \text{when } r<r_0,\\ v_J(r)=\langle\mathcal{P}_{JM'}(r)\rangle_{M'}/\mu & \text{when } r>r_0,\end{cases} \tag{14}$$

and $r_{JM}^{(TP)}$ is the coordinate of the classical turning point in channel M, with angular momentum $\vec{J}$.

Two different situations may be examined in the limits that $r_{JM}^{(TP)}$ is larger or smaller than r_0.

$r_{JM}^{(TP)}<r_0$. The incident particle first reaches the radius r_0 at a time t_J^- which is M independent assuming a common trajectory $r_J(t)$ for $-\infty<t<t_J^-$ (since this interval corresponds to $r>r_0$). In Eq. (11) we replace $b^-_{JM}(r)$ by $c_{JM}(t)$ defined by

$$c_{JM}(t)=b^-_{JM}(r_J(t)),\quad t<t_J^- \tag{15}$$

and find that $c_{JM}(t)$ obeys the differential equation

$$\frac{d}{dt}c_{JM}(t)=\sum_{M'}B^J_{MM'}(t)c_{JM'}(t),\quad t<t_J^- \tag{16}$$

where

$$B^J_{MM'}(t)=\frac{\dot{R}}{2i\mu}[X^+_{JM}(r_J(t))\delta_{M',M+1}+X^-_{JM}(r_J(t))\delta_{M',M-1}] \tag{17}$$

$$\times\exp\frac{i}{\hbar}\int_{t_J^-}^{t}[V_M(r_J(t'))-V_{M'}(r_J(t'))]dt'\quad t<t_J^-.$$

In arriving at Eqs. (16) and (17), we set $(\mathcal{P}_{JM}\mathcal{P}_{JM'})^{1/2}\simeq(\mathcal{P}_{JM}+\mathcal{P}_{JM'})/2\simeq\mu v_J(r)$ and evaluate the phase difference $(i/\hbar)\int_{r_0}^{r}(\mathcal{P}_{JM}-\mathcal{P}_{JM'})dr'$ to first order in $V_M-V_{M'}$.

In the region $r<r_0$, the $b^{\pm}_{JM}(r)$ are constant owing

to the adiabatic nature of the collision for $r < r_0$. There is a classical trajectory r_{JM} which may be associated with each helicity state and a corresponding classical turning point $r_{JM}^{(TP)}$. The JWKB connection formulas are used at the turning point to relate $b_{JM}^{+}(r)$ and one finds

$$ib_{JM}^{+}(r_{JM}^{(TP)})e^{iQ_{JM}(r_{JM}^{(TP)})} = b_{JM}^{-}(r_{JM}^{(TP)})e^{-iQ_{JM}(r_{JM}^{(TP)})} . \quad (18a)$$

Since the $b_{JM}^{\pm}(r)$ are constant for $r < r_0$, Eq. (18a) may be written

$$ib_{JM}^{+}(r_0) = b_{JM}^{-}(r_0)e^{-2iQ_{JM}(r_{JM}^{(TP)})} . \quad (18b)$$

Connection with the time-dependent $c_{JM}(t)$ amplitudes is achieved by associating

$$c_{JM}(t) = \begin{cases} b_{JM}^{-}(r_{JM}(t)) , & t < \dfrac{t_J^{-} + t_{JM}^{+}}{2} \quad (19a) \\ ib_{JM}^{+}(r_{JM}(t)) , & t > \dfrac{t_J^{-} + t_{JM}^{+}}{2} \quad (19b) \end{cases}$$

where t_{JM}^{+} is the M-dependent time at which a classical particle moving along the r_{JM} trajectory would exit the $r < r_0$ region. Using Eqs. (19), (18), and (6) we find

$$c_{JM}(t_{JM}^{+}) = c_{JM}(t_J^{-})\exp\left(-\frac{i}{\hbar}\int_{t_J^{-}}^{t_{JM}^{+}} \frac{\mathcal{P}_{JM}^{2}(r_{JM}(\tau))d\tau}{\mu}\right). \quad (20)$$

Finally, for times $t > t_{JM}^{+}$, we are again in the $r > r_0$ zone. Each r_{JM} trajectory created for $r < r_0$ now continues into the $r > r_0$ region without further splitting. *Thus, each trajectory can be labeled by its M value in the $r < r_0$ region.* For $t > t_{JM}^{+}$ (i.e., $r > r_0$) there is again coupling of the $b_{JM}^{+}(r)$ along each trajectory. Defining

$$c_{JM}^{M'}(t) = ib_{JM}^{+}(r_{JM'}(t)) , \quad t > t_{JM}^{+} \quad (21)$$

where $r_{JM'}(t)$ is the extension of the trajectory associated with $M = M'$ in the $r < r_0$ region, one finds that $c_{JM}^{M'}$ obeys equations analogous to (16) and (17). The final value for $b_{JM}^{+}(\infty)$ is given by a sum over all trajectories, i.e.,

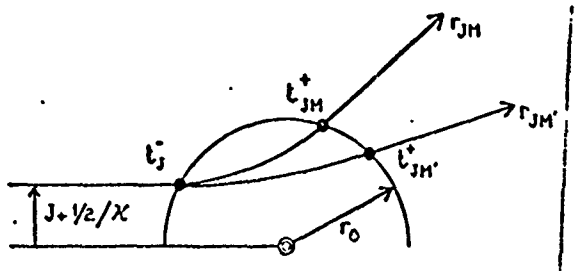

FIG. 4. An atom in a superposition state enters the interaction region with an impact parameter $(J + \frac{1}{2})/K$. From time t_J^{-} to t_{JM}^{+} or $t_{JM'}^{+}$ no transition occurs between substates and their respective trajectories may part from each other. After t_{JM}^{+} or $t_{JM'}^{+}$ a single trajectory starts from the point reached at t_{JM}^{+} or $t_{JM'}^{+}$.

$$ib_{JM}^{+}(\infty) = i\sum_{M'} b_{JM}^{+}(r_{JM'}(\infty)) = \sum_{M'} c_{JM}^{M'}(\infty) . \quad (22)$$

This equation can be put into a more transparent form if time evolution operators are introduced such that

$$c_{JM}(t) = \sum_{M''} U_{M''M}^{J}(t', t)c_{JM''}(t') , \quad t < t_J^{-} \quad (23a)$$

$$c_{JM}^{M'}(t) = \sum_{M''} U_{M''M}^{JM'}(t', t)c_{JM''}(t') , \quad t > t_{JM'}^{+} . \quad (23b)$$

One can combine Eqs. (22), (23), and (20) to obtain

$$ib_{JM}^{+}(\infty) = \sum_{M''M'} U_{M'M}^{JM'}(t_{JM'}^{+}, \infty)\exp\left(\frac{i}{\hbar\mu}\right.$$
$$\left.\times\int_{t_J^{-}}^{t_{JM'}^{+}} \mathcal{P}_{JM'}^{2}(r_{JM'}(\tau))d\tau\right)$$
$$\times U_{M''M'}^{J}(-\infty, t_J^{-})b_{JM''}^{-}(-\infty) . \quad (24)$$

Equation (24) may be given a simple physical interpretation (see Fig. 4). In order to calculate the contribution of the Jth partial wave to the scattering amplitude, one starts a collision at $t = -\infty$ with $b_{JM''}^{-}(-\infty)$. For $-\infty < t < t_J^{-}$, collisions mix all states along an average common trajectory and this mixing is represented by $U_{M''M'}^{J}(-\infty, t_J^{-})$. For $t_J^{-} < t < t_{JM'}^{+}$, the adiabatic states are not mixed by the collisions and one evaluates elastic scattering phase shifts along each trajectory. Finally, the states are again mixed along each of the final trajectories as represented by $U_{M''M'}^{JM'}(t_{JM'}^{+}, \infty)$ (recall that the superscript M' labels the trajectory in the *adiabatic* region). The time-evolution operators describe the mixing and shifting of atomic substates as the atoms move along classical trajectories. The spatial coordinates have been changed from quantum-mechanical variables into time-dependent parameters. However, there subsists in Eq. (24) an exponential phase factor which attests to the quantum-mechanical character of the translational motion in the region where $r < r_0$.

To get expressions for the time-evolution operators, one may use Eqs. (23), (16), and (17) to obtain

$$\frac{d}{dt}U_{M'M}^{J}(t', t) = \sum_{M''} B_{M'M''}^{J}(t)U_{M''M}^{J}(t', t) , \quad t < t_J^{-} \quad (25a)$$

$$\frac{d}{dt}U_{M''M}^{JM'}(t_{JM'}^{+}, t) = \sum_{M''} B_{M'M''}^{JM'}(t)U_{M''M}^{JM'}(t_{JM'}^{+}, t) , \quad t > t_{JM'}^{+} \quad (25b)$$

subject to

$$U_{M'M}^{J}(t, t) = \delta_{M'M} , \quad U_{M''M}^{JM'}(t_{JM'}^{+}, t_{JM'}^{+}) = \delta_{M'M''} , \quad (25c)$$

where $E^J_{M'M}$ is given by Eq. (17) and $E^{JM''}_{M''M}(t)$ is also given by Eq. (17) with $r_J(t)$ replaced by $r_{JM''}(t)$ (recall that $r_{JM''}$ indicates the trajectory associated with the M'' helicity state in the *adiabatic* region).

An expression for S-matrix elements is obtained by substituting Eq. (24) into Eq. (7) and making a comparison with Eq. (3). One finds[21]

$$S^J_{-M',M} = (-1)^J \sum_{M''} U^J_{M',M''}(-\infty, t_J^-) U^{JM''}_{M''M}(t^+_{JM''}, \infty) \times \exp(i\Delta^{JM''}_{M'M} + 2i\eta_{JM''}), \quad (26)$$

where

$$\eta_{JM''} = \lim_{r\to\infty} \int_{r^{(TP)}_{JM''}}^{r} \frac{\mathcal{P}_{JM''}(r')}{\hbar} dr' - Kr + (J+\tfrac{1}{2})\frac{\pi}{2} \quad (27a)$$

and

$$\Delta^{JM''}_{M'M} = \frac{1}{\hbar}\int_{-\infty}^{t_J^-} [V_{M'}(r_J(\tau)) - V_{M''}(r_J(\tau))]d\tau + \frac{1}{\hbar}\int_{t^+_{JM''}}^{\infty} [V_{M'}(r_{JM''}(\tau)) - V_M(r_{JM''}(\tau))]d\tau. \quad (27b)$$

$r^{(TP)}_{JM} > r_0$. In this case the time interval $[t_J^-, t^+_{JM}]$, during which the trajectories part from one another, collapses, so that t_J^- and t^+_{JM} may be set to 0 in Eq. (22) which reduces to

$$S^J_{-M',M} = (-1)^J U^J_{M',M}(-\infty, \infty)\exp(i\eta_{JM'} + i\eta_{JM}). \quad (28)$$

where

$$U^J_{M',M}(-\infty,\infty) = \sum_{M''} U^J_{M',M''}(-\infty, 0) U^J_{M'',M}(0,\infty).$$

This region corresponds to weak (large impact parameter) collisions.

This is the farthest point which can be reached in the direction of a semiclassical picture under the approximation $\lambda \ll r_c$. As has already been noted in Sec. II, the classical trajectories which have been hitherto considered may not be regarded as actual paths since deflection in direction $\theta\varphi$, which is described by the scattering amplitude [Eq. (2)] involves contribution from all the impact parameters $(J+\frac{1}{2})/K$.

The final step of the semiclassical approximation is possible provided $\sqrt{\lambda} \ll \sqrt{r_c}$. It consists in using the stationary-phase method to calculate the scattering amplitude [Eq. (2)]. This calculation is performed in Appendix B. In the simplest case, that of a purely repulsive interaction, one obtains

$$f^{tel}_{-M',M}(\theta,\varphi) = \frac{(-1)^J}{K(\chi'\sin\theta)^{1/2}} \sum_{M''} (J_{\theta M''})^{1/2} U^{J_{\theta M''}}_{M',M''}(-\infty, t_J^-) U^{J(\theta M'')}_{M''M}(t^+_{JM''}, \infty)\exp(i\Delta^{J_{\theta M''}M''}_{M'M} + 2i\eta_{J_{\theta M''}M''}) \times \left(\frac{\partial\theta}{\partial J_{\theta M''}}\right)^{-1/2} * \exp\left(-\frac{i\pi}{2} - i(M'+M)\frac{\pi}{2} - iJ_{\theta M''}\theta\right)\exp(-iM\varphi)\frac{1}{\left(\frac{\partial\theta}{\partial J_{\theta M''}}\right)^{1/2}}, \quad (29)$$

where $J_{\theta M''}$ is the angular momentum giving rise to scattering at $\theta\varphi$ for an atom following trajectory M'' in the adiabatic region. This result is valid provided that $\sqrt{\lambda} \ll \sqrt{r_0}$ and $J_{\theta M}\theta \gg 1$. The former condition allows one to use a stationary-phase method, and the latter condition implies that validity of Eq. (29) breaks down in the small-angle diffractive region.

As in elastic scattering, the major contribution in the sum over J comes from specific values of J, linking these values and the scattering direction $(\theta\varphi)$. However, Eq. (24) differs from the usual elastic scattering amplitude in the fact that for a given deflection direction $\theta\varphi$, a distinct impact parameter $(J_{\theta M''}+\frac{1}{2})/K$ is associated with each intermediate internal substate M''. For more general forms of the interaction potential, a rainbow angle may be defined and when θ is smaller than it, several values of J are generally involved in the scattering amplitude for given θ and M''.

Throughout this section mention has been made of classical trajectories. However, this notion is actually meaningful, only when collisional effects on observables are considered. Then scattering cross sections instead of scattering amplitudes are involved. The aim of the next section is to discuss the classical trajectory picture of depolarizing collisions on the observables which are accessible in laser spectroscopy.

IV. DEPOLARIZING COLLISIONS IN LASER SPECTROSCOPY

In a gas cell, the quantum-mechanical state of atoms within a small domain of position-velocity space around $(\vec{r}, \vec{v})$ is most conveniently described by the density-matrix elements $\rho_{\alpha\alpha'}(\vec{r}, \vec{v})$ where α and α' label internal states. We shall limit the discussion to the case where α and α' belong to the same j level since we are interested in studying the effect of depolarizing collisions. The general transport equation which determines the collisional evolution of density-matrix elements of "active atoms" immersed in a perturber bath is given by[2]

$$\left.\frac{d}{dt}\rho^{j}_{\alpha\beta}\right|_{\text{coll}} = -\sum_{\alpha'\beta'}\Gamma^{\alpha'\beta'}_{\alpha\beta}(\vec{v})\rho^{j}_{\alpha'\beta'}(\vec{r},\vec{v},t) + \sum_{\alpha'\beta'}\int d^3v' W^{\alpha'\beta'}_{\alpha\beta}(\vec{v}',\vec{v})\rho^{j}_{\alpha'\beta'}(\vec{r},\vec{v}',t), \tag{30a}$$

where

$$\Gamma^{\alpha'\beta'}_{\alpha\beta}(\vec{v}) = N\int d^3v_p W_p(\vec{v}_p)\left(\frac{2\pi\hbar}{i\mu}[f_{\alpha\alpha'}(\vec{v}_r,\vec{v}_r)\delta_{\beta\beta'} - f^{*}_{\beta\beta'}(\vec{v}_r,\vec{v}_r)\delta_{\alpha\alpha'}]\right) \tag{30b}$$

and

$$W^{\alpha'\beta'}_{\alpha\beta}(\vec{v}',\vec{v}) = N\int d^3v_r \int d^3v_r'\,\delta(\vec{v}'-\vec{v}-\vec{\Upsilon})W_p(\vec{v}-\vec{v}_r'+\vec{\Upsilon})\delta(v_r-v_r')v_r^{-1}f_{\alpha'\alpha}(\vec{v}_r',\vec{v}_r)f^{*}_{\beta'\beta}(\vec{v}_r',\vec{v}_r), \tag{30c}$$

where $\vec{v}_r$ is the relative velocity between active atom and perturber, $W_p(\vec{v}_p)$ is the perturber equilibrium velocity distribution, $\vec{\Upsilon} = (\mu/m)(\vec{v}_r' - \vec{v}_r)$, N is the perturber density, and $f_{\alpha'\alpha}(\vec{v}_r',\vec{v}_r)$ is the $\alpha',\vec{v}_r' - \alpha,\vec{v}_r$ inelastic scattering amplitude. In our case the internal state is labeled by the magnetic number m and the relevant scattering amplitudes are $f_{mm'}(\vec{v}_r',\vec{v}_r,\hat{A})$ where m and m' are taken along a fixed quantization axis $\hat{A}$. This scattering amplitude may be expressed as a function of the scattering amplitude in the helicity representation by

$$f_{mm'}(\vec{v}_r',\vec{v}_r,\hat{A}) = \sum_{MM'}\mathfrak{D}^{j*}_{mM}(\mathcal{R}')\mathfrak{D}^{j}_{m'M'}(\mathcal{R})f^{\text{hel}}_{MM'}(\vec{v}_r',\vec{v}_r), \tag{31}$$

where $\mathcal{R} = (\varphi_{v_r}, \theta_{v_r}, 0)$ and $\mathcal{R}' = (\varphi_{v_r'}, \theta_{v_r'}, 0)$ and φ and θ are polar angles with respect to $\hat{A}$.

In traditional optical pumping experiments in which depolarizing collisions are studied,[4] neither the vapor excitation nor the signal detection is velocity selective. In these experiments, the broadband excitation creates density-matrix elements $\rho^{j}_{mm'}(\vec{r},\vec{v},t)$ in a state of given j and the intensity of radiation emitted (or absorbed) from these mm' substates in a given direction and with a specific polarization is monitored. With broadband excitation and detection, the signal is a function of velocity-averaged density-matrix elements

$$\rho^{j}_{mm'}(\vec{r},t) = \int d^3v\,\rho^{j}_{mm'}(\vec{r},\vec{v},t)$$

and provides some measure of the effects of depolarizing collisions in level j. Integrating Eq. (30a) over velocity we find

$$\left.\frac{d}{dt}\rho^{j}_{mm'}(\vec{r},t)\right|_{\text{coll}} = -\sum_{m''m'''}\int d\vec{v}\,\gamma^{m''m'''}_{mm'}(\vec{v})\rho^{j}_{m''m'''}(\vec{r},\vec{v},t), \tag{32a}$$

where

$$\gamma^{m''m'''}_{mm'} = \Gamma^{m''m'''}_{mm'}(\vec{v}) - \int d^3v' W^{m''m'''}_{mm'}(\vec{v},\vec{v}'). \tag{32b}$$

Equation (32a) does not decouple γ and ρ; however, an approximation that is often made[22] is to neglect the $\vec{v}$ dependence of the γ's. In effect, one replaces $\gamma^{m''m'''}_{mm'}(\vec{v})$ by

$$\gamma^{m''m'''}_{mm'} = \int d^3v W(\vec{v})\gamma^{m''m'''}_{mm'}(\vec{v}), \tag{33}$$

where $W(\vec{v})$ is the active atom velocity distribution. A good approximation to Eq. (32a) is then

$$\left.\frac{d}{dt}\rho^{j}_{mm'}(\vec{r},t)\right|_{\text{coll}} = -\sum_{m''m'''}\gamma^{m''m'''}_{mm'}\rho^{j}_{m''m'''}(\vec{r},t). \tag{34}$$

The $\gamma^{m''m'''}_{mm'}$ describe the (velocity-averaged) coupling between magnetic sublevels and, as such, reflect the nature of the collisional interaction. Thus the structure of the $\gamma^{m''m'''}_{mm'}$ can provide some insight into the collisional process. By combining Eqs. (33), (32b), (30b), and (30c) and performing some of the integrations, one may obtain[2]

$$\gamma^{m''m'''}_{mm'} = N\int d^3v_r W_r(\vec{v}_r)v_r\left(\frac{2\pi}{ik}[f_{m''m}(\vec{v}_r,\vec{v}_r)\delta_{m'm'''} - f^{*}_{m'''m'}(\vec{v}_r,\vec{v}_r)\delta_{mm''}] - \int d\Omega_{v_r}\,f_{m''m}(\vec{v}_r',\vec{v}_r)f^{*}_{m'''m'}(\vec{v}_r',\vec{v}_r)\right). \tag{35}$$

This expression can be written in terms of S-matrix elements if Eqs. (31) and (2) are used for the scattering amplitudes. The resulting equation can be simplified by using the relation $\mathfrak{D}^{j}_{\nu M'}(\theta,\varphi,0) = \sum_{\nu'}\mathfrak{D}^{j}_{\nu M''}(\mathcal{R})\mathfrak{D}^{j*}_{\nu' M''}(\mathcal{R}')$ and other elementary properties of the $\mathfrak{D}$ matrices. The integrals over $d\Omega_{v_r}$ and $d\Omega_{v_r'}$ can be carried out and, after some cancellation of terms, one is left with

$$\gamma_{mm}^{m''m'''} = \frac{4\pi^2 N}{K^2} \sum (-1)^q (2J+1)(2J'+1)(2f+1) \begin{pmatrix} j & j & f \\ m & -m' & q \end{pmatrix} \begin{pmatrix} j & j & f \\ m'' & -m''' & q \end{pmatrix} \begin{pmatrix} j & j & f \\ M & -M' & q \end{pmatrix} \begin{pmatrix} J & J' & f \\ M'' & -M''' & q \end{pmatrix}$$

$$\times \begin{pmatrix} J & J' & f \\ M'' & -M''' & q \end{pmatrix} \int dv_r W_r(v_r) v_r^3 (\delta_{MM'} \delta_{M'M'''} - S_{MM}^J S_{M'''M'}^{J'*}), \tag{36}$$

where the sum is over all repeated indices (except j). Equation (36) contains the selection rule $m - m'' = m' - m'''$ which may also be obtained from symmetry considerations. One can verify that $\sum_m \gamma_{mm}^{m''m'''} = 0$, reflecting the conservation of probability $\sum_m dp_{mm}(\vec{r}, t)/dt = 0$.

Using Eq. (26), one can write the dynamical factor appearing in Eq. (36) as

$$\delta_{M''M'} \delta_{MM'''} - S_{M''M'}^{J'*} S_{MM'''}^{J} = \delta_{M''M'} \delta_{MM'''} - \sum_{m'n'} U_{-M''m'}^{J*}(-\infty, t_{J'}^-) U_{-Mm}^{J}(-\infty, t_J^-) U_{m'M'}^{J'}(t_{J'n'}^+, +\infty)$$

$$\times U_{nM'''}^{J'}(t_{Jn}^+, +\infty) \exp[-i(\Delta_{-M''M'}^{J'n'} - \Delta_{-MM'''}^{Jn})] \exp[-2i(\eta_{J'n'} - \eta_{Jn})]. \tag{37}$$

In writing Eq. (37) we have implicitly used the selection rule $|J - J'| \leq j$ which is imposed by the $3-j$ symbols appearing in Eq. (36). Since $J \gg j$, differences between J and J' can be neglected in all but phase factors. In the previous section it has been shown that the quantum-mechanical aspect of the translational motion is concentrated in the factors $\exp[-2i(\eta_{J'n'} - \eta_{Jn})]$. The other factors describe the evolution of internal substates along classical paths $r_{Jn}(t)$. Let $\hbar J_0$ be the angular momentum for which $r_{JM}^{(TP)} = r_0$. In Eq. (36), the sum over J may be regarded as a sum over the impact parameter $(J + \frac{1}{2})/K$. In analogy with the classical mechanics calculation. In the region where $J > J_0$ [or $r_0 < r_{JM}^{(TP)}$] a common motion approximation is valid. Since $|J - J'| \ll J$, the phase difference in Eq. (37) can be expanded under the form

$$\eta_{J'n'} - \eta_{Jn} = \eta_{J'n'} - \eta_{Jn} + (J' - J) \frac{\partial \eta_{Jn'}}{\partial J}, \tag{38}$$

where $\partial \eta_{Jn'}/\partial J$ can be identified as the classical deflection angle Θ_J (see Appendix B). Then, following Eq. (28) one reduces Eq. (37) to

$$\delta_{M''M'} \delta_{MM'''} - S_{M''M'}^{J'*} S_{MM'''}^{J} = \delta_{M''M'} \delta_{MM'''} - U_{-M''M'}^{J*}(-\infty, +\infty) U_{-MM'''}^{J}(-\infty, +\infty)$$

$$\times \exp \frac{i}{\hbar} \int_0^\infty [V_{-M''M'}(r_J(t)) + V_{MM'''}(r_J(t)) - V_{-M''M'''}(r_J(t)) - V_{MM'}(r_J(t))] dt \exp[-\tfrac{1}{2} i (J' - J) \Theta_J], \tag{39}$$

where $(\eta_{Jn} - \eta_{Jn'})$ have been expanded to lowest order in the potentials. This expression describes the substate mixing along a single trajectory $r_J(t)$.

When $J < J_0$ [or $r_0 > r_{JM}^{(TP)}$], it may be verified that $|\eta_{Jn} - \eta_{J'n'}| \gg 1$ and that the factor $\exp[-2i(\eta_{J'n'} - \eta_{Jn})]$ averages to zero by summation over J and J' for $|n| \neq |n'|$. A classical trajectory r_{Jn} may still be assigned to elements of the density matrix which are diagonal (in the helicity representation) on entering the region $r < r_0$ but the classical picture fails for nondiagonal elements. In other words at $r = r_0$ the magnetic substate populations ρ_{JnJn} are scattered along separate trajectories r_{Jn} but the coherence between substates is lost owing to trajectory separation. After the departure from the region $r < r_0$, substate mixing starts again along each separate trajectory. In some sense the images given in Figs. 2(a) and 2(b) are valid when the interatomic distance r is, respectively, larger or smaller than r_0. To work out this semiclassical picture, the only needed condition on the de Broglie wavelength has been

$\lambda \ll r_c$. This condition is not sufficient to regard the atoms as wave packets of dimension much smaller than the interaction distance. Thus, in analogy with JWKB calculations of scattering amplitudes, the classical trajectories that we have mentioned are not really followed by the atoms. A specific evaluation of $\gamma_{mm}^{m''m'''}$ will be given in a future work.

Velocity selective laser spectroscopy

In velocity selective laser spectroscopy, the relevant quantity which describes collisional effects is the collision kernel $W_{mm}^{m''m'''}(\vec{v}', \vec{v})$. Calculation of this kernel from Eqs. (30c) and (31) requires the knowledge of products of differential scattering amplitudes of the form

$$f_{M''m'M'}^{bel}(\vec{v}_r', \vec{v}_r) f_{M''m''M}^{bel*}(\vec{v}_r', \vec{v}_r).$$

The stringent condition $\sqrt{\lambda} \ll \sqrt{r_c}$ is needed to obtain a semiclassical approximation of this quantity. We consider still the simple case of purely repulsive interaction for which a semiclassical

scattering amplitude has been calculated (Eq. 29). Since Eq. (29) is valid only if $J_{\theta M}\theta \gg 1$, a supplementary assumption is needed to take into account small-angle scattering. We suppose that the width of $\rho_{mm'}(\vec{r},\vec{v},t)$ in velocity space is much larger than the velocity change which corresponds to the deflection angle defined by $J_{\theta M}\theta = 1$. Thus, the collisional transport equation may be written

$$\left.\frac{d\rho_{mm'}}{dt}\right|_{coll} = \sum_{m''m'''} -\Gamma^{m''m'''}_{mm'}(\vec{v})\rho_{m''m'''}(\vec{r},\vec{v},t)$$

$$+ \sum_{m''m'''} \rho_{m''m'''}(\vec{r},\vec{v},t)\int d^3v' W^{m''m'''}_{mm'>}(\vec{v}',\vec{v})$$

$$+ \sum_{m''m'''} \int d^3v' W^{m''m'''}_{mm'>}(\vec{v}',\vec{v})\rho_{m''m'''}(\vec{r},\vec{v}',t), \tag{40}$$

where $W^{m''m'''}_{mm'>}(\vec{v}',\vec{v})$ describes collisions which are such that $J_{\theta M}\theta > 1$ and $W^{m''m'''}_{mm'<}(\vec{v}',\vec{v})$ describes the remaining very small-angle collisions. The first two terms may be calculated in the same way as $\gamma^{m''m'''}_{mm'}$.

The semiclassical approximation of scattering amplitudes is needed to determine $W^{m''m'''}_{mm'>}(\vec{v}',\vec{v})$.

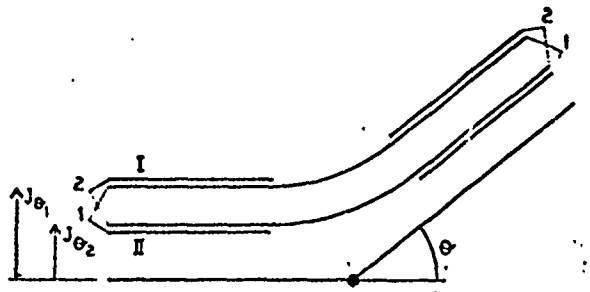

FIG. 5. The scattering of 2-substate atoms at angle θ results from the contribution of two trajectories: the one which enters the $r < r_0$ region in substate 1 at impact parameter $(J_{\theta_1} + \frac{1}{2})\hbar$ (I) and the one which enters the $r < r_0$ region in substate 2 at impact parameter $(J_{\theta_2} + \frac{1}{2})\hbar$ (II). Along each trajectory mixing between substates occurs for $r < r_0$. The trajectories of substate 2 in I and substate 1 in II would lead to scattering at an angle *other than* θ and are, therefore, not continued into the $r < r_0$ region.

As above, two collision regions may be distinguished depending on whether $J_{\theta M}$ is larger or smaller than J_0. When $J_{\theta M} > J_0$, a single trajectory is available and one obtains

$$f^{*hel}_{M'''M'}(\theta,\varphi) f^{hel}_{M''M}(\theta,\varphi) = \frac{J_\theta}{K^2\pi\sin\theta\left|\frac{d\theta}{dJ_\theta}\right|} U^{J_\theta}_{-M'''M'}(-\infty,+\infty)^* U^{J_\theta}_{-M''M}(-\infty,+\infty)$$

$$\times \exp\frac{i\mu}{\hbar}\int_0^\infty dt[V_{-M'''}(r_{J_\theta}(t)) - V_{-M''}(r_{J_\theta}(t)) + V_{M'}(r_{J_\theta}(t)) - V_M(r_{J_\theta}(t))]$$

$$\times \exp\left(-i(M''' - M'' + M - M')\frac{\pi}{2}\right) \tag{41}$$

for use in Eqs. (30c) and (31). This result contains the product of a semiclassical elastic differential scattering cross section by a factor which accounts for the MM' transitions along this trajectory.

When $J_{\theta M} > J_0$, distinct trajectories corresponding to distinct substates may contribute to scattering at $\theta\varphi$ and

$$f^{*hel}_{M'''M'}(\theta,\varphi) f^{hel}_{M''M}(\theta,\varphi) = \frac{1}{K^2\pi\sin\theta}\sum_{nn'}(J_{\theta n}J_{\theta n'})^{1/2} U^{J_{\theta n}}_{-M'''M'}(-\infty,t_j^-)^* U^{J_{\theta n'}}_{-M''M}(-\infty,t_{j'}^-) U^{J_{\theta n}}_{nM'}(t_{j_n}^+,\infty)^* U^{J_{\theta n'}}_{n'M}(t_{j_{n'}}^+,\infty)$$

$$\times \exp[-i(\Delta^{J_{\theta n}}_{-M'''M'} - \Delta^{J_{\theta n'}}_{-M''M})]\exp[-i(M''' - M' - M'' + M)\frac{\pi}{2} + i(M' - M)\varphi]$$

$$\times \left(\frac{\partial\theta}{\partial J_{\theta n}}\frac{\partial\theta}{\partial J_{\theta n'}}\right)^{1/2}\exp[2i(\eta_{J_{\theta n}n'} - \eta_{J_{\theta n}n}) + i(J_{\theta n} - J_{\theta n'})\theta]. \tag{42}$$

The last factor in Eq. (42) represents interference effects between diverging trajectories. Its angular dependence is given by

$$\frac{d}{d\theta}[2(\eta_{J_{\theta n}n'} - \eta_{J_{\theta n}n}) - (J_{\theta n'} - J_{\theta n})\theta] = J_{\theta n} - J_{\theta n'}. \tag{43}$$

This angular dependence leads to oscillations of $W^{m''m'''}_{mm'>}(\vec{v}',\vec{v})$ as a function of $\vec{v}$ and $\vec{v}'$. In $\int W^{m''m'''}_{mm'>}(\vec{v}',\vec{v})\rho_{m''m'''}(\vec{v}')d^3v'$, the integral over v' averages to zero for terms with $|n| \neq |n'|$ *provided* $(\mu/m)u|J_{\theta n} - J_{\theta n'}|^{-1}$ is much smaller than the width of $\rho_{mm'}(\vec{v})$ in velocity space, where u is the active-atom mean speed.

The net effect of scattering in direction $\theta\varphi$ for a two-level system in this limit is shown in Fig. 5. The angular momenta $J_{\theta i}(i = 1, 2)$ correspond to scattering of an atom in state i through the

angle $\theta\varphi$. For $r > r_0$ the substates are mixed by the collisional interaction along each of the two trajectories I and II. For $r < r_0$ the two states in each of trajectories I and II are split by the collisional interaction, but only *one* trajectory in each leads to scattering at $(\theta\varphi)$. Finally, the states in a given trajectory are again mixed for $r > r_0$. The internal final state is a combination of internal states which have experienced the history shown in Fig. 5. When the above conditions are not fulfilled, no simple picture can be given. It should be noticed that the phase factor in Eq. (42) cannot be clearly separated into a "spatial phase shift" which would represent interference effects between diverging trajectories, and an "internal phase shift" which results from internal substate mixing and which is present along a common classical trajectory.

Thus, the methods used to calculate $\gamma_{mm'}^{m''m'''}$ and $W_{mm'}^{m''m'''}(\vec{v}', \vec{v})$ are perfectly consistent with the JWKB and classical trajectory approximations, respectively, that are used to calculate total and differential scattering cross sections. Assuming $\lambda \ll r_c$, the result for $\gamma_{mm'}^{m''m'''}$ can be interpreted in terms of a large number of partial waves giving rise to scattering at angle $\theta\varphi$ with *no* classical correspondence between impact parameter and scattering angle; however, the relevant phase shifts and substate coupling *are* calculated along classical trajectories (just as the η_l are calculated along classical trajectories in the JWKB evaluation of collision cross sections). Under the more stringent condition $\sqrt{\lambda} \ll \sqrt{r_c}$, the derived expression for the kernel $W_{mm'}^{m''m'''}(\vec{v}', \vec{v})$ can be interpreted as arising from collisions having the appropriate impact parameter to give rise to classical scattering at $\theta\varphi$. There may be a number of such impact parameters reflecting the different interaction potentials for the various magnetic substates.

We have not attempted to give an interpretation to $W_{mm'}^{m''m'''}(\vec{v}', \vec{v})$ under the less restrictive semiclassical condition $\lambda \ll r_c$; in this limit the large number of partial waves contributing to each scattering amplitude leads to a very complicated expression when bilinear products of the scattering amplitudes are taken to form the collision kernel. Only when *total* cross sections, such as those represented by $\gamma_{mm'}^{m''m'''}$, are evaluated does one regain a result with a simple physical interpretation.

V. SUMMARY

In view of understanding the signal formation in laser spectroscopic experiments when depolarizing collisions are present, we have developed a semiclassical theory of these collisions. First we have shown that single-trajectory approximation and adiabatic approximation can be combined to obtain a generally valid expression for the semiclassical phase shifts (provided $\lambda \ll r_c$). An explicit calculation of this phase shift has been outlined in the simple case of a continuously decreasing difference of the substate dependent interatomic potentials. The conditions of validity for using a semiclassical scattering amplitude have been examined and the case of a purely repulsive interaction has been treated in some detail. Using semiclassical approximations to the scattering amplitudes, we investigated the nature of the depolarization collision kernels and rates which enter into laser spectroscopic experiments. For these two quantities a picture of the scattering, in terms of classical trajectories, has been given. In a forthcoming paper, expressions that we have obtained will be used in a numerical calculation of the corresponding signal profiles which could be observed in laser spectroscopic experiments.

ACKNOWLEDGMENTS

The authors wish to thank Professor J. Delos for a helpful discussion. The research of one of the authors (P.R.B.) was supported by the U. S. Office of Naval Research. This research was supported in part by the NSF under Grant No. INT 792 1530.

APPENDIX A: DERIVATION OF THE RADIAL EQUATION[17]

A convenient set of commuting observables in the center-of-mass frame consists of the Hamiltonian H, j^2, and the total angular-momentum operators J^2, J_z, where J_z is taken along a laboratory fixed axis of quantization Oz. The corresponding eigenfunctions are $\Psi^{JM_J}(\vec{r}, \vec{\rho})$ where M_J is an eigenvalue of J_z and $\vec{\rho}$ denotes the ensemble of electronic coordinates of the colliding atoms. The total Hamiltonian H is

$$H = H_0(\vec{\rho}) + \frac{P^2}{2\mu} + V(\vec{r}, \vec{\rho}),$$

where $H_0(\vec{\rho})$ is the internal Hamiltonian, $V(\vec{r}, \vec{\rho})$ is the interatomic potential, and

$$P^2 = -\hbar^2 \frac{\partial^2}{\partial r^2} + \frac{(J^2 + j^2 - 2\vec{J}\cdot\vec{j})}{r^2}\hbar^2.$$

The Hamiltonian, without internuclear motion, is

$$H_0 = H_0(\vec{\rho}) + \frac{j^2\hbar^2}{2\mu r^2} + V(\vec{r}, \vec{\rho}).$$

Its eigenfunctions are $\phi_{\nu'}^{l'}(r, \vec{\rho})$ where M' is the simultaneous eigenvalue of $J_{z'}$ and $j_{z'}$ along the

rotating axis of quantization $\vec{r}$. The expansion of $\Psi^{JlM}(\vec{r},\vec{\rho})$ in terms of $\mathcal{O}^l_M(r,\vec{\rho})$, and the wave function $\underline{\underline{\Psi}}^{Jl}_M(r)$ describing the scattering is[17]

$$\Psi^{JlMJ}(\vec{r},\vec{\rho}) = \frac{1}{r}\sum_{M'} \mathfrak{D}^{J*}_{M,M'}(\mathfrak{R})\underline{\underline{\Psi}}^{Jl}_{M'}(r)\varphi^l_{M'}(r,\vec{\rho}),$$

where $\mathfrak{R}$ is the rotation which brings $\vec{r}$ along Oz. We substitute this expression into the Schrödinger equation

$$\frac{\hbar^2K^2}{2\mu}\Psi^{JlMJ}(\vec{r},\vec{\rho}) = H\Psi^{JlMJ}(\vec{r},\vec{\rho}),$$

where K is the magnitude of the relative motion wave vector. Projection on $\varphi^{l*}_M(r,\vec{\rho})$ leads to the radial equation

$$\left(-\frac{\hbar^2}{2\mu}\frac{d^2}{dr^2} - \frac{\hbar^2}{2\mu}\bar{\pi}\frac{d}{dr} - \frac{\hbar^2K^2}{2\mu} + \langle M|V|M\rangle\right)\underline{\underline{\Psi}}^{Jl}_M(r)$$

$$= -\sum_{M'\neq M}\langle M|V|M'\rangle\underline{\underline{\Psi}}^{Jl}_{M'}(r),$$

where

$$\bar{\pi} = \int d\vec{\rho}\,\varphi^{l*}_M(r,\vec{\rho})\frac{\partial}{\partial r}\varphi^l_M(r,\vec{\rho}),$$

$$\langle M|V|M'\rangle = \left(V_M(r) + \frac{J(J+1) - 2M^2 + j(j+1)}{2\mu r^2}\hbar^2\right)\delta_{MM'}$$

$$-\frac{\hbar^2}{2\mu r^2}[\lambda_+(J,M)\lambda_+(j,M)\delta_{MM'+1}$$

$$+\lambda_-(j,M)\lambda_-(J,M)\delta_{MM'-1}],$$

$\lambda_\pm(J,M') = [J(J+1) - M'(M'\pm 1)]^{1/2}$ and $V_M(r)$ is the value of the interatomic potential in substate M. In the diagonal term, the contributions which contain $\bar{\pi}$ and $j(j+1) - 2M^2$ may be neglected as they are of the order of $\hbar/r_c$.

The boundary-value condition which is necessary to select the appropriate solution of the radial equation is determined by the asymptotic form of a scattered plane wave which is

$$\Psi \sim e^{i\vec{K}\cdot\vec{r}}\bar{\varphi}^l_M(\vec{\rho}) + \sum_{M'}\frac{e^{iKr}}{r}f^{\text{hel}}_{MM'}(\theta,\vec{\rho})\varphi^l_{M'}(\infty,\vec{\rho}),$$

where $\bar{\varphi}^l_M(\vec{\rho})$ is the electronic wave function assuming that the quantization axis is along $\vec{K}$, and $f^{\text{hel}}_{MM'}(\theta,\vec{\rho})$ is the scattering amplitude in the helicity representation. The connection between $\bar{\varphi}^l_M(\vec{\rho})$ and $\varphi^l_{M'}(\infty,\vec{\rho})$ is

$$\bar{\varphi}^l_M(\vec{\rho}) = \sum_{M'}\mathfrak{D}^{l*}_{MM'}(\mathfrak{R})\varphi^l_{M'}(\infty,\vec{\rho}).$$

Expansion of the plane-wave function in terms of spherical harmonics leads to

$$e^{i\vec{K}\vec{r}}\bar{\varphi}^l_M(\vec{\rho}) - \frac{1}{2iKr}\sum_{lM'j}(2l+1)(2J+1)(e^{iKr} - (-1)^l e^{-iKr})$$

$$\times\begin{pmatrix} l & j & J \\ 0 & M & -M\end{pmatrix}\begin{pmatrix} l & j & J \\ 0 & M' & -M'\end{pmatrix}$$

$$\times\mathfrak{D}^J_{-M-M'}(\mathfrak{R})\varphi^l_{M'}(\infty,\vec{\rho}).$$

Summing over l and using Eq. (2) one finally obtains

$$\Psi \sim \frac{1}{2iKr}\sum_{JM'}(2J+1)[-(-1)^{J+l}\delta_{M',-M}e^{-iKr} + S^J_{MM'}e^{iKr}]$$

$$\times(-1)^{M-M'}\mathfrak{D}^{J*}_{MM'}(\mathfrak{R})\varphi^l_{M'}(\infty,\vec{\rho}).$$

Since $\Psi = \sum_{JM'}\Psi^{Jl}_{M'}(\vec{r},\vec{\rho})$, we see that the asymptotic form of the radial wave function is[21]

$$\lim_{r\to\infty}\underline{\underline{\Psi}}^{Jl}_M(r) = -\frac{2J+1}{2iK}(-1)^{M-M'+l+J}$$

$$\times[\delta_{-MM'}e^{-iKr} - (-1)^{l+J}S^J_{MM'}e^{iKr}].$$

APPENDIX B: STATIONARY-PHASE CALCULATION

The needed approximation for $\mathfrak{D}_{MM'}(\varphi,\theta,0)$ for large J values is given by Brussaard and Tolhoek[23]

$$\mathfrak{D}^J_{MM'}(0,\theta,0) = \left(\frac{\pi}{2}\sin\theta k(\theta)\right)^{-1/2}\sin\left(\frac{\pi}{4} + M\pi + W^J_{MM'}(\theta)\right), \tag{B1}$$

where

$$k(\theta) = [J^2 - (M^2 + M'^2 - 2MM'\cos\theta)/\sin^2\theta]^{1/2} \tag{B2}$$

and

$$W^J_{MM'}(\theta) = J\cos^{-1}[(J^2\cos\theta - MM')/(J^2 - M^2)^{1/2}(J^2 - M'^2)^{1/2}]$$

$$-M\cos^{-1}[(M\cos\theta - M')/\sin\theta(J^2 - M^2)^{1/2}] - M'\cos^{-1}[(M'\cos\theta - M)/\sin\theta(J^2 - M'^2)^{1/2}]. \tag{B3}$$

This approximation is valid provided $W^J_{M'M}(\theta) \gg 1$. This expression is substituted into Eq. (2). The sum of the term involving $\delta_{M'M}$ vanishes[17] and one is left with

$$f^{\rm bel}_{M'M}(\theta,\varphi) = \frac{(-1)^{M-M'}}{2iK}\sum_J (2J+1) S^J_{M'M} d^J_{M'M}(\varphi,\theta,0), \tag{B4}$$

where $S^J_{M'M}$ is to be given by Eq. (26). The quantities $U^{J\eta''}_{M'M}(t,t')$ and $\exp(i\Delta^{J\eta''}_{M'M})$, appearing in Eq. (26) are slowly varying functions of J with respect to $\exp(2i\eta_{JM''})$. Thus, they can be taken out of the sum over J and evaluated at a point of maximum contribution to the sum. One may use the stationary-phase method to calculate

$$\int dJ \exp[2i\eta_{JM''} \pm iW^J_{M'M}(\theta)]. \tag{B5}$$

The stationary-phase condition is $d/dJ[2\eta_{JM''} \pm W^J_{M'M}(\theta)] = 0$ which leads to

$$2\frac{d\eta_{JM''}}{dJ} = \pm\cos^{-1}\left(\frac{J^2\cos\theta - MM'}{(J^2-M^2)^{1/2}(J^2-M'^2)^{1/2}}\right) \tag{B6}$$

or, when $M \ll J$,

$$2\frac{d\eta_{JM''}}{dJ} = \pm\theta + O\left(\frac{M^2}{J^2}, \frac{MM'}{J^2}, \frac{M'^2}{J^2}\right). \tag{B7}$$

The classical deflection angle Θ is defined by

$$\Theta = 2\frac{d\eta_{JM''}}{dJ}, \tag{B8}$$

where $d\eta_{JM''}/dJ$ satisfies Eq. (B7) to first order in M'/J. A set of angular momenta $J_{\theta M''}$ may satisfy Eq. (B8). We restrict now our calculation to the single case of a purely repulsive potential. Then $\theta = \Theta$ and the semiclassical scattering amplitude may be evaluated from Eqs. (B4), (22), and (B1) using the method of stationary phase. One obtains

$$f^{\rm bel}_{-M',M}(\theta,\varphi) = \frac{1}{K(\sin\theta)^{1/2}}\sum_{M''}(J_{\theta M''})^{1/2}\left|\frac{\partial\theta}{\partial J_{\theta M''}}\right|^{-1/2} U^{J_{\theta M''}M''}_{M'M''}(-\infty,t_J^-)U^{J_{\theta M''}M''M}_{M''M}(t_{JM''}^+,\infty)\exp(i\Delta^{J_{\theta M''}M''M}_{M'M''M} + 2i\eta_{J_{\theta M''}M''M})$$
$$\times \exp\left(-i\frac{\pi}{2} - i(M'+M)\frac{\pi}{2} - iJ_{\theta M'}\theta\right)\exp(-iM\varphi). \tag{B9}$$

This expression is bound to the validity of the stationary-phase approximation which requires that

$$\left|\frac{\partial^2\theta}{\partial J^2}\left(\frac{\partial\theta}{\partial J}\right)^{-3/2}\right| \ll 1. \tag{B10}$$

This condition generally reduces to $\sqrt{\lambda} \ll \sqrt{r_c}$. One has to also take account of the condition of validity of the approximation used for $d^J_{M'M}(0,\theta,0)$. To first order in M/J the approximation demands that

$$|J_{M''0}\sin\theta| \gg 1 \tag{B11}$$

The points of stationary phase for channels M and M' are well separated provided that

$$|J_{M\theta} - J_{M'\theta}| \gg (\partial\theta/\partial J)^{-1/2}. \tag{B12}$$

The fulfillment of this condition implies that the wave packets in channels M and M' do not overlap. When condition (B12) is not fulfilled the distinct wave packets coalesce into a single one, but Eq. (B9) is still valid, since Eq. (B8) still has a single solution for a given value of M''.

---

[a]Laboratoire associé à l'Université Paris-Sud.

[1]For a comprehensive bibliography see R. Vetter and P. R. Berman, Comments At. Mol. Phys. 10, 69 (1981).

[2]P. R. Berman, Phys. Rev. A 5, 927; 6, 2157 (1972).

[3]V. A. Alekseev, T. L. Andreeva, and I. I. Sobelman, Zh. Eksp. Teor. Fiz. ??, xxx (19??) [Sov. Phys.—JETP 35, 325 (1972).

[4]W. Happer, Rev. Mod. Phys. 44, 169 (1972).

[5]M. Gorlicki, A. Peuriot, and M. Dumont, J. Phys. (Paris) Lett. 41, L275 (1980) and private communication; J.-L. Le Gouët and R. Vetter, J. Phys. B 13, L147 (1980).

[6]The scattering can depend strongly on the internal state, although the exchange of angular momentum between internal and external motion is very small with regard to the translational angular momentum.

[7]W. D. Held, J. Schöttler, and J. P. Toennies, Chem. Phys. Lett. 6, 304 (1970); H. Udseth, C. F. Giese, and W. R. Gentry, J. Chem. Phys. 54, 3643 (1971).

[8]D. Secrest and B. P. Johnson, J. Chem. Phys. 45, 4556 (1966); B. R. Johnson, D. Secrest, W. A. Lester, and R. B. Bernstein, Chem. Phys. Lett. 1, 396 (1967).

[9]H. F. Helbig and E. Everhart, Phys. Rev. 140, 715 (1965); J. C. Houvier, P. Fayeton, and M. Barat, J. Phys. B 7, 1353 (1974).

[10]W. H. Miller, J. Chem. Phys. 53, 1949 (1970); 54, 5386 (1971).

[11]R. A. Marcus, J. Chem. Phys. 54, 3965 (1971); J. N. L. Connor and R. A. Marcus, *ibid.* 55, 5636 (1971).

[12]M. D. Pattengill, C. F. Curtiss, and R. B. Bernstein,

J. Chem. Phys. 54, 2197 (1971); C. F. Curtiss, Ibid. 52, 4832 (1970).
[13]D. R. Bates and D. S. F. Crothers, Proc. R. Soc. London Ser. A 315, 465 (1970) and references therein.
[14]J. B. Delos, W. R. Thorson, and S. K. Knudson, Phys. Rev. A 6, 709 (1972); 6, 720 (1972).
[15]C. Gaussorgues, C. Le Sech, F. Masnou-Seeuws, and R. Mac Caroll, J. Phys. B 8, 239, 253 (1975).
[16]P. Pechukas, Phys. Rev. 181, 166 (1969); 181, 174 (1969).
[17]M. S. Child, *Molecular Collision Theory* (Academic, London, 1974). Note we follow the notation of Child when we use $f_{MM'}$ or $S_{MM'}$ to indicate transition from M to M'.
[18]E. C. Kemble, Phys. Rev. 48, 549 (1935).
[19]M. Jacob and G. C. Wick, Ann. Phys. (N.Y.) 7, 404 (1959).
[20]In the classical picture of the adiabatic limit, the momentum $\vec{j}$ processes rapidly around $\vec{r}$ and this motion is much faster than the rotation of the internuclear vector around the center of mass. The classical S-matrix problem is then reduced to the solution of one differential equation for each value of $\vec{j}\cdot\vec{r}/r$.
[21]We insist upon the fact that in $S^J_{M'M}$, M' is taken along $\vec{K}$ while M is measured along $\vec{r}$. Thus, in the absence of any collisional interaction, looking in the forward direction one observes a final momentum M along $\vec{r}$, which is equal to the initial momentum M' along direction $\vec{K}$. This implies that $S^J_{MM'}$ is diagonal in M. On the other hand, in the adiabatic approximation, as the internal momentum is linked to the internuclear axis, a final momentum M corresponds to the same momentum along the initial internuclear axis, i.e., to the opposite value $-M$ along direction $\vec{K}$. Thus $S^J_{MM'}$ is proportional to $\delta_{-MM'}$.
[22]A. Omont, J. Phys. Radium 26, 26 (1965). P. R. Berman and W. E. Lamb, Phys. Rev. 187, 221 (1969).
[23]P. J. Brussard and H. A. Tolhoek, Physica (Utrecht) 23, 955 (1957).

ThI4. Pressure Dependence of Gratings Produced by DFWM in Na. L. M. HUMPHREY, P. F. LIAO, AND P. R. BERMAN,* *Bell Telephone Laboratories, Crawfords Corner Road, Holmdel, New Jersey 07733.*—Degenerate four-wave mixing may be viewed as the simultaneous production and reading of two real-time holographic gratings. If the oppositely propagating pump beams have orthogonal polarizations, it is possible to control which grating is produced and read by changing the polarization of the probe. We have investigated the foreign gas pressure dependence of the two possible gratings far off resonance and have found striking differences. Our experiments were performed in Na vapor using a single-mode cw dye laser, at ~589 nm, whose output was passed through an E-O modulator set up to give 25-ns pulses. With an angle between probe and pump of 0.014 rad, the probe beam polarization was set to produce a grating with a 2.9×10^{-5} cm spacing. Helium gas was introduced into the Na cell. The conjugate wave intensity decreased by a factor of 10 by 10 Torr helium. With the probe beam polarization set to produce a grating with 4.2×10^{-3} cm spacing, the conjugate wave intensity increased with increasing gas pressure before leveling off near 100 Torr, a factor of 5 larger than with no gas. These results are explained in terms of the adiabatic following model. (13 min.)

• Supported by the U.S. Office of Naval Research.

Supported by the U.S. Office of Naval Research under Contract No. N00014-77-C-0553.

PHYSICAL REVIEW A VOLUME 22, NUMBER 5 NOVEMBER 1980

Coherence effects in radiatively assisted inelastic collisions: General theory

Paul R. Berman

*Laboratoire Aimé Cotton, Centre National de la Recherche Scientifique II, Bâtiment 505, 91405 Orsay-Cedex, France and Physics Department, New York University, 4 Washington Place, New York, New York 10003**

(Received 21 March 1980)

A radiatively assisted inelastic collision (RAIC) is one in which two atoms collide in the presence of a radiation field to produce a reaction of the form $A^* + B + \hbar\Omega \rightarrow A + B^*$. In this paper, a general theory of RAIC is developed with special attention given to the final-state coherences produced by RAIC. These final-state coherences can be monitored by standard experimental techniques (polarization of fluorescence, quantum beats), enabling one to use such studies to gain information on the interatomic potentials that are relevant to the RAIC under consideration.

I. INTRODUCTION

There has been considerable recent interest in reactions of the form

$$A_i + A'_{i'} + \hbar\Omega \rightarrow A_f + A'_{f'} \tag{1}$$

in which two atoms (A and A') undergo a collision while simultaneously absorbing a photon of energy $\hbar\Omega$ from an external radiation field to take the atoms from some initial state $A_i A'_{i'}$ to a final state $A_f A'_{f'}$. In many cases, the direct transition $A_i + A'_{i'} \rightarrow A_f + A'_{f'}$ is energetically forbidden; consequently, the transition can take place only in the presence of the radiation field, with the photon providing the energy mismatch $(E_f + E_{f'}) - (E_i + E_{i'})$.[1] Such processes have been referred to as radiative collisions[2] (RC), laser-induced collisional energy transfer[3] (LICET), or radiatively assisted inelastic collisions[4] (RAIC) and have been the subject of a large number of theoretical[5] and a lesser number of experimental[3,6] investigations. By studying the RAIC cross section as a function of frequency Ω, one can gain important information about the initial- and final-state AA' interatomic potentials.

Typically, the RAIC cross section can be measured by monitoring the fluorescence from one of the final states ($A'_{f'}$, for example) since the total RAIC cross section can be simply related to the *total* fluorescence rate. It is apparent, however, that additional information is contained in the polarization of the fluorescence, i.e., in the coherence properties of the final states. It is the purpose of this paper to present a general theory of RAIC which allows one to calculate the final-state coherence properties as well as the total RAIC cross section. Experimentally, the final-state coherence can be probed by standard methods (absorption, emission, or quantum beats originating from one of the final states).

A few calculations[7,8] have already appeared which include magnetic degeneracy effects in RAIC and in the related problem of collisionally assisted radiative excitation (CARE). However, these calculations were restricted to specific J values for the various levels and to specific forms for the interatomic potentials; moreover, only total cross sections were obtained.

A more global picture of the collisional process is achieved if levels of arbitrary J and interatomic potentials of a quite general nature are considered. The calculations, including an averaging over different collision orientations, are conveniently carried out using techniques involving irreducible tensor operators. The final-state coherence resulting from RAIC can then be interpreted in terms of the symmetry properties of the interatomic potential and the characteristic properties (polarization, frequency, intensity) of the external light field participating in the RAIC reaction.

A general formalism for RAIC is given in this paper. The physical system is described in Sec. II, the equations of motion are given in Sec. III (and derived in Appendix A), and a formal solution is obtained in Sec. IV. A discussion of the results is given in Sec. V. In Appendix B, I present a diagrammatic interpretation of the operators that appear in the equations of motion.

Solutions of the RAIC equations in the limit where the external field is weak and the collision-induced level shifts of the atomic energy levels can be neglected will be presented in a following paper. In future work, solutions of the RAIC equations will be sought that are valid for arbitrary field strengths and include level-shifting effects.

II. PHYSICAL SYSTEM

The physical system consists of a low density ($\lesssim$ several hundred Torr) atomic vapor containing two types of atoms, A and A', to which a light pulse is applied. The atomic energy levels for

Supported by the U.S. Office of Naval Research under Contract No. N00014-77-C-0553.

atoms A and A' are shown in Fig. 1. Levels of atom A are designated by unprimed variables and those of atom A' by primed ones. It is assumed that the levels of each atom can be separated into subgroups of levels (see Fig. 1), with the energy separation between sublevels in a given group having some upper bound $\hbar\omega_g$ (to be established below). Specifically, the sublevels within a group are generally different fine structure, hyperfine structure, or Zeeman sublevels of a given electronic state. The atoms are prepared in a linear superposition of states $|ii'\rangle$, where i and i' represent any of the sublevels in the i and i' groups, respectively.

The light pulse is taken to be of the form

$$\vec{E}(\vec{R},t)=\tfrac{1}{2}[\vec{\mathcal{E}}(\vec{R},t)e^{-i\Omega t}+\vec{\mathcal{E}}(\vec{R},t)^{*}e^{i\Omega t}], \qquad (2)$$

where the envelope function $|\vec{\mathcal{E}}(\vec{R},t)|$ is characterized by a duration T and a maximum amplitude $|\mathcal{E}_0|$ (Fig. 2). It is assumed that the pulse envelope varies very slowly in an optical period ($\Omega T \gg 1$) and that the frequency Ω is very far detuned from any transition frequency in atom A or in atom A'. On the other hand, the field is assumed to be in near resonance with the transition in the *composite* AA' system from some initial state $|ii'\rangle$ to a final state $|ff'\rangle$. In other words

$$\hbar\Omega \approx E_f + E_{f'} - (E_i + E_{i'}), \qquad (3)$$

where E_α is the energy of a given level α.

Thus, the field can induce transitions only in the composite system AA', implying that excitation can occur only if there is an $A-A'$ collision during the on-time of the light pulse. Let us suppose that such a collision occurs, centered at time $t=t_c$, position $\vec{R}=\vec{R}_c$, and is characterized by a collision duration $\tau_c = b/v$, where b is the impact

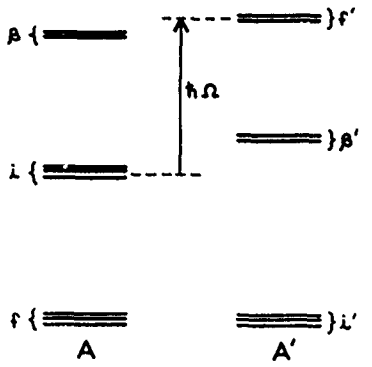

FIG. 1. Energy levels for the atoms A and A' under consideration. The groups of levels represented by a single letter are degenerate or near degenerate, with a maximum frequency separation ω_g such that $\omega_g\tau_c \ll 1$ (τ_c = duration of a collision). The field frequency Ω is such that $\hbar\Omega \approx E_f + E_{f'} - (E_i + E_{i'})$.

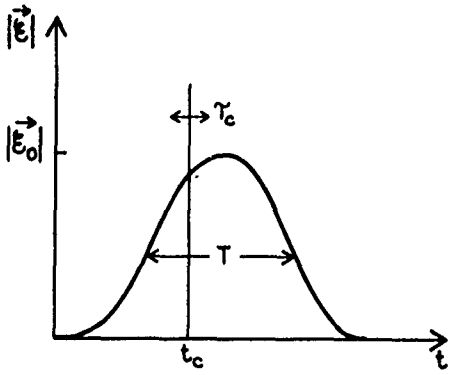

FIG. 2. Field-pulse envelope as a function of time. A collision occurs, centered in time at $t=t_c$, with a duration $\tau_c \ll T$.

parameter and v_r the relative atomic speed associated with the collision. Collision durations are on the order of 10^{-12} sec so that it is reasonable to assume that

$$\tau_c \ll T, \qquad (4)$$

since pulse durations $T \gtrsim 1.0$ nsec are typical. Thus, excitation occurs on the time scale τ_c; on this time scale, the field amplitude $\vec{\mathcal{E}}(\vec{R},t)$ is essentially constant and may be evaluated as $\vec{\mathcal{E}}(\vec{R}_c,t_c)$ (Fig. 2). In calculating excitation probabilities, it is generally necessary to average over all possible t_c and $\vec{R}_c$ during the light pulse and to average over all collision impact parameters, orientations, and relative speeds. The average over $\vec{R}_c$ is equivalent to an average over the spatial profile of the light pulse.

The following assumptions are adopted: (1) Collisional excitation exchange between atoms A and A' does not occur in the absence of the light field (i.e., all such exchange processes are assumed to be nonresonant). (2) The frequency ω_g is chosen such that

$$\omega_g \tau_c \ll 1, \qquad (5)$$

ensuring that all sublevels in a given group are, in effect, degenerate during a collision. (3) There is no population decay or buildup of Doppler phase during a collision; that is,

$$\gamma\tau_c \ll 1, \quad ku\tau_c \ll 1, \qquad (6)$$

where γ is a decay rate associated with the initial or final states, $\vec{k}$ is a wave vector associated with the field, and u is an atomic speed. (4) Each atom undergoes, at most, one collision, on average, during the pulse time T, enabling one to ignore multiple-collision effects [valid for densities $\ll 10^{19}$ atoms/cm^3 T (nsec)]. (5) The collision trajectory is treated classically, which implies that the change in kinetic energy resulting from

RAIC is small, i.e., that

$$|\omega_{fi}+\omega_{f'i'}-\Omega|\tau_c \lesssim 1, \tag{7}$$

where

$$\omega_{\alpha\beta}=\omega_\alpha-\omega_\beta, \quad \omega_\alpha=E_\alpha/\hbar. \tag{7a}$$

If condition (7) were not satisfied, one could not assign a unique classical trajectory to the collision.

To summarize, I am considering the radiatively assisted collisional reaction

$$A_i+A'_{i'}+\hbar\Omega \rightarrow A_f+A'_{f'}$$

from initial states $|ii'\rangle$ to final states $|ff'\rangle$, in which the photon is provided by an electromagnetic pulse. Several assumptions relating to the time scales in the problem have been made which are valid for many systems of practical interest. All information on final-state coherence is contained in the density matrix following the RAIC. The final-state density matrix for one of the atoms can be obtained by taking the trace of the final-state density matrix for the composite system over the final-state variables of the other atom. Experimentally, it is generally such a single-particle density matrix that is monitored (e.g., by fluorescence from the final state of one of the atoms).

III. EQUATIONS OF MOTION

By assumption, the collision trajectory is treated classically. That is, relative to a fixed laboratory frame, a collision is characterized by an impact parameter b, relative speed $v_r=|\vec{v}-\vec{v}'|$ ($\vec{v}$ and $\vec{v}'$ being, respectively, the velocities of atoms A and A'), and orientation Θ relative to the fixed frame. The Hamiltonian for the RAIC can be written

$$H(t;b,v_r,\Theta,\vec{R}_c,t_c)=H_0(\vec{r})+H'_0(\vec{r}') - \tfrac{1}{2}(\vec{\mu}+\vec{\mu}')\cdot[\vec{\mathcal{E}}(\vec{R}_c,t_c)e^{-i\Omega t}+\text{c.c.}] +\mathcal{V}(\vec{r},\vec{r}',\vec{R}(t)), \tag{8}$$

where H_0 and H'_0 are the free-atom Hamiltonians for atoms A and A', respectively, $\vec{\mu}$ and $\vec{\mu}'$ are the dipole-moment operators for atoms A and A', respectively (the atom-field interaction is treated in the dipole approximation), and $\mathcal{V}$ is the A-A' interaction Hamiltonian. The collision is centered in time at $t=t_c$ and $\vec{R}_c$ is the position of the center of mass of the atoms when $t=t_c$. All effects of atomic motion are contained implicitly in the interatomic separation $\vec{R}(t)$, calculated for a classical trajectory. In writing the approximate Hamiltonian (8), conditions (4), (6), and (7) were used.

According to the assumptions of Sec. II, states $|ii'\rangle$ can be coupled only to states $|i_1i'_1\rangle$ (i_1 is another state in the i group) or to states $|ff'\rangle$. The corresponding equations of motion for the probability amplitudes $a_{ii'}(t)$, $a_{ff'}(t)$ (in the interaction representation), as derived in Appendix A starting from the Schrödinger equation with the Hamiltonian (8), are given by

$$i\hbar\dot{a}_{ii'}=\sum_{i_1i'_1}\langle ii'|\hat{S}(ii';t,b,v_r,\Theta,\vec{R}_c,t_c)|i_1i'_1\rangle a_{i_1i'_1} + \sum_{ff'}\langle ii'|\hat{T}(ff',ii';t,b,v_r,\Theta,\vec{R}_c,t_c)|ff'\rangle e^{i\Delta t}a_{ff'}, \tag{9a}$$

$$i\hbar\dot{a}_{ff'}=\sum_{f_1f'_1}\langle ff'|\hat{S}(ff';t,b,v_r,\Theta,\vec{R}_c,t_c)|f_1f'_1\rangle a_{f_1f'_1} + \sum_{ii'}\langle ff'|\hat{T}(ii',ff';t,b,v_r,\Theta,\vec{R}_c,t_c)|ii'\rangle e^{-i\Delta t}a_{ii'}, \tag{9b}$$

where the detuning Δ is defined by

$$\Delta=\Omega-(\omega_{fi}+\omega_{f'i'}), \tag{10}$$

and the operators $\hat{S}$ and $\hat{T}$ are defined below.

The operator $\hat{S}(\alpha\alpha';t,b,v_r,\Theta,\vec{R}_c,t_c)$ is an operator that acts *only* in the $\alpha\alpha'$ subspace ($\alpha\alpha'=ii'$ or ff'); it shifts and couples levels within that subspace. Explicitly (see Appendix A),

$$\hat{S}(\alpha\alpha';t,b,v_r,\Theta,\vec{R}_c,t_c)=\hat{S}_L+\hat{S}_c, \tag{11}$$

$$\hat{S}_L=\frac{-1}{4\hbar}\sum_{\beta\beta'}\left(\frac{\vec{\mu}_T\cdot\vec{\mathcal{E}}(\vec{R}_c,t_c)^*|\beta\beta'\rangle\langle\beta\beta'|\vec{\mu}_T\cdot\vec{\mathcal{E}}(\vec{R}_c,t_c)}{\omega_{\beta\alpha}+\omega_{\beta'\alpha'}-\Omega}+\frac{\vec{\mu}_T\cdot\vec{\mathcal{E}}(\vec{R}_c,t_c)|\beta\beta'\rangle\langle\beta\beta'|\vec{\mu}_T\cdot\vec{\mathcal{E}}(\vec{R}_c,t_c)^*}{\omega_{\beta\alpha}+\omega_{\beta'\alpha'}+\Omega}\right), \tag{11a}$$

$$\hat{S}_c=-\hbar^{-1}\sum_{\beta\beta'}\frac{\mathcal{V}(\vec{R}(t))|\beta\beta'\rangle\langle\beta\beta'|\mathcal{V}(\vec{R}(t))}{\omega_{\beta\alpha}+\omega_{\beta'\alpha'}}, \tag{11b}$$

where

$$\vec{\mu}_T = \vec{\mu} + \vec{\mu}' . \tag{12}$$

The operator $\hat{S}$ may appear to be complicated, but it has a well-known physical interpretation. The term $\hat{S}_L$ involves only field variables and gives rise to the shifting (light shifts) and coupling of $\alpha\alpha'$ levels produced by an *off-resonant* external electromagnetic field. The summation over intermediate states $\beta\beta'$ represents the virtual excitation of these levels by the field. The term $\hat{S}_c$ [Eq. (11b)] involves only collision variables and gives rise to collisionally induced shifting and coupling of levels in the $\alpha\alpha'$ group. The shift of the levels is the origin of the pressure broadening and shifting of spectral lines, while the coupling within the $\alpha\alpha'$ group leads to collisionally induced relaxation of any alignment, orientation, etc., that may be present in that group of levels. Again one finds a summation over an infinite number of virtual excitations $|\beta\beta'\rangle$.

The transition operator $\hat{T}$ that couples groups of states $|ii'\rangle$ to $|ff'\rangle$ is given by (see Appendix A)

$$\hat{T}(ii',ff';t,b,v_r,\Theta,\vec{R}_c,t_c) = \frac{1}{2\hbar}\sum_{\beta\beta'}\left(\frac{\mathfrak{u}(\vec{R}(t))|\beta\beta'\rangle\langle\beta\beta'|\vec{\mu}_T}{\omega_{\beta f}+\omega_{\beta' f'}} + \frac{\vec{\mu}_T|\beta\beta'\rangle\langle\beta\beta'|\mathfrak{u}(\vec{R}(t))}{\omega_{\beta i}+\omega_{\beta' i'}}\right)\cdot\vec{\mathcal{E}}(\vec{R}_c,t_c) \tag{13}$$

and represents the combined effect of the (field + collision) in producing the transition from initial to final states. The corresponding transition operator which couples states $|ff'\rangle$ to $|ii'\rangle$ is given by[9]

$$\hat{T}(ff',ii';t,b,v_r,\Theta,\vec{R}_c,t_c) = \frac{1}{2\hbar}\sum_{\beta\beta'}\left(\frac{\vec{\mu}_T|\beta\beta'\rangle\langle\beta\beta'|\mathfrak{u}(\vec{R}(t))}{\omega_{\beta f}+\omega_{\beta' f'}} + \frac{\mathfrak{u}(\vec{R}(t))|\beta\beta'\rangle\langle\beta\beta'|\vec{\mu}_T}{\omega_{\beta i}+\omega_{\beta' i'}}\right)\cdot\vec{\mathcal{E}}(\vec{R}_c,t_c)^* . \tag{14}$$

Note that the matrix elements of $\hat{T}$ appearing in Eq. (9) are related by

$$\langle ii'|\hat{T}(ff',ii';t)|ff'\rangle = \langle ff'|T(ii',ff';t)|ii'\rangle^* . \tag{15}$$

A diagrammatic interpretation of $\hat{S}$ and $\hat{T}$ is given in Appendix B.

To obtain the RAIC excitation probability, one must solve Eqs. (9) for $a_{ff'}(t_c^+)$ subject to the initial conditions

$$a_{ii'}(t_c^-)\neq 0, \quad a_{ff'}(t_c^-)=0 , \tag{16}$$

where $t_c^-(t_c^+)$ are times before (after) the collision. Since $\tau_c \ll T$ [Eq. (4) or Fig. 2], the times $t_c^\pm$ can be set equal to $\pm\infty$ when integrating Eqs. (9) without introducing significant error.

The validity conditions for Eqs. (9) are discussed in detail in Appendix A. If

$$\bar{\omega}\tau_c \gg 1 , \tag{17}$$

where $\bar{\omega}$ is any of the frequency denominators appearing in the operators $\hat{T}$ and $\hat{S}$, and if Eqs. (3)–(7) are satisfied, then Eqs. (9) are valid over a wide range of field strengths.[10] Condition (17) ensures that the intermediate states act only as *virtual* levels in the RAIC problem. The virtual excitations are represented by the summations over β and β' in the $\hat{S}$ and $\hat{T}$ operators, and the problem is reduced to an effective two groups of levels problem for the states $|ii'\rangle$ and $|ff'\rangle$. It should be noted that Eqs. (9) reduce to the corresponding equations derived by other authors in various limiting cases.[5]

IV. FORMAL SOLUTION

It is useful to make use of Eq. (15) and to rewrite Eqs. (9) in matrix form as

$$i\hbar\dot{\vec{a}}_I = S(I,t)\vec{a}_I + [T(IF,t)]^\dagger e^{i\Delta t}\vec{a}_F , \tag{18a}$$

$$i\hbar\dot{\vec{a}}_F = S(F,t)\vec{a}_F + T(IF,t)e^{-i\Delta t}\vec{a}_I , \tag{18b}$$

$$\vec{a}_I(t_c^-)\neq 0, \quad \vec{a}_F(t_c^-)=0 , \tag{18c}$$

where $\vec{a}_I$ ($\vec{a}_F$) is a vector containing all possible states $|ii'\rangle$ ($|ff'\rangle$) in the initial (final) group of levels and $S(I,t)$, $S(F,t)$, and $T(IF,t)$ are matrix representations of the corresponding operators appearing in Eqs. (9). A solution of the form

$$\vec{a}_K(t) = G_K(t,t_c^-)\vec{A}_K(t), \quad K=I,F \tag{19}$$

is sought, where the matrix $G_K(t,t')$ is chosen to satisfy the equations

$$i\hbar\frac{\partial G_K(t,t')}{\partial t} = S(K,t)G_K(t,t') , \tag{20a}$$

$$G_K(t,t)=1, \quad K=I,F \tag{20b}$$

and the symbols I and F represent the entire ii' and ff' subspaces, respectively. Substituting Eqs. (19) and (20) into Eqs. (18) and making use of the relations

$$\begin{aligned}&(G_K(t,t'))^{-1} = G_K(t',t) ,\\ &G_K(t,t_1)G_K(t_1,t_2) = G_K(t,t_2) ,\end{aligned} \tag{21}$$

which follow directly from Eqs. (19) and (20), one obtains

$$i\hbar\dot{\vec{A}}_I = G_I(t_c^-,t)(T(IF,t))^\dagger G_F(t,t_c^-)e^{i\Delta t}\vec{A}_F , \tag{22a}$$

$$i\hbar\dot{\vec{A}}_F = G_F(t_c^-, t)T(IF, t)G_I(t, t_c^-)e^{-i\Delta t}\vec{A}_I, \quad (22b)$$

$$\vec{A}_I(t_c^-) = \vec{a}_I'(t_c^-), \quad \vec{A}_F(t_c^-) = 0. \quad (22c)$$

In this form, all effects of shifting and coupling within the ii' and ff' subspaces are contained in the matrices $G_I(t, t')$ and $G_F(t, t')$, respectively.

Once a solution to Eqs. (22) is found, final-state density matrix elements of the form

$$\tilde{\rho}_{ff';f_1f_1'}(t_c^+; b, v_r, \Theta, \vec{R}_c, t_c) = a_{ff'}(t_c^+)[a_{f_1f_1'}(t_c^+)]^* = [G_F(t_c^+, t_c^-)\vec{A}_F(t_c^+)]_{ff'}[G_F(t_c^+, t_c^-)\vec{A}_F(t_c^+)]^*_{f_1f_1'} \quad (23)$$

may be constructed (the tilde is a reminder that results are expressed in the interaction representation). The (complex) rate at which RAIC create density matrix elements $\tilde{\rho}_{ff';f_1f_1'}(t_c^+; v_r, t_c)$ at time t_c during the light pulse for atoms A and A' having relative speed v_r starting from an initial density matrix element $\tilde{\rho}_{ii';i_1i_1'}(t_c^-)$ is given by

$$\Gamma^{II_1}_{FF_1}(v_r, t_c) = \mathfrak{N}_A\mathfrak{N}_{A'}v_r\int_0^\infty 2\pi b\,db\int(8\pi^2)^{-1}d\Theta\int d\vec{R}_c\,\frac{d[\tilde{\rho}_{FF_1}(t_c^+; b, v_r, \Theta, \vec{R}_c, t_c)]}{d[\tilde{\rho}_{II_1}(t_c^-)]}, \quad (24)$$

where $\mathfrak{N}_\alpha$ is the α-atom density (assumed to be independent of position) and the shorthand notation

$$I = ii', \quad F = ff', \quad I_1 = i_1i_1', \quad F_1 = f_1f_1', \quad (25)$$

etc., has been adopted. The integral over $\vec{R}_c$ in Eq. (24) is limited to the interaction region of the atoms and light field; it is essentially an integration over the spatial profile of the light beam.

Thus, *during the light pulse*, the density matrix evolves as

$$\frac{\partial\tilde{\rho}_{FF_1}(\vec{v}, \vec{v}', t_c)}{\partial t_c} = \sum_{II_1}\Gamma^{II_1}_{FF_1}(v_r, t_c)\tilde{\rho}_{II_1}(\vec{v}, \vec{v}', t_c) + [\tilde{X}(t_c)\tilde{\rho}(v, v', t_c)]_{FF_1}, \quad (26)$$

where $\vec{v}_r = \vec{v} - \vec{v}'$. The assumption that an atom undergoes at most one collision during the light pulse is contained implicitly in Eq. (26), otherwise, terms such as

$$\Gamma^{F_2F_3}_{FF_1}\tilde{\rho}_{F_2F_3}$$

would be present. The term with $\tilde{X}(t_c)$ represents changes produced by processes *other* than RAIC (i.e., level decay, other external fields, etc.).[11] It is an equation of the form (26) *plus* a corresponding equation for times when the light pulse is *off* which must be solved in order to make connection with a given experimental situation (of course, there are no RAIC terms in the equations with the field off). For example, if the pulse time T is short enough so that the bracketed term in Eq. (26) may be neglected, then the final-state density matrix following the light pulse is simply

$$\tilde{\rho}_{FF_1}(\vec{v}, \vec{v}', T^+) = \sum_{II_1}\left(\int_{T^-}^{T^+}\Gamma^{II_1}_{FF_1}(v_r, t_c)dt_c\right)\times\tilde{\rho}_{II_1}(\vec{v}, \vec{v}', T^-), \quad (27)$$

where $T^-(T^+)$ indicates a time just before (after) the pulse. One can then monitor the final-state density matrix via absorption or emission experiments to obtain values for the various rates $\Gamma^{II_1}_{FF_1}$. For longer pulse times T, it may be necessary to integrate Eq. (26) to obtain the net effect of the light pulse.

To be consistent with other authors, I define a RAIC transfer rate per pulse from some initial state described by $\tilde{\rho}_{II_1}$ to a final state described by $\tilde{\rho}_{FF_1}$ as

$$\Gamma^{II_1}_{FF_1}(v_r) = \frac{1}{T^+ - T^-}\int_{T^-}^{T^+}\Gamma^{II_1}_{FF_1}(v_r, t_c)dt_c \quad (28)$$

and a RAIC transfer cross section per pulse by

$$\sigma^{II_1}_{FF_1}(v_r) = \Gamma^{II_1}_{FF_1}(v_r)\Big/\left(\mathfrak{N}_A\mathfrak{N}_{A'}v_r\int d\vec{R}_c\right), \quad (29)$$

where the $\vec{R}_c$ integration is over the interaction volume.[12] The rate and cross section for transfer of *population* from some initial state $|I\rangle$ to a final state $|F\rangle$ is obtained by setting $I_1 = I$, $F_1 = F$ in Eqs. (28) and (29). Finally, one can define an average RAIC rate and cross section by

$$\bar{\Gamma}(v_r) = \frac{1}{N_I}\sum_{II}\Gamma^{II}_{FF}(v_r), \quad (30a)$$

$$\bar{\sigma}(v_r) = \frac{1}{N_I}\sum_{II}\sigma^{II}_{FF}(v_r), \quad (30b)$$

where N_I is the number of initial states. Equation (30b) defines a quantity that has been typically referred to as the RAIC cross section.[5]

V. DISCUSSION

In general, it is difficult to obtain solutions to Eqs. (22) and perform the necessary averaging

over collision orientations. However, certain general features of the solutions may be understood by examining some of the limiting forms of these equations.

A. Nondegenerate levels

In this limit, the matrices S and T in Eqs. (18) become scalars. Equation (20) is easily integrated and one finds that Eqs. (22) take the form

$$i\hbar\dot{A}_I = T(IF,t)^* \exp\{i[\Delta t - \varphi_c(t)]\}A_F , \tag{31a}$$

$$i\hbar\dot{A}_F = T(IF,t) \exp\{-i[\Delta t - \varphi_c(t)]\}A_I , \tag{31b}$$

where

$$\varphi_c(t) = \int_{t_c^-}^{t} [S(F,t') - S(I,t')]\,dt' \tag{32}$$

and I and F are nondegenerate states. The phase $\varphi_c(t)$ contains the effects of the level shifts produced by the off-resonant light field and the collisional interaction. Equations (31) have been studied by many authors using a variety of analytical and numerical techniques.[5,13] The resulting RAIC profile exhibits a marked asymmetry for large $|\Delta|$, resulting from the action of the level-shifting term. For one sign of Δ, the I-F transition can be brought into instantaneous resonance with the field during a collision, leading to enhanced excitation; for the other sign of Δ, no such instantaneous resonance is possible. Equations (31) also contains saturation effects which can appear for large field strengths or small impact parameters.

B. Perturbation-theory limit

By neglecting the level-shifting terms in Eqs. (22) and taking $\Delta = 0$, one can estimate that a perturbation solution is valid provided

$$\frac{|\mathcal{U}(t=t_c)|\tau_c\chi}{\hbar\bar{\omega}} \ll 1 , \tag{33}$$

where $\mathcal{U}(t=t_c)$ is the interatomic potential at the time of closest approach, $\tau_c = b/v_r$ is the collision time, χ is a Rabi frequency (e.g., $\chi = \langle\beta'|\mu'|f\rangle|\mathcal{E}|/2\hbar$), and $\bar{\omega}$ is some characteristic frequency denominator appearing in the transition operator $\hat{T}$ [Eq. (13)]. For nonzero Δ, Eq. (33) is replaced by a less severe condition. Since $|\mathcal{U}(t=t_c)|\tau_c/\hbar \approx 1$ in the range of impact parameters that contributes to excitation,[14] the perturbation theory fails for field strengths $\chi \gtrsim \bar{\omega}$. Regardless of field strength, inequality (33) always fails to hold for sufficiently small impact parameters [$\mathcal{U}(t=t_c)$ varies typically as b^{-n}]; this domain can be treated by using a cutoff procedure.[5]

In the perturbation-theory limit, Eq. (22b) can be integrated directly after setting $\vec{A}_I(t) = \vec{a}_I(t_c^-)$. Using Eqs. (22), (19), and (21), one may obtain

$$\vec{a}_F(t_c^+) = (i\hbar)^{-1} \int_{t_c^-}^{t_c^+} G_F(t_c^+,t')T(IF,t') \times G_I(t',t_c^-)e^{-i\Delta t'}\vec{a}_F(t_c^-)\,dt' . \tag{34}$$

To be consistent with the perturbation-theory limit, the contributions to G_F and G_I arising from the light-shift operator should be neglected. Equation (34) may be given a simple interpretation. Starting in the state represented by $\vec{a}_I(t_c^-)$, one has a mixing and shifting of the initial levels from time $t = t_c^-$ to time $t = t'$ [represented by $G_I(t',t_c^-)$], a transition from initial to final state at time $t = t'$ [represented by $T(IF,t')$] and a mixing and shifting of final-state levels from time $t = t'$ to time $t = t_c^+$ [represented by $G_F(t_c^+,t')$]; an integration over all possible t' is included. Thus, it appears that reorientation effects in the initial and final states are correlated with both the shifting of these levels and the changes that occur in the $I \rightarrow F$ transition. In particular, if there are times at which instantaneous resonances occur for a given detuning $|\Delta|\tau_c \gtrsim 1$, the T matrix can be evaluated at such times and the integral (34) evaluated by a stationary-phase method. This condition can help to simplify the calculations, although the average over collision orientations can still pose considerable problems. Experimentally, one should expect to find a variation-of final-state coherence as a function of detuning.

C. Perturbation theory neglecting level shifts

Additional simplifications of Eq. (34) are possible for a range of impact parameters if one limits the detuning to the impact core of the RAIC profile ($|\Delta|\tau_c \ll 1$). If $|\Delta|\tau_c \ll 1$, the effects of instantaneous resonances are not important, since the phase factor $\exp(i\Delta t)$ is slowly varying; all times t' in the range (t_c^-, t_c^+) contribute to the integral in Eq. (34). Since the matrix S is quadratic in the collision interaction potential while the T matrix is linear in it, there exists a range of impact parameters where one can neglect the collisional contributions to S. Contributions to S from the light field have already been neglected owing to the perturbation-theory limit. Thus, in this limit where all level shifting and mixing in the initial and final states are ignored, $S(I,t) = S(F,t) = 0$ and, $G_I(t,t') = G_F(t,t') = 1$. Equation (34) reduces to

$$\vec{a}_F(t_c^+) = (i\hbar)^{-1} \int_{t_c^-}^{t_c^+} dt'\, T(IF,t')e^{-i\Delta t'}\vec{a}_I(t_c^-) . \tag{35}$$

This expression is evaluated explicitly in the following paper, where the appropriate averaging over collision orientations and impact parameters is carried out. Since the interatomic potential appears linearly in Eq. (35) and, consequently, bilinearly in Eqs. (23) and (24), the averaging over collision orientations is easily performed using techniques involving irreducible tensor operators. One can show that the collsion produces the same type of final-state coherence properties that would be produced by replacing the collision by an unpolarized field having the same multipolar properties as the collision operator (e.g., a dipole collision operator is replaced by an unpolarized electric field). This result is not difficult to understand. Excitation is produced in a single collision; when averaged over all collision orientations, the net effect is similar to that produced by an unpolarized field of the corresponding multipolarity.

It is relatively easy in this case to predict the final-state coherence properties for various polarizations of the external field. The final-state coherence may be observed by monitoring the polarization of fluorescence or the quantum beats originating from one of the final states.

D. General case

If perturbation theory fails (power densities $\gtrsim 10^{10}$ W/cm^2), the solutions of Eqs. (22) exhibit saturation effects. Unless a way can be found to perform the averaging over collision orientations and beam intensity profiles, one is faced with the costly task of integrating Eqs. (22) numerically as a function of collision orientation Θ and field amplitude $\mathcal{E}(\vec{R}_c, t_c)$. There has been limited work in this area, although a few related calculations have appeared.[7]

A general formalism for calculating the final-state coherences produced by radiatively-assisted inelastic collisions has been given. In the following paper, the RAIC transfer cross section is calculated in the perturbation-theory limit, neglecting level-shifting effects. In future work, it is hoped that the more general problem will be addressed.

ACKNOWLEDGMENT

This work was carried out while I was a guest at the Laboratoire Aimé Cotton, Orsay, France. The hospitality shown to me during my stay is gratefully acknowledged. I should also like to acknowledge financial support from the Fulbright Foundation. This research was also supported by the U. S. Office of Naval Research.

APPENDIX A

In this appendix, starting from the Hamiltonian (8) and using the assumptions of Sec. II, I derive Eqs. (9). The wave vector is written as

$$|\Psi(t)\rangle = \sum_M a_M(t) e^{-i\omega_M t} |M\rangle , \tag{A1}$$

where

$$|M\rangle = |mm'\rangle = |m\rangle |m'\rangle' ,$$
$$\omega_M = \omega_m + \omega_{m'} ,$$

and (ω_m and $\omega_{m'}$) and ($|m\rangle$ and $|m'\rangle'$) are eigenfrequencies and eigenkets of free atoms A and A', respectively [i.e., eigenfrequencies and eigenkets of the Hamiltonians $H_0(\vec{r})$ and $H_0'(\vec{r}')$, respectively, appearing in Eq. (8)]. I adopt the notation that a captial Roman letter represents a composite state of the AA' system [e.g., $|I\rangle = |ii'\rangle$, $\omega_{F_1} = \omega_{f_1} + \omega_{f_1'}$, etc.]. Using Schrödinger's equation with the Hamiltonian (8), one can derive the following equation for the probability amplitude (in the interaction representation) $a_M(t)$:

$$i\hbar \dot{a}_M = \{ -\tfrac{1}{2}\langle M|\vec{\mu}_T|B\rangle \cdot [\vec{\mathcal{E}} e^{-i\Omega t} + \vec{\mathcal{E}}^* e^{i\Omega t}] + \langle M|\mathcal{U}(t)|B\rangle \} e^{i\omega_{MB} t} a_B , \tag{A2}$$

where $\vec{\mu}_T = \vec{\mu} + \vec{\mu}'$, $\omega_{MB} = \omega_M - \omega_B$, and the summation convention is used.

According to the assumptions of Sec. II, the only states that are significnatly coupled are $|I\rangle$ and $|F\rangle$. However, this coupling does not yet appear directly in Eq. (A2) since the I-F coupling is via virtual intermediate states. To see the coupling directly, one writes Eq. (A2) for $\dot{a}_F$, replacing the a_B which appears on the right-hand side of this equation by the value obtained by formally integrating Eq. (A2) for $\dot{a}_B$. In this way, one finds

$$i\hbar \dot{a}_F = e^{i\omega_{FB} t} [-\tfrac{1}{2}\langle F|\vec{\mu}_T|B\rangle \cdot (\vec{\mathcal{E}} e^{-i\Omega t} + \vec{\mathcal{E}}^* e^{i\Omega t}) + \langle F|\mathcal{U}(t)|B\rangle] \times \left(a_B(t_c^-) + (i\hbar)^{-1} \int_{t_c^-}^{t} dt' \, e^{i\omega_{BM} t'} [-\tfrac{1}{2}\langle B|\vec{\mu}_T|M\rangle \cdot (\vec{\mathcal{E}} e^{-i\Omega t'} + \vec{\mathcal{E}}^* e^{i\Omega t'}) + \langle B|\mathcal{U}(t')|M\rangle] a_M(t') \right) . \tag{A3}$$

The term proportional to $a_B(t_c^-)$ can be neglected using the assumption that the field and collision must act *simultaneously* to produce a transition. The validity conditions for the neglect of this term are

$$\bar{\omega}_c T \gg 1 , \quad \bar{\omega}_c \tau_c \gg 1 , \tag{A4}$$

where $\bar{\omega}_c$ and $\bar{\omega}_c$ are some appropriate frequency

mismatches for the atom-field and atom-atom interactions, respectively.[15]

The integral term in Eq. (A3) is treated as follows: (1) The only terms $a_M(t')$ of importance are assumed to be $a_{F_1}(t')$ and $a_I(t')$, where $|F_1\rangle$ is in the final-state group of levels. This assumption is equivalent to asserting that there is negligible population in all states outside the I and F groups (i.e., that there are only *virtual* excitations of the intermediate states). For this approximation to be valid one must again require conditions (A4) to hold. In addition, one must require that the cross section for transfer within a *given* atom from either its initial or final state to some intermediate state be negligible. This cross section is precisely that associated with collisionally-aided radiative excitation (CARE).[4] For $\bar{\omega}_c\tau_c \gg 1$ and $\chi \ll \bar{\omega}_c$, CARE is unimportant. However, CARE may become significant in the strong-field regime $\chi \approx \bar{\omega}_c$; in that case, one would have to expand the basis to include those states coupled to either $|I\rangle$ or $|F\rangle$ by CARE. (2) Antiresonance terms in Eq. (A3) varying as $\exp[\pm i(\omega_{FI}+\Omega)t]$ or $\exp(\pm 2i\Omega t)$ are neglected. (3) The functions $\langle B|\mathcal{U}(t')|M\rangle$ and $a_M(t')$ are assumed to be slowly varying with respect to the exponential factors and are evaluated at time $t'=t$. For this assumption to be valid, one must have

$$\bar{\omega}_c\tau_c \gg 1, \quad \omega_c\tau_c \gg 1. \tag{A5}$$

There is a supplementary condition which must also be satisfied related to the time variation of $a_I(t')$ (see below). (4) Frequency differences $\omega_{FF_1}, \omega_{II_1}$ are neglected with respect to $\bar{\omega}_c$ or $\bar{\omega}_c$ and factors such as $\exp(i\omega_{II_1}t)$ or $\exp(i\omega_{FF_1}t)$ are set equal to unity. These approximations are valid owing to Eqs. (5) and (A5).

With these assumptions, one can easily carry out the integration in Eq. (A3) and obtain

$$i\hbar\dot{a}_F = \left[-\frac{1}{4\hbar}\left(\frac{\langle F|\vec{\mu}_T|B\rangle\cdot\vec{\mathcal{E}}^*\langle B|\vec{\mu}_T|F_1\rangle\cdot\vec{\mathcal{E}}}{\omega_{BF}-\Omega} + \frac{\langle F|\vec{\mu}_T|B\rangle\cdot\vec{\mathcal{E}}\langle B|\vec{\mu}_T|F_1\rangle\cdot\vec{\mathcal{E}}^*}{\omega_{BF}+\Omega}\right) - \frac{1}{\hbar}\frac{\langle F|\mathcal{U}(t)|B\rangle\langle B|\mathcal{U}(t)|F_1\rangle}{\omega_{BF}}\right]a_{F_1}$$
$$+\frac{1}{2\hbar}\left(\frac{\langle F|\vec{\mu}_T|B\rangle\langle B|\mathcal{U}(t)|I\rangle}{\omega_{BI}} + \frac{\langle F|\mathcal{U}(t)|B\rangle\langle B|\vec{\mu}_T|I\rangle}{\omega_{BF}-\Delta}\right)\cdot\vec{\mathcal{E}}e^{-i\Delta t}a_I, \tag{A6}$$

where there is no sum on F and Δ is defined by Eq. (10). The quantity Δ appearing in the frequency denominator can be neglected in comparison with ω_{BF} and it should be dropped for consistency (see below). Equation (A6) is then identical to Eqs. (9b), (11), and (13), using the notation $I=ii'$, $F=ff'$, $B=\beta\beta'$, and $F_1=f_1f_1'$. Similarly, Eq. (9a) can be verified.

Finally, one can check to see if $a_I(t)$ is slowly varying compared with $\exp(i\bar{\omega}t)$ as has been assumed ($\bar{\omega}=\bar{\omega}_c$ or $\bar{\omega}_c$). By examining Eqs. (9), one can deduce that $|\dot{a}_I/a_I|_{\max}$ is given by the largest of either $|\Delta|$, $\omega_c=1/\tau_c$, or $\hbar\mathcal{U}(t=t_c)\chi/\bar{\omega}$, where χ is a Rabi frequency in the problem. Thus, in order to neglect all but the groups I and F, one must have

$$\bar{\omega}/|\Delta| \gg 1, \quad \bar{\omega}\tau_c \gg 1,$$
$$\left[\frac{|\mathcal{U}(t=t_c)|\tau_c}{\hbar}\left(\frac{\chi}{\bar{\omega}}\right)\right]\frac{1}{\bar{\omega}\tau_c} \ll 1. \tag{A7}$$

Note that one may retain a consistent solution even in the strong-field limit, $\hbar^{-1}|\mathcal{U}(t=t_c)|\tau_c\chi/\bar{\omega} \gtrsim 1$, provided that $\bar{\omega}\tau_c$ is large enough to assure the validity of the last inequality in conditions (A7).

APPENDIX B

A simple diagrammatic interpretation of the operators $\hat{T}$ and $\hat{S}$ appearing in Eqs. (9) can be given. The interaction between the field and the atoms is represented by

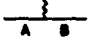

(B1)

The field takes the atom from the composite state $A=\alpha\alpha'$ to $B=\beta\beta'$. Actually this diagram may be thought of as the sum of two diagrams,

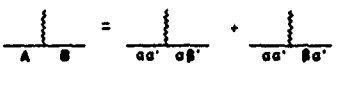

in which the field acts on each atom separately. The collisional interaction is represented by

(B2)

taking the atoms from states A to B.

With these definitions, it is relatively easy to draw the diagrams corresponding to the operators $\hat{S}_L$, $\hat{S}_c$ and $\hat{T}(IF)$ appearing in Eqs. (11) and (13), and these are shown in Fig. 3. Figure 3(a) corresponds to the light-shift operator $\hat{S}_L(F)$ which acts

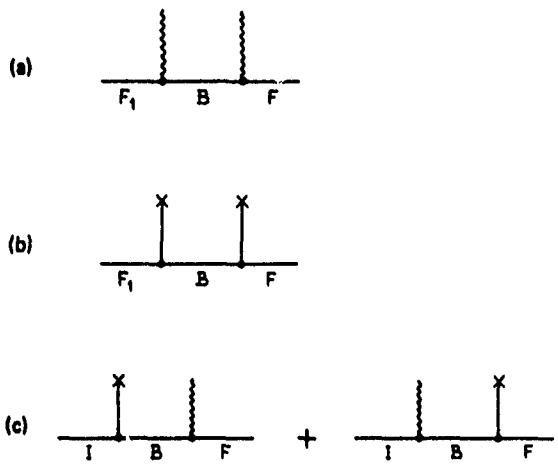

FIG. 3. Diagrammatic interpretation of the operators (a) $\hat{S}_L(F)$, (b) $\hat{S}_c(F)$, and (c) $\hat{T}(IF)$. In each diagram a wavy-line vertex refers to an atom-field interaction and a straight-line vertex to a collisional interaction.

in the final-state subspace [a similar diagram can be drawn for $\hat{S}_L(I)$]. The field excites either of the atoms to some intermediate virtual state and then de-excites the atom back to the final-state manifold. Figure 3(b) corresponds to the collisional operator $\hat{S}_c(F)$; the collision excites the atoms to some intermediate state $B=\beta\beta'$ and then de-excites them to the final-state manifold. Finally, Fig. 3(c) corresponds to the operator $\hat{T}(IF)$. The field and collision combine to excite the atoms from initial state I to final state F via the virtual intermediate state B. These diagrams immediately illustrate the nature of the operators appearing in the RAIC equations (i.e., $\hat{S}_L$ varies as $|\mathcal{E}|^2$, $\hat{S}_c$ as $\mathcal{U}^2$, and $\hat{T}$ as $\mathcal{U}\mathcal{E}$).

It is also possible to directly construct the operators from the diagrams. More precisely, the following rules enable one to calculate the matrix representation of the operators in the interaction representation.

(1) Assign a factor $(-1)^{N-1}$ (N=number of vertices) and a factor $e^{i\omega_{GH}t}$ (G=final state, H=initial state) to each diagram.

(2) Each vertex of the form (B1) is assigned the value $-\langle B|\vec{\mu}_T\cdot\vec{E}(t)|A\rangle$, where $\vec{E}(t)$ is given by Eq. (2). Each vertex of the form (B2) is assigned the value $\langle B|\mathcal{U}(t)|A\rangle$.

(3) In the resulting expression, reject all rapidly varying terms (e.g., terms varying as $\exp(\pm 2i\Omega t)$ or $\exp[\pm i(\Omega+\omega_{FI})t]$).

(4) For a vertex of the form (B1) assign an energy denominator $\hbar(\omega_{BI}\pm\Omega)$, with the (+) sign used if $\vec{\mathcal{E}}$ appears in the B-A matrix element and the (−) sign if $\vec{\mathcal{E}}^*$ appears in the B-A matrix element. For a vertex of the form (B2) assign an energy denominator $\hbar\omega_{BA}$. Energy denominators are assigned for *all but the last vertex* in any diagram.

(5) Sum over all intermediate states.

As an example, I calculate Fig. 3(a) and the second diagram in Fig. 3(c). Following rules (1) and (2) for Fig. 3(a) gives

$$-\tfrac{1}{4}e^{i\omega_{FF}t}\langle B|\vec{\mu}_T\cdot(\vec{\mathcal{E}}e^{-i\Omega t}+\vec{\mathcal{E}}^*e^{i\Omega t})|F_1\rangle \times\langle F|\vec{\mu}_T\cdot(\vec{\mathcal{E}}e^{-i\Omega t}+\vec{\mathcal{E}}^*e^{i\Omega t})|B\rangle .$$

Keeping only the slowly varying terms [rule (3)] yields

$$-\tfrac{1}{4}e^{i\omega_{FF}t}[\langle F|\vec{\mu}_T\cdot\vec{\mathcal{E}}^*|B\rangle\langle B|\vec{\mu}_T\cdot\vec{\mathcal{E}}|F_1\rangle +\langle F|\vec{\mu}_T\cdot\vec{\mathcal{E}}|B\rangle\langle B|\vec{\mu}_T\cdot\vec{\mathcal{E}}^*|F_1\rangle] . \tag{B3}$$

An energy denominator is assigned only to the first vertex and is $\hbar(\omega_{BF}-\Omega)$ for the first term in (B3) (since $\vec{\mathcal{E}}$ appears in the B-F_1 matrix element) and is $\hbar(\omega_{BF}+\Omega)$ for the second term in (B3) (since $\vec{\mathcal{E}}^*$ appears in the B-F_1 matrix element). Therefore,

$$\langle F|\hat{S}_L|F_1\rangle=-\frac{1}{4\hbar}e^{i\omega_{FF}t}\times\left(\frac{\langle F|\vec{\mu}_T\cdot\vec{\mathcal{E}}^*|B\rangle\langle B|\vec{\mu}_T\cdot\vec{\mathcal{E}}|F_1\rangle}{\omega_{BF_1}-\Omega} +\frac{\langle F|\vec{\mu}_T\cdot\vec{\mathcal{E}}|B\rangle\langle B|\vec{\mu}_T\cdot\vec{\mathcal{E}}^*|F_1\rangle}{\omega_{BF_1}+\Omega}\right)$$

in agreement with the first two terms of Eq. (A6) [recall that I set $\exp(i\omega_{FF_1}t)=1$ and $\omega_{BF}\approx\omega_{BF_1}$ in that equation].

Similarly, applying rules (1) and (2) to the second diagram of Fig. 3(c) yields

$$\tfrac{1}{2}e^{i\omega_{FI}t}\langle B|\vec{\mu}_T\cdot(\vec{\mathcal{E}}e^{-i\Omega t}+\vec{\mathcal{E}}^*e^{i\Omega t})|I\rangle\langle F|\mathcal{U}|B\rangle .$$

Keeping the slowly varying term which varies as $\vec{\mathcal{E}}\exp[i(\omega_{FI}-\Omega)t]=\vec{\mathcal{E}}e^{-i\Delta t}$ and applying rules (3)–(5) gives

$$\frac{1}{2\hbar}e^{-i\Delta t}\frac{\langle F|\mathcal{U}|B\rangle\langle B|\vec{\mu}_T\cdot\mathcal{E}|I\rangle}{\omega_{BI}-\Omega},$$

which agrees with the last term of Eq. (A6) since $\omega_{BI}-\Omega=\omega_{BF}-\Delta$.

*Permanent address.

[1]Part of the energy mismatch can also be compensated for by a change in the translational energy of the atoms.

[2]L. I. Gudzenko and S. I. Yakovlenko, Zh. Eksp. Teor. Fiz. 62, 1686 (1972) [Sov. Phys.—JETP 35, 877 (1972)].

[3]Ph. Cahuzac and P. E. Toschek, Phys. Rev. Lett. 40, 1087 (1978).

[4]S. Yeh and P. R. Berman, Phys. Rev. A 19, 1106 (1979).

[5]Extensive lists of references can be found in two recent articles which address the problem of RAIC. See S. I. Yakovlenko, Kvant. Elektron (Moscow) 5, 259 (1978) [Sov. J. Quantum Electron. 8, 151 (1978)]; M. G. Payne, V. E. Anderson, and J. E. Turner, Phys. Rev. A 20, 1032 (1979).

[6]S. E. Harris, J. F. Young, W. R. Green, R. W. Falcone, J. Lukasik, J. C. White, J. R. Willison, M. D. Wright, and G. A. Zdasiuk, in *Laser Spectroscopy IV*, edited by H. Walther and K. W. Rothe (Springer, Berlin, 1979), p. 349 and references therein; C. Bréchignac, Ph. Cahuzac, and P. E. Toschek, Phys. Rev. A 21, 1969 (1980).

[7]S. P. Andreev and V. S. Lisitsa, Zh. Eksp. Teor. Fiz. 72, 73 (1977) [Sov. Phys.—JETP 45, 38 (1977)]; J. Light and A. Szoke, Phys. Rev. A 18, 1363 (1978).

[8]S. E. Harris and J. C. White, IEEE J. Quantum Electron. 13, 972 (1977).

[9]The operator appearing in Eq. (14) appears to be the adjoint of the operator in Eq. (13). However, as defined, these operators act in different spaces [i.e., $\hat{T}(ii';ff')$ is defined to couple only states $|ii'\rangle$ to $|ff'\rangle$, implying $\langle ii'|\hat{T}(ii',ff')|ff'\rangle \equiv 0$].

[10]See Eq. (A7) for a more precise statement of the validity conditions.

[11]In situations where one starts from initial states having a nonthermal velocity distribution, effects of velocity-changing collisions may have to be included in Eq. (26). In that case, the first term on the right-hand side of Eq. (26) would be replaced by an integral giving the transfer from initial states with velocities $\vec{v}_1$, $\vec{v}_1'$ to final states with velocities $\vec{v}$, $\vec{v}'$.

[12]As defined, the transfer rates and cross sections are generally complex quantities.

[13]E. J. Robinson, J. Phys. B 12, 1451 (1979); *ibid.* B 13, 2359 (1980).

[14]The impact parameter b_w for which $|\mathcal{U}(t=t_c)|\,\tau_c/\hbar = 1$ is the so-called Weisskopf radius and represents a characteristic length in the problem.

[15]Since some energy mismatch can also be provided by a change in the atom's translational motion, the condition $\bar{\omega}_c\tau_c \gg 1$ can be replaced by the somewhat stronger condition $\hbar\bar{\omega}_c >$ (thermal energy).

PHYSICAL REVIEW A VOLUME 22, NUMBER 5 NOVEMBER 1980

Theory of coherences produced by radiatively assisted inelastic collisions: Weak-field impact-core limit

Paul R. Berman

*Laboratoire Aimé Cotton, Centre National de la Recherche Scientifique II, Bâtiment 505, 91405 Orsay-Cedex, France and Physics Department, New York University, 4 Washington Place, New York, New York 10003**

(Received 21 March 1980)

A theoretical calculation of the final-state coherences produced by a radiatively assisted inelastic collision (RAIC) is presented. Two atoms, A and A', collide in the presence of an external radiation field to produce the RAIC reaction $A_i+A_i'+\hbar\Omega\rightarrow A_f+A_f'$, where $|ii'\rangle$ is the initial state, $|ff'\rangle$ is the final state, and Ω is the frequency of the external field. It is assumed that the final states consist of a number of nearly degenerate levels and the coherences produced in these levels by the RAIC reaction is calculated. These final-state coherences can be monitored by standard techniques (polarization of fluorescence, quantum beats) enabling one to use the final-state coherences as a probe of the RAIC reaction. The calculation is limited to the weak-field (perturbation-theory) limit and is valid only in the impact core of the RAIC profile.

I. INTRODUCTION

In a previous paper[1] (to be referred to as RAIC I), a general theory or radiatively assisted inelastic collisions (RAIC) was developed. These collisions represent processes of the form

$$A_i+A_i'+\hbar\Omega\rightarrow A_f+A_f',$$

in which two atoms (A and A') are excited from initial states ii' to final states ff' by the combined action of the collision and the absorption of a photon from an external pulsed radiation field. Whereas most previous theories of RAIC considered only one possible excitation channel (from non degenerate state ii' to nondegenerate state ff'), the theory presented in RAIC I allowed for the more general RAIC excitation from a group of initial levels characterized by some appropriate density matrix to a group of final levels. An expression was obtained for the final-state density matrix which completely described both the population and coherence properties of the excitation process. The final-state coherences can be monitored by standard experimental techniques (e.g., measurement of the polarization of fluorescence or quantum beats originating from the final states of one of the atoms); alternatively, one can monitor the final-state populations (e.g., by measuring the total fluorescence rate from one of the final states). It turns out, however, that measurements of final-state coherences provide a more sensitive probe of the RAIC interatomic potentials than do measurements of final-state populations. Thus, it appears useful to develop a theory of RAIC which permits one to calculate the induced-final-state coherences.

In this paper, a perturbative solution of the RAIC equations is obtained which is valid provided (1) the external field is sufficiently weak and (2) the detunings are restricted to the impact core of the RAIC profile. Starting with some arbitrary initial density matrix and assuming interatomic potentials and external-field polarizations of a quite arbitrary nature, the final-state density matrix for the system is calculated. The most general case leads to rather lengthy expressions which are presented in the Appendices. Specific results are given in the body of the paper for the reduced density matrix of atom A' in the limits of (1) dipole-dipole interatomic potential, (2) straight-line collisional trajectory, (3) linearly polarized external field, (4) central tuning, (5) unpolarized initial state, (6) final states of a given atom characterized by the same J quantum number, and (7) a summation over intermediate virtual states that reduces to one term, owing to a nearly satisfied resonance condition. It is shown that the fluorescence emitted from the final states of one of the atoms directly reflects the nature of the interatomic potential. Thus, in contrast with normal RAIC experiments where one must record an entire RAIC profile as a function of detuning to test interatomic potentialmodels, a polarization measurement at central tuning (where the signal is largest) serves to probe the interatomic potential.

It may seem strange that collisions *induce* coherence, since it is generally thought that collisions *destroy* coherence. In fact, it will be seen that the collisional interaction may be viewed as two unpolarized (but possibly correlated) "fields" incident on the atoms from all directions. The fields are chosen to have the same multipolar properties as the collisional interactions they represent (e.g., a dipole operator is replaced by a dipole field). In this way the final-state coher-

Supported by the U.S. Office of Naval Research under Contract No. N00014-77-C-0553.

ence can be understood as the combined action of *three* fields; two unpolarized fields plus the external field. It is the external field which may be polarized and possesses a well-defined directionality in any case, that is the origin of the final-state coherence. The collisional interaction responsible for the RAIC reaction will, in general, modify the final-state coherence.

In Sec. II, the physical system is described and an expression for the final-state amplitude given. An outline of the calculation is presented in Sec. III, with the details given in the Appendices. The final-state density matrix is given in Sec. IV for the case outlined above. In Sec. V the RAIC excitation cross sections and the polarization of the fluoresence emitted from the final state of atom A' are calculated using a cutoff procedure to treat collisions with small impact parameters. A discussion and physical interpretation of the results are given in Sec. VI.

It should be noted that this paper is essentially self-contained. However, the reader is referred to RAIC I for a general overview of the problem, for a detailed derivation of the RAIC equations including validity conditions, and for references to previous work.

II. PHYSICAL SYSTEM AND TRANSITION AMPLITUDE

The physical system consists of two atoms, A and A', undergoing a collision in the presence of a pulsed radiation field. The time of closest approach during the collision is $t=t_c$ and the center-of-mass position of the atoms at this time is $\vec{R}=\vec{R}_c$. The amplitude of the pulsed field is assumed to vary slowly during the collision and is evaluated at $(\vec{R}_c, t_c)$; the field is taken to be of the form

$$\vec{\mathcal{E}}(t;\vec{R}_c,t_c)=\tfrac{1}{2}[\vec{\mathcal{E}}_c e^{-i\Omega t}+\vec{\mathcal{E}}_c^{*}e^{i\Omega t}], \tag{1}$$

where $|\vec{\mathcal{E}}_c|$ is the field amplitude at $(\vec{R}_c, t_c)$.

The energy levels of atoms A and A' are shown in Fig. 1. Each label in the figure represents a group of levels having a maximum frequency separation $\omega_\epsilon \ll \tau_c^{-1}$, where τ_c is the duration of a collision. Since

$$\omega_\epsilon \tau_c \ll 1, \tag{2}$$

levels within a given group may be considered as degenerate during the RAIC. The levels associated with atom A are represented by lower-case unprimed variables and those associated with atom A' by primed ones. A capital letter refers to a state of the composite system ($I=i\,i'$, $E=e\,e'$, $F_1=f_1 f_1'$, etc.) and the convention

$$\omega_I=\omega_i+\omega_{i'},\quad \omega_F=\omega_f+\omega_{f'}, \tag{3}$$

etc., is adopted, where $\omega_\alpha=E_\alpha/\hbar$ and E_α is the energy associated with state α.

Before the collision, the atoms are in an arbitrary linear superposition of the states $|I\rangle = |ii'\rangle = |i\rangle|i'\rangle$, where i and i' represent any of the levels in the i and i' groups, respectively. The field is assumed to be nearly resonant with the $I \rightarrow F$ transition in the composite system, i.e., $\Omega \approx \omega_F - \omega_I$. More precisely, the detuning Δ defined by

$$\Delta=\Omega-\omega_{FI}\ , \tag{4}$$

$$\omega_{FI}=\omega_F-\omega_I \tag{4a}$$

is limited, in this work, to the impact core of the RAIC profile

$$|\Delta|\,\tau_c \ll 1\ . \tag{5}$$

All other atom-atom or atom-field interactions are assumed to be nonresonant; in other words, all levels outside the I and F groups enter the problem only as *virtual* levels. The contribution of these virtual levels can be included in effective operators that act in the IF subspace only. The problem is to determine the final-state density matrix following the collision since it provides a complete description of the final-state coherences and populations produced by RAIC.

The RAIC can be characterized by three operators which have been discussed in RAIC I. First, there is the "light-shift" operator $\hat{S}_L$ which couples and shifts the levels *within* both the initial and final groups of levels. This light-shift operator represents the virtual excitation and de-excitation of either of the atoms by the external field. The effects produced by $\hat{S}_L$, which are second order in the field, are neglected in this work, since the field is treated in a perturbation-theory limit.

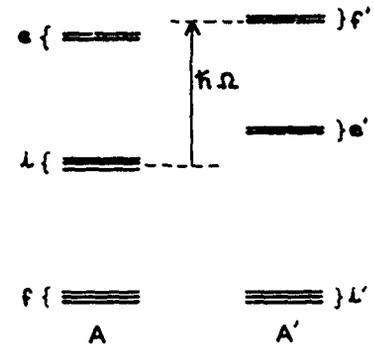

FIG. 1. Energy-level diagram of atoms A and A'. Each group of levels labeled by a single letter is nearly degenerate with a maximum frequency spacing between levels within a group less than an inverse collision time. The external-field frequency Ω is such that $\hbar\Omega \approx (E_f + E_{f'}) - (E_i + E_{i'})$.

Second, there is the collisional operator $\hat{S}_c$ which also couples and shifts the levels *within* the initial and final groups of levels. This operator is second order in the collisional interaction, representing the collision-induced virtual excitation and de-excitation of the composite AA' system in either its initial or final state. The operator $\hat{S}_c$ is the origin of the pressure broadening and shifting of spectral profiles. The relative importance of $\hat{S}_c$ is dependent on (i) the detuning Δ and (ii) the impact parameter associated with a given collision. Owing to condition (5), the collision possesses sufficient frequency components to effectively compensate for the detuning Δ. Thus, in contrast to the case $|\Delta|\tau_c > 1$, where collisional shifts can significantly enhance excitation cross sections by bringing the atomic transition frequency into instantaneous resonance with the field, all effects produced by the operator $\hat{S}_c$ related to the detuning may be neglected. The dependence of $\hat{S}_c$ on the impact parameter is discussed following the description of the transition operator.

The transition operator $\hat{T}(IF)$ represents the combined action of the (field + collision) in *coupling* the initial state $|I\rangle$ to final state $|F\rangle$ via a virtual excitation of intermediate states. This operator can be represented diagrammatically by the four terms shown in either Fig. 2 or Fig. 3. In Figs. 2(a) and 3(a), the collision (represented by non-wavy lines) acts to virtually excite the atoms from state $|ii'\rangle$ to state $|ef'\rangle$ and the field (represented by wavy lines) then acts on atom A to complete the excitation to the final state $|ff'\rangle$. In Figs. 2(b) and 3(b) the collision excites the virtual state $|fe'\rangle$ and the field acts on atom A' to complete the excitation. In Figs. 2(c) and 3(c) the field acts on atom A to excite the virtual state $|ei'\rangle$ and the collision completes the excitation to the final state $|ff'\rangle$. Finally, in Figs. 2(d) and 3(d), the field acts on atom A' to excite the virtual state $|ie'\rangle$ and the collision completes the excitation.

It may be seen from Fig. 2 that the transition operator is linear in both the field and collisional interaction. Explicitly,[1] one finds matrix elements of $\hat{T}(IF)$ to be

$$\langle F|\hat{T}(IF;t,b,v_r,\Theta,\vec{R}_c,t_c)|I\rangle = \frac{1}{2\hbar}\left(\frac{\langle F|\vec{\mu}_T|E\rangle\langle E|\mathcal{U}(\vec{R}(t))|I\rangle}{\omega_{EI}} + \frac{\langle F|\mathcal{U}(\vec{R}(t))|E\rangle\langle E|\vec{\mu}_T|I\rangle}{\omega_{EF}}\right)\cdot\vec{\delta}_c\ , \quad (6)$$

where t is the time during the collision; b, v_r,

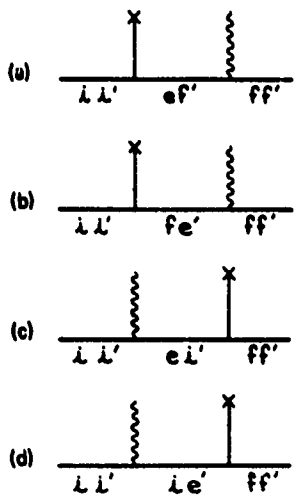

FIG. 2. Diagrams representing matrix elements of the transition operation from initial state $|ii'\rangle$ to final state $|ff'\rangle$. A straight-line vertex corresponds to a collision interaction and wavy-line vertex to an atom-field interaction. The states e and e' represent some arbitrary intermediate (virtual) states in atoms A and A', respectively.

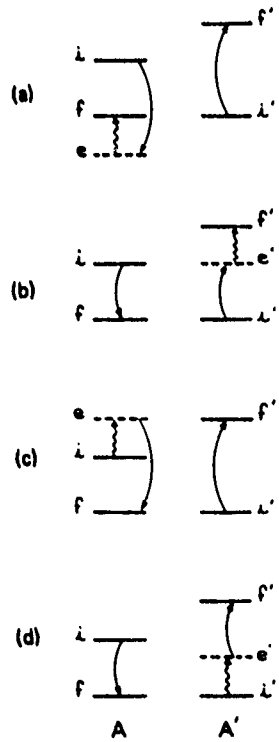

FIG. 3. A schematic representation of the contributions to the final-state RAIC amplitude complementary to that shown in Fig. 2. Each diagram corresponds to the similarly labeled diagram in Fig. 2. Solid lines with arrows represent the collisional interaction and wavy lines represent the atom-field interaction. States e and e' are virtual states excited in the RAIC reaction. Each level actually corresponds to a group of nearly degenerate levels.

and Θ are the impact parameter, relative speed, and collision orientation, respectively, associated with the collision

$$\vec{\mu}_T = \vec{\mu} + \vec{\mu}' \tag{7}$$

where $\vec{\mu}$ and $\vec{\mu}'$ are the electric-dipole operators for atoms A and A', respectively; and $\mathcal{U}(\vec{R}(t))$ is the collision interaction Hamiltonian calculated assuming a classical interatomic collision trajectory $\vec{R}(t)$. In writing Eq. (6), I have used the fact that $\omega_\epsilon \ll \omega_{EI}$, ω_{EF} (recall that ω_ϵ is the maximum frequency separation within a group of levels) and have adopted a summation convention in which any repeated state label (*not* including its appearance in a phase factor or frequency denominator) is summed over (e.g., in Eq. (6), there is a sum over E but not over I or F).[2] Since $\vec{\mu}_T$ is the sum of two terms, one can readily identify Eq. (6) with the four figures of Fig. 2. An analogous calculation for the operator $\hat{T}(FI)$ yields

$$\langle I|\hat{T}(FI;t)|F\rangle = \langle F|\hat{T}(IF;t)|I\rangle^* . \tag{8}$$

Since $\hat{T}(IF)$ varies linearly in $\mathcal{U}$ and $\hat{S}_c$ varies as $(\mathcal{U})^2$, and since $\mathcal{U}$ varies typically as b^{-n} $(n>0)$, one can conclude that, for collisions with "large" impact parameters, the effects produced by $\hat{S}_c$ may be neglected in comparison with those produced by $\hat{T}(IF)$. For "smaller" impact parameters, the contribution of $\hat{S}_c$ can no longer be ignored. For the present, I consider only those collisions with $b>b_0$, where b_0 is the minimum impact parameter for which the contribution from $\hat{S}_c$ can be neglected. In Sec. V a simple model is developed for treating collisions with $b<b_0$.

Thus, during collisions with $b>b_0$, the probability amplitudes (in the interaction representation) for the initial and final states obey the equations of motion

$$i\hbar\dot{a}_F = \langle F|T(IF,t)|I\rangle e^{-i\Delta t}a_I , \tag{9a}$$

$$i\hbar\dot{a}_I = \langle F|\hat{T}(IF,t)|I\rangle^* e^{i\Delta t}a_F , \tag{9b}$$

where it has been assumed that changes in a_I or a_F resulting from level decay and atomic motion (Doppler effect) are negligible on the time scale of a collision. Furthermore, it is now assumed that the field strength is weak enough so that Eqs. (9) can be solved by perturbation theory with initial conditions $a_I(t_c^-)\neq 0$, $a_F(t_c^-)=0$, where t_c^- is a time just before the collision. Integrating Eqs. (9) in the perturbation-theory limit, one finds a final-state amplitude at time t_c^+ just following the collision given by

$$a_F(t_c^+) = (i\hbar)^{-1}\left(\int_{t_c^-}^{t_c^+}\langle F|\hat{T}(IF,t)|I\rangle e^{-i\Delta t}\,dt\right)a_I(t_c^-) . \tag{10}$$

Perturbation theory is valid provided that $|a_F(t)|^2 \ll 1$ for all t during a collision having $b=b_0$. Under typical experimental conditions, perturbation theory is valid for power densities $\lesssim 10^{10}\,\mathrm{W/cm^2}$.

It remains to carry out the integration in Eq. (10), to form final-state density-matrix elements, and to average over all appropriate collision parameters.

III. OUTLINE OF CALCULATION

Forming final-state density-matrix elements from the amplitude (10) and carrying out the average over collision orientations Θ, one obtains[3]

$$\rho_{FF_1}(t_c^+;b,v_r,\vec{R}_c,t_c) = R^{II_1}_{FF_1}(b,v_r,\vec{R}_c,t_c)\rho_{II_1}(t_c^-), \tag{11a}$$

where

$$R^{II_1}_{FF_1}(b,v_r,\vec{R}_c,t_c) = \hbar^{-2}(8\pi^2)^{-1}\int d\Theta\int_{t_c^-}^{t_c^+}\langle F|\hat{T}(IF,t)|I\rangle e^{-i\Delta t}\,dt\int_{t_c^-}^{t_c^+}\langle F_1|\hat{T}(IF,t')|I_1\rangle^* e^{i\Delta t'}\,dt' . \tag{11b}$$

The dependence of $\hat{T}$ on $(b,v_r,\Theta,\vec{R}_c,t_c)$ has been suppressed in Eqs. (10) and (11). In this section, a method for evaluating Eqs. (11) is outlined; details of the calculation are given in the Appendices. The averaging over b and $\vec{R}_c$ is deferred to Sec. V.[4]

The matrix elements of $\hat{T}$ needed in Eq. (11b) may be calculated using Eq. (6) once the interatomic potential $\mathcal{U}$ and the field $\vec{\mathcal{E}}_c$ are specified. An arbitrary potential can be written in the form

$$\mathcal{U}(t-t_c,\,b,v_r,\Theta) = A^{kk'}_{qq'}(t-t_c,b,v_r,\Theta)T^k_q\,T'^{k'}_{q'}, \tag{12}$$

where T^k_q and $T'^{k'}_{q'}$ are components of irreducible tensor operators of rank k and k' (assumed integral), respectively, which act on states of atoms A and A', respectively. In the form (12), the potential can be viewed as the sum of correlated multipolar fields acting on each of the atoms, the correlation provided by the coupling constants

$A^{kk'}_{qq'}$. The average over all collision orientations needed in Eq. (11b) is equivalent to including all possible directions of incidence and polarizations for these multipolar fields. In some sense, therefore, the collisions can be viewed as producing the same effect as a sum of unpolarized, but correlated, multipolar fields acting on atoms A and A'. This picture of the collisional process can be useful in understanding the coherences produced by RAIC and is used in Sec. VI to help explain the results obtained for the various RAIC cross sections.

In order to carry out the average over Θ, it is convenient to rewrite Eq. (12) in the form

$$\mathfrak{A}(t-t_c;b,v_r,\Theta)={}^{kk'}A^K_Q(t-t_c;b,v_r,\Theta)\,{}^{kk'}V^K_Q\,, \tag{13}$$

where

$${}^{kk'}V^K_Q=\begin{bmatrix} k & k' & K \\ q & q' & Q \end{bmatrix} T^k_q\,T^{k'}_{q'}\,, \tag{14a}$$

$${}^{kk'}A^K_Q=\begin{bmatrix} k & k' & K \\ q & q' & Q \end{bmatrix} A^{kk'}_{qq'}\,, \tag{14b}$$

and the quantity in brackets is a Clebsch-Gordon coefficient. Since the V^K_Q transform as the components of an irreducible tensor operator under rotation, the expansion coefficients A^K_Q transform as

$${}^{kk'}A^K_Q(t-t_c;b,v_r,\Theta)$$

$$={\mathfrak{R}^{(K)}_{QQ'}}^{*}(\Theta)\,{}^{kk'}A^K_{Q'}(t-t_c;b,v_r,0)\,, \tag{15}$$

where the $\mathfrak{R}^{(K)}_{QQ'}$ are matrix elements of the irreducible representation of order (K) of the rotation group and $\Theta=0$ is some arbitrary collision geometry. The Θ dependence is now contained totally in the $\mathfrak{R}^{(K)}_{QQ'}$, enabling one to easily perform the Θ integration required in Eq. (11b) (see below). In anticipation of the time integrals also required in Eq. (11b), I define the quantities

$$A^{kk'}_{qq'}(b,v_r,\Theta;\Delta)=(v_r/b)\int_{t_c^--t_c}^{t_c^+-t_c} A^{kk'}_{qq'}(\tau,b,v_r,\Theta)\times e^{-i\Delta(\tau+t_c)}\,d\tau \tag{16a}$$

and

$${}^{kk'}A^K_Q(b,v_r,\Theta;\Delta)=(v_r/b)\int_{t_c^--t_c}^{t_c^+-t_c} {}^{kk'}A^K_Q(\tau,b,v_r,\Theta)\times e^{-i\Delta(\tau+t_c)}\,d\tau\,, \tag{16b}$$

which are also related via Eq. (14b). Equation (15) remains valid for ${}^{kk'}A^K_Q(b,v_r,\Theta;\Delta)$.

It remains to specify the atom-field interaction $\vec{\mu}_T\cdot\vec{\mathcal{E}}_c$. The field amplitude may be written

$$\vec{\mathcal{E}}_c=\hat{\epsilon}\,\mathcal{E}_c\,,\quad |\hat{\epsilon}|=1 \tag{17}$$

where $\hat{\epsilon}$ is a complex polarization vector. One then finds

$$\vec{\mu}_T\cdot\vec{\mathcal{E}}_c=(-1)^q(\mu_T)^{(1)}_q\,\epsilon_{-q}\,\mathcal{E}_c\,, \tag{18}$$

where

$$\epsilon_1=-(\epsilon_x+i\epsilon_y)/\sqrt{2}\,,$$

$$\epsilon_{-1}=(\epsilon_x-i\epsilon_y)/\sqrt{2}\,, \tag{19}$$

$$\epsilon_0=\epsilon_z\,,$$

and

$$(\mu_T)^{(1)}_1=-[(\mu_T)_x+i(\mu_T)_y]/\sqrt{2}\,,$$

$$(\mu_T)^{(1)}_{-1}=[(\mu_T)_x-i(\mu_T)_y]/\sqrt{2}\,,\quad (\mu_T)^{(1)}_0=(\mu_T)_z\,. \tag{20}$$

The quantities $(\mu_T)^{(1)}_q$ are the components of an irreducible tensor operator of rank 1.

Since all the operators appearing in Eq. (6) have now been expressed in terms of the components of irreducible tensor operators, the matrix elements appearing in Eq. (6) are easily calculated using the Wigner-Eckart theorem[5] (see Appendix A). The resulting expressions for $\langle F|\,T(IF,t)|I\rangle$ and $\langle F_1|\,T(IF,t)|\,I_1\rangle^*$ are then inserted into Eq. (11b) and the integration over Θ is performed using the fact that[6]

$$(8\pi^2)^{-1}\int d\Theta\,\mathfrak{R}^K_{QQ'}(\Theta)\,(\mathfrak{R}^{\bar{K}}_{\bar{Q}\bar{Q}'}(\Theta))^*=(2K+1)^{-1}\,\delta_{K\bar{K}}\delta_{Q\bar{Q}}\delta_{Q'\bar{Q}'} \tag{21}$$

to arrive at a value for $R^{II_1}_{FF_1}(b,v_r,\vec{R}_c,t_c)$ [Eq. (11b)] and $\rho_{FF_1}(t_c^+;b,v_r,\vec{R}_c,t_c)$ [Eq. (11a)]. The final expressions are rather lengthy and are given in Appendix A along with the details of the calculation.

Experimentally, one often observes the final-state properties of only one of the atoms. Imagine, for example, that one monitors the final-state coherence of atom A'. Mathematically, this coherence is described by the reduced density matrix obtained by tracing ρ_{FF_1} over the final-state variables of atom A. Explicitly, these reduced density-matrix elements $\rho^{f'}_{f'_1}$ are given by setting $F=ff'$, $F_1=ff'_1$ and summing over f, i.e.,

$$\rho^{f'}_{f'_1}(t_c^+;b,v_r,\vec{R}_c,t_c)=\rho_{ff';ff'_1}(t_c^+;b,v_r,\vec{R}_c,t_c)\,. \tag{22}$$

A calculation of these reduced matrix elements, those of atom A, and the connection between the two is also given in Appendix A.

The coherence properties of a system are conveniently expressed in terms of the irreducible tensor components of the density matrix. The transformation between matrix elements is given by

$$f'f'_1\rho'^K_Q = (-1)^{J_{f'_1}-m_{f'_1}} \begin{bmatrix} J_{f'} & J_{f'_1} & K \\ m_{f'} & -m_{f'_1} & Q \end{bmatrix} \times \langle f' J_{f'} m_{f'} | \rho' | f' J_{f'_1} m_{f'_1} \rangle , \quad (23a)$$

along with the inverse transform

$$\langle f' J_{f'} m_{f'} | \rho' | f' J_{f'_1} m_{f'_1} \rangle = (-1)^{J_{f'_1}-m_{f'_1}} \begin{bmatrix} J_{f'} & J_{f'_1} & K \\ m_{f'} & -m_{f'_1} & Q \end{bmatrix} f'f'_1\rho'^K_Q , \quad (23b)$$

where it has been assumed that a state $|\alpha\rangle$ may be labeled by $|\alpha J_\alpha m_\alpha\rangle$ and that states within a given group of levels differ only in their J and m_J quantum numbers.[7] The ρ^K_Q are matrix elements of the density matrix expanded in an irreducible tensor basis. When expressed in this fashion, one can see directly if there is any final-state coherence. The quantity ρ^0_0 is given by

$$f'f'_1\rho'^0_0 = (2J_{f'}+1)^{-1/2} \langle f' J_{f'} m_{f'} | \rho' | f' J_{f'} m_{f'} \rangle \delta_{J_{f'} J_{f'_1}} \quad (24)$$

and is proportional to the total final-state *population*. Any nonzero value of ρ'^K_Q for $K>0$ indicates that final-state coherence exists, since a totally unpolarized final state leads to $\rho'^K_Q = 0$ for $K \neq 0$.

In Appendix A, general expressions for $\rho'_{f'f'_1}$ and ρ'^K_Q are obtained, assuming an arbitrary initial state. These expressions are evaluated in detail in Appendix B for the case of an unpolarized initial state. In the following section, certain limiting cases of these calculations are discussed.

IV. RESULTS FOR A SPECIFIC MODEL

In order to illustrate the physical principles involved in the RAIC process, I consider a limiting case of the general results presented in Appendices A and B. The following model is adopted: (1) Each group of levels α can be represented by a single angular momentum quantum number J_α (valid for fine-structure splittings $> \tau_c^{-1}$). (2) The initial state is unpolarized. (3) Owing to a nearly satisfied resonance condition, only *one* group of levels enters in the summation over intermediate virtual states. In this limit, the reduced density matrix for atom A' is calculated. Since the final state of atom A' is characterized by a single J value $J_{f'} = J_{f'_1}$, the calculation of $f'f'\rho'^K_Q$ is essentially one in which the Zeeman coherences of level f' are determined.

In order for condition (3) to be satisfied *one* of the virtual levels shown in Fig. 3 must be nearly coincident with a real atomic level. This condition can be achieved with any of the level schemes shown in Fig. 4. For example, if the level scheme is as shown in Fig. 4(a), then the dominant contribution to the final-state amplitude comes from the diagram of Fig. 2(a) with the sum over intermediate states e restricted to the single group of states $e=r$; contributions from states $e \neq r$ as well as from the other diagrams of Figs. 2(b)–2(d) are relatively unimportant in this case in comparison with this nearly resonant contribution. Similarly, if the level scheme is as shown in Figs. 4(b)–4(d), the dominant contribution comes from the diagrams of Figs. 2(b)–2(d) with the summation over intermediate states restricted to $e=r$ or r'.

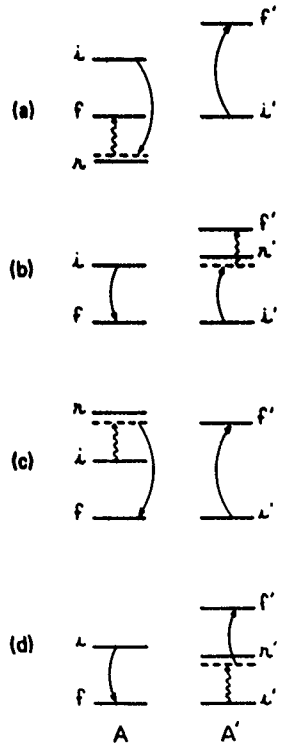

FIG. 4. Four different cases of energy-level schemes that lead to a single term dominating the sum over intermediate virtual states. Each level corresponds to a group of nearly degenerate levels.

The frequency mismatches associated with Figs. 4(a)–4(d) are

$$\Delta_a = \omega_r + \omega_{f'} - \omega_I \ , \tag{25a}$$

$$\Delta_b = \omega_f + \omega_{r'} - \omega_I \ , \tag{25b}$$

$$\Delta_c = \omega_r + \omega_{i'} - \omega_F \ , \tag{25c}$$

$$\Delta_d = \omega_i + \omega_{r'} - \omega_F \ , \tag{25d}$$

respectively. Although these frequencies are small in comparison with those associated with other virtual states, they still are assumed to satisfy $|\Delta_\alpha|\tau_c \gg 1$ ($\alpha = a - d$) to ensure that states r or r' still act as virtual states in the RAIC process. Experimentally, one often seeks level schemes similar to those shown in Fig. 4 in order to enhance excitation probabilities.

For the level scheme of Fig. 4(a), the final-state reduced density matrix for atom A' is obtained from Eqs. (B3), (B4), and (25a) as

$$\begin{aligned}{}^{f'f'}\rho_Q'^K(t_c^+; b, v_r, \vec{R}_c, t_c)_a = (b\mathcal{S}_c/\hbar v_r)^2 N_I^{-1}\, {}^{kk'}A_Q^{K'}(b, v_r, 0; \Delta)[{}^{pp'}A_Q^{K'}(b, v_r, 0; \Delta)]^* \\ \times P_{KQ}\Delta_a^{-2}(-1)^{J_f - J_{f'} - J_i - J_{i'} + K' + p' + k'} |\langle f\|\mu^{(1)}\|r\rangle|^2 \langle r\|T^{(k)}\|i\rangle \\ \times \langle r\|T^{(p)}\|i\rangle^* \langle f'\|T'^{(k')}\|i'\rangle \langle f'\|T'^{(p')}\|i'\rangle^* \begin{Bmatrix} 1 & 1 & K \\ J_r & J_r & J_f \end{Bmatrix} \\ \times \begin{Bmatrix} k & p & K \\ J_r & J_r & J_i \end{Bmatrix} \begin{Bmatrix} k' & p' & K \\ p & k & K' \end{Bmatrix} \begin{Bmatrix} k' & p' & K \\ J_{f'} & J_{f'} & J_{i'} \end{Bmatrix}, \end{aligned} \tag{26}$$

where N_I is the number of initial states,

$$P_{KQ} = (-1)^{Q_s} \epsilon_j^* \epsilon_s \begin{bmatrix} 1 & 1 & K \\ Q_j & -Q_s & Q \end{bmatrix}, \tag{27a}$$

$\langle \| \cdots \| \rangle$ is a reduced matrix element, $\{\cdots\}$ is a 6-J symbol, and

$$Q_1 = 1 \ , \ Q_{-1} = -1 \ , \ Q_0 = 0 \tag{27b}$$

as defined in Eq. (A17).

Equation (26) has a simple interpretation in terms of Fig. 4(a). The collision excites the atoms from state ii' to virtual state rf'; this process is represented by the product of the ${}^{kk'}A_Q^{K'}[{}^{pp'}A_Q^{K'}]^*$ factor and the reduced matrix elements of the collision operators T^k, T^p, $T^{k'}$, $T'^{p'}$. The field then acts on atom 1 to excite the system from state rf' to state ff'; this process is represented by the factor $P_{KQ}|\langle f\|\mu^{(1)}\|r\rangle|^2$, with P_{KQ} containing the polarization properties of the field. The 6-J and Clebsch-Gordon coefficients which appear are geometrical factors which arise when the various J levels are coupled by either the collisional interaction or the field.

For the level scheme shown in Fig. 4(b), the result is given by Eqs. (B3), (B6), and (25b) as

$$\begin{aligned}{}^{f'f'}\rho_Q'^K(t_c^+; b, v_r, \vec{R}_c, t_c)_b = \mathcal{G}(k, k', p, p', K, K', Q; \Delta)\Delta_b^{-2}(-1)^{K + J_{f'} + J_{r'}}[(2J_{r'}+1)(2k+1)(2k'+1)]\delta_{kp}\delta_{k'p'} \\ \times |\langle f'\|\mu'^{(1)}\|r'\rangle|^2 |\langle f\|T^{(k)}\|i\rangle|^2 |\langle r'\|T'^{(k')}\|i'\rangle|^2 \\ \times \begin{Bmatrix} 1 & 1 & K \\ J_{f'} & J_{f'} & J_{r'} \end{Bmatrix}, \end{aligned} \tag{28}$$

where

$$\mathcal{G}(k, k', p, p', K, K', Q; \Delta) = (b\mathcal{S}_c/\hbar v_r)^2 N_I^{-1}\, {}^{kk'}A_Q^{K'}(b, v_r, 0; \Delta)[{}^{pp'}A_Q^{K'}(b, v_r, 0; \Delta)]^* P_{KQ}. \tag{29}$$

This result is interpreted in terms of Fig. 4(b) as a collisional excitation from ii' to fr' followed by a field exciation of atom A' to the final state ff'.

For the level scheme of Fig. 4(c), one obtains from Eqs. (B3), (B11), and (25c),

$$\rho'^{K}_{Q}(t_c^+;b,v_r,\vec{R}_c,t_c)_c=\mathcal{C}(k,k',p,p',K,K',Q;\Delta)\Delta_c^{-2}(-1)^{-J_i-J_{i'}-J_{f'}+k+k'+p+p'-2J_r-J_f+K'}$$
$$\times\left|\langle r\|\mu^{(1)}\|i\rangle\right|^2\langle f\|T^{(k)}\|r\rangle\langle f\|T^{(p)}\|r\rangle^*\langle f'\|T'^{(k')}\|i'\rangle$$
$$\times\langle f'\|T'^{(p')}\|i'\rangle^*\begin{Bmatrix}1&1&K\\J_r&J_r&J_i\end{Bmatrix}\begin{Bmatrix}k'&p'&K\\J_{f'}&J_{f'}&J_{i'}\end{Bmatrix}\begin{Bmatrix}k&p&K\\p'&k'&K'\end{Bmatrix}\begin{Bmatrix}k&p&K\\J_r&J_r&J_f\end{Bmatrix}. \tag{30}$$

In terms of Fig. 4(c), one interprets this result as a field excitation from ii' to ri' followed by a collisional excitation to ff'.

Finally, for the level scheme of Fig. 4(d), one finds from Eqs. (B3), (B13), and (25d)

$$\rho'^{K}_{Q}(t_c^+;b,v_r,\vec{R}_c,t_c)_d=\mathcal{C}(k,k',p,p',K,K',Q;\Delta)\Delta_c^{-2}(-1)^{J_{i'}+2J_{r'}+J_{f'}+k'}[(2k+1)(2k'+1)]^{-1}$$
$$\times\delta_{k,p}\delta_{k',p'}\left|\langle r'\|\mu'^{(1)}\|i'\rangle\right|^2\left|\langle f\|T^{(k)}\|i\rangle\right|^2\left|\langle f'\|T'^{(k')}\|r'\rangle\right|^2$$
$$\times\begin{Bmatrix}J_{f'}&J_{f'}&K\\J_{r'}&J_{r'}&k'\end{Bmatrix}\begin{Bmatrix}1&1&K\\J_{r'}&J_{r'}&J_{i'}\end{Bmatrix}. \tag{31}$$

In terms of Fig. 4(d), this result corresponds to a field excitation from ii' to ir' followed by a collisional excitation to state ff'.

Equations (26)–(31) characterize the final-state coherence of atom A' for the level schemes of Fig. 4. This coherence can be monitored by measuring the polarization of the fluorescence emitted by atom A' from state f' (see Sec. V).

A. Dipole-dipole interaction

As a somewhat more specific example, I now consider the case where the collisional interaction is of a dipole-dipole nature. For such an interaction, $k=k'=p=p'=1$, $T=\mu$, and $T'=\mu'$. The corresponding ${}^{11}A^{K}_{Q}(b,v_r,0;\Delta)$ are calculated in Appendix C, assuming straight-line collision trajectories.

The results for the dipole-dipole limit are conveniently expressed in terms of the Rabi frequencies

$$\chi^{c}_{\alpha\beta}=\tfrac{1}{2}\langle\alpha\|\mu^{(1)}\|\beta\rangle\mathcal{E}_c/\hbar, \tag{32a}$$
$$\chi'^{c}_{\alpha'\beta'}=\tfrac{1}{2}\langle\alpha'\|\mu'^{(1)}\|\beta'\rangle\mathcal{E}_c/\hbar, \tag{32b}$$

and a characteristic length $b^{\alpha'\beta'}_{\alpha\beta}$ defined by

$$b^{\alpha'\beta'}_{\alpha\beta}=\left|2\langle\alpha\|\mu^{(1)}\|\beta\rangle\langle\alpha'\|\mu'^{(1)}\|\beta'\rangle/\hbar v_r\right|^{1/2}. \tag{33}$$

The quantity $b^{\alpha'\beta'}_{\alpha\beta}$ is a radius that typically appears in theories of resonance broadening ("Weisskopf radius" for resonant broadening) and usually has a value in the 10 to 40 Å range. Moreover, it is useful to define the dimensionless quantity

$$D_K(\Delta b/v_r)=b^6\sum_{Q}\left|{}^{11}A^{K}_{Q}(b,v_r,0;\Delta)\right|^2. \tag{34}$$

For the level scheme of Fig. 4(a), the dipole-dipole limit of Eq. (26) is

$$\rho'^{K}_{Q}(t_c^+;b,v_r,\vec{R}_c,t_c)_a=N_i^{-1}(-1)^{\varphi_a}\left|\chi^{c}_{fr}/\Delta_a\right|^2(b^{fr}_{ri}/b)^4D_{K'}(\Delta b/v_r)$$
$$\times(-1)^{K'}P_{KQ}\begin{Bmatrix}1&1&K\\J_r&J_r&J_f\end{Bmatrix}\begin{Bmatrix}1&1&K\\J_r&J_r&J_i\end{Bmatrix}\begin{Bmatrix}1&1&K\\1&1&K'\end{Bmatrix}\begin{Bmatrix}1&1&K\\J_{f'}&J_{f'}&J_{i'}\end{Bmatrix}, \tag{35a}$$

where

$$\varphi_a=J_f-J_{f'}-J_i-J_{i'}. \tag{35b}$$

For the level scheme of Fig. 4(b), the dipole-dipole limit of Eq. (28) is

$$\rho'^{K}_{Q}(t_c^+;b,v_r,\vec{R}_c;t_c)_b=N_i^{-1}(-1)^{\varphi_b}\left|\chi'^{c}_{fr'}/\Delta_b\right|^2(b^{fr'}_{fi}/b)^4[9(2J_{r'}+1)]^{-1}$$
$$\times D_{K'}(\Delta b/v_r)(-1)^{K}P_{KQ}\begin{Bmatrix}1&1&K\\J_{f'}&J_{f'}&J_{r'}\end{Bmatrix}, \tag{36a}$$

where

$$\varphi_b = J_{f'} + J_{r'} . \tag{36b}$$

For the level scheme of Fig. 4(c), the dipole-dipole limit of Eq. (30) is

$$^{f'f'}\rho_Q'^K(t_c^+; b, v_r, \vec{R}_c, t_c)_c = N_I^{-1}(-1)^{\varphi_c}|\chi_{rl}^c/\Delta_c|^2(b_{fr}^{f'i'}/b)^4 D_{K'}(\Delta b/v_r)$$
$$\times(-1)^{K'}P_{KQ}\begin{Bmatrix}1 & 1 & K\\ J_r & J_r & J_i\end{Bmatrix}\begin{Bmatrix}1 & 1 & K\\ J_{f'} & J_{f'} & J_{i'}\end{Bmatrix}\begin{Bmatrix}1 & 1 & K\\ 1 & 1 & K'\end{Bmatrix}\begin{Bmatrix}1 & 1 & K\\ J_r & J_r & J_f\end{Bmatrix}, \tag{37a}$$

where

$$\varphi_c = -J_i - J_{i'} - J_{f'} - 2J_r - J_f . \tag{37b}$$

For the level scheme of Fig. 4(d), the dipole-dipole limit of Eq. (31) is

$$^{f'f'}\rho_Q'^K(t_c^+; b, v_r, \vec{R}_c, t_c)_d = \tfrac{1}{6}N_I^{-1}(-1)^{\varphi_d}|\chi_{r'i'}^c/\Delta_d|^2(b_{fi}^{f'r'}/b)^2 D_{K'}(\Delta b/v_r)$$
$$\times P_{KQ}\begin{Bmatrix}J_{f'} & J_{f'} & K\\ J_{r'} & J_{r'} & 1\end{Bmatrix}\begin{Bmatrix}1 & 1 & K\\ J_{r'} & J_{r'} & J_{i'}\end{Bmatrix}, \tag{38a}$$

where

$$\varphi_d = J_{i'} + 2J_{r'} + J_{f'} + 1 . \tag{38b}$$

Equations (35)–(38) characterize the final-state coherence of atom A' for collisions having impact parameters $b > b_0$, assuming a dipole-dipole collisional interaction.

V. CROSS SECTIONS AND FINAL-STATE COHERENCES FOR A DIPOLE-DIPOLE COLLISIONAL INTERACTION

This section is divided into two parts. In the first part, the RAIC cross sections are calculated for the limiting cases represented in Fig. 4 and discussed in the previous section. In the second part, the polarization of the fluorescence emitted from state f' of atom A' is evaluated.

A. Cross sections

The RAIC cross section is a function of t_c, reflecting the fact that a collision can occur at any time during the on time of the radiation pulse. However, one can define an *average* cross section per pulse for RAIC excitation of $^{f'f'}\rho_Q'^K(v_r)$ in atom A' as

$$^{f'f'}\sigma_Q'^K(v_r, \Delta) = \frac{2\pi\int_0^\infty b\,db\int_{T^-}^{T^+}dt_c\int d\vec{R}_c\; r'^K\rho_Q'^K(t_c^+; b, v_r, \vec{R}_c, t_c)}{(T^+ - T^-)\int d\vec{R}_c}, \tag{39}$$

where $T^-(T^+)$ represent times just before (after) the radiation pulse and the $\vec{R}_c$ integration is over the atom-field interaction volume. In order to evaluate Eq. (39), an integration over all impact parameters is required. However, the calculation of $^{f'f'}\rho_Q'^K(t_c^+; b, v_r, \vec{R}_c, t_c)$ presented in Sec. IV is valid only for $b > b_0$, where b_0 is the impact parameter at which the collisional level-shifting operator $\hat{S}_c$ becomes important (see discussion of Sec. II). Thus, some type of cutoff procedure is needed to account for collisions with $b < b_0$.

In this paper, the region $b < b_0$ is treated in an extremely simplified fashion; basically, the contribution from $b < b_0$ is ignored. This overly simplified procedure is, nevertheless, somewhat justified. The parameter b_0 is essentially the Weisskopf radius associated with the level-shifting operator, i.e., that radius at which

$$\varphi_0 = \frac{1}{\hbar}\int_{-\infty}^{\infty}\bar{S}_c(b_0, t)dt = 1 , \tag{40}$$

where $\bar{S}_c$ represents the expectation value of $\hat{S}_c$ in the final-state manifold (typically, $5 < b_0 < 15$ Å). For $b < b_0$ the operator $\hat{S}_c$ strongly couples all final-state magnetic sublevels; it is therefore reasonable to assume that final-state coherences cannot be created for collisions with $b < b_0$. Consequently, the b integral for $\sigma_Q'^K$ $(K > 0)$ can be evaluated from b_0 to ∞. Moreover, collisions with $b < b_0$ can be estimated to contribute less than 20% to the RAIC excitation of final-state *populations*.[8] Thus, the b integral for $\sigma_0'^0$ can also be cut off for $b < b_0$, although the RAIC cross section evaluated in this manner underestimates by 10 to 20% the corresponding cross section calculated without using a cutoff.

In summary, the cutoff procedure adopted is

one in which the lower limit of the b integral in Eq. (39) is replaced by b_0. This procedure underestimates σ'^0_0 by 10 to 20% and provides a good approximation for σ'^K_Q ($K>0$). The perturbation theory results are valid if ${}^{f'f'}\rho'^0_0(t_c, b_0, v_r, \vec{R}_c, t) \ll 1$ (i.e., the final-state population is much less than unity). From Eqs. (32)–(38), and (C14), one can derive the validity condition

$$|\chi^c/\Delta_\alpha|^2(b_R/b_0)^4 \ll 1, \tag{41}$$

where χ^c is a Rabi frequency defined by Eq. (32), b_R is one of the characteristic *resonant* Weisskopf radii defined by Eq. (33), and Δ_α is a frequency mismatch defined by Eq. (25). Since $b_R/b_0 \lesssim 4$ and $|\Delta_\alpha| \gg 10^{12}$ sec^{-1}, Eq. (41) is easily satisfied for a large range of field strengths.

The RAIC excitation cross sections may now be easily obtained for the limiting cases of Fig. 4. For the case of *central tuning*, the RAIC cross section in the dipole-dipole limit for the level scheme corresponding to Fig. 4(a) may be obtained from Eqs. (39), (35a), and (C14) as

$$ {}^{f'f'}\sigma'^K_Q(v_r, 0)_a = 8\pi N_I^{-1}(-1)^{q_a}(\langle|\chi^c_{f_r}|^2\rangle/\Delta_a^2)(b'^{f'f'}_{r_i}/b_0)^2(-1)^{Q_s}\epsilon^*_j\epsilon_s \begin{bmatrix} 1 & 1 & K \\ Q_j & -Q_s & Q \end{bmatrix} $$
$$ \times \begin{Bmatrix} 1 & 1 & K \\ J_r & J_r & J_f \end{Bmatrix}\begin{Bmatrix} 1 & 1 & K \\ J_r & J_r & J_i \end{Bmatrix}\begin{Bmatrix} 1 & 1 & K \\ 1 & 1 & 2 \end{Bmatrix}\begin{Bmatrix} 1 & 1 & K \\ J_{f'} & J_{f'} & J_{i'} \end{Bmatrix}(b'^{f'i'}_{r_i})^2, \tag{42}$$

where

$$\langle|\chi^c_{\alpha\beta}|^2\rangle = |\chi^c_{\alpha\beta}|^2\langle\mathcal{E}_c^2\rangle/\mathcal{E}_c^2 \tag{43}$$

and

$$\langle\mathcal{E}_c^2\rangle = \frac{1}{T^+ - T^-}\int d\vec{R}_b \int_{T^-}^{T^+} dt_c |\mathcal{E}_c(\vec{R}_c, t_c)|^2 \Big/ \int d\vec{R}_c. \tag{44}$$

Similarly, for the level scheme of Fig. 4(b), from Eqs. (39), (36a), and (C14) one may obtain

$$ {}^{f'f'}\sigma'^K_Q(v_r, 0)_b = 8\pi N_I^{-1}(-1)^{q_b}[9(2J_{r'}+1)]^{-1}(\langle|\chi'^c_{f_{r'}}|^2\rangle/\Delta_b^2)(b'^{r'i'}_{f_i}/b_0)^2 $$
$$ \times(-1)^{Q_s}\epsilon^*_j\epsilon_s \begin{bmatrix} 1 & 1 & K \\ Q_j & -Q_s & Q \end{bmatrix}(-1)^K \begin{Bmatrix} 1 & 1 & K \\ J_{f'} & J_{f'} & J_{r'} \end{Bmatrix}(b'^{r'i'}_{f_i})^2, \tag{45}$$

where

$$\langle|\chi'^c_{\alpha'\beta'}|^2\rangle = |\chi'^c_{\alpha'\beta'}|^2\langle\mathcal{E}_c^2\rangle/\mathcal{E}_c^2. \tag{46}$$

For the level scheme of Fig. 4(c), the RAIC cross section calculated from Eqs. (39), (37a), and (C14) is

$$ {}^{f'f'}\sigma'^K_Q(v_r, 0)_c = 8\pi N_I^{-1}(-1)^{q_c}(\langle|\chi^c_{r_i}|^2\rangle/\Delta_c^2)(b'^{f'i'}_{f_r}/b_0)^2(-1)^{Q_s}\epsilon^*_j\epsilon_s $$
$$ \times \begin{bmatrix} 1 & 1 & K \\ Q_j & -Q_s & Q \end{bmatrix}\begin{Bmatrix} 1 & 1 & K \\ J_r & J_r & J_i \end{Bmatrix}\begin{Bmatrix} 1 & 1 & K \\ J_{f'} & J_{f'} & J_{i'} \end{Bmatrix}\begin{Bmatrix} 1 & 1 & K \\ 1 & 1 & 2 \end{Bmatrix}\begin{Bmatrix} 1 & 1 & K \\ J_r & J_r & J_f \end{Bmatrix}(b'^{f'i'}_{f_r})^2. \tag{47}$$

Finally, for the level scheme of Fig. 4(d), one may use Eqs. (39), (38a), and (C14) to obtain

$$ {}^{f'f'}\sigma'^K_Q(v_r, 0)_d $$
$$ = \tfrac{8}{5}\pi N_I^{-1}(-1)^{q_d}(\langle|\chi'^c_{r'i'}|^2\rangle/\Delta_d^2)(b'^{f'r'}_{f_i}/b_0)^2(-1)^{Q_s}\epsilon^*_j\epsilon_s \begin{bmatrix} 1 & 1 & K \\ Q_j & -Q_s & Q \end{bmatrix}\begin{Bmatrix} J_{f'} & J_{f'} & K \\ J_{r'} & J_{r'} & 1 \end{Bmatrix}\begin{Bmatrix} 1 & 1 & K \\ J_{r'} & J_{r'} & J_{i'} \end{Bmatrix}(b'^{f'r'}_{f_i})^2. \tag{48}$$

Equations (42), (45), (47), and (48) give the RAIC excitation cross sections for level schemes corresponding to Fig. 4 in the limit of a dipole-dipole collisional interaction. It should be recalled that these are the RAIC cross sections for excitation from an *unpolarized initial state*; the quantities ϵ_j ($j=1, 0, -1$) specify the polarization of the external field. As defined by Eqs. (33) and (40), the characteristic radii $b^{\alpha'\beta'}_{\alpha\beta}$ and b_0 are functions of v_r; $b^{\alpha'\beta'}_{\alpha\beta}$ is proportional to $v_r^{-1/2}$ and b_0 is proportional to $v_r^{1/(n-1)}$ for a level-shifting operator which varies as R^{-n} ($n>3$).

The physical significance of the various RAIC cross sections is discussed in Sec. VI. It may be noted at this point, however, that the RAIC cross sections vary as

$$\sigma' = |\Psi(\langle|\chi^c|^2\rangle/\Delta_\alpha^2)(b_R/b_0)^2 b_R^2 , \tag{49}$$

where Ψ is a constant of order unity. Combining Eqs. (41) and (49), one finds that, if the perturbation theory is valid, then

$$\sigma' \ll b_0^2 . \tag{50}$$

Since $b_0 \approx 10$ Å, the maximum RAIC cross sections obtainable with fields satisfying the perturbation-theory requirement (41) are of the order of 100 Å^2. For larger field strengths, where Eq. (41) no longer holds, a strong-field (nonperturbative) theory is needed.

Corresponding results for noncentral tuning ($\Delta \neq 0$) may be obtained from Eqs. (39), (35)–(38), and (C13).

B. Fluorescence

The final-state coherence of atom A' is conveniently monitored by measuring the polarization or quantum beats in the fluorescence emitted from state f'. In this paper, the polarization of the fluorescence is calculated assuming that the external field participating in the RAIC excitation is linearly polarized in the z direction,

$$\epsilon_{\pm 1} = 0, \quad \epsilon_0 = 1 , \tag{51}$$

and propagates in the y direction.

The fluorescence signal emitted from state f' to some lower state g' (characterized by an angular momentum quantum number $J_{g'}$) in atom A' is given by[9]

$$S \propto (-1)^{Q_n} \bar{\epsilon}_i^* \bar{\epsilon}_n (-1)^K \begin{bmatrix} 1 & 1 & K \\ Q_n & -Q_i & Q \end{bmatrix} \times \begin{Bmatrix} 1 & 1 & K \\ J_{f'} & J_{f'} & J_{g'} \end{Bmatrix} \langle {}^{f'f'}\rho_Q'^K(v_r)\rangle , \tag{52}$$

where the $\bar{\epsilon}_i$ ($i = -1, 0, 1$) specify the polarization of the fluorescence according to Eq. (19) (replacing the external-field polarization vector $\vec{\epsilon}$ by the vacuum-field polarization vector $\vec{\bar{\epsilon}}$) and $\langle {}^{f'f'}\rho_Q'^K\rangle$ is the average value of the reduced density-matrix element ${}^{f'f'}\rho_Q'^K$ of atom A'. Adopting a simple model, I assume that the lifetimes of the various ${}^{ff'}\rho_Q'^K$, once created by RAIC, are determined only by the natural decay rate $\gamma_{f'}$ of level f' (i.e., the natural decay rate is much greater than the collision rate and the frequency separation of the final states). In that limit

$$\langle {}^{f'f'}\rho_Q'^K(v_r)\rangle = \mathfrak{N}_A v_r {}^{f'f'}\sigma_Q'^K(v_r) \times [N_p(T^+ - T^-)/\gamma_{f'}] , \tag{53}$$

where $\mathfrak{N}_A$ is the A-atom density and N_p is the number of pulses per second, each of duration $(T^+ - T^-)$. Thus, from Eqs. (52) and (53), one finds

$$S \propto (-1)^{Q_n} \bar{\epsilon}_i^* \bar{\epsilon}_n (-1)^K \begin{bmatrix} 1 & 1 & K \\ Q_n & -Q_i & Q \end{bmatrix} \times \begin{Bmatrix} 1 & 1 & K \\ J_{f'} & J_{f'} & J_{g'} \end{Bmatrix} {}^{f'f'}\sigma_Q'^K(v_r) . \tag{54}$$

For an external field polarized according to (51), it is convenient to measure the fluorescence also propagating in the y direction and polarized in either the x or z direction (Fig. 5). That is, one measures a signal S_x characterized by

$$\bar{\epsilon}_x = 1, \quad \bar{\epsilon}_y = \bar{\epsilon}_z = 0; \quad \bar{\epsilon}_1 = -\bar{\epsilon}_{-1} = \frac{-1}{\sqrt{2}}, \quad \bar{\epsilon}_0 = 0 , \tag{55a}$$

a signal S_z characterized by

$$\bar{\epsilon}_x = \bar{\epsilon}_y = 0, \quad \bar{\epsilon}_z = 1; \quad \bar{\epsilon}_{\pm 1} = 0, \quad \bar{\epsilon}_0 = 1 , \tag{55b}$$

and forms the ratio

$$P = (S_z - S_x)/(S_z + S_x) . \tag{56}$$

Before explicitly calculating this ratio, it is useful to note that the general expression for $\rho_Q'^K$ and, consequently, for $\sigma_Q'^K$ is proportional to

$$P_{KQ} = \epsilon_j^* \epsilon_s (-1)^{Q_s} \begin{bmatrix} 1 & 1 & K \\ Q_j & -Q_s & Q \end{bmatrix}$$

so that, for the excitation scheme of Eq. (51) with the Q_i defined by Eq. (27b), one has

$$P_{KQ} = -(1/\sqrt{3})\,\delta_{K0}\delta_{Q0} + (2/\sqrt{6})\,\delta_{K2}\delta_{Q0} . \tag{57}$$

Thus only $\sigma_0'^0$ and $\sigma_0'^2$ enter the summation in Eq. (54). Using this fact and Eqs. (54)–(56), one can derive a polarization ratio

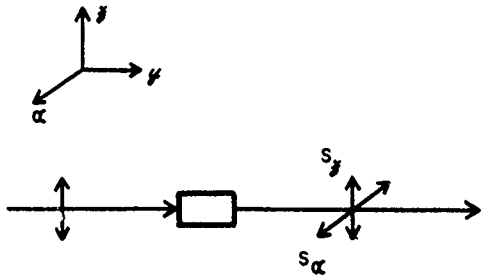

FIG. 5. Excitation-detection scheme. The external field is linearly polarized in the z direction and is incident in the y direction. The fluorescence from the $f' \rightarrow g'$ transition of atom A', propagating in the y direction and polarized in either the x direction (S_x) or z direction (S_z), is monitored.

$$P(\Delta)=3\left(\frac{2\sqrt{6}(-1)^{J_{f'}+J_{g'}}}{3(2J_{f'}+1)^{1/2}}\begin{Bmatrix}1 & 1 & 2\\ J_{f'} & J_f & J_{g'}\end{Bmatrix}^{-1}\frac{f'f'\sigma'^0_0(v_r,\Delta)}{f'f'\sigma'^2_0(v_r,\Delta)}+1\right)^{-1}. \tag{58}$$

Within the confines of the adopted model, the ratio P depends only on *relative* RAIC cross sections and not on *absolute* cross sections. Consequently, it is a useful parameter in comparing theory with experiment.

The ratio P is now calculated for the level schemes of Fig. 4. For the level scheme of Fig. 4(a), it follows from Eqs. (58), (42), and (51) that, for central tuning, $\Delta=0$,

$$P_a(0)=3\left(\frac{20(-1)^{J_f+J_{g'}-J_i-J_{i'}}}{9(2J_{f'}+1)(2J_r+1)\begin{Bmatrix}1 & 1 & 2\\ J_{f'} & J_f & J_{g'}\end{Bmatrix}\begin{Bmatrix}1 & 1 & 2\\ J_r & J_r & J_f\end{Bmatrix}\begin{Bmatrix}1 & 1 & 2\\ J_r & J_r & J_i\end{Bmatrix}\begin{Bmatrix}1 & 1 & 2\\ J_{f'} & J_f & J_{i'}\end{Bmatrix}}+1\right)^{-1}. \tag{59}$$

For the specific case,

$$J_{i'}=J_{g'}=J_i=J_f=0;\quad J_{f'}=J_r=1;\quad P_a(0)=\tfrac{1}{7}, \tag{60}$$

while, for higher J values, $P_a(0)$ is smaller. For the level scheme of Fig. 4(b), one may derive from Eqs. (58), (45), and (51),

$$P_b(0)=3\left(\frac{2(-1)^{J_r-J_{g'}}}{3(2J_{f'}+1)\begin{Bmatrix}1 & 1 & 2\\ J_{f'} & J_f & J_{g'}\end{Bmatrix}\begin{Bmatrix}1 & 1 & 2\\ J_{f'} & J_f & J_{r'}\end{Bmatrix}}+1\right)^{-1}. \tag{61}$$

Some specific cases are

$$J_{g'}=J_{r'}=1,\quad J_{f'}=2,\quad P_b(0)=\tfrac{21}{47}, \tag{62a}$$

$$J_{g'}=J_{r'}=0,\quad J_{f'}=1,\quad P_b(0)=1. \tag{62b}$$

For the level scheme of Fig. 4(c), it follows from Eqs. (58), (47), and (51) that

$$P_c=P_a. \tag{63}$$

This result is unique to the dipole-dipole interaction. For the level scheme of Fig. 4(d), one may derive from Eqs. (58), (48), and (51) that

$$P_d(0)=3\left(\frac{2(-1)^{J_{g'}+J_{i'}}}{3(2J_{f'}+1)(2J_{r'}+1)\begin{Bmatrix}1 & 1 & 2\\ J_{f'} & J_f & J_{g'}\end{Bmatrix}\begin{Bmatrix}J_{f'} & J_{f'} & 2\\ J_{r'} & J_{r'} & 1\end{Bmatrix}\begin{Bmatrix}1 & 1 & 2\\ J_{r'} & J_{r'} & J_{i'}\end{Bmatrix}}+1\right)^{-1}. \tag{64}$$

Some specific cases are

$$J_{i'}=0,\quad J_{g'}=J_{r'}=1,\quad J_{f'}=2,\quad P_d(0)=\tfrac{21}{47}, \tag{65a}$$

$$J_{i'}=J_{f'}=1,\quad J_{g'}=J_{r'}=0,\quad P_d(0)=0. \tag{65b}$$

The physical significance of these results is discussed in the following section.

VI. DISCUSSION

A RAIC is one of the most basic forms of photochemistry. It is, therefore, of fundamental interest to understand the collisional interactions taking part in these reactions. The nature of the collisional interaction is reflected in (1) the total RAIC cross sections, (2) the dependence of RAIC cross sections on detuning Δ, and (3) the final-state coherences produced by RAIC. Total cross-section measurements are not very useful in distinguishing between various collisional interactions since accurate theoretical expressions are not available for comparison with experiment (i.e., there do not exist theoretical calculations in which matrix elements are accurately calculated along with a proper treatment of small-impact-parameter collisions). The dependence of RAIC total cross sections on Δ *does* provide a signature for the collisional interaction, provided one uses de-

tunings outside the impact core of the line $|\Delta|\tau_c > 1$. A limited number of experiments of this type have been performed,[10] but no definite conclusion on the interaction potential was reached. It should be noted that, for $|\Delta|\tau_c > 1$, the RAIC excitation cross sections are relatively small. The study of final-state coherences produced by RAIC offers an additional method for probing the collisional interaction. In many cases (see below), measurements of RAIC-induced final-state coherences at central tuning $\Delta = 0$ (where signal is the largest) are sufficient to provide information concerning the collisional interaction.

Perhaps the most important aspect connected with the study of RAIC-induced coherences is the additional insight one can gain into the RAIC process. The calculation of final-state coherences introduces features into the problem that need not be considered when one calculates *total* RAIC cross sections. A particularly interesting feature can be already seen in the calculation presented in this paper, valid in the impact core of the RAIC profile and in the perturbation-theory limit. The collisional interaction can be viewed as the interaction of two unpolarized multipolar fields with atoms A and A'; the fields are incident from all directions and lead to the simultaneous (virtual) excitation of atoms A and A'. Although the fields are unpolarized, they are, in general, correlated to one another by the coupling coefficients of the collisional interaction [see the discussion of Fig. 4(a) below].

The unpolarized nature of the fields arises from the average over all possible collision orientations. This result may be seen mathematically in Eqs. (A20) and (B2). In Eq. (A20), starting from initial density matrix elements $\rho^{K'}_{Q'}$, one excites final-state density-matrix elements ρ^{K}_{Q} with $|K - K'| \leq 2$. This type of selection rule is precisely that produced by the external field acting alone. In other words, the averaged collisional interaction does not modify the selection rule determined by the external field alone—an average collision acts as a scalar, i.e., as an unpolarized field. Similarly, in Eq. (B2), one sees that, starting from an unpolarized initial state, one excites reduced density-matrix elements ρ'^{K}_{Q} with $K \leq 2$; the selection rule is that associated with the external field only. In contrast to these results, one finds that, for a collision with a *specific* orientation, one could excite density-matrix elements ρ^{K}_{Q} from initial density-matrix elements $\rho^{K'}_{Q'}$ such that $|K - K'| > 2$. It is only the *averaged* collisional interaction that acts as a scalar.

Thus the total RAIC reaction can be viewed as two unpolarized (but correlated) multipolar fields *plus* the external radiation field acting on atoms A and A' to produce the $ii' \rightarrow ff'$ transition. To simulate the collisional interaction, the unpolarized fields are taken to act simultaneously on atoms A and A'; one field acts only on atom A while the other acts only on atom A' (in analogy with the fact that the collision operators act on either atom A or A', but not both). The external field acts on either atom A or A'. Using this model it is relatively easy to give a physical interpretation to the results obtained in Secs. IV and V for the level schemes of Fig. 4.

Figure 4(b). For the level scheme of Fig. 4(b), the collision first acts to produce the virtual state $|fr'\rangle$. If the collision is now replaced by two unpolarized multipolar fields incident from all directions, the coherence properties of this intermediate state are immediately determined. Since the initial state was unpolarized and the average collision operator now acts as a scalar, the intermediate state must also be unpolarized. Thus, when the external field completes the RAIC reaction by acting on atom A', the coherence properties of the final state f' of atom A' are the same as those produced by a radiation field exciting the $r' \rightarrow f'$ transition in atom A' for an initially unpolarized state r'. The factor

$$\epsilon^*_f \epsilon_s (-1)^{Q_s} \begin{bmatrix} 1 & 1 & K \\ Q_f & -Q_s & Q \end{bmatrix} \begin{Bmatrix} 1 & 1 & K \\ J_f, & J_f, & J_r \end{Bmatrix}$$

appearing in Eq. (45) for the excitation cross section is precisely that associated with the one-photon $r' \rightarrow s'$ transition, assuming state r' to be unpolarized.

The collisional interaction affects the magnitude of the RAIC cross sections through a multiplicative factor. Consequently, the polarization ratio $P_b(0)$ discussed in Sec. V B is independent of the collisional interaction; it depends only on the values J_r, J_f, J_g, reflecting the field excitation from $r' \rightarrow f'$ followed by spontaneous emission from f' to g'. Thus, the level scheme [Fig. 4(b)] is not particularly well suited for probing the collisional interaction via polarization studies at line center; RAIC cross sections as a function of frequency are needed.

Figure 4(d). For the level scheme of Fig. 4(d), the field produces a polarized virtual state $|ir'\rangle$ and the two unpolarized fields (collision) complete the transition to state $|ff'\rangle$. The final-state coherence of atom A' can then be thought to be produced by the external field acting on the $i' \rightarrow r'$ transition and an unpolarized multipolar field incident from all directions acting on the transition $r' \rightarrow f'$. The transition amplitude for the $r' \rightarrow f'$ transition depends on the multipolarity of the collision interaction; this dependence is given by the weighting factor

$$\begin{Bmatrix} J_f, & J_f, & K \\ J_r, & J_r, & k' \end{Bmatrix}$$

appearing in Eq. (48). Since this weighting factor couples K and k', the final-state coherence and the polarization ratio P_ℓ can be used to distinguish different collisional interactions.

For the dipole-dipole interaction, $k'=1$, and the collision interaction on atom A' can be replaced by an unpolarized electric field incident from all directions producing the $r' \rightarrow f'$ transition. Thus the coherence properties of state f' of atom A' are the same as those produced by *two-photon excitation* of atom A', the first photon provided by the external field producing the transition $i' \rightarrow r'$ and the second by an unpolarized electric field incident from all directions producing the transition $r' \rightarrow f'$. The polarization ratio $P_\ell(0)$ for the excitation-detection scheme of Fig. 5 is then easily calculated to be the simple function of $J_{i'}, J_{r'}, J_{f'}, J_{\ell'}$ given by Eq. (64).

Figure 4(a). For the level scheme of Fig. 4(a), the two unpolarized multipolar fields incident from all directions first excite the virtual state $|rf'\rangle$ and the external field acts on atom A to complete the transition to state $|ff'\rangle$. One might think that the final state f' of atom A' would be unpolarized since it was produced by an unpolarized field incident from all directions. However, this conclusion need not be true owing to *correlation* effects between the unpolarized fields. This effect is best illustrated by the case of $J_i = J_f = 0$, $J_r = 1$, and an external field polarized linearly in the z direction. In order for the overall $\Delta m = 0$ selection rule to be satisfied, only that part of the unpolarized field producing a $\Delta m = 0$ transition is utilized. Thus, only a *part* of the unpolarized field acting on atom A is used. Owing to the coupling coefficients $A_{qq'}^{kk'}$ in the collisional interaction, this result implies that, correspondingly, only a *part* of the unpolarized multipolar field acting on atom A' contributes in the $i' \rightarrow f'$ excitation. This result, in turn, implies that state f' can be polarized. For the conditions of Eq. (60), a polarization ratio $P_\ell(0) = \frac{1}{7}$ was found. Since the polarization ratio for case Fig. 4(a) is a function of the multipolarity of the collisional interaction, it can be used to provide an indication of the collisional processes participating in RAIC.

Figure 4(c). The analysis of the level scheme of Fig. 4(c) is similar to that for Fig. 4(a), except that the field acts on atom A' rather than on atom A. For the dipole-dipole interaction, in which the external field and the collisional operators have the same multipolarity ($k = k' = p = p' = 1$), the RAIC cross sections for cases Figs. 4(a) and 4(d) are proportional to one another; for other collisional interactions, this proportionality is lost.

In order to have a more complete picture of the final-state coherences produced by RAIC, it is desirable to extend the theory to include the cases of large detuning ($|\Delta|\tau_c > 1$) and large field strengths (nonperturbative solution). Such extensions may pose some interesting problems in the average over collision orientations, since the collision interaction no longer enters linearly in the final-state amplitude. Owing to this nonlinearity, the analog between an average collision and an unpolarized field may no longer be useful.

In summary, I have presented a calculation of the final-state coherences produced by RAIC in the weak-field limit that is valid in the impact core of the RAIC excitation profile. The resulting final-state coherences can be monitored by standard techniques (polarization of fluorescence, quantum beats) and may provide information on the collisional interactions occurring in the RAIC reaction.

ACKNOWLEDGMENT

This research was carried out while I was a guest at the Laboratoire Aimé Cotton, Orsay, France. The hospitality shown to me during my stay is deeply acknowledged as are conversations with C. Bréchignac, Ph. Cahuzac, J. L. Le Gouët, J. L. Picqué, and R. Vetter. I should also like to acknowledge financial support from the Fulbright Foundation. This research was also supported by the U. S. Office of Naval Research.

APPENDIX A

Appendix A is divided into three parts. In part A, some notation is introduced and the relationship between the direct product and irreducible-tensor subspaces is established. In part B, the relationship between the two-particle and single-particle (reduced) density-matrix elements is given. Finally, in part C, the final-state density-matrix for RAIC is calculated.

A. Relationship between bases

A state of the composite AA' system is represented by a capital letter, e.g.,

$$|F\rangle = |ff'\rangle = |f\rangle|f'\rangle' \equiv |fJ_f m_f\rangle|f'J_{f'} m_{f'}\rangle', \tag{A1}$$

where it has been assumed that the angular momentum of a level can be represented by a J quantum number. The angular momenta appearing in the direct product basis (A1) can be coupled in the standard fashion,

$$|\bar{F}\rangle \equiv |ff'J_fJ_{f'}J_F m_F\rangle = \begin{bmatrix} J_f & J_{f'} & J_F \\ m_f & m_{f'} & m_F \end{bmatrix} |fJ_f m_f\rangle |f'J_{f'} m_{f'}\rangle' , \quad \text{(A2)}$$

where the bar indicates this coupled basis. As in the main text, I use a summation convention in which all repeated indices (not including their appearance in phase factors or frequency denominators) are summed over.[2]

Matrix elements of the density-matrix operator in the barred basis are related to those in an irreducible tensor basis, ${}^{\bar{F}\bar{F}_1}\rho_Q^K$, via the transformations

$$\rho_{\bar{F}\bar{F}_1} = \langle \bar{F}|\rho|\bar{F}_1\rangle = (-1)^{J_{\bar{F}_1} - m_{\bar{F}_1}} \begin{bmatrix} J_{\bar{F}} & J_{\bar{F}_1} & K \\ m_{\bar{F}} & -m_{\bar{F}_1} & Q \end{bmatrix} {}^{\bar{F}\bar{F}_1}\rho_Q^K , \quad \text{(A3a)}$$

$${}^{\bar{F}\bar{F}_1}\rho_Q^K = (-1)^{J_{\bar{F}_1} - m_{\bar{F}_1}} \begin{bmatrix} J_{\bar{F}} & J_{\bar{F}_1} & K \\ m_{\bar{F}} & -m_{\bar{F}_1} & Q \end{bmatrix} \times \langle \bar{F} J_{\bar{F}} m_{\bar{F}} |\rho| \bar{F}_1 J_{\bar{F}_1} m_{\bar{F}_1}\rangle , \quad \text{(A3b)}$$

where the total J and m_f values of the barred basis are explicitly written in the right-hand side of Eq. (A3b).

The time rate of change of density-matrix elements produced by RAIC can be expressed as[4]

$$\dot{\rho}_{FF_1} = \Gamma^{II_1}_{FF_1} \rho_{II_1} \quad \text{(A4a)}$$

or

$${}^{\bar{F}\bar{F}_1}\dot{\rho}_Q^K = \Gamma^{K'Q'}_{KQ}(\bar{F}, \bar{F}_1, \bar{I}, \bar{I}_1)^{\bar{I}\bar{I}_1} \rho_{Q'}^{K'} . \quad \text{(A4b)}$$

The relationship between the Γ's may be obtained from Eqs. (A1)–(A4) as

$$\Gamma^{K'Q'}_{KQ}(\bar{F}, \bar{F}_1, \bar{I}, \bar{I}_1) = (-1)^{\bar{I}_1 - m_{\bar{I}_1}} (-1)^{\bar{F}_1 - m_{\bar{F}_1}} \begin{bmatrix} J_f & J_{f'} & J_{\bar{F}} \\ m_f & m_{f'} & m_{\bar{F}} \end{bmatrix} \begin{bmatrix} J_{f_1} & J_{f_1'} & J_{\bar{F}_1} \\ m_{f_1} & m_{f_1'} & m_{\bar{F}_1} \end{bmatrix}$$
$$\times \begin{bmatrix} J_{\bar{F}} & J_{\bar{F}_1} & K \\ m_{\bar{F}} & -m_{\bar{F}_1} & Q \end{bmatrix} \begin{bmatrix} J_i & J_{i'} & J_{\bar{I}} \\ m_i & m_{i'} & m_{\bar{I}} \end{bmatrix} \begin{bmatrix} J_{i_1} & J_{i_1'} & J_{\bar{I}_1} \\ m_{i_1} & m_{i_1'} & m_{\bar{I}_1} \end{bmatrix} \begin{bmatrix} J_{\bar{I}} & J_{\bar{I}_1} & K' \\ m_{\bar{I}} & -m_{\bar{I}_1} & Q' \end{bmatrix}$$
$$\times \Gamma^{II_1}_{FF_1}(m_f, m_{f'}, m_{f_1}, m_{f_1'}, m_{i'}, m_{i_1'}, m_{i_1}, m_{i_1'}) \quad \text{(A5)}$$

along with the corresponding inverse transformation.

B. Reduced density-matrix elements

The reduced density-matrix elements for atom A' are defined by

$$\rho'_{f'f_1'} = \langle ff'|\rho|ff_1'\rangle . \quad \text{(A6)}$$

In terms of the matrix elements of irreducible-tensor operators defined by Eq. (23a), one can use Eqs. (A1)–(A3) and some elementary properties of the Clebsch-Gordon coefficient to derive

$$f'f_1'\rho_Q'^K = (-1)^{J_{f_1'} + J_{\bar{F}} + J_f - K} [(2J_{\bar{F}}+1)(2J_{\bar{F}_1}+1)]^{1/2} \begin{Bmatrix} J_{\bar{F}} & J_{\bar{F}_1} & K \\ J_{f_1'} & J_{f_1} & J_f \end{Bmatrix} {}^{\bar{F}\bar{F}_1}\rho_Q^K (ff'J_fJ_{f'}, J_{\bar{F}}; ff_1'J_fJ_{f_1'}J_{\bar{F}_1}) . \quad \text{(A7)}$$

Equation (A7), in which the $\{\ \}$ represents a 6-J symbol, enables one to calculate the reduced density-matrix elements of atom A' from the two-particle density-matrix elements. Similarly, reduced matrix elements of atom A are given by

$$\rho_{ff_1} = \langle ff'|\rho|f_1f'\rangle \quad \text{(A8)}$$

and

$${}^{ff_1}\rho_Q^K = (-1)^{J_f + J_{\bar{F}_1} + J_{f'} - K} [(2J_{\bar{F}}+1)(2J_{\bar{F}_1}+1)]^{1/2} \begin{Bmatrix} J_{\bar{F}} & J_{\bar{F}_1} & K \\ J_{f_1} & J_f & J_{f'} \end{Bmatrix} {}^{\bar{F}\bar{F}_1}\rho_Q^K (ff'J_fJ_{f'}, J_{\bar{F}}; f_1f'J_{f_1}J_{f'}, J_{\bar{F}_1}) . \quad \text{(A9)}$$

C. Calculation of ${}^{\overline{FF}_1}\rho_Q^K$

Starting from Eq. (10), I now derive an expression for ${}^{\overline{FF}_1}\rho_Q^K(t_c^+; b, v_r, \vec{R}_c, t_c)$. Equation (10) may be written

$$a_F(t_c^+) = \langle F | \tilde{T} | I \rangle a_I(t_c^-) , \tag{A10a}$$

where

$$\langle F | \tilde{T} | I \rangle = (i\hbar)^{-1} \int_{t_c^-}^{t_c^+} \langle F | \hat{T}(IF, t) | I \rangle e^{-i\Delta t} dt . \tag{A10b}$$

Equation (A10a) could equally well be given in the coupled (barred) basis as

$$a_{\overline{F}}(t_c^+) = \langle \overline{F} | \tilde{T} | \overline{I} \rangle a_{\overline{I}}(t_c^-) , \tag{A11}$$

so that the final-state density matrix is

$$\rho_{\overline{FF}_1}(t_c^+; b, v_r, \Theta, \vec{R}_c, t_c) = \langle \overline{F} | \tilde{T} | \overline{I} \rangle \langle \overline{F}_1 | \tilde{T} | \overline{I}_1 \rangle^* \rho_{\overline{II}_1}(t_c^-) . \tag{A12}$$

The matrix elements of $\tilde{T}$ are expanded as

$$\langle \overline{F} | \tilde{T} | \overline{I} \rangle = (-1)^{J_{\overline{I}} - m_{\overline{I}}} \begin{bmatrix} J_{\overline{F}} & J_{\overline{I}} & G \\ m_{\overline{F}} & -m_{\overline{I}} & g \end{bmatrix} {}^{\overline{FI}}\tilde{T}_g^G . \tag{A13}$$

Equation (A3a) is used, and some identities involving the angular momentum coupling coefficients are employed to transform equation (A12) into

$${}^{\overline{FF}_1}\rho_Q^K(t_c^+; b, v_r, \vec{R}_c, t_c) = (-1)^{2J_{\overline{F}} + G' + 2J_{\overline{I}} + K'} (-1)^{g'+Q'} [(2G+1)(2G'+1)(2K+1)(2K'+1)]^{1/2}$$

$$\times \begin{bmatrix} K & K' & X \\ Q & -Q' & m_x \end{bmatrix} \begin{bmatrix} G & G' & X \\ g & -g' & m_x \end{bmatrix} \begin{Bmatrix} \overline{F} & \overline{F}_1 & K \\ \overline{I} & \overline{I}_1 & K' \\ G & G' & X \end{Bmatrix} H(\overline{F}, \overline{F}_1, \overline{I}, \overline{I}_1, G, G', g, g') {}^{\overline{II}_1}\rho_Q^{K'}(t_c^-) , \tag{A14}$$

where

$$H(\overline{F}, \overline{F}_1, \overline{I}, \overline{I}_1, G, G', g, g') \equiv (8\pi^2)^{-1} \int d\Theta \, {}^{\overline{FI}}\tilde{T}_g^G (\overline{F}_1 \overline{I}_1 \tilde{T}_{g'}^{G'})^* \tag{A15}$$

and the quantity in large curly brackets is a 9-J symbol. The quantities ${}^{\overline{FI}}\tilde{T}_g^G$ may be calculated by (i) using Eqs. (A13), (A10b), (6), (13), (18); (ii) expanding all intermediate states appearing in Eq. (6) in terms of the barred basis; and (iii) using the Wigner-Eckart theorem to evaluate matrix elements of $(\mu_T)_q^1$ and ${}^{kk'}V_Q^K$. One obtains

$$\begin{aligned} {}^{\overline{FI}}\tilde{T}_g^G = {} & (-1)^{3J_{\overline{F}} + J_{\overline{I}} + 2J_{\overline{E}} + K + 1} \langle \overline{F} \| (\mu_T)^{(1)} \| \overline{E} \rangle \langle \overline{E} \| {}^{kk'}V^{(K)} \| \overline{I} \rangle (\omega_{EI})^{-1} \\ & \times (i\hbar)^{-1} \left(\frac{b}{v_r} \right) {}^{kk'}A_Q^K(b, v_r, \Theta; \Delta) \epsilon_j^* \begin{bmatrix} K & 1 & G \\ Q & Q_j & g \end{bmatrix} \begin{Bmatrix} K & 1 & G \\ J_{\overline{I}} & J_{\overline{F}} & J_{\overline{E}} \end{Bmatrix} \mathcal{E}_c \\ & + (-1)^{J_{\overline{F}} + J_{\overline{I}} + G} \langle \overline{F} \| {}^{kk'}V^{(K)} \| \overline{E} \rangle \langle \overline{E} \| (\mu_T)^{(1)} \| \overline{I} \rangle (\omega_{EF})^{-1} \\ & \times (i\hbar)^{-1} \left(\frac{b}{v_r} \right) {}^{kk'}A_Q^K(b, v_r, \Theta; \Delta) \epsilon_j^* \begin{bmatrix} K & 1 & G \\ Q & Q_j & g \end{bmatrix} \begin{Bmatrix} K & 1 & G \\ J_{\overline{I}} & J_{\overline{F}} & J_{\overline{E}} \end{Bmatrix} \mathcal{E}_c \end{aligned} \tag{A16}$$

where ${}^{kk'}A_Q^K(b, v_r, \Theta; \Delta)$ is defined by Eq. (16b), $\langle \| \cdots \| \rangle$ is a reduced matrix element, ϵ_j is defined by Eqs. (17)–(19), and

$$Q_1=1,\ Q_{-1}=-1,\ Q_0=0. \tag{A17}$$

Equation (A16) and its complex conjugate are now inserted into Eq. (A15), and Eqs. (15) and (21) are used to arrive at

$$H(\bar{F},\bar{F}_1,\bar{I},\bar{I}_1,\ G,G',g,g')=\left(\frac{b\mathcal{E}_a}{\hbar v_r}\right)^2(2K+1)^{-1}\epsilon_j^*\epsilon_s\,{}^{kk'}A_Q^K(b,v_r,0;\Delta)[{}^{pp'}A_{Q'}^K(b,v_r,0;\Delta)]^*$$
$$\times\begin{bmatrix}K & 1 & G\\ Q & Q_j & g\end{bmatrix}\begin{bmatrix}K & 1 & G'\\ Q' & Q_s & g'\end{bmatrix}C(\bar{F},\bar{I},G,k,k',K)[C(\bar{F}_1,\bar{I}_1,G',p,p',K)]^*, \tag{A18}$$

where

$$C(\bar{F},\bar{I},G,k,k',K)=(-1)^{3J_{\bar{F}}+J_{\bar{I}}+2J_{\bar{E}}+K+1}(\omega_{\bar{E}\bar{I}})^{-1}\langle\bar{F}||(\mu_T)^{(1)}||\bar{E}\rangle\langle\bar{E}||{}^{kk'}V^{(K)}||\bar{I}\rangle\begin{Bmatrix}K & 1 & G\\ J_{\bar{F}} & J_{\bar{I}} & J_{\bar{E}}\end{Bmatrix}$$
$$+(-1)^{J_{\bar{F}}+J_{\bar{I}}+G}(\omega_{\bar{E}\bar{F}})^{-1}\langle\bar{F}||{}^{kk'}V^{(K)}||\bar{E}\rangle\langle\bar{E}||(\mu_T)^{(1)}||\bar{I}\rangle\begin{Bmatrix}K & 1 & G\\ J_{\bar{I}} & J_{\bar{F}} & J_{\bar{E}}\end{Bmatrix}. \tag{A19}$$

The quantity C is easily identified with the four diagrams of Figs. 2 and 3.

Combining Eqs. (A18) and (A19) and carrying out the summations over magnetic quantum numbers, one obtains

$${}^{\bar{F}\bar{F}_1}\rho_Q^K(t_c^+;b,v_r,\vec{R}_c,t_c)=(-1)^{2J_{\bar{I}}+2J_{\bar{F}}+G+K'+\tilde{K}+X}(-1)^{Q'+Q_j+m_x}\left(\frac{b\mathcal{E}_a}{\hbar v_r}\right)^2$$
$$\times\epsilon_j^*\epsilon_s[(2G+1)(2G'+1)(2K+1)(2K'+1)]^{1/2}\begin{bmatrix}K & K' & X\\ Q & -Q' & m_x\end{bmatrix}$$
$$\times\begin{bmatrix}1 & 1 & X\\ Q_j & -Q_s & m_x\end{bmatrix}{}^{kk'}A_Q^{\tilde{K}}(b,v_r,0;\Delta)[{}^{pp'}A_Q^{\tilde{K}}(b,v_r,0;\Delta)]^*\begin{Bmatrix}1 & 1 & X\\ G & G' & \tilde{K}\end{Bmatrix}\begin{Bmatrix}\bar{F} & \bar{F}_1 & K\\ \bar{I} & \bar{I}_1 & K'\\ G & G' & X\end{Bmatrix}$$
$$\times C(\bar{F},\bar{I},G,k,k',\tilde{K})[C(\bar{F}_1,\bar{I}_1,G',p,p',\tilde{K})]^*{}^{\bar{I}\bar{I}_1}\rho_{Q'}^{K'}(t_c^-). \tag{A20}$$

It is clear from this equation that $|K'-K|<2$, i.e., that the collision acts in some way as a scalar operator (see Sec. VI). Reduced density-matrix elements may be obtained from Eq. (A20) by use of Eqs. (A7) and (A9). Density-matrix elements in the magnetic sublevel basis are related to those in the irreducible tensor basis by Eqs. (A3) and (A2) or, for reduced density-matrix elements, by Eq. (23b).

APPENDIX B

Unpolarized initial state

In Appendix B, the reduced density-matrix elements for atom A' are calculated *for an unpolarized initial state.* An unpolarized initial state corresponds to

$${}^{\bar{I}\bar{I}_1}\rho_Q^K(t_c^-)=(2J_{\bar{I}}+1)^{1/2}N_I^{-1}\delta_{\bar{I}\bar{I}_1}\delta_{K0}\delta_{Q0}, \tag{B1}$$

where N_I is the total number of initial states. Using Eqs. (A7), (A20), and (B1), one may obtain after a little algebra[5] the reduced density-matrix elements for atom A',

$${}^{f'f_1'}\rho_{Q'}^{K'}(t_c^+;b,v_r,\vec{R}_c,t_c)=\sum_j(-1)^{J_f+J_{f_1'}+K+K'+G+G'}\left(\frac{b\mathcal{E}_c}{\hbar v_r}\right)^2(2G+1)(2G'+1)$$
$$\times[(2J_{\bar{F}}+1)(2J_{\bar{F}_1}+1)]^{1/2}[N_I(2K'+1)]^{-1}{}^{kk'}A_{Q'}^{K'}(b,v_r,0;\Delta)$$
$$\times{}^{pp'}A_{Q'}^{K'}(b,v_r,0;\Delta)]^*\epsilon_j^*\epsilon_s(-1)^{Q_s}\begin{bmatrix}1 & 1 & K\\ Q_j & -Q_s & Q\end{bmatrix}\begin{Bmatrix}1 & 1 & K\\ G & G' & K'\end{Bmatrix}$$
$$\times\begin{Bmatrix}G & G' & K\\ J_{\bar{F}_1} & J_{\bar{F}} & J_{\bar{I}}\end{Bmatrix}\begin{Bmatrix}J_{\bar{F}_1} & J_{\bar{F}} & K\\ J_{f'} & J_{f_1'} & J_f\end{Bmatrix}C(\bar{F},\bar{I},G,k,k',K')$$
$$\times[C(\bar{F}_1,\bar{I},G',p,p',K')]^*. \tag{B2}$$

The product of the C's can be calculated explicitly and the final expression simplified using identities involving the angular momenta coupling coefficients.[5]

One obtains 16 terms corresponding to the square of the four terms contributing to the amplitude in Fig. 2. The result may be written in the form

$$f'f'_1\rho'^{K}_{Q}(t_c^+;b,v_r,\vec{R}_c,t_c)=\left(\frac{b\mathcal{E}_c}{\hbar v_r}\right)^2 N_I^{-1}i^{k-k'}A^{K'}_{Q'}(b,v_r,0;\Delta)[i^{p-p'}A^{K'}_{Q'}(b,v_r,0;\Delta)]^*\epsilon^*_j\epsilon_a(-1)^{Q_a}\begin{bmatrix}1 & 1 & K\\ Q_j & -Q_a & Q\end{bmatrix}$$

$$\times\sum_{\alpha,\beta=a}^{d}\mathcal{S}_{\alpha\beta}(k,k',p,p',K,K',f',f'_1)\,, \tag{B3}$$

where $\mathcal{S}_{\alpha\beta}$ represents the contribution from diagram α and the complex conjugate of diagram β in Fig. 2. Explicitly,

$$\mathcal{S}_{aa}=[(\omega_e+\omega_{f'}-\omega_I)(\omega_e+\omega_{f'}-\omega_I)]^{-1}(-1)^{J_e-J_d-J_{f'}+J_f-J_i-J_{i'}+K'+p'+k'}$$
$$\times\langle f\,||\mu^{(1)}||e\rangle\langle f\,||\mu^{(1)}||d\rangle^*\langle e||T^{(k)}||i\rangle\langle d||T^{(p)}||i\rangle^*\langle f'||T'^{(k')}||i'\rangle\langle f'_1||T'^{(p')}||i'\rangle^*$$
$$\times\begin{Bmatrix}1 & 1 & K\\ J_e & J_d & J_f\end{Bmatrix}\begin{Bmatrix}k & p & K\\ J_d & J_e & J_i\end{Bmatrix}\begin{Bmatrix}k' & p' & K\\ p & k & K'\end{Bmatrix}\begin{Bmatrix}k' & p' & K\\ J_{f'_1} & J_{f'} & J_{i'}\end{Bmatrix}, \tag{B4}$$

$$\mathcal{S}_{ab}=[(\omega_e+\omega_{f'}-\omega_I)(\omega_f+\omega_{d'}-\omega_I)]^{-1}(-1)^{K-2J_e+J_{d'}+J_f-J_i-J_{i'}+k'+p'}$$
$$\times\langle f\,||\mu^{(1)}||e\rangle\langle f'_1||\mu'^{(1)}||d'\rangle^*\langle e||T^{(k)}||i\rangle\langle f\,||T^{(p)}||i\rangle^*\langle f'||T'^{(k')}||i'\rangle\langle f'_1||T'^{(p')}||d'\rangle^*$$
$$\times\begin{Bmatrix}1 & 1 & K\\ J_{f'} & J_{f'_1} & J_{d'}\end{Bmatrix}\begin{Bmatrix}k & p & 1\\ k' & p' & K'\end{Bmatrix}\begin{Bmatrix}k & p & K'\\ J_f & J_e & J_i\end{Bmatrix}\begin{Bmatrix}k' & p' & 1\\ J_{d'} & J_{f'} & J_{i'}\end{Bmatrix}, \tag{B5}$$

$$\mathcal{S}_{bb}=[(\omega_f+\omega_{e'}-\omega_I)(\omega_p+\omega_{d'}-\omega_I)]^{-1}(-1)^{K+J_{f'}+J_{e'}}[(2J_{e'}+1)(2k+1)(2k'+1)]^{-1}$$
$$\times\delta_{J_{e'}J_{d'}}\delta_{kp}\delta_{k'p'}\langle f'||\mu'^{(1)}||e'\rangle\langle f'_1||\mu'^{(1)}||d'\rangle^*|\langle F||T^{(k)}||i\rangle|^2\langle e'||T'^{(k')}||i'\rangle$$
$$\times\langle d'||T'^{(k')}||i'\rangle^*\begin{Bmatrix}1 & 1 & K\\ J_{f'} & J_{f'_1} & J_{e'}\end{Bmatrix}, \tag{B6}$$

$$\mathcal{S}_{cc}=[(\omega_e+\omega_{f'}-\omega_I)(\omega_d+\omega_{i'}-\omega_p)]^{-1}(-1)^{J_i+J_{i'}+J_d-J_e+K'+K+J_{f'}+k'+p+p'+J_{f'_1}}$$
$$\times\langle f||\mu^{(1)}||e\rangle\langle d||\mu^{(1)}||i\rangle^*\langle e||T^{(k)}||i\rangle\langle f||T^{(p)}||d\rangle^*\langle f'||T'^{(k')}||i'\rangle\langle f'_1||T'^{(p')}||i'\rangle^*$$
$$\times\begin{Bmatrix}k' & p' & K\\ p & k & K'\end{Bmatrix}\begin{Bmatrix}k' & p' & K\\ J_{f'_1} & J_{f'} & J_{i'}\end{Bmatrix}\begin{Bmatrix}1 & 1 & K\\ J_d & J_f & p\\ J_i & J_e & k\end{Bmatrix}, \tag{B7}$$

$$\mathcal{S}_{dd}=[(\omega_e+\omega_{f'}-\omega_I)(\omega_i+\omega_{d'}-\omega_p)]^{-1}(-1)^{J_i+J_{i'}+J_{d'}+J_{f'}+2J_f+k'+J_e+K}$$
$$\times\langle f\,||\mu^{(1)}||e\rangle\langle d'||\mu'^{(1)}||i'\rangle^*\langle e||T^{(k)}||i\rangle\langle f\,||T^{(p)}||i\rangle^*\langle f'||T'^{(k')}||i'\rangle$$
$$\times\langle f'_1||T'^{(p')}||d'\rangle^*$$
$$\times\begin{Bmatrix}k & p & 1\\ p' & k' & K'\end{Bmatrix}\begin{Bmatrix}k & p & 1\\ J_f & J_e & J_i\end{Bmatrix}\begin{Bmatrix}1 & K & 1\\ J_{d'} & J_{f'_1} & p'\\ J_{i'} & J_{f'} & k'\end{Bmatrix}, \tag{B8}$$

$$\mathcal{S}_{bc}=[(\omega_f+\omega_{e'}-\omega_I)(\omega_d+\omega_{i'}-\omega_p)]^{-1}(-1)^{J_{i'}-J_i+1-J_{f'}+K-J_f+J_{f'_1}+K'-J_{e'}+k+k'+p+p'}$$
$$\times\langle f'||\mu'^{(1)}||e'\rangle\langle d||\mu^{(1)}||i\rangle^*\langle f\,||T^{(k)}||i\rangle\langle f\,||T^{(p)}||d\rangle^*\langle e'||T'^{(k')}||i'\rangle$$
$$\times\langle f'_1||T'^{(p')}||i'\rangle^*$$
$$\times\begin{Bmatrix}1 & 1 & K\\ J_{f'} & J_{f'_1} & J_{e'}\end{Bmatrix}\begin{Bmatrix}k & p & 1\\ J_d & J_i & J_f\end{Bmatrix}\begin{Bmatrix}k' & p' & 1\\ p & k & K'\end{Bmatrix}\begin{Bmatrix}k' & p' & 1\\ J_{f'_1} & J_{e'} & J_{i'}\end{Bmatrix}, \tag{B9}$$

$$\mathcal{G}_{bd} = [(\omega_f + \omega_{e'} - \omega_I)(\omega_i + \omega_{d'} - \omega_F)]^{-1}(-1)^{2J_i+1-J_{f'}-J_f+K'+J_{d'}+k'}$$
$$\times [(2k+1)(2k'+1)]^{-1}\delta_{pk}\delta_{p'k'}\langle f'||\mu'^{(1)}||e'\rangle\langle d'||\mu'^{(1)}||i'\rangle^*$$
$$\times |\langle f||T^{(k)}||i\rangle|^2\langle e'||T'^{(k')}||i'\rangle\langle f_1'||T'^{(k')}||d'\rangle^* \begin{Bmatrix} 1 & 1 & K \\ J_{f'} & J_{f_1'} & J_{e'} \end{Bmatrix} \begin{Bmatrix} J_{f_1'} & J_{d'} & k' \\ J_i & J_e & 1 \end{Bmatrix}, \tag{B10}$$

$$\mathcal{G}_{cc} = [(\omega_e + \omega_{i'} - \omega_F)(\omega_d + \omega_{i'} - \omega_F)]^{-1}(-1)^{-J_i-J_{i'}-J_{f'}+k+k'+p+p'-J_d-J_e-J_f+K'}$$
$$\times \langle e||\mu^{(1)}||i\rangle\langle d||\mu^{(1)}||i\rangle^*\langle f||T^{(k)}||e\rangle\langle f||T^{(p)}||d\rangle^*\langle f'||T'^{(k')}||i'\rangle\langle f_1'||T'^{(p')}||i'\rangle^*$$
$$\times \begin{Bmatrix} 1 & 1 & K \\ J_e & J_d & J_i \end{Bmatrix} \begin{Bmatrix} k' & p' & K \\ J_{f_1'} & J_{f'} & J_{i'} \end{Bmatrix} \begin{Bmatrix} k & p & K \\ p' & k' & K' \end{Bmatrix} \begin{Bmatrix} k & p & K \\ J_d & J_e & J_f \end{Bmatrix}, \tag{B11}$$

$$\mathcal{G}_{cd} = [(\omega_e + \omega_{i'} - \omega_F)(\omega_i + \omega_{d'} - \omega_F)]^{-1}(-1)^{J_i+J_{i'}+J_{d'}+K+K'+p+k+k'+J_f+2J_{f'}}$$
$$\times \langle e||\mu^{(1)}||i\rangle\langle d'||\mu'^{(1)}||i'\rangle^*\langle f||T^{(k)}||e\rangle\langle f||T^{(p)}||i\rangle^*\langle f'||T'^{(k')}||i'\rangle\langle f_1'||T'^{(p')}||d'\rangle^*$$
$$\times \begin{Bmatrix} k & p & 1 \\ p' & k' & K' \end{Bmatrix} \begin{Bmatrix} k & p & 1 \\ J_i & J_e & J_f \end{Bmatrix} \begin{Bmatrix} J_{f_1'} & K & J_{f'} \\ J_{d'} & 1 & J_{i'} \\ p' & 1 & k' \end{Bmatrix}, \tag{B12}$$

$$\mathcal{G}_{dd} = [(\omega_i + \omega_{e'} - \omega_F)(\omega_i + \omega_{d'} - \omega_F)]^{-1}(-1)^{J_i+J_{i'}+2J_{d'}+J_{f_1'}+k'}[(2k+1)(2k'+1)]^{-1}$$
$$\times \delta_{kp}\delta_{k'p'}\langle e'||\mu'^{(1)}||i'\rangle\langle d'||\mu'^{(1)}||i'\rangle^*|\langle f||T^{(k)}||i\rangle|^2\langle f'||T'^{(k')}||e'\rangle$$
$$\times \langle f_1'||T'^{(k')}||d'\rangle^* \begin{Bmatrix} J_{f_1'} & J_{f'} & K \\ J_{e'} & J_{d'} & k' \end{Bmatrix} \begin{Bmatrix} 1 & 1 & K \\ J_{e'} & J_{d'} & J_{i'} \end{Bmatrix}, \tag{B13}$$

and

$$\mathcal{G}_{\alpha\beta}(k,k',p,p',K,K',f',f_1') = (-1)^{J_{f_1'}-J_{f'}}[\mathcal{G}_{\beta\alpha}(p,p',k,k',K,K',f_1',f')]^*. \tag{B14}$$

Some of these terms may vanish owing to the selection rules appropriate to the level-coupling scheme and interatomic potential under consideration.

APPENDIX C

Dipole-dipole interaction

In Appendix C, the quantities $A_{ee'}^{kk'}$ and ${}^{kk'}A_Q^K$ are evaluated, assuming a dipole-dipole collisional interaction between atom A (dipole-moment operator $\vec{\mu}$) and atom A' (dipole-moment operator $\vec{\mu}'$) of the form

$$\mathcal{U} = (\vec{\mu}\cdot\vec{\mu}'R^2 - 3\vec{\mu}\cdot\vec{R}\,\vec{\mu}'\cdot\vec{R})/R^5, \tag{C1}$$

where $\vec{R}$ is the separation between the atoms. For a given collision geometry, $\vec{R}$ is a function of $\tau = t - t_c$ (the collision is centered in time at $t = t_c$), b, v_r, and Θ.

Writing $\vec{\mu}$ and $\vec{\mu}'$ in the form of Eq. (20) and defining

$$R_1 = -\frac{(R_x - iR_y)}{\sqrt{2}}, \quad R_{-1} = \frac{R_x + iR_y}{\sqrt{2}}, \quad R_0 = R_z, \tag{C2}$$

one may rewrite Eq. (C1) as

$$\mathcal{U} = A_{ee'}^{11}(\tau, b, v_r, \Theta)\mu_q^1(\mu')_{e'}^1, \tag{C3}$$

where

$$A^{11}_{qq'}(\tau, b, v_r, \Theta) = [R^2(\delta_{q0}\delta_{q'0} - \delta_{q1}\delta_{q',-1} - \delta_{q,-1}\delta_{q'1}) - 3R_qR_{q'}]/R^5 . \tag{C4}$$

Equation (C3) has exactly the same form as Eq. (12) since μ^1_q and $(\mu')^1_q$ are components of irreducible tensors of rank 1.

The quantities of interest in evaluating RAIC cross sections are the Fourier transform of the $A^{11}_{qq'}$ defined by Eq. (16a). Using Eqs. (C2), (C4), and (16a), one finds

$$A^{11}_{qq'}(b, v_r, \Theta; \Delta) = (v_r/b)e^{-i\Delta t_c}\int_{t_c^- - t_c}^{t_c^+ - t_c} A^{11}_{qq'}(\tau, b, v_r, \Theta)e^{-i\Delta\tau}d\tau , \tag{C5}$$

where

$$A^{11}_{11}(\tau, b, v_r, \Theta) = [A^{11}_{-1-1}(\tau, b, v_r, \Theta)]^* = -3(R_x^2 - R_y^2 - 2iR_xR_y)/2R^5 , \tag{C6a}$$

$$A^{11}_{10}(\tau, b, v_r, \Theta) = A^{11}_{01}(\tau, b, v_r, \Theta) = -[A^{11}_{-10}(\tau, b, v_r, \Theta)]^*$$

$$= -[A^{11}_{0-1}(\tau, b, v_r, \Theta)] = 3R_z(R_x - iR_y)/\sqrt{2}\,R^5 , \tag{C6b}$$

$$A^{11}_{00}(\tau, b, v_r, \Theta) = (R^2 - 3R_z^2)/R^5 , \tag{C6c}$$

$$A^{11}_{1-1}(\tau, b, v_r, \Theta) = A^{11}_{-11}(\tau, b, v_r, \Theta) = \tfrac{1}{2}A^{11}_{00}(\tau, b, v_r, \Theta) . \tag{C6d}$$

The corresponding equations for the ${}^{11}A^K_Q$ defined by Eq. (14b) are

$${}^{11}A^K_Q(b, v_r, \Theta; \Delta) = (v_r/b)e^{-i\Delta t_c}\int_{t_c^- - t_c}^{t_c^+ - t_c} {}^{11}A^K_Q(\tau, b, v_r, \Theta)e^{-i\Delta\tau}d\tau , \tag{C7}$$

$${}^{11}A^0_0(\tau, b, v_r, \Theta) = 0 , \tag{C8a}$$

$${}^{11}A^1_Q(\tau, b, v_r, \Theta) = 0 \quad (Q = 1, 0, -1) , \tag{C8b}$$

$${}^{11}A^2_2(\tau, b, v_r, \Theta) = [{}^{11}A^2_{-2}(\tau, b, v_r, \Theta)]^* = -3(R_x^2 - R_y^2 - 2iR_xR_y)/2R^5 , \tag{C8c}$$

$${}^{11}A^2_1(\tau, b, v_r, \Theta) = -[{}^{11}A^2_{-1}(\tau, b, v_r, \Theta)]^* = 6R_z(R_x - iR_y)/R^5 , \tag{C8d}$$

$${}^{11}A^2_0(\tau, b, v_r, \Theta) = 3(R^2 - 3R_z^2)/6^{1/2}R^5 . \tag{C8e}$$

It should be noted that the RAIC cross sections depend only on the quantity

$${}^{kk'}_{\lambda\lambda'}A_{K'}(b, v_r; \Delta) = {}^{kk'}_{\lambda\lambda'}A^{K'}_{Q'}(b, v_r, \Theta; \Delta)\,{}^{\lambda\lambda'}_{QQ'}A^{K'}_{Q'}(b, v_r, \Theta; \Delta)]^* . \tag{C9}$$

The fact that $A_{K'}$ is independent of Θ follows directly from Eq. (15) and the orthogonality properties of the rotation matrices; from a physical viewpoint, this result is to be expected since the calculated cross sections cannot depend on the choice of the reference geometry $\Theta = 0$.

Straight-line trajectories

Under the assumption of straight-line collision trajectories, the various A's are easily calculated. Taking as a reference geometry $R_x = v\tau$, $R_y = 0$, $R_z = b$, and letting $(t_c^{\pm} - t_c) \to \pm\infty$ in Eqs. (C5) and (C7), ore obtains

$$A^{11}_{11}(b, v_r, 0; \Delta) = -e^{-i\Delta t_c}\,b^{-3} \times[\alpha K_1(\alpha) - \alpha^2 K_0(\alpha)], \tag{C10a}$$

$$A^{11}_{10}(b, v_r, 0; \Delta) = -\sqrt{2}\,e^{-i\Delta t_c}\,b^{-3}\alpha^2 K_1(\alpha), \tag{C10b}$$

$$A_{00}^{11}(b, v_r, 0; \Delta) = -2e^{-i\Delta t_c} b^{-3} \times [\alpha^2 K_2(\alpha) - \alpha K_1(\alpha)], \quad \text{(C10c)}$$

$$^{11}A_2^2(b, v_r, 0; \Delta) = A_{11}^{11}(b, v_r, 0; \Delta), \quad \text{(C11a)}$$

$$^{11}A_1^2(b, v_r, 0; \Delta) = \sqrt{2}\, A_{10}^{11}(b, v_r, 0; \Delta), \quad \text{(C11b)}$$

$$^{11}A_0^2(b, v_r, 0; \Delta) = 3A_{10}^{11}(b, v_r, 0; \Delta)/\sqrt{6}, \quad \text{(C11c)}$$

where

$$\alpha = \Delta b / v_r \quad \text{(C12)}$$

and $K_i(\alpha)$ is a modified Bessel function. The dimensionless quantity

$$D_K(\alpha) = b^6 \sum_{\alpha} |^{11}A_Q^K(b, v_r; \Delta)|^2$$

is given by

$$D_K(\alpha) = \{2[\alpha K_1(\alpha) - \alpha^2 K_0(\alpha)]^2 + 8\alpha^4 [K_1(\alpha)]^2 + 6[\alpha^2 K_2(\alpha) - \alpha K_1(\alpha)]^2\} \delta_{K2}. \quad \text{(C13)}$$

For central tuning, $\alpha = 0$, Eq. (C13) reduces to

$$D_K(0) = 8\delta_{K2}. \quad \text{(C14)}$$

---

*Permanent address.

[1] P. R. Berman, Phys. Rev. A 22, 1838 (1980).

[2] Labels appearing on *both* sides of an equation are not to be summed over.

[3] The final-state density-matrix elements are the same whether calculated in the "normal" or the interaction representation, owing to condition (2).

[4] In RAIC I, a quantity $\Gamma_{FF_1}^{II_1}(v_r, t_c)$ was defined giving the (complex) rate at which RAIC produces a final-state density-matrix element ρ_{FF_1} from an initial one ρ_{II_1}. If Eq. (11) is multiplied by the number of collisions per unit time with the impact parameter between b and $b+db$ and relative speed v_r, and if an average over b and $\vec{R}_c$ is performed one finds

$$(\partial \rho_{FF_1}(v_r, t_c)/\partial t)_{\text{RAIC}} = \Gamma_{FF_1}^{II_1}(v_r, t_c) \rho_{II_1}(v_r, t_c),$$

where

$$\Gamma_{FF_1}^{II_1}(v_r, t_c) = \mathcal{N}_A \mathcal{N}_A v_r \int 2\pi b\, db \int d\vec{R}_c R_{FF_1}^{II_1}(b, v_r, \vec{R}_c, t_c),$$

$\mathcal{N}_\alpha$ is the α-atom density, and the $\vec{R}_c$ integral is over the atom-field interaction volume.

[5] A. R. Edmonds, *Angular Momentum Theory in Quantum Mechanics* (Princeton University Press, Princeton, N.J., 1957).

[6] In averaging over Θ, it has been assumed that all Θ are equally likely, which is equivalent to assuming a uniform distribution of relative velocities. If one or both of the atoms is velocity selected, this assumption is no longer strictly true. One can incorporate the effects of a nonuniform relative velocity distribution into the average over Θ, but the results take on a much more complicated form.

[7] The symbol $f'(f_1')$ as a superscript on ρ_Q^K is a shorthand notation for $f'J_{f'}(f'J_{f_1'})$; consequently, there is no summation on $J_{f'}$ or $J_{f_1'}$ in Eqs. (23).

[8] M. G. Payne, V. E. Anderson, and J. E. Turner, Phys. Rev. A 20, 1032 (1979); E. J. Robinson, J. Phys. B 13, 2359 (1980).

[9] S. Haroche, in *High Resolution Laser Spectroscopy*, edited by K. Shimoda (Springer, Berlin, 1976), pp. 275–279.

[10] S. E. Harris, J. F. Young, W. R. Green, R. W. Falcone, J. Lukasik, J. C. White, J. R. Willison, M. D. Wright, and G. A. Zdasiuk, in *Laser Spectroscopy IV*, edited by H. Walther and K. W. Rothe (Springer, Berlin, 1979), p. 349 and references therein; C. Bréchignac, Ph. Cahuzac, and P. E. Toschek, Phys. Rev. A 21, 1969 (1980).

Radiative Collisions with Impact Level Shifts II: Strong Fields

E.J. Robinson
Department of Physics
New York University
4 Washington Place
New York, N.Y. 10003 USA

Supported by the U.S. Office of Naval Research
under Contract No. N00014-77-C-0553.

An earlier, analytically solvable model of radiative collisions, in which the level shifting potential is taken to be a delta function, is generalized to the case of arbitrary fields by simulating the dipole-dipole R^{-3} coupling term by a hyperbolic secant. The equations which describe the time evolution of the system are thereby reduced to a simple generalization of those which apply to the Rosen-Zener problem. Results generated by the model exhibit most of the qualitative features found in numerical calculations.

There has recently been a surge of both experimental and theoretical interest in the subject of "radiative collisions," i.e., light-induced inelastic scattering events (Falcone et.al. 1976a,b, Geltman 1976, Gudzenko and Yakovlenko 1972, Harris and Lidow 1974, 1975, Harris and White 1977, Knight 1977, Gallagher and Holstein 1977, Cahuzac and Toschek 1978, Brechignac et. al. 1980, Lisitsa and Yakovlenko 1974, Payne and Nayfeh 1976, Robinson 1979, 1980). Apart from Harris and White, who have presented numerical calculations valid in the strong field case, the theoretical efforts in this field have largely been formulated perturbatively, that is, for situations in which the amplitude of the initial state in the interaction representation remains essentially unity throughout the interaction time. (Geltman, while in fact performing a calculation via perturbation theory, utilizes a cutoff procedure based on the saturation of the lowest order result to obtain a high intensity approximation.) The purpose of the present paper is to extend a previous analytic calculation (Robinson 1979), hereafter designated as I, valid at low intensities, to arbitrary power densities. We accomplish this by making an apparently minor modification of the functional form of the coupling potential.

Let us briefly review the dynamics of the process. The system consists of two dissimilar atoms, A and B, with atom B initially in its ground state B_1 and A in excited state A_2. This is composite state $|1\rangle$. As a result of the combined effect of a collision between A and B and the absorption of a photon of energy $\hbar\omega$, there is a transition to state $|2\rangle$, which finds B in excited state B_3 and A in ground state A_1.

(See Figure 1 of I.) Since the energy defect between $|1\rangle$ and $|2\rangle$ greatly exceeds thermal energies, and since each atom undergoes a change of state, both the collision and the radiation field are needed to effect the transfer.

To render the problem tractable, it is treated in the rotating wave approximation. By summing over virtual transitions, one may approximately describe the time evolution of the system by an effective two level Hamiltonian H_{eff}, given, for detuning Δ, by

$$H_{eff} = H_a + \sum_{i=1}^{2} a_i^{\dagger} a_i \, (Q_i R^{-6} + C_i E^2/2)$$
$$+ (EBR^{-3})(a_2^{\dagger} a_1 \exp(-i\Delta t) + a_1^{\dagger} a_2 \exp(+i\Delta t)/)2, \qquad (1)$$

where H_a is the atomic Hamiltonian at infinite separation, Q_i, C_i the van der Waals' and Stark coefficients of state $|i\rangle$, E the amplitude of the electric field, and B an approximately constant parameter obtained by averaging sums over off-diagonal matrix elements of the actual Hamiltonian. Detailed discussion of this averaging procedure is given by Harris and White. The operators $a_i^{\dagger}$, a_i create and annihilate the system in state $|i\rangle$. The nuclear motion is taken to be a classical straight line path, so that its effect is to generate a temporally varying potential for the electrons. The time-dependent Schroedinger equation in the interaction representation becomes a pair of simultaneous equations for the state amplitudes α_1 and α_2,

$$i\dot{\alpha}_1 = \frac{EB}{2R^3}\alpha_2 \exp\left[i\left\{\left(\Delta - \frac{(c_1-c_2)E^2}{2}\right)t - (Q_1-Q_2)\int_{-\infty}^{t} R^{-6}(s)\,ds\right\}\right], \quad (2a)$$

$$i\dot{\alpha}_2 = \frac{EB}{2R^3}\alpha_1 \exp\left[-i\left\{\left(\Delta - \frac{(c_1-c_2)}{2}E^2\right)t - (Q_1-Q_2)\int_{-\infty}^{t} R^{-6}(s)\,ds\right\}\right]. \quad (2b)$$

In the weak field limit $|\alpha_1| = 1$, and the transition amplitude is given by the quadrature

$$\lim_{t\to\infty}\alpha_2(t) = -\frac{iEB}{2}\int_{-\infty}^{\infty} R^{-3}(t)\exp\left\{-i\Delta t - (Q_1-Q_2)\int_{-\infty}^{t} R^{-6}(s)\,ds\right\}dt. \quad (3)$$

The model used in I replaced the level-shifting potential $R^{-6}(t)$, by the delta function $\phi\delta(t)$, while the R^{-3} coupling term was included exactly. The integrated phase ϕ is given by $\phi = (Q_1-Q_2)\int_{-\infty}^{\infty}\frac{dt}{(v^2t^2+\rho^2)^3}$

While the impact ansatz of replacing the R^{-6} potential by a delta function enabled us to integrate equation (3) for weak fields in terms of modified Bessel and related functions, we did not succeed in finding an analytic solution to equations (2) valid at all intensities. To generalize our results to arbitrary fields, we substitute a hyperbolic secant for the R^{-3} coupling term. A weak field model which simulates R^{-3} by a hyperbolic secant and R^{-6} by the square of this function has been shown to generate results not very different from those obtained by numerical calculations with the exact power law potentials (Robinson 1980).

The problem of a two-level system coupled by a hyperbolic secant potential without level shifts was first solved by Rosen and Zener (1932). More recently, Robiscoe extended the solution to the case of decaying states. The equations of motion in the present problem will differ from the Rosen-Zener problem only for times near t = 0, when the delta function level shifting potential is present.

The time dependent Schroedinger equation in the model system is for $t \neq 0$,

$$i\dot{\alpha}_1 = K\,\mathrm{sech}\,\frac{\pi t}{T}\,e^{i\Delta' t}\,\alpha_2 \quad (4a)$$

$$i\dot{\alpha}_2 = K\,\mathrm{sech}\,\frac{\pi t}{T}\,e^{-i\Delta' t}\,\alpha_1, \quad \text{where } \Delta' = \Delta - \frac{c_1-c_2}{2}E^2 \text{ and} \quad (4b)$$

where $K = \frac{EB}{2B^3}$ and $T = \frac{2\rho}{v}$. For $t \neq 0$ this is of the form

$$i\dot{\alpha}_1 = V_T\,e^{i\Delta' t}\,\alpha_2, \quad (5a)$$

$$i\dot{\alpha}_2 = V_T\,e^{-i\Delta' t}\,\alpha_1, \quad (5b)$$

with V_T real, which may be uncoupled by converting to the second order equations (Robiscoe)

$$\ddot{\alpha}_1 - \left(\frac{\dot{V}_T}{V_T} + i\Delta'\right)\dot{\alpha}_1 + V_T^2\alpha_1 = 0, \quad (6a)$$

$$\ddot{\alpha}_2 - \left(\frac{\dot{V}_T}{V_T} - i\Delta'\right)\dot{\alpha}_2 + V_T^2\alpha_2 = 0. \quad (6b)$$

For $V_T = K\,\mathrm{sech}\pi t/T$, equations (6) become

$$\ddot{\alpha}_1 + \left(\frac{\pi}{T}\tanh\frac{\pi t}{T} - i\Delta'\right)\dot{\alpha}_1 + k^2\,\mathrm{sech}^2\frac{\pi t}{T}\,\alpha_1 = 0, \quad (7a)$$

$$\ddot{\alpha}_2 + \left(\frac{\pi}{T}\tanh\frac{\pi t}{T} + i\Delta'\right)\dot{\alpha}_2 + k^2\,\mathrm{sech}^2\frac{\pi t}{T}\,\alpha_2 = 0. \quad (7b)$$

Following previous authors (Rosen and Zener, Robiscoe), we make the change of variable $z = (\tanh \pi t/T + 1)/2$. In the new representation, equations (7) become

$$z(1-z)\alpha_1'' + [c_1 - (a+b+1)z]\alpha_1' - ab\,\alpha_1 = 0, \quad (8a)$$

$$z(1-z)\alpha_2'' + [c_2 - (a+b+1)z]\alpha_2' - ab\,\alpha_2 = 0, \quad (8b)$$

where $a = -b = \frac{kT}{\pi}$, $c_1 = 1/2 - i\Delta T/(2\pi)$, $c_2 = c_1^*$. Equations (8) both conform to the hypergeometric equation, and are to be solved subject to the initial conditions at $z = 0$ ($t = -\infty$) $\alpha_1 = 1$ and $\alpha_2 = 0$, with starting slopes derived from the first order equations (5). If level shifts were absent, these solutions would hold for all z in the range $0 \le z \le 1$, which corresponds to all t between $\pm\infty$. In the present problem, these solutions hold only for negative times ($z \le \frac{1}{2}$). As $z \to \frac{1}{2}$, they are disturbed by the level shifting delta function. Since only the relative level shift is of importance, we assume, without loss of generality, that $\phi\,\delta(t)$ operates only in the final state. Thus in passing from $z = 1/2 - \varepsilon$ to $z = 1/2 + \varepsilon$, ε arbitrarily small and positive, the phase, but not the magnitude of α_2 changes, and $d\alpha_2/dz$, which is proportional to α_1, is unchanged. This creates new initial conditions for equation (8b) in the positive time

domain ($z > 1/2$).

Using the original initial conditions, α_2 and $d\alpha_2/dz$ at $z = 1/2 - \varepsilon$ are

$$\alpha_2\left(\tfrac{1}{2}-\varepsilon\right) = B_2\left(\tfrac{1}{2}\right)^{1-c_2} F\left(a-c_2+1,\ b-c_2+1,\ 2-c_2,\ \tfrac{1}{2}\right),$$

$$\alpha_2'\left(\tfrac{1}{2}-\varepsilon\right) = B_2\left[(1-c_1)\left(\tfrac{1}{2}\right)^{-c_2} F\left(a-c_2+1,\ b-c_2+1,\ 2-c_2,\ \tfrac{1}{2}\right)\right.$$

$$\left. + \frac{(a-c_2+1)(b-c_2+1)}{(2-c_2)}\left(\tfrac{1}{2}\right)^{1-c_2} F\left(a-c_2+2,\ b-c_2+2,\ 3-c_2,\ \tfrac{1}{2}\right)\right],$$

where the F's are hypergeometric functions, whose representation in terms of Gauss series is everywhere convergent along the real axis in the range $0 \le z \le 1$. B_2 is given by $B_2 = KT/\pi|(1 - c_2)|$. The general solution for positive times is

$$\alpha_2 = \bar{A}_2 F(a, b, c_2, z) + \bar{B}_2 z^{1-c_2} F(a-c_2+1, b-c_2+1, 2-c_2, z), \quad (9)$$

where $\bar{A}_2$ and $\bar{B}_2$ are determined from the $z = 1/2 + \varepsilon$ initial conditions, which are

$$\alpha_2\left(\tfrac{1}{2}+\varepsilon\right) = e^{i\phi}\,\alpha_2\left(\tfrac{1}{2}-\varepsilon\right)$$

$$\alpha_2'\left(\tfrac{1}{2}+\varepsilon\right) = \alpha_2'\left(\tfrac{1}{2}-\varepsilon\right)$$

to be

$$\bar{A}_2 = (G_C H_B - G_B H_C)/\Gamma, \quad \bar{B}_2 = (G_A H_C - G_C H_A)/\Gamma,$$

Using the result (Abramowitz and Stegun) that the hypergeometric functions

$$F(a,b,c;z) \to \frac{\Gamma(c)\Gamma(c-a-b)}{\Gamma(c-a)\Gamma(c-b)} \qquad \text{as } z \to 1,$$

and the reflection properties of gamma functions, and denoting $a_2(t=\infty)$ as $\tilde{a}_2$,

$$\tilde{a}_2 = \bar{A}_2 \left[\Gamma(c_2)\right]^2 / \Gamma(c_2-a)\,\Gamma(c_2+a) + \bar{B}_2 \left(\Gamma(2-c_2)\right)^2 \frac{\sin\pi a}{\pi a} . \qquad (10)$$

For $\beta = 0$, $\bar{A}_2 = 0$, and the result reduces to the Rosen-Zener solution, $\tilde{a}_2 = \frac{\sin\pi a}{\pi a}$.

Lineshapes, normalized to their maximum values, are plotted in figures 2 and 3 for the Ca-Sr system. In conformity with the work reported in I, we have performed the integration over impact parameter with a cutoff at a minimum internuclear separation, since the repulsive core of the potential prevents the atoms from approaching too closely. Note that since the present treatment builds in unitarity, a cutoff is not needed to assure convergence of the transition amplitude. Following I, we have chosen 7 Å for our minimum impact parameter for the Ca-Sr system. Using the constants of Harris and White for this pair of atoms, we find that the weak field and strong field formulations with hyperbolic secant coupling potentials and delta function level shifts are identical to within three significant figures up to intensities of 2×10^6 W/cm^2. (See Appendix). As the intensity is increased beyond

where $\nabla = (G_A H_B - G_B H_A)$, $G_A = \frac{ab}{c_2} F(a+1, b+1, c_2+1, \frac{1}{2})$,

$$G_B = \left\{(1-c_2)\left(\tfrac{1}{2}\right)^{-c_2} F(a-c_2+1, b-c_2+1, 2-c_2, \tfrac{1}{2}) + \left(\tfrac{1}{2}\right)^{1-c_2} \frac{(a-c_2+1)(b-c_2+1)}{(2-c_2)} F(a-c_2+2, b-c_2+2, 3-c_2, \tfrac{1}{2})\right\},$$

$$G_C = B_2 G_B, \quad H_A = F(a, b, c_2, \tfrac{1}{2}),$$

$$H_B = \left(\tfrac{1}{2}\right)^{1-c_2} F(a-c_2+1, b-c_2+1, 2-c_2, \tfrac{1}{2}),$$

$$H_C = B_2 e^{-i\phi} H_B.$$

The relevant hypergeometric functions may be expressed in terms of gamma functions (Abramowitz and Stegun)

$$F(a,b,c,\tfrac{1}{2}) = \frac{\pi^{1/2}}{a} 2^{-c_2} \Gamma(c_2)\left\{\frac{1}{\Gamma\left(\frac{c_2+1+a}{2}\right)\Gamma\left(\frac{c_2-a}{2}\right)} + \frac{1}{\Gamma\left(\frac{c_2+a}{2}\right)\Gamma\left(\frac{c_2+1-a}{2}\right)}\right\}; \quad F(a-c_2+1, b-c_2+1, 2-c_2, \tfrac{1}{2}) = \frac{\pi^{1/2}}{a}\Gamma(2-c_2)\left\{\frac{1}{\Gamma\left(\frac{a-c_2+1}{2}\right)\Gamma\left(\frac{b-c_2+2}{2}\right)} - \frac{1}{\Gamma\left(\frac{a-c_2+2}{2}\right)\Gamma\left(\frac{b-c_2+1}{2}\right)}\right\};$$

$$F(a-c_2+2, b-c_2+2, 3-c_2, \tfrac{1}{2}) = \frac{\pi^{1/2}}{a}\Gamma(3-c_2)\left\{\frac{1}{\Gamma\left(\frac{a-c_2+1}{2}\right)\Gamma\left(\frac{b-c_2+3}{2}\right)} - \frac{1}{\Gamma\left(\frac{a-c_2+3}{2}\right)\Gamma\left(\frac{b-c_2+2}{2}\right)}\right\}; \quad F(a+1, b+1, c_2+1, \tfrac{1}{2}) = \frac{2^{-c_2}\pi^{1/2}}{a}\Gamma(1+c_2)\left\{\frac{1}{\Gamma\left(\frac{a+c_2+1}{2}\right)\Gamma\left(\frac{c_2+a}{2}\right)} + \frac{1}{\Gamma\left(\frac{c_2+a}{2}\right)\Gamma\left(\frac{c_2+1-a}{2}\right)}\right\}.$$

this point, we see, at first, divergences in the transition probabilities at small impact parameters, but little discrepancies in total cross sections. These differences are associated with saturation effects, which occur initially for small impact parameters, which make a lesser relative contribution to the integral

$$Q = 2\pi \int_{\rho_{min}}^{\infty} \rho \, |a_2(\rho)|^2 \, d\rho,$$ where Q is the cross section and ρ the impact parameter, as the field is allowed to increase. At 15.6 GW/cm^2, we see a major reduction in the width of the integrated cross section due to the change in the relative weight of different atomic seperations. The shift in the position of the maximum is also quite pronounced. The displacement to the red of the peak may be understood almost entirely in terms of the numerical value of the Stark coefficient C_1-C_2. Nearly absent in the total cross section is the shift toward the blue due to the direct effect of the coupling potential. That this component of the shift is unimportant is a consequence of its being greatest at small impact parameters, where the relative contribution to Q falls off at high intensities. The Stark effect, on the other hand, is the same for all impact parameters.

The high intensity narrowing evident in the numerical work of Harris and White also occurs in this model. This effect also may be understood in terms of the smaller relative contributions of close collisions. The van der Waals' level shift, which is independent of field intensity in all these models is greatest at small ρ. The greater

contribution of collisions at large separation therefore implies that these level shifts are of lesser importance.

For low power, the total cross section at the spectral maximum (zero detuning) increases linearly with intensity. As saturation becomes a factor, this growth becomes sublinear ($I^{1/2}$), and the position of the peak is shifted toward the red.

Our work is therefore in qualitative agreement with the numerical work of Harris and White, in that if an experimenter wished to optimize the population of B_3 by radiative collisions, it would be desirable to detune toward the red as the power was raised. Sharper tuning would also be in order for strong fields.

Evidently, saturation imposes a type of upper limit of about 10^{10} W/cm^2 on the intensity that may be used for energy transfer via radiative collisions. Beyond this, one experiences diminishing returns. In addition, 10^{10} W/cm^2 represents a rough upper limit in another sense since photoionization of A_2 and/or B_3 should compete strongly with radiative collisions at this level of intensity.

To summarize, we have generalized our previous impact level shift model for radiative collisions to laser fields of arbitrary strength, retaining the closed form nature of the solution at the small price of substituting a suitably parametrized hyperbolic secant function of time for the $R^{-3}(t)$ occurring in nature. At high intensities, our model exhibits the same dominance of large impact parameters and red shift of the spect

maximum appearing in the numerical calculations of Harris and White, as well as a sublinear dependence on the intensity. It also predicts a similar line narrowing.

Appendix

For the purposes of comparison, we have solved the weak field problem of a hyperbolic secant coupling potential and a delta function level shift. We require

$$i\tilde{\alpha}_2^* = K\int_{-\infty}^{\infty} \operatorname{sech}\frac{\pi t}{T}\, e^{i\theta\phi}\, e^{i\Delta t}\, dt, \quad \theta = \begin{cases} 0, & t<0 \\ 1, & t>0 \end{cases}.$$

$$i\tilde{\alpha}_2^* = K\left\{\int_{-\infty}^{0} \operatorname{sech}\frac{\pi t}{T}(\cos\Delta t + i\sin\Delta t)\,dt + e^{i\phi}\int_0^{\infty} \operatorname{sech}\frac{\pi t}{T}(\cos\Delta t + i\sin\Delta t)\,dt\right\} =$$

$$K\left\{(e^{i\phi}+1)\int_0^{\infty} \operatorname{sech}\frac{\pi t}{T}\cos\Delta t\,dt + i(e^{i\phi}-1)\int_0^{\infty} \operatorname{sech}\frac{\pi t}{T}\sin\Delta t\,dt\right\}$$

$$= 2K e^{\frac{i\phi}{2}}\left\{\cos\frac{\phi}{2}\int_0^{\infty} \operatorname{sech}\frac{\pi t}{T}\cos\Delta t\,dt + \sin\frac{\phi}{2}\int_0^{\infty} \operatorname{sech}\frac{\pi t}{T}\sin\Delta t\,dt\right\}.$$

These are known integrals (Abramowitz and Stegun). In dimensionless form

$$I_c = \int_0^{\infty} \cos ax\, \operatorname{sech}\beta x\, dx = \frac{\pi}{2\beta}\operatorname{sech}\frac{a\pi}{2\beta},$$

$$I_s = \int_0^{\infty} \sin ax\, \operatorname{sech}\beta x\, dx = -\frac{\pi}{2\beta}\tanh\frac{a\pi}{2\beta} + \frac{\operatorname{Im}\psi\left(\frac{1}{4}+i\frac{a}{4\beta}\right)}{\beta},$$

where ψ is the gamma function.

The author is indebted to Professor Paul R. Berman and Dr. S. Yeh for stimulating discussions of this and related problems.

This work was supported by the U.S. Office of Naval Research.

References

Abramowitz M and Stegun I A 1964, Handbook of Mathematical Functions (Washington, D.C.: NBS).

Brechignac C, Cahuzac Ph and Toschek P E 1980 Phys. Rev. A 21, 1969.

Cahuzac Ph and Toschek P E 1978 Phys. Rev. Letters 40, 1087.

Falcone R W, Green W R, White J C, and Harris S E 1976a Phys. Rev. Lett. 36, 462.

-----1976b Phys. Rev. Lett. 37, 1590.

Gallagher A and Holstein T 1977 Phys. Rev. A 16, 2413.

Gudzenko L I and Yakovlenko S I 1972, Sov. Phys.-J.E.T.P. 35, 877.

Harris S E and Lidow D B 1974 Phys. Rev. Lett. 33, 674.

-----1975 Phys. Rev. Lett. 34, 172.

Harris S E and White J C 1977 I E E E J. Quant. Electr. QE-13 972.

Knight P L 1977 J. Phys. B: Atom. Molec. Phys. 10, L195.

Lisitsa V S and Yakovlenko S E 1974, Sov. Phys. J E T P 39, 759.

Payne M G and Mayfeh M H, 1976 Phys. Rev., A 13, 596

Robinson E J 1979 J. Phys. B: Atom. Molec. Phys. 12, 1451.

Robinson E J 1980 J. Phys. B: Atom. Molec. Phys. 13, 2359.

Robiscoe R T 1978 Phys. Rev. A 17, 247.

Rosen N and Zener C 1932, Phys. Rev. 40, 502.

Figure Cantions

Figure 1: Comparison of the functions $EB/2(v^2t^2+\rho^2)^{3/2}$ and $Ksech\pi t/T$, with $K = EB/2\rho^3$ and $T = 2\rho/v$.

Δ Power law potential

● Hyperbolic secant potential

Figure 2: Radiative collision spectra in the strong field case, hyperbolic secant coupling potential. Cross sections normalized to their maxima. The ordinate is in arbitrary units.

X 62.5 MW/cm^2

▲ 625 MW/cm^2

o 15.6 GW/cm^2

Figure 3: Radiative collision spectra in the strong field case, hyperbolic secant coupling potential cross sections normalized to maxima. Stark shifts set equal to zero to exhibit the residual shift due to the coupling. The ordinates in arbitrary units are

X 625 MW/cm^2

o 15.6 GW/cm^2

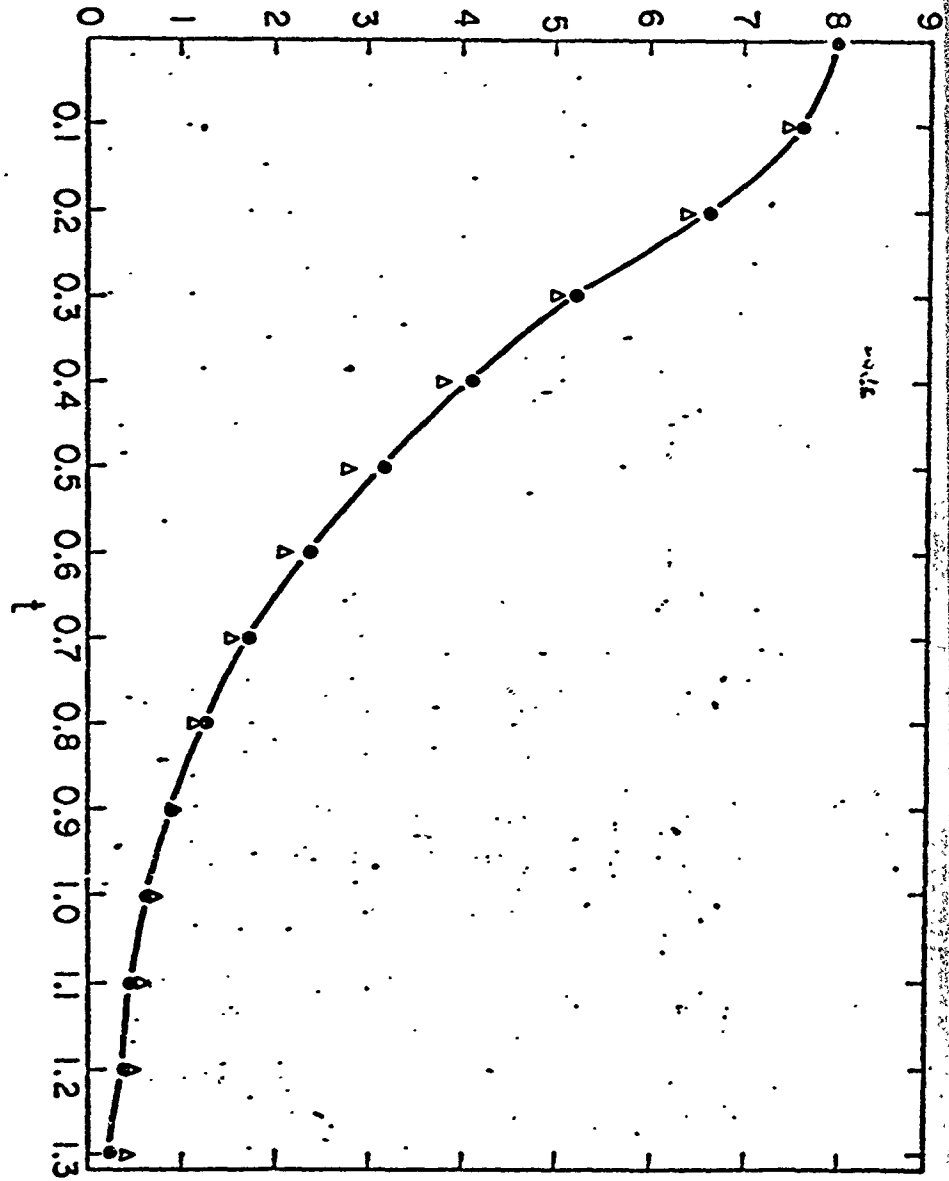

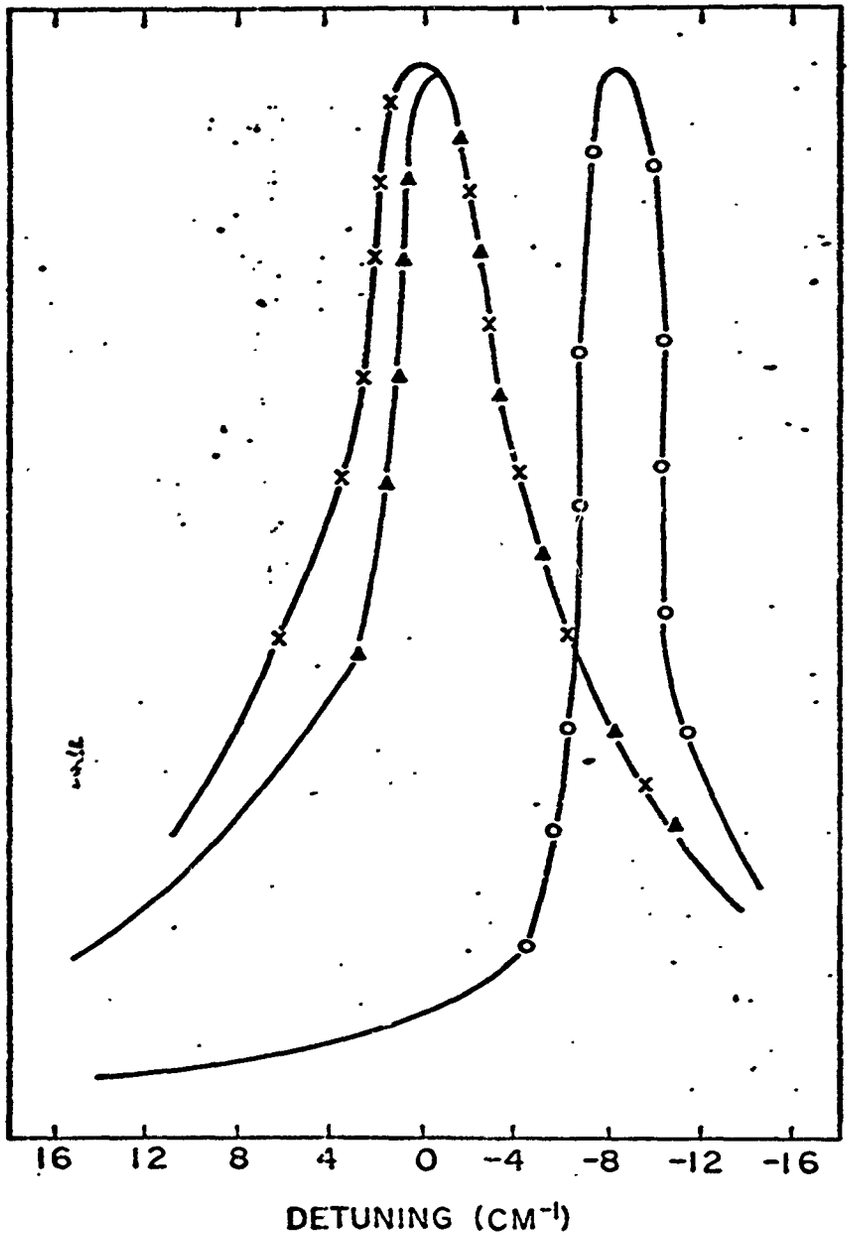
16 12 8 4 0 -4 -8 -12 -16
DETUNING (CM⁻¹)

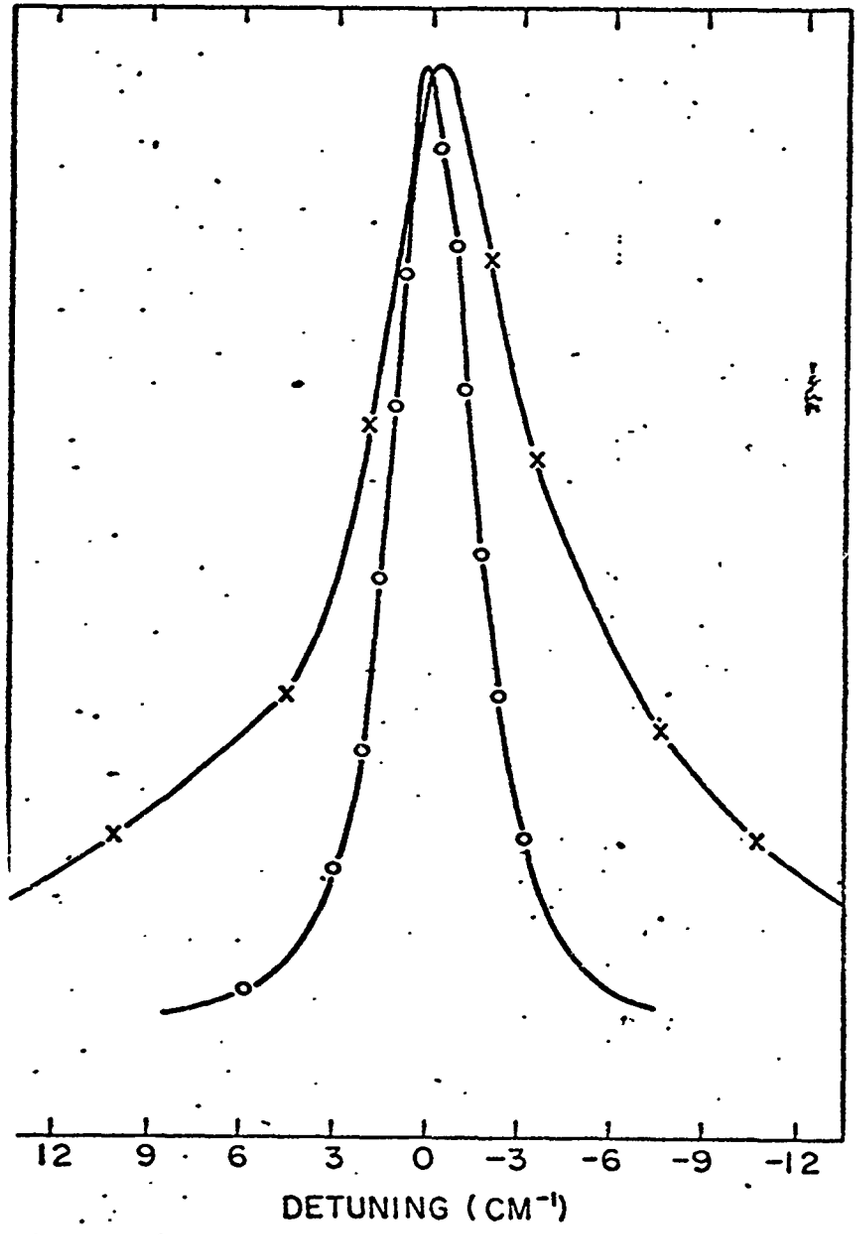
12 9 6 3 0 -3 -6 -9 -12
DETUNING (CM⁻¹)

PHYSICAL REVIEW A VOLUME 22, NUMBER 4 OCTOBER 1980

Theory of collisionally aided radiative excitation in three-level systems

S. Yeh* and P. R. Berman
Department of Physics, New York University, 4 Washington Place, New York, New York 10003
(Received 18 March 1980)

A theory of collisionally aided radiative excitation (CARE) for three-level systems in the weak-field limit is presented. Cross sections for the excitation of three-level atoms by two off-resonant pulsed radiation fields in the presence of collisions with structureless perturbers are calculated. Analytic expressions for the cross sections as functions of atom-field detunings are obtained under usual classical-trajectory and rotating-wave approximations using perturbation theory for various regions of detunings. Examples for the resulting excitation line shapes are given mostly for van der Waals potentials. A dressed-atom picture of the CARE processes is discussed. Emphasis is put on an interesting effect arising from the interference between the "stepwise" and the "direct" channel of excitation. Such an interference effect manifests itself as modulations in the total excitation cross section as a function of relative interatomic speed in some cases.

I. INTRODUCTION

In this paper, we present a theory of collisionally aided radiative excitation (CARE) for three-level systems in the weak-field limit. CARE in two-level systems has been the subject of many recent studies.[1] Approximation schemes, valid in different regions of atom-field detunings, have been used and verified by numerical calculations.[2] In three-level systems, however, calculations have been limited to a narrow range of detunings.[3] It is thus desirable to have a theory which is free from such limitations.

In Sec. II, we state the problem to be investigated and define the conditions under which the treatment of this paper are applicable. The complexity of a three-level CARE problem over its two-level counterpart is due partly to the fact that there are two detunings which can be independently varied. In addition, the collision-induced energy shifts of these three levels can be of either a positive or a negative sign (relative to the detunings), leading to different physical situations. It becomes necessary, for the convenience of presentation, to classify the cases according to the sizes and signs (relative to those of the collision-induced energy-level shifts) of the detunings. This is done in Sec. III. A "dressed-atom" picture of the physical processes will be given in Sec. IV with discussions of interesting interference effects for some cases. In Sec. V, the basic equations involved are given. The solutions and results for cases as classified in Sec. III are obtained in Sec. VI. In Sec. VII, we discuss the advantages of using CARE over conventional atom-atom collision techniques to study the atom-atom interactions. The paper is concluded in Sec. VIII. Appendices A and B provide some calculational details.

II. THE PROBLEM

Consider a three-level active atom, which may have one of the configurations shown in Fig. 1 with level separations $\hbar\omega_{21}$ and $\hbar\omega_{32}$, subjected to two off-resonant incident pulsed radiation fields of frequencies ω and ω' and amplitudes $E(t)$ and $E'(t)$. The atom simultaneously undergoes a collision with a structureless perturber. Under some conditions to be stated in this section, we calculate the $1 \rightarrow 3$ excitation cross section as a function of detunings.

The fields $E(t)$ and $E'(t)$ are assumed to drive only 1-2 and 2-3 transitions, respectively, with interactions characterized by the coupling strengths $\chi(t) = \mu_{12}E/2\hbar$ and $\chi'(t) = \mu_{23}E'/2\hbar$, respectively, where μ_{12} and μ_{23} are the dipole matrix elements of the respective transitions. The collisions are assumed only to shift the energies of the active-atomic levels without coupling them (sometimes referred to as adiabatic approximation), a generally good assumption in the case of electronic transitions in the optical regime because of the lack of interatomic potential curve crossings (except perhaps at extremely small internuclear distance which cannot be reached with ordinary thermal energy).

If the atom-field detunings Δ and Δ', defined as $\Delta = \omega - \omega_{21}$ and $\Delta' = \omega' - \omega_{32}$, are larger than the Doppler width, and/or if the incident pulsed fields are adiabatic, the excitation cross section are negligibly small in the absence of collisions. In both cases, the collision can greatly enhance the excitation by either breaking the adiabaticity or shifting the energy levels of the active atom into resonance (instantaneously) with the external fields. We shall confine the discussion of this paper to detunings larger than the Doppler width and assume that the pulses are slow enough such

Supported by the U.S. Office of Naval Research under Contract No. N00014-77-C-0553.

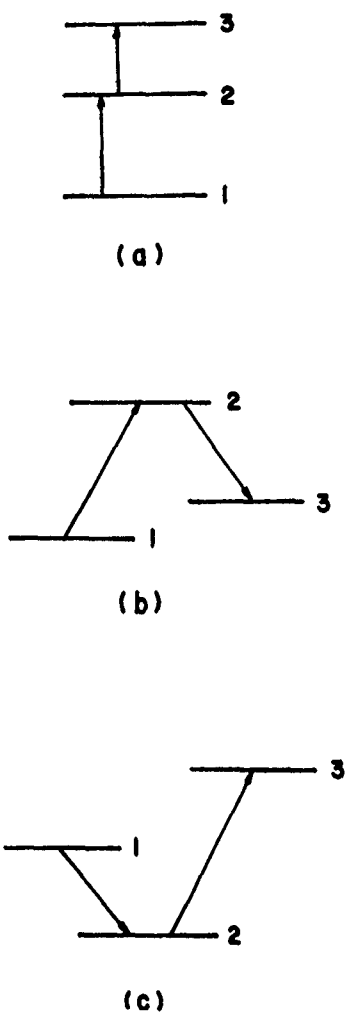

FIG. 1. Configurations of a three-level active atom for CARE. (a) Upward cascade, (b) inverse V, and (c) V.

that the pulse durations are much larger than the collision time, and that during a collision the field amplitudes are constants; that is,

$$|\Delta|, |\Delta'| > W_D, \tag{2.1}$$

where W_D is the Doppler width,

$$\lim_{t\to\pm\infty} \chi(t), \chi'(t) \to 0, \tag{2.2}$$

$$\frac{d\chi}{dt}, \frac{d\chi'}{dt} \to 0, \tag{2.3}$$

and

$$\chi(t) \to \chi_0, \chi'(t) \to \chi_0' \tag{2.4}$$

during a collision.

In addition to conditions (2.1)–(2.4), the perturber density is assumed to be low enough that the time between collisions is much longer than the inverse of the detunings and the pulse durations. In such a pressure regime, one can take the CARE rate to be linear in the perturber density and calculate the CARE cross section for a single collision, from which the CARE rate is obtained by averaging over all possible collisions. This procedure is followed throughout this paper.

The conditions on the pulsed radiation [Eqs. (2.1)–(2.4)] can be met by ordinary laser pulses which have typical pulse lengths ($\gtrsim 10^{-9}$ sec) much longer than the collision time ($\sim 10^{-12}$ sec). The pressure range we are considering is typically of the order of 10 Torr or less in order to satisfy the conditions stated above.

III. CLASSIFICATION

For the convenience of presentation, the three-level atom is assumed to have a configuration shown in Fig. 1(a), unless otherwise stated. The theory to be presented is equally applicable to other configurations with suitable changes of the signs of detunings and of the relative energy-level shifts.

Consider such a three-level active atom [Fig. 1(a)] undergoing a collision with a structureless perturber. The energy levels are shifted during a collision, as shown schematically in Fig. 2, for some specific collision impact parameter b and relative velocity v in a manner depending on the assumed interatomic potential. The relative shifts of these levels can lead to an increase or decrease in the atomic transition frequencies over their unperturbed values. In the case shown in Fig. 2(a), both the 1-2 and 2-3 transition frequencies decrease (shift toward the red), and one speaks of (relative) attractive interatomic potentials. Conversely, the transition frequencies increase for repulsive potentials. Although different combinations of attractive and repulsive potentials for the 1-2, 2-3, and 1-3 (two-photon) transitions may occur in a three-level system, we shall be concerned only with attractive interatomic potentials. This restriction (to the attractive relative interatomic potentials) is for the convenience of the presentation; the theory to be presented is, nevertheless, applicable to all types of interatomic potentials.

What is essential in the theory is the existence (or lack thereof) of the collision-induced instantaneous resonances during a collision. When the detunings equal (both in signs and in magnitudes) the relative energy-level shifts, resonances occur. In Fig. 2(a), instantaneous resonances occur at $\pm\tau_0$ for 1-2 transitions, $\pm\tau_0'$ for 2-3 transition, and $\pm\tau_0''$ for 1-3 two-photon transition. Such instantaneous resonances enhance the absorption of radiation, especially in the case of large detunings.

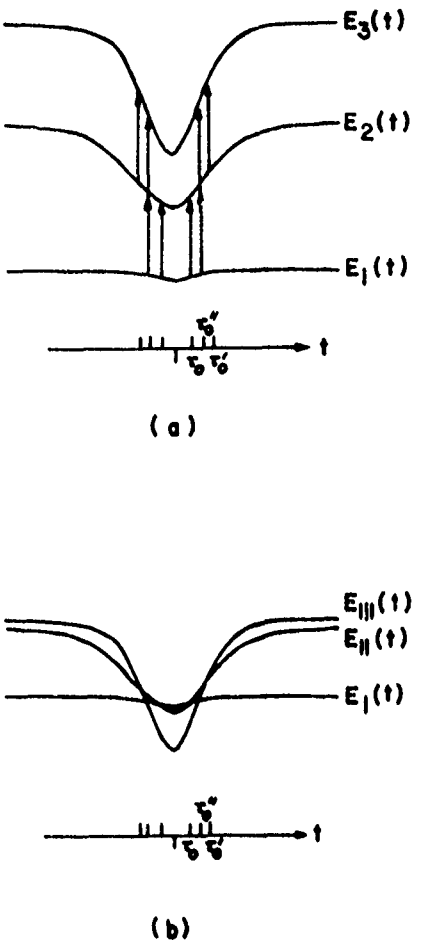

FIG. 2. Energy levels of a three-level active atom during a collision, schematically shown for a relatively attractive interatomic potential. (a) In a bare-state–classical-field picture, the energy levels, thus the detunings, are time dependent. As shown, resonances occur at $\pm\tau_0$ for 1-2 transition, $\pm\tau_0'$ for 2-3 transition, and $\pm\tau_0''$ for 1-3 two-photon transition. (b) In a dressed-state picture, the resonance points in (a) are transformed into level crossings of the dressed states.

The studies of two-level CARE (Ref. 2) have led to the understanding that the instantaneous resonances are important when the detunings are much larger than the inverse collision time τ_c^{-1}, i.e., $|\text{detuning}|\tau_c \gg 1$. For $|\text{detuning}|\tau_c \ll 1$ [impact region (*I*)], the existence or lack thereof of instantaneous resonances is unimportant, and the absorption cross section varies as $|\text{detuning}|^{-2}$ irrespective of the sign of the detuning. The case of $|\text{detuning}|\tau_c \sim 1$ can be divided into two regions according to the sign of the detuning relative to the interatomic potential: the quasistatic (*Q*) region where the instantaneous resonances can occur (e.g., red detunings for attractive potentials), and the antistatic (*A*) regions where *no* instantaneous resonance can occur (e.g., blue detunings for attractive potentials).[4] In the three-level problem, classification of the cases is complicated by the possible combinations of *I*, *Q*, and *A* regions for Δ, Δ', and $\Delta+\Delta'$. If there is no constraint, there would be a total of 27 cases to be discussed; the fact that $\Delta+\Delta'$ cannot be independently varied and that we restrict our discussion to attractive potentials reduces the number to 13 cases.

The cases to be considered are listed in Table I according to the region of each detuning. In the third column, the conditions, appropriate for attractive potentials only, are also listed to help clarify the cases considered. In subsequent sections, results are given mainly for attractive van der Waals potentials, although the treatments are generally applicable to other types of potentials. Table I exhausts all possible cases where attractive potentials only are considered. It does not, however, include all cases for a general interatomic potential. We choose not to include all possible cases because it is impractical to do so and may lead to confusion. At any rate, for the cases *not* included, one can find applicable treatments in one of the cases included.

It is natural to group together the cases in Table I for which the mathematical treatments are similar. In Sec. VI, we present the solutions and the results according to these groups. We group cases A, B, and C (Δ in the *I* region), cases D and E (Δ' in the *I* region), and cases F and G ($\Delta+\Delta'$ in the *I* region). Cases H and I, which have two of the three detunings in the *Q* region and the third detuning in the *A* region, will be grouped together. Case J, with all three detunings in the *Q* region, is the last and the most interesting case to be treated. Cases K, L, and M will not be discussed since at least two of the detunings are in the *A* region, leading to exponentially small excitation cross sections. Although numerical calculations can be performed to obtain cross sections for these cases, reliable analytic approximation schemes have yet to be developed.

IV THE DRESSED-ATOM PICTURE AND GENERAL CONSIDERATIONS

In this section we shall give a general description of the physical processes in terms of the "dressed-atom" picture[5] (sometimes referred to as the atom-field diabatic representation)[6] in which the eigenstates of the Hamiltonian of free atom + free fields + atom-field interactions (i.e.,

TABLE I. Classification of cases.

Δ	Δ'	$\Delta+\Delta'$	Conditions appropriate for attractive potentials	Case
I	I	I	$\lvert\Delta\rvert\tau_c \ll 1,\ \lvert\Delta'\rvert\tau_c \ll 1,\ \lvert\Delta+\Delta'\rvert\tau_c \ll 1$	A
I	Q	Q	$\lvert\Delta\rvert\tau_c \ll 1,\ \lvert\Delta'\rvert\tau_c \gg 1,\ \lvert\Delta+\Delta'\rvert\tau_c \gg 1,\ \Delta'<0, \Delta+\Delta'<0$	B
I	A	A	$\lvert\Delta\rvert\tau_c \ll 1,\ \lvert\Delta'\rvert\tau_c \gg 1,\ \lvert\Delta+\Delta'\rvert\tau_c \gg 1,\ \Delta'>0, \Delta+\Delta'>0$	C
Q	I	Q	$\lvert\Delta\rvert\tau_c \gg 1,\ \lvert\Delta'\rvert\tau_c \ll 1,\ \lvert\Delta+\Delta'\rvert\tau_c \gg 1,\ \Delta<0, \Delta+\Delta'<0$	D
A	I	A	$\lvert\Delta\rvert\tau_c \gg 1,\ \lvert\Delta'\rvert\tau_c \ll 1,\ \lvert\Delta+\Delta'\rvert\tau_c \gg 1,\ \Delta>0, \Delta+\Delta'>0$	E
Q	A	I	$\lvert\Delta\rvert\tau_c \gg 1,\ \lvert\Delta'\rvert\tau_c \gg 1,\ \lvert\Delta+\Delta'\rvert\tau_c \ll 1,\ \Delta<0, \Delta'>0$	F
A	Q	I	$\lvert\Delta\rvert\tau_c \gg 1,\ \lvert\Delta'\rvert\tau_c \gg 1,\ \lvert\Delta+\Delta'\rvert\tau_c \ll 1,\ \Delta>0, \Delta'<0$	G
Q	A	Q	$\lvert\Delta\rvert\tau_c \gg 1,\ \lvert\Delta'\rvert\tau_c \gg 1,\ \lvert\Delta+\Delta'\rvert\tau_c \gg 1,\ \Delta<0, \Delta'>0, \Delta+\Delta'<0$	H
A	Q	Q	$\lvert\Delta\rvert\tau_c \gg 1,\ \lvert\Delta'\rvert\tau_c \gg 1,\ \lvert\Delta+\Delta'\rvert\tau_c \gg 1,\ \Delta>0, \Delta'<0, \Delta+\Delta'<0$	I
Q	Q	Q	$\lvert\Delta\rvert\tau_c \gg 1,\ \lvert\Delta'\rvert\tau_c \gg 1,\ \lvert\Delta+\Delta'\rvert\tau_c \gg 1,\ \Delta<0, \Delta'<0, \Delta+\Delta'<0$	J
Q	A	A	$\lvert\Delta\rvert\tau_c \gg 1,\ \lvert\Delta'\rvert\tau_c \gg 1,\ \lvert\Delta+\Delta'\rvert\tau_c \gg 1,\ \Delta<0, \Delta'>0, \Delta+\Delta'>0$	K[a]
A	Q	A	$\lvert\Delta\rvert\tau_c \gg 1,\ \lvert\Delta'\rvert\tau_c \gg 1,\ \lvert\Delta+\Delta'\rvert\tau_c \gg 1,\ \Delta>0, \Delta'<0, \Delta+\Delta'>0$	L[a]
A	A	A	$\lvert\Delta\rvert\tau_c \gg 1,\ \lvert\Delta'\rvert\tau_c \gg 1,\ \lvert\Delta+\Delta'\rvert\tau_c \gg 1,\ \Delta>0, \Delta'>0, \Delta+\Delta'>0$	M[a]

[a] Not treated in this paper.

atomic dressed states) are taken as stationary states and the collision, which couples the dressed states as well as shifts their energies, is treated as a perturbation. The dressed states are generally linear combinations of the "bare states" (i.e., eigenstates of free atom + free-field Hamiltonian) and, in the weak-field limit, can be approximated as

$$
\begin{aligned}
|\mathrm{I}\rangle &= (1-\chi^2/2\Delta^2)|1,n,n'\rangle + (\chi/\Delta)|2,n-1,n'\rangle + [\chi\chi'/\Delta(\Delta+\Delta')]|3,n-1,n'-1\rangle,\\
|\mathrm{II}\rangle &= (-\chi/\Delta)|1,n,n'\rangle + (1-\chi^2/2\Delta^2-\chi'^2/2\Delta'^2)|2,n-1,n'\rangle + (\chi'/\Delta')|3,n-1,n'-1\rangle,\\
|\mathrm{III}\rangle &= [\chi\chi'/\Delta'(\Delta+\Delta')]|1,n,n'\rangle - (\chi'/\Delta')|2,n-1,n'\rangle + (1-\chi'^2/2\Delta'^2)|3,n-1,n'-1\rangle,
\end{aligned}
\tag{4.1}
$$

with eigenenergies

$$
\begin{aligned}
E_{\mathrm{I}} &= E_1 + n\hbar\omega + n'\hbar\omega' + \chi^2/\Delta,\\
E_{\mathrm{II}} &= E_2 + (n-1)\hbar\omega + n'\hbar\omega' - \chi^2/\Delta + \chi'^2/\Delta',\\
E_{\mathrm{III}} &= E_3 + (n-1)\hbar\omega + (n'-1)\hbar\omega' - \chi'^2/\Delta',
\end{aligned}
\tag{4.2}
$$

where E_1, E_2, and E_3 are energies of the atomic states 1, 2, and 3, respectively, with separations $E_2 - E_1 = \hbar\omega_{21}$ and $E_3 - E_2 = \hbar\omega_{32}$; the fields are represented by number states with photon numbers n and n' for fields E and E', respectively. For adiabatic pulses χ and χ', n and n' take on the instantaneous values.

In the weak-field limit, from Eqs. (4.1), the dressed states $|\mathrm{I}\rangle$, $|\mathrm{II}\rangle$, and $|\mathrm{III}\rangle$ are composed almost entirely of only states $|1,n,n'\rangle$, $|2,n-1,n'\rangle$, and $|3,n-1,n'-1\rangle$, respectively, with some small corrections; their energy separation are approximately $E_{\mathrm{II}} - E_{\mathrm{I}} \simeq -\Delta$, $E_{\mathrm{III}} - E_{\mathrm{II}} = -\Delta'$, and $E_{\mathrm{III}} - E_{\mathrm{I}} \simeq -(\Delta+\Delta')$; during a collision, the time dependence of E_{I}, E_{II}, and E_{III} are almost the same as E_1, E_2, and E_3. Thus, the instantaneous resonance points in Fig. 2(a) (i.e., $\pm\tau_0$, $\pm\tau_0'$, and $\pm\tau_0''$) are transformed into crossing points as shown in Fig. 2(b), and a physical picture of CARE can be established similar to that of ordinary (radiationless) inelastic atomic collision, which has been under active research for several decades.

The coupling between the dressed states by the collision is characterized by the off-diagonal matrix elements

$$
\begin{aligned}
&\langle\mathrm{I}|U(t)|\mathrm{II}\rangle = \langle\mathrm{II}|U(t)|\mathrm{I}\rangle \simeq (\chi/\Delta)V(t),\\
&\langle\mathrm{II}|U(t)|\mathrm{III}\rangle = \langle\mathrm{III}|U(t)|\mathrm{II}\rangle \simeq (\chi'/\Delta')V'(t),\\
&\langle\mathrm{I}|U(t)|\mathrm{III}\rangle = \langle\mathrm{III}|U(t)|\mathrm{I}\rangle\\
&\qquad \simeq [\chi\chi'/\Delta(\Delta+\Delta')]V'(t) - [\chi\chi'/\Delta'(\Delta+\Delta')]V(t),
\end{aligned}
\tag{4.3}
$$

where $U(t)$ is the collision interaction which is diagonal in the atomic bare-state basis. $V(t) = \langle 2|U(t)|2\rangle - \langle 1|U(t)|1\rangle$ and $V'(t) = \langle 3|U(t)|3\rangle - \langle 2|U(t)|2\rangle$ are the collision-induced relative energy-level shifts between states 1,2 and states 2,3, respectively. The off-diagonal matrix element $\langle\mathrm{I}|U(t)|\mathrm{III}\rangle$ is responsible for the "direct" (I → III) excitation corresponding to two-photon absorption in the bare-state picture, while $\langle\mathrm{I}|U(t)|\mathrm{II}\rangle$ and $\langle\mathrm{II}|U(t)|\mathrm{III}\rangle$ form the chain for "stepwise" (I → II → III) excitation. By studying these matrix elements we can better understand dominant excitation processes in different regions of detunings. It is clear that when $|\Delta+\Delta'| \ll |\Delta|, |\Delta'|$, the direct process is the dominant one. When $|\Delta|$ (or $|\Delta'|$) is smaller than the other two detunings, Eq. (4.3) suggest that the "direct"

and the "stepwise" processes have comparable contributions. However, as we shall see later, cancellation between the two processes occurs, and the stepwise process remains dominant. This will be seen when the detailed calculations are given.

In the above discussion, the effects of the collision-induced curve crossings (i.e., of the collision-induced shifts of the dressed states) have not been included. As discussed earlier, the crossings are particularly important when the detunings are large, corresponding to large separations between the dressed states. When the detunings are small (corresponding to small-level separations between the dressed states), however, the crossings do not provide major contributions to the excitation, since Fourier frequencies are induced by the collision to cover the energy mismatch. To show the importance of curve crossings, we choose, in the remainder of this section, to discuss only the case where all the detunings are in the Q region, since an interesting interference effect occurs in this limit.

The interference effect is better described using a classical-trajectory approximation of the collision event. In this approximation, crossings, as shown in Fig. 2(b) in the time domain, occur at corresponding internuclear distances $R(\tau_0) = R_0$, $R(\tau_0') = R_0'$, and $R(\tau_0'') = R_0''$. For collision impact parameters such that the closest approach between the active atom and the perturber is smaller than R_0, R_0', and R_0'', all the crossings occur during the collision. For larger impact parameters, some or all of the crossings are not induced, and the excitation probability is reduced (as compared to the all-crossing case) by orders of magnitude. Hence, collisions with larger impact parameters do not contribute significantly to the excitation cross section and can be ignored. Consequently, we consider only the collisions with impact parameters small enough to induce all the crossings. Furthermore, since the radiation pulses are assumed to be adiabatic, the atom-field system is in its dressed state $|\mathrm{I}\rangle$ before the collision (which comes from adiabatic following of bare atomic state 1), and only the dressed state $|\mathrm{III}\rangle$ will adiabatically follow the pulses back to bare atomic state 3. Hence, calculating the $|\mathrm{I}\rangle \rightarrow |\mathrm{III}\rangle$ transition probability is equivalent to calculating the $1 \rightarrow 3$ transition probability.

When the detunings are large ($|\Delta|$, $|\Delta'|$, $|\Delta + \Delta'| \gg$ inverse collision time), all the transitions occur well localized near the crossings. It is not difficult to see that there are four channels for the $|\mathrm{I}\rangle \rightarrow |\mathrm{III}\rangle$ transition to occur, two from the stepwise process ($\mathrm{I} \rightarrow \mathrm{II} \rightarrow \mathrm{III}$) and two from the direct process ($\mathrm{I} \rightarrow \mathrm{III}$). With reference to Fig. 2(b), these four channels are

$$\left.\begin{array}{l} |\mathrm{I}\rangle \xrightarrow[-\tau_0]{} |\mathrm{II}\rangle \xrightarrow[\tau_0']{} |\mathrm{III}\rangle \\ |\mathrm{I}\rangle \xrightarrow[\tau_0]{} |\mathrm{II}\rangle \xrightarrow[\tau_0']{} |\mathrm{III}\rangle \end{array}\right\} \text{stepwise}$$

$$\left.\begin{array}{l} |\mathrm{I}\rangle \xrightarrow[-\tau_0'']{} |\mathrm{III}\rangle \\ |\mathrm{I}\rangle \xrightarrow[\tau_0'']{} |\mathrm{III}\rangle \end{array}\right\} \text{direct},$$

where the times below the arrows correspond to the crossing times shown in Fig. 2(b) and indicate when each transition takes place. Each of these four channels contributes to the $|\mathrm{I}\rangle \rightarrow |\mathrm{III}\rangle$ transition amplitude, and interference between them can exhibit interesting phenomena. In a recent article,[7] we have demonstrated that this interference effect gives rise to an oscillatory structure in the total excitation cross section as a function of the active-atom-perturber relative speed when the crossings are well separated and the interatomic potentials are such that the "stepwise" and "direct" processes have comparable contributions to the transition amplitude. This effect is similar to that discussed by Rosenthal and Foley[8,9] regarding He-He$^+$ charge-exchange inelastic collision in which the atom-ion interatomic potential curves are similar to those of CARE in the dressed-atom diabatic representation discussed here. In this paper, we provide a detailed calculation to supplement the discussion in Ref. 7. This interference phenomena is quite general and should be expected to occur in many systems where excitation is possible *via* several channels.

The interference effect discussed above requires a special crossing configuration, i.e., three well-separated crossings occurring at R_0, R_0', and R_0''. Since the existence of crossings and their positions and slopes depend on the interatomic potential as well as the detunings, other crossing configurations may occur leading to different manifestations of the interference effect in the total excitation cross section. In this paper, a treatment for the general case is given, and results for special cases follow.

We note that the interference between the stepwise and the direct processes occurs even in the case of small detunings. However, the interference does not give rise to interesting effects such as the oscillatory total excitation cross sections discussed above for the case of large detunings because, in the case of small detunings, the transitions do not occur at well-defined instants, which is required to obtain a definite phase relationship between amplitudes arising from the stepwise and the direct processes.

V. THE HAMILTONIAN AND THE EQUATIONS OF MOTION

The equations of motion to be derived in this section do not differ for quantized or classical fields. To be more in line with the discussion in the dressed-atom picture given earlier, we take the fields to be quantized and use the photon-number representation; however, the calculation is carried out in the bare-atom picture. Let us consider a system consisting of a three-level active atom interacting with two external fields and a perturber atom. The Hamiltonian of this system can be written as

$$H = H_A + H_R + H_{AR} + U(t), \tag{5.1}$$

where the following hold. (i) The free-atom Hamiltonian H_A has three eigenstates $|1\rangle, |2\rangle, |3\rangle$ with eigenenergies E_1, E_2, and E_3; $E_2 - E_1 = \hbar\omega_{21}$ and $E_3 - E_2 = \hbar\omega_{32}$. (ii) $H_R = \hbar\omega a_\omega^\dagger a_\omega + \hbar\omega' a_{\omega'}^\dagger a_{\omega'}$ is the quantized free-field Hamiltonian describing a two-mode external field with photon energies $\hbar\omega$ and $\hbar\omega'$, where $a_\omega^\dagger$, $a_{\omega'}^\dagger$, and $a_\omega, a_{\omega'}$ are the usual creation and annihilation operators of the photons for each mode. (iii) The active-atom-field interaction is given in the rotating-wave approximations by

$$H_{AR} = \hbar\xi_\omega (a_\omega R_{12}^\dagger + a_\omega^\dagger R_{12}) + \hbar\xi_{\omega'} (a_{\omega'} R_{23}^\dagger + a_{\omega'}^\dagger R_{23}), \tag{5.2}$$

where $R_{12}^\dagger$, $R_{23}^\dagger$ and R_{12}, R_{23} are the raising and lowering operators of the active-atomic states, the indices referring to the transition involved, and ξ_ω and $\xi_{\omega'}$ are the coupling constants related to the interaction strengths introduced in Sec. I by $\chi = n^{1/2}\xi_\omega$ and $\chi' = n'^{1/2}\xi_{\omega'}$ with n, n' the photon numbers. (iv) The effective interaction with the perturber $U(t)$ is taken to be time dependent, since the internuclear motion is not quantized, and is diagonal in the basis of $|1,n,n'\rangle$, $|2,n-2,n'\rangle$, and $|3,n-1,n'-1\rangle$ (eigenstates of $H_A + H_R$),

$$V_1(t) = \langle 1,n,n'|U(t)|1,n,n'\rangle,$$
$$V_2(t) = \langle 2,n-1,n'|U(t)|2,n-1,n'\rangle,$$
$$V_3(t) = \langle 3,n-1,n'-1|U(t)|3,n-1,n'-1\rangle \tag{5.3}$$
$$\langle 1,n,n'|U(t)|2,n-1,n'\rangle = \langle 2,n-1,n'|U(t)|3,n-1,n'-1\rangle = \langle 3,n-1,n'-1|U(t)|1,n,n'\rangle = 0,$$

owing to the absence of inelastic collisions.

The wave function of the system

$$|\Psi(t)\rangle = C_1(t)\, e^{-i(E_1 + n\hbar\omega + n'\hbar\omega')t/\hbar} + C_2(t)\, e^{-i(E_2 + (n-1)\hbar\omega + n'\hbar\omega')t/\hbar} + C_3(t)\, e^{-i(E_3 + (n-1)\hbar\omega + (n'-1)\hbar\omega')t/\hbar}$$

satisfies the time-dependent Schrödinger equation

$$i\hbar \frac{\partial}{\partial t}|\Psi(t)\rangle = H|\Psi(t)\rangle,$$

from which the equation of motion for the probability amplitudes $C_1(t)$, $C_2(t)$, and $C_3(t)$ are obtained,

$$\begin{aligned} i\dot{C}_1 &= C_1 V_1(t) + \chi C_2 e^{i\Delta t}, \\ i\dot{C}_2 &= \chi C_1 e^{-i\Delta t} + C_2 V_2(t) + \chi' C_3 e^{i\Delta' t}, \\ i\dot{C}_3 &= \chi' C_2 e^{-i\Delta' t} + C_3 V_3(t). \end{aligned} \tag{5.4}$$

With the substitution

$$C_1 = \tilde{C}_1 \exp\left(-i\int_{-\infty}^{t} V_1(t')dt'\right),$$

$$C_2 = \tilde{C}_2 \exp\left(-i\int_{-\infty}^{t} V_2(t')dt'\right),$$

and

$$C_3 = \tilde{C}_3 \exp\left(-i\int_{-\infty}^{t} V_3(t')dt'\right),$$

the equations become

$$\begin{aligned} i\dot{\tilde{C}}_1 &= \chi\tilde{C}_2 \exp\left[i\left(\Delta t - \int_{-\infty}^{t} V(t')dt'\right)\right], \\ i\dot{\tilde{C}}_2 &= \chi\tilde{C}_1 \exp\left[-i\left(\Delta t - \int_{-\infty}^{t} V(t')dt'\right)\right] + \chi'\tilde{C}_3 \exp\left[i\left(\Delta' t - \int_{-\infty}^{t} V'(t')dt'\right)\right], \\ i\dot{\tilde{C}}_3 &= \chi'\tilde{C}_2 \exp\left[-i\left(\Delta' t - \int_{-\infty}^{t} V'(t')dt'\right)\right], \end{aligned} \tag{5.5}$$

where $V(t) = V_2(t) - V_1(t)$ and $V'(t) = V_3(t) - V_2(t)$ are the relative energy shifts of the active-atomic levels during a collision. All the relaxation rates are neglected in this equation owing to the condition of large detunings in Eqs. (2.1)–(2.4).

Equations (5.5) will be solved using the perturbation theory with the initial conditions $\tilde{C}_1(t=-\infty) = 1$, $\tilde{C}_2(t=-\infty) = 0$, and $\tilde{C}_3(t=-\infty) = 0$ corresponding to a three-level atom initially prepared in state 1. The probability of exciting the atom to state 3 is given by $|\tilde{C}_3(t=\infty)|^2$, and the corresponding total cross section is obtained by integrating over the impact parameter b,

$$\sigma = \int_0^\infty |\tilde{C}_3(t=\infty)|^2 2\pi b\, db. \tag{5.6}$$

VI. SOLUTIONS AND RESULTS

In the perturbation limit, Eqs. (5.5) are easily solved to obtain a formal expression for $\tilde{C}_3(t=\infty)$,

$$\tilde{C}_3(t=\infty)=-\int_{-\infty}^{\infty}\chi'(t)\exp\left[-i\left(\Delta' t-\int_0^t V'(t')dt'\right)\right]\int_{-\infty}^{t}\chi(t_1)\exp\left[i\left(\Delta t_1-\int_0^{t_1}V(t')dt'\right)\right]dt_1dt\,, \tag{6.1}$$

where an overall phase factor has been suppressed since it does not change the probability $|\tilde{C}_3(t=\infty)|^2$.

Equation (6.1) has to be evaluated using different techniques in different regions of detunings corresponding to different physical situations. We follow the classification of Table I.

A. Cases A, B, C

In this group, Δ is in the I region. We integrate by parts the t_1 integral in Eq. (6.1), neglecting the term containing $d\chi/dt$ owing to the conditions (2.1)–(2.4), and obtain

$$\tilde{C}_3(t=\infty)=\frac{1}{i\Delta}\left\{\int_{-\infty}^{\infty}\chi(t)\chi'(t)\exp\left[-i\left((\Delta+\Delta')t-\int_0^t[V(t')+V'(t')]dt'\right)\right]dt\right.$$
$$\left.-i\int_{-\infty}^{\infty}\chi'(t)\exp\left[-i\left(\Delta' t-\int_0^t V'(t')dt'\right)\right]\int_{-\infty}^{t}\chi(t_1)V(t_1)\exp\left[-i\left(\Delta t_1-\int_0^{t_1}V(t')dt'\right)\right]dt_1dt\right\}. \tag{6.2}$$

Since $\chi(t)$ is a constant χ_0 over the range of $V(t)$, and $|\Delta|\tau_c\ll 1$, we can take $\chi(t_1)$ out of the t_1 integral in the second term of Eq. (6.2) and set $e^{-i\Delta t_1}\simeq 1$. One finds

$$\tilde{C}_3(t=\infty)=\frac{1}{i\Delta}\left\{\int_{-\infty}^{\infty}\chi(t)\chi'(t)\exp\left[-i\left((\Delta+\Delta')t-\int_0^t[V(t')+V'(t')]dt'\right)\right]dt\right.$$
$$-\chi_0\int_{-\infty}^{\infty}\chi'(t)\exp\left[-i\left(\Delta' t-\int_0^t[V(t')+V'(t')]dt'\right)\right]dt$$
$$\left.+\chi_0\int_{-\infty}^{\infty}\chi'(t)\exp\left[-i\left(\Delta' t-\int_0^t V'(t')dt'\right)\right]dt\right\}. \tag{6.3}$$

Up to this point, we have used the assumptions that the field, $E(t)$, is a slow pulse and that Δ is in the I region, which are common to all three cases A, B, and C. Further evaluation of Eq. (6.3) involves the other field, $E'(t)$, and the other detunings, Δ' and $\Delta+\Delta'$.

1. Case A

In this case, all the detunings are in the I region. We use the same technique used to obtain Eq. (6.3) from Eq. (6.2) to evaluate the integrals in Eq. (6.3). Namely, we integrate by parts once on each of these integrals, neglect the terms containing the derivatives of $\chi(t)$ and $\chi'(t)$, replace $e^{-i\Delta t}$, $e^{-\Delta' t}$, and $e^{-i(\Delta+\Delta')t}$ by 1, and set $\chi'(t)=\chi_0'$ to obtain the excitation amplitude

$$\tilde{C}_3(t=\infty)=-\chi_0\chi_0'\left(\frac{1-e^{i\theta'}}{\Delta\Delta'}-\frac{1-e^{i(\theta+\theta')}}{\Delta'(\Delta+\Delta')}\right), \tag{6.4}$$

where $\theta=\int_{-\infty}^{\infty}V(t')dt'$ and $\theta'=\int_{-\infty}^{\infty}V'(t')dt'$ are the usual impact phases associated with pressure broadening theories.[10] The amplitude depends on the collision impact parameter b, implicitly through $V(t)$ and $V'(t)$.

The excitation probability is obtained by squaring Eq. (6.4):

$$|\tilde{C}_3(t=\infty)|^2=\chi_0^2\chi_0'^2\left(\frac{2(1-\cos\theta)}{\Delta\Delta'^2(\Delta+\Delta')}+\frac{2(1-\cos\theta')}{\Delta^2\Delta'(\Delta+\Delta')}\right.$$
$$\left.-\frac{2(1-\cos\theta'')}{\Delta\Delta'(\Delta+\Delta')^2}\right), \tag{6.5}$$

with $\theta''=\theta+\theta'$. Equation (6.5) exhibits some interesting features. The first term dominates when $|\Delta'|\ll|\Delta|, |\Delta+\Delta'|$, and only the impact phase associated with the 1-2 transition θ appears. This suggests that the collisionally enhanced excitation to state 3 is determined by the collision rate associated with the 1-2 transition only. When $|\Delta|\ll|\Delta'|, |\Delta+\Delta'|$, the second term dominates, and the only relevant collision rate is that associated with the 2-3 transition. From the point of view of CARE, these two terms can be regarded as "stepwise," since no collision rate associated with 1-3 transition is involved. When $|\Delta+\Delta'|\ll|\Delta|, |\Delta'|$, however, the third term dominates, indicating that the "direct" process is responsible for the excitation. When $|\Delta|$, $|\Delta'|$ and $|\Delta+\Delta'|$ are comparable, contributions from both the "direct" and the "stepwise" processes interfere with each other.

The excitation cross section is obtained by integrating Eq. (6.5) over the impact parameter [i.e., Eq. (5.6)]:

$$\sigma=\frac{4\pi\chi_0^2\chi_0'^2}{\Delta\Delta'(\Delta+\Delta')}\left(\frac{A}{\Delta'}+\frac{B}{\Delta}+\frac{C}{\Delta+\Delta'}\right), \tag{6.6}$$

where

$$A=\int_0^\infty (1-\cos\theta)b\,db\,,$$

$$B=\int_0^\infty (1-\cos\theta')b\,db\,,$$

$$C=\int_0^\infty (\cos\theta''-1)b\,db\,.$$

This result does not specify the type of interatomic potential. For a given potential, A, B, and C can be calculated analytically or numerically. For van der Waals potentials with the straight-line-trajectory approximation

$$V(t)=C_{\rm VDW}/[R(t)]^6$$

and

$$V'(t)=C'_{\rm VDW}/[R(t)]^6$$

with $R(t)=(b^2+v^2t^2)^{1/2}$, analytic results can be obtained,

$$\sigma=\frac{4\pi\chi_0^2\chi_0'^2}{\Delta\Delta'(\Delta+\Delta')}\left(\frac{3\pi}{8v}\right)^{2/5}(-\Gamma(-\tfrac{2}{5})\cos\tfrac{1}{5}\pi)\times\left(\frac{|C_{\rm VDW}|^{2/5}}{\Delta'}+\frac{|C'_{\rm VDW}|^{2/5}}{\Delta}-\frac{|C''_{\rm VDW}|^{2/5}}{\Delta+\Delta'}\right),\tag{6.7}$$

with

$$-\Gamma(-\tfrac{2}{5})\cos(\tfrac{1}{5}\pi)\simeq 3\,,$$

where v is the active-atom-perturber relative speed and $C''_{\rm VDW}=C_{\rm VDW}+C'_{\rm VDW}$.

2. Case B

Since Δ' and $\Delta+\Delta'$ are in the Q region, the integrals appearing in Eq. (6.3) can be evaluated by the stationary-phase method.[11] The first term and the second term in Eq. (6.3) cancel each other approximately because of the condition $|\Delta|\tau_c \ll 1$. The third term yields

$$\tilde{C}_3(t=\infty)=(-i\chi_0\chi_0'/\Delta)(\pi/\alpha')^{1/2}2\cos(\phi'+\tfrac{1}{4}\pi)\,,\tag{6.8}$$

where

$$\alpha'=\frac{1}{2}\left|\left(\frac{dV'}{dt}\right)_{\tau_0'}\right|,\quad \phi'=-\Delta'\tau_0'+\int_0^{\tau_0'}V'(t')dt'$$

and τ_0' is the stationary-phase point defined to be the positive solution of $V'(t')=\Delta'$.

In obtaining Eq. (6.8), we have assumed that the impact parameter b is small enough such that the crossings are induced during a collision (i.e., we neglect collisions with large impact parameter which do not contribute significantly to the total cross section since no crossing is induced), and that $t=0$ is the time of closest approach between the active atom and the perturber.

Apart from the factor χ_0/Δ, Eq. (6.8) takes the form of the two-level result,[12] and a standard treatment for obtaining the total excitation cross section can be used. The excitation probability is obtained by taking the square of Eq. (6.8)

$$|\tilde{C}_3(t=\infty)|^2=(\chi_0^2\chi_0'^2/\Delta^2)(\pi/\alpha')4\cos^2(\phi'+\tfrac{1}{4}\pi)\,,\tag{6.9}$$

from which the total excitation cross section is calculated using

$$\sigma=\int_0^{R_0'}|\tilde{C}_3(t=\infty)|^2 2\pi b\,db\,.\tag{6.10}$$

The upper limit in this integral has been changed to R_0', the internuclear distance at which the instantaneous resonance for the 2-3 transition occurs, since for collision impact parameter larger than R_0', the excitation is negligibly small due to lack of crossings and Eq. (6.9) fails to be valid. Equation (6.9) diverges as the impact parameter approaches R_0'; however, Eq. (6.10) remains finite since α' varies as $(b^2-R_0'^2)^{1/2}$. The cutoff at R_0' may lead to an error of up to 15%, depending on the detuning. Better results can be achieved by numerical calculations for impact parameters near $b\simeq R_0'$, or by a uniform approximation[13] specially designed to overcome the difficulty of divergence.

For van der Waals potentials, $R_0'=(C'_{\rm VDW}/\Delta')^{1/6}$, and Eq. (6.10) leads to the total excitation cross section

$$\sigma=\frac{4\pi^2\chi_0^2\chi_0'^2|C'_{\rm VDW}|^{1/2}}{3\Delta^2 v|\Delta'|^{3/2}},\tag{6.11}$$

where $\cos^2(\phi'+\frac{1}{4}\pi)$ has been approximated by $\frac{1}{2}$, and v is the active-atom-perturber relative speed.

This result shows that the line shape varies as Δ^{-2} (since Δ is in the I region) and varies as $|\Delta'|^{-3/2}$, reflecting the fact that Δ' is in the Q region.[12]

3. Case C

In this case, Δ' and $\Delta+\Delta'$ are both in the A region. No crossing occurs for the 2-3 transition and the 1-3 two-photon transition at any collision impact parameter. Since Δ is in the I region ($|\Delta|\tau_c\ll 1$), the first two terms in Eq. (6.3) approximately cancel each other as in case B, leading to the excitation amplitude

$$\tilde{C}_3(t=\infty)=\frac{-i\chi_0}{\Delta}\times\int_{-\infty}^{\infty}\chi'(t)\exp\left[-i\left(\Delta' t-\int_0^t V'(t')dt'\right)\right]dt\,.\tag{6.12}$$

This equation is easily recognized as simply a two-level excitation amplitude (2-3 transition) multiplied by a factor χ_0/Δ. Results for the two-level excitation probability are available from the numerical study of Yeh and Berman[2] for van der Waals potentials and Lennard-Jones–type potentials. Also available are approximate analytic results of Tvorogov and Fomin[14] and Szudy and Baylis[15] using saddle-point methods.[11] We now give only the essential features of the results. For details, the readers are referred to Refs. 2, 14, and 15.

The cross section, obtained by integrating $|\tilde{C}_3(t=\infty)|^2$ over the impact parameter b, shows a Δ^{-2} dependence as is clear from Eq. (6.12). The dependence on Δ' follows the antistatic wing behavior. For a van der Waals potential, Fig. 6 of Yeh and Berman[7] exhibits a line shape going as

$$|\Delta'|^{-7/3}\exp(-\beta|\Delta'|^{5/6})$$

with β a constant, which is in agreement with asymptotic results[14,15] to within a multiplicative factor of order 1.

B. Cases D, E

In these cases, Δ' is in the I region, while Δ and $\Delta+\Delta'$ are in the Q region (case D) or A region (case E). Since Δ' is in the I region, the integration-by-parts technique used in cases A, B, and C can be applied to the t integral in Eq. (6.1) for its evaluation.

We write Eq. (6.1) in the following form:

$$\tilde{C}_3(t=\infty)=-\int_{-\infty}^{\infty}\chi'(t)\exp\left[-i\left(\Delta' t-\int_0^t V'(t')dt'\right)\right]G(t)dt\,, \tag{6.13}$$

where

$$G(t)=\int_{-\infty}^{t}\chi(t_1)\exp\left[-i\left(\Delta t_1-\int_0^{t_1}V(t')dt'\right)\right]dt_1\,. \tag{6.14}$$

An integration by parts is performed on Eq. (6.13), neglecting the term containing $d\chi'/dt$, setting $\chi'(t)=\chi_0'$ over the range of $V'(t)$, and setting $e^{-\Delta' t}\simeq 1$ to obtain

$$\begin{aligned}\tilde{C}_3(t=\infty)=\frac{-i\chi_0'}{\Delta'}\Bigg\{&e^{i\theta'}\int_{-\infty}^{\infty}\chi(t)\exp\left[-i\left(\Delta t-\int_0^t V(t')dt'\right)\right]dt\\&-\int_{-\infty}^{\infty}\chi(t)\exp\left[-i\left(\Delta t-\int_0^t[V(t')+V'(t')]dt'\right)\right]dt\\&+\int_{-\infty}^{\infty}\chi(t)\exp\left[-i\left((\Delta+\Delta')t-\int_0^t[V(t')+V'(t')]dt'\right)\right]dt\Bigg\}\,.\end{aligned} \tag{6.15}$$

The second and the third terms approximately cancel each other because of the condition $|\Delta'|\tau_c \ll 1$, and we get

$$\tilde{C}_3(t=\infty)=\frac{-i\chi_0'}{\Delta'}e^{i\theta'}\times\int_{-\infty}^{\infty}\chi(t)\exp\left[-i\left(\Delta t-\int_0^t V(t')dt'\right)\right]dt\,, \tag{6.16}$$

where $\theta'=\int_{-\infty}^{\infty}V'(t')dt'$ is the impact phase[10] associated with the 2-3 transition.

Equation (6.16) is simply the 1-2 two-level transition amplitude multiplied by the factor $(\chi_0'/\Delta')e^{i\theta'}$. Its evaluation depends on the region of Δ. For case D (Δ in Q region) a stationary phase method[11] is used, and for case E (Δ in the A region) a method of steepest descent[16] or a numerical calculation[2] can be carried out.

1. Case D

The integral in Eq. (6.16) is evaluated using a stationary-phase method to yield

$$\tilde{C}_3(t=\infty)=(-i\chi_0\chi_0'/\Delta')e^{i\theta'}(\pi/\alpha)^{1/2}2\cos(\phi+\tfrac{1}{4}\pi)\,, \tag{6.17}$$

where

$$\alpha=\frac{1}{2}\left|\left(\frac{dV}{dt}\right)_{\tau_0}\right|\,,$$

$$\phi=-\Delta\tau_0+\int_0^{\tau_0}V(t')dt'\,,$$

and τ_0 is the stationary-phase point of the integrand in Eq. (6.16), i.e., the solution of the equation $\Delta=V(t)$. τ_0 is taken to be positive, and we have taken $t=0$ to be the time of closest approach so that $\pm\tau_0$ are both stationary-phase points.

Equation (6.17) holds only for collision impact

parameter small enough such that potential curve crossings (in the dressed-atom picture) are induced during a collision. In the straight-line-path approximation, this amounts to restricting the impact parameter to values smaller than R_0, the internuclear distance at which the resonance between the 1-2 transition and the field E occurs. For $b \geq R_0$, Eq. (6.17) is not valid, and the contribution to the total excitation cross section is negligible due to lack of induced resonance.

The excitation probability is given by

$$|\tilde{C}_3(t=\infty)|^2 = (\chi_0^2\chi_0'^2/\Delta'^2)(\pi/\alpha)4\cos^2(\phi+\tfrac{1}{4}\pi). \quad (6.18)$$

To obtain the total excitation cross section, Eq. (6.18) is integrated over the impact parameter from $b=0$ to $b=R_0$ according to the discussion leading to Eq. (6.10). For a van der Waals potential $R_0=(C_{\mathrm{VDW}}/\Delta)^{1/6}$, an analytic result can be obtained provided that $\cos^2(\phi+\frac{1}{4}\pi)$ is approximated by its average value $\frac{1}{2}$, which is a good approximation since $\cos^2(\phi+\frac{1}{4}\pi)$ is rapidly oscillating as a function of b. We get

$$\sigma = \int_0^{R_0} |\tilde{C}_3(t=\infty)|^2 2\pi b\, db$$

$$= \frac{4\pi^2\chi_0^2\chi_0'^2}{3\Delta'^2 v}\frac{|C_{\mathrm{VDW}}|^{1/2}}{|\Delta|^{1/2}}. \quad (6.19)$$

The Δ'^{-2} and $|\Delta|^{-3/2}$ dependences in this equation are expected because Δ' is in the I region and Δ is in the Q region.

2. Case E

Since Δ is in the A region, Eq. (6.16) has to be evaluated using saddle-point methods or numerical methods. We do not have to reiterate the discussion given in case C. Let us just state the results for van der Waals potentials: Both the numerical method and the saddle-point method give a total excitation cross section going as

$$\Delta'^{-2}|\Delta|^{-7/3}\exp(-\beta|\Delta|^{5/6}),$$

with a difference of a multiplicative factor of order 1.

C. Cases F, G

In these cases, Δ and Δ' are large ($|\Delta|\tau_c \gg 1$, $|\Delta'|\tau_c \gg 1$) and $\Delta+\Delta'$ is in the I region. This can occur when Δ and Δ' are of opposite signs and differ by at most $1/\tau_c$ in magnitude. According to the discussions in Sec. IV, the direct excitation process is expected to be dominant. Since $\Delta+\Delta'$ is in the I region, large contributions to the total excitation cross section come from collisions with impact parameters near the Weisskopf radius[17] associated with the 1-3 interatomic potential. Near such impact parameters, $V(t)/\Delta \ll 1$, so that approximations can be made to neglect terms containing such a factor in evaluating Eq. (6.1). When an integration by parts is performed on the t_1 integral in Eq. (6.1), such as the one leading to Eq. (6.2), a factor of $V(t)/\Delta$ is produced in the second term of Eq. (6.2) and is subsequently neglected. Further integrations by parts produce additional factors of $V(t)/\Delta$. Hence, to a good approximation, the 1-3 excitation amplitude can be written as

$$\tilde{C}_3(t=\infty) = \frac{1}{i\Delta}\int_{-\infty}^{\infty}\chi(t)\chi'(t)\exp\left[-i\left((\Delta+\Delta')t - \int_0^t [V(t')+V'(t')]dt'\right)\right]dt. \quad (6.20)$$

Since $\Delta+\Delta'$ is in the I region, Eq. (6.20) can be evaluated easily by integrating by parts once, neglecting terms containing $d(\chi\chi')/dt$, setting $e^{-i(\Delta+\Delta')t} \approx 1$, and evaluating $\chi(t)\chi'(t)$ as $\chi_0\chi_0'$. One obtains

$$\tilde{C}_3(t=\infty) = [\chi_0\chi_0'/\Delta(\Delta+\Delta')](1-e^{i\theta''}), \quad (6.21)$$

where

$$\theta'' = \theta+\theta' = \int_{-\infty}^{\infty}[V(t')+V'(t')]dt'.$$

In this approximation, the region of Δ(Q or A) does not play an important role, because the contribution to the total excitation cross section comes mainly from collision with impact parameters near the Weisskopf radius associated with the 1-3 direct transition. At such (large) impact parameters, no instantaneous resonance can be induced during a collision, even in the Q region. This suggests that when $\Delta+\Delta'$ is in the I region and Δ, Δ' are large ($|\Delta|\tau_c \gg 1$, $|\Delta'|\tau_c \gg 1$), the direct excitation process dominates, and the collision-induced potential curve crossings for the 1-2 and 2-3 transitions, which occur at much smaller internuclear distances than the Weisskopf radius, have only higher-order effects on the excitation cross section. Consequently, cases F and G are equivalent in this approximation.

The excitation probability is given by

$$|\tilde{C}_3(t=\infty)|^2 = [\chi_0^2\chi_0'^2/\Delta^2(\Delta+\Delta')^2]2(1-\cos\theta''), \quad (6.22)$$

and the total excitation cross section by

$$\sigma = [4\pi\chi_0^2\chi_0'^2/\Delta^2(\Delta+\Delta')^2]\int_0^{\infty}(1-\cos\theta'')b\,db. \quad (6.23)$$

For a van der Waals potential, the total excita-

tion cross section is given by

$$\sigma=\frac{4\pi\chi_0^2\chi_0'^2}{\Delta^2(\Delta+\Delta')^2}\left(\frac{3\pi|C''_{\mathrm{VDW}}|}{8v}\right)^{2/5}\left(\frac{-\Gamma(-\frac{2}{5})\cos\frac{1}{5}\pi}{5}\right), \tag{6.24}$$

where $C''_{\mathrm{VDW}}=C_{\mathrm{VDW}}+C'_{\mathrm{VDW}}$ is the van der Waals constant for the 1-3 relative potential, and $-\Gamma(-\frac{2}{5})\cos\frac{1}{5}\pi\approx 3$.

The line shape varying as $\Delta^{-2}(\Delta+\Delta')^{-2}$ is typical of the impact region when the direct excitation process is dominant over the stepwise process. The line exhibits a Δ^{-2} rather than exponential Δ dependence, even though Δ is in the A region; in some sense, the direct excitation serves to break the adiabatic following of the field $\chi(t)$ on the 1-2 transition and changes the dependence from exponential to power law.

D. Cases H, I

In these two cases, Δ and Δ' are large ($|\Delta|\tau_c \gg 1$, $|\Delta'|\tau_c \gg 1$) and of opposite signs, and their sum $(\Delta+\Delta')$ is still in the Q region. We further focus our attention to the region of $|\Delta+\Delta'| \ll |\Delta|$, $|\Delta'|$. This region is of particular interest because the direct two-photon excitation process is dominant over the stepwise process and, by varying $|\Delta+\Delta'|$, the effects of stepwise process on the direct two-photon line shape can be determined. Moreover, this further restriction of detunings makes the mathematical treatment to be given below much simplified and equally applicable to both case H and case I.

If the condition $|\Delta+\Delta'| \ll |\Delta|, |\Delta'|$ holds, the instantaneous resonance for the direct $(1-3)$ transition occurs at an internuclear distance (R_0'') much larger than that for the 1-2 transition (R_0) or the 2-3 transition (R_0') (i.e., $R_0'' \gg R_0, R_0'$). Thus, in the straight-line-path approximation, for collisions with impact parameter b such that $R_0'' > b > R_0, R_0'$, only the 1-3 instantaneous resonances occur during a collision. Collisions within this range of impact parameters give a major contribution to the total excitation cross section because of the condition $R_0'' \gg R_0, R_0'$, the weighting factor $b\,db$ in the definition of the total cross section [Eq. (5.6)], and the fact that collisions with impact parameters b larger than R_0'' do not contribute, due to lack of collision-induced resonance. Hence, we can do repeated integrations by parts on the t_1 integral in Eq. (6.1), each integration by parts producing a factor $|V(t)/\Delta| \ll 1$ for the range of impact parameters of importance determined by the $(\Delta+\Delta')$ crossing. The excitation amplitude is thus given, keeping only terms up to first order in $V'(t)/\Delta$, by

$$\tilde{C}_3(t=\infty)=\frac{-i}{\Delta}\left\{\int_{-\infty}^{\infty}\chi(t)\chi'(t)\exp\left[-i\left((\Delta+\Delta')t-\int_0^t[V(t')+V'(t')]dt'\right)\right]dt + \int_{-\infty}^{\infty}\chi(t)\chi'(t)[V(t)/\Delta]\exp\left[-i\left((\Delta+\Delta')t-\int_0^t[V(t')+V'(t')]dt'\right)\right]dt\right\}. \tag{6.25}$$

Since $\Delta+\Delta'$ is in the Q region, Eq. (6.25) is evaluated using the stationary-phase method to obtain

$$\tilde{C}_3(t=\infty)=(-i\chi_0\chi_0'/\Delta)(\pi/\alpha'')^{1/2}2\cos(\phi''+\tfrac{1}{4}\pi)[1+V(\tau_0'')/\Delta], \tag{6.26}$$

where

$$\alpha''=\frac{1}{2}\left|\left(\frac{d(V+V')}{dt}\right)_{\tau_0''}\right|,$$

$$\phi''=-(\Delta+\Delta')\tau_0''+\int_0^{\tau_0''}[V(t')+V'(t')]dt',$$

with $\tau_0''>0$ satisfying $\Delta+\Delta'=V(\tau_0'')+V'(\tau_0'')$. As before, we have taken $t=0$ to be the time of closest approach between the active atom and the perturber.

The first term in Eq. (6.26) represents the direct two-photon process since it contains only quantities relevant to the 1-3 transition α'' and ϕ''. The second term represents the correction due to stepwise process, which affects the line shape somewhat, and may become important when $|\Delta+\Delta'|$ is increased, as will be shown below.

The excitation probability is given by

$$|\tilde{C}_3(t=\infty)|^2=(4\pi\chi_0^2\chi_0'^2/\Delta^2\alpha'')\cos^2(\phi''+\tfrac{1}{4}\pi) \times[1+2V(\tau_0'')/\Delta]. \tag{6.27}$$

The excitation cross section is obtained as usual by integrating over the impact parameter, cutting off the integral at $b=R_0''$, and approximating $\cos^2(\phi''+\frac{1}{4}\pi)$ by its average value $\frac{1}{2}$. For van der Waals potentials, we obtain

$$\sigma=\frac{4\pi^2\chi_0^2\chi_0'^2}{3\Delta^2 v}\frac{|C''_{\mathrm{VDW}}|^{1/2}}{|\Delta+\Delta'|^{3/2}} \times\left[1+2\left(\frac{C_{\mathrm{VDW}}}{C''_{\mathrm{VDW}}}\right)\left(\frac{\Delta+\Delta'}{\Delta}\right)\right], \tag{6.28}$$

where v is the active-atom-perturber relative speed and C_{VDW} and C''_{VDW} are the van der Waals constants corresponding to the 1-2 and 1-3 relative interatomic potentials, respectively.

This equation has been obtained in a recent

paper by Nayfeh[3] using a Landau-Zener–type approximation and discussed in connection with the collision-induced three-photon ionization in which two photons are used to excite the atom, *via* CARE, to a bound excited state. A third photon then ionizes the atom. The present discussion makes clear the conditions under which Eq. (6.28) is valid.

The correction term in Eq. (6.28) shows the effect of the stepwise process on the direct two-photon process. It falls off as $|\Delta+\Delta'|^{-1/2}$ for fixed Δ, which is slower then the main part going as $|\Delta+\Delta'|^{-3/2}$. It is thus easier to observe such an effect at a larger $|\Delta+\Delta'|$; however, the correction term cannot become larger than the main part, since the treatment presented here ceases to be valid.

Digression. Before we go on to present the next case, it is advisable to show a spectrum so that we can have a better overall view of all the cases presented so far. In Fig. 3, the total excitation cross section is shown as a function of Δ' for a fixed $\Delta=-1.5\times10^{12}$ sec^{-1} and an attractive van der Waals potential with constants $C_{VDW}=-1.2\times10^{18}$ Å^6 sec^{-1}, $C'_{VDW}=-1.5\times10^{18}$ Å^6 sec^{-1}. In showing such a "complete" spectrum, we cannot avoid regions where *none* of the approximations employed in cases A through I is good (i.e., regions with detunings $|\sim 1/\tau_c$). Hence, the line shape from numerical integrations of Eqs. (5.5) and Eq. (5.6) is also shown for comparison and to aid in gaining an appreciation of regions of each case. Since there are many curves on Fig. 3, and each curve only has a limited region of validity (for some cases the regions do not fall within this figure), the following points will help in reading this graph:

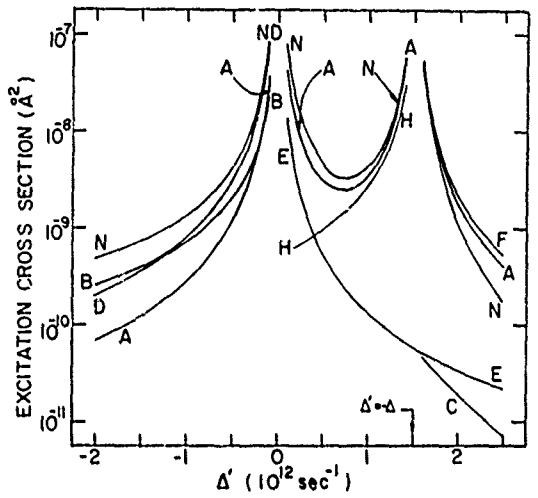

FIG. 3. Excitation cross sections versus Δ' for a fixed $\Delta=-1.5\times10^{12}$ sec^{-1} and an attractive van der Waals potential of constants $C_{VDW}=-1.2\times10^{18}$ Å^6 sec^{-1}, $C'_{VDW}=-1.5\times10^{18}$ Å^6 sec^{-1}, and $v=10^5$ cm sec^{-1}, $\chi_0=\chi'_0=10^9$ sec^{-1}. Curve N is the result of numerical integrations of Eqs. (5.5) and (5.6); others are plotted according to the equations in Table II. Only the regions, where at least the signs of the detunings are correct, are shown. See the text for discussion.

(1) Curves A, B, C, D, E, F, and H, representing cases covered so far, are plotted according to equations shown in Table II, and curve N is from numerical integrations of Eqs. (5.5) and Eq. (5.6). For curves B, C, D, E, and F, only the

TABLE II. Line shapes.

Case	Excitation cross section
A	$\frac{4\pi\chi_0^2\chi_0'^2}{\Delta\Delta'(\Delta+\Delta')}\left(\frac{3\pi}{8v}\right)^{2/5}\left(\frac{-\Gamma(-\frac{2}{5})\cos\frac{1}{5}\pi}{5}\right)\left(\frac{\lvert C_{VDW}\rvert^{2/5}}{\Delta'}+\frac{\lvert C'_{VDW}\rvert^{2/5}}{\Delta}-\frac{\lvert C''_{VDW}\rvert^{2/5}}{\Delta+\Delta'}\right)$
B	$\frac{4\pi^2\chi_0^2\chi_0'^2}{3v\Delta^2}\frac{\lvert C'_{VDW}\rvert^{1/2}}{\lvert\Delta'\rvert^{3/2}}$
C[a]	$\frac{\chi_0^2\chi_0'^2\pi^{5/2}}{0.952\Delta^2}\lvert C'_{VDW}\rvert^{1/3}\lvert\Delta'\rvert^{-7/3}e^{-1.2(\lvert C_{VDW}\rvert^{1/6}/v)\lvert\Delta'\rvert^{5/6}}$
D	$\frac{4\pi^2\chi_0^2\chi_0'^2}{3v\Delta'^2}\frac{\lvert C_{VDW}\rvert^{1/2}}{\lvert\Delta\rvert^{3/2}}$
E[a]	$\frac{\chi_0^2\chi_0'^2\pi^{5/2}}{0.952\Delta'^2}\lvert C_{VDW}\rvert^{1/3}\lvert\Delta\rvert^{-7/3}e^{-1.2(\lvert C_{VDW}\rvert^{1/6}/v)\lvert\Delta\rvert^{5/6}}$
F, G	$\frac{4\pi\chi_0^2\chi_0'^2}{\Delta^2(\Delta+\Delta')^2}\left(\frac{3\pi\lvert C''_{VDW}\rvert}{8v}\right)^{2/5}\left(\frac{-\Gamma(-\frac{2}{5})\cos\frac{1}{5}\pi}{5}\right)$
H, I	$\frac{4\pi^2\chi_0^2\chi_0'^2}{3v\Delta^2}\frac{\lvert C''_{VDW}\rvert^{1/2}}{\lvert\Delta+\Delta'\rvert^{3/2}}\left[1+2\left(\frac{C_{VDW}}{C''_{VDW}}\right)\left(\frac{\Delta+\Delta'}{\Delta}\right)\right.$

[a] The exponential line shape from the two-level asymptotic calculation of Tvorogov and Fomin (Ref. 14) is adopted.

portions, where at least the signs of detunings are correct, are shown.

(2) The conditions in the fourth column of Table I should be kept in mind in reading this figure.

(3) The detuning, $\Delta=-1.5\times10^{12}$ sec^{-1} ($|\Delta|\tau_c\sim1$), is in neither the impact region nor the quasistatic region. Hence, only in the cases when Δ is unimportant, does the agreement with the numerical result become good, e.g., cases A, F, and G near $|\Delta+\Delta'|\tau_c\ll1$.

(4) Curve B has the tendency of having the same Δ' dependence with the numerical result, if we extend the value of Δ' well into Q region. The numerical difference comes from the Δ^{-2} variation in case B, which is not a very good approximation for $\Delta=-1.5\times10^{12}$ sec^{-1}. The same statement holds for case C if we extend the value of Δ' well into the A region of $\Delta+\Delta'$.

(5) Curve E does not have any region of validity in this figure because of the sign and size of Δ. We show it for comparison.

E. Case J

We return now to case J, which is perhaps the most interesting case, since all the detunings are in the Q region and the curve crossings can interfere with each other, leading to a new type of interference effect. For the convenience of presentation, we give some of the details of the calculation in the Appendices and separate the discussions to calculations on (1) the amplitude and (2) the cross section. Since the detunings involved are large (typically of the order of 10^{13} sec^{-1}) in this case, a large amount of energy per collision ($\sim10^{-1}$ eV) is transferred from the atomic motion to the internal degrees of freedom. Some consideration of the energetics seems to be advisable to ensure the validity of the calculations below.

For such large kinetic energies, a temperature higher than the room temperature ($\gtrsim100$°C) is required, which in turn reduces the atomic collision time ($\tau_c\propto1/v$). This, however, will not violate the condition for the Q region (|detunings|$\tau_c\gg1$) in general, since one can keep this condition with a thermal energy ($\propto v^2$) $>\hbar$|detunings|. To be more specific, an estimate of the relevant quantities ($\hbar|\Delta|, E_{\text{thermal}}, v, |\Delta|\tau_c$) is given. For the largest detuning considered in case J ($\Delta=-8\times10^{13}$ sec^{-1}) and an atomic mass of forty times proton mass, $\hbar|\Delta|=5.31\times10^{-2}$ eV, $T=410$ K, $v=5.04\times10^{4}$ cm/sec, $\tau_c=9.85\times10^{-13}$ sec, and $|\Delta|\tau_c\simeq79\gg1$. Hence, at a temperature higher than 137 °C, the kinetic energy will be large enough to overcome the energy mismatch ($\hbar|\Delta|$) while simultaneously maintaining the condition of the Q region ($|\Delta|\tau_c\gg1$).

1. The amplitude

In this case, the instantaneous resonances for 1-2, 2-3, and 1-3 two-photon transitions occur at internuclear distances R_0, R_0', and R_0'', respectively, during a collision if the impact parameter is such that the distance of closest approach between the active atom and the perturber is smaller than the smallest of R_0, R_0', or R_0''. At such impact parameters, radiative excitation is enhanced owing to the collision-induced instantaneous resonances. At larger impact parameters, some of the instantaneous resonances cannot be induced, giving rise to a negligible contribution (compared with contributions from collisions with smaller b) to the total cross section. Therefore, in the straight-line-path approximation, it is sufficient to consider collisions with impact parameter $b<R_0$, R_0', or R_0''.

The instantaneous resonance points in the time domain correspond to the stationary-phase points of the integrals appearing in Eq. (6.1) and, owing to the conditions $|\Delta|\tau_c\gg1$, $|\Delta'|\tau_c\gg1$, and $|\Delta+\Delta'|\tau_c\gg1$, major contributions to these integrals are from the neighborhood of these points. Hence, a stationary-phase method, of which the details are shown in Appendix A, is used to evaluate Eq. (6.1).

Assuming that the time of instantaneous resonances are all far from $t=0$, where the collision is centered, the amplitude is given by

$$\bar{C}_3(t=\infty)=-\tfrac{1}{2}\chi_0\chi_0'(\pi/\alpha)^{1/2}[A_1+A_2+A_3], \quad (6.29)$$

where

$$A_1=(\pi/\alpha')^{1/2}e^{-i(\phi+\phi'+s\pi/4+s'\pi/4)}[1-s_1-i\sqrt{2}\,s's_1(f_1^2+g_1^2)^{1/2}e^{is'(\theta_1+\pi/4)-is'\pi Z_1^2/2}]$$
$$-i\sqrt{2}\,ss_2(\pi/\alpha'')^{1/2}(f_0^2+g_0^2)^{1/2}e^{i\delta\theta_0-i(\phi''+s''\pi/4)}[1+i\sqrt{2}\,s''(f_2^2+g_2^2)^{1/2}e^{is''(\theta_2+\pi/4)-is''\pi Z_2^2/2}], \quad (6.30)$$

$$A_2=(\pi/\alpha')^{1/2}e^{i(\phi+\phi'+s\pi/4+s'\pi/4)}[1+s_1-i\sqrt{2}\,s's_1(f_1^2+g_1^2)^{1/2}e^{-is'(\theta_1+\pi/4)+is'\pi Z_1^2/2}]$$
$$-i\sqrt{2}\,ss_2(\pi/\alpha'')^{1/2}(f_0^2+g_0^2)^{1/2}e^{-is\theta_0+i(\phi''+s''\pi/4)}[1-i\sqrt{2}s''(f_2^2+g_2^2)^{1/2}e^{-is''(\theta_2+\pi/4)+is''\pi Z_2^2/2}], \quad (6.31)$$

$$A_3=2(\pi/\alpha')^{1/2}e^{-i(\phi-\phi'+s\pi/4-s'\pi}, \quad (6.32)$$

$$\alpha=\frac{1}{2}\left|\left(\frac{dV}{dt}\right)_{r_0}\right|, \quad \alpha'=\frac{1}{2}\left|\left(\frac{dV}{dt}\right)_{r_0'}\right|, \quad \alpha''=\frac{1}{2}\left|\left(\frac{d(V+V')}{dt}\right)_{r_0''}\right|, \quad (6.33)$$

where

$$s=\mathrm{sgn}\left(\frac{dV}{dt}\right)_{\tau_0},\quad s'=\mathrm{sgn}\left(\frac{dV'}{dt}\right)_{\tau_0'},\quad s''=\mathrm{sgn}\left(\frac{d(V+V')}{dt}\right)_{\tau_0''},\tag{6.34}$$

$$\phi=-\Delta\tau_0+\int_0^{\tau_0}V(t)dt,\quad \phi'=-\Delta'\tau_0'+\int_0^{\tau_0'}V'(t)dt,\quad \phi''=-(\Delta+\Delta')\tau_0''+\int_0^{\tau_0''}[V(t)+V'(t)]dt,\tag{6.35}$$

$$\theta_i=\tan^{-1}(g_i/f_i);\tag{6.36}$$

g_i, f_i are the auxiliary functions of Fresnel integrals evaluated at z_i,

$$z_0=\left|(2\alpha/\pi)^{1/2}(\tau_0''-\tau_0)\right|,\quad z_1=\left|(2\alpha'/\pi)^{1/2}(\tau_0'-\tau_0)\right|,\quad z_2=\left|(2\alpha''/\pi)^{1/2}(\tau_0''-\tau_0)\right|,\tag{6.37}$$

$$s_1=\mathrm{sgn}(\tau_0'-\tau_0),\quad s_2=\mathrm{sgn}(\tau_0''-\tau_0),\tag{6.38}$$

and $\tau_0, \tau_0', \tau_0''$ are the positive solutions of

$$\Delta=V(t),\quad \Delta'=V'(t),\quad \Delta+\Delta'=V(t)+V'(t),\tag{6.39}$$

respectively. If any of the times of instantaneous resonances is near $t=0$ (i.e., $\tau_0\simeq 0$, $\tau_0'\simeq 0$, or $\tau_0''\simeq 0$), the corresponding time derivative of the potential (α, α', or α'') approaches 0, and Eq. (6.29) becomes singular and is a poor approximation to the amplitude. Apart from this, Eqs. (6.29)–(6.39) provide good approximations for the amplitude, regardless of the type of potentials and the ordering of τ_0, τ_0', and τ_0'', as long as the conditions for this case (case J) hold. The essential difference between various types of potentials in determining the transition amplitude lies in the derivatives and their signs at the times of instantaneous resonance, which are given by α, α', and α'' and s, s', and s''. The ordering of τ_0, τ_0', and τ_0'' determines the values of s_1 and s_2. For given interatomic potentials and detunings, these parameters can be determined, and Eqs. (6.29)–(6.39) are greatly simplified.

In Eq. (6.29), it is natural to interpret the terms containing α' as the contribution coming from the stepwise process and the terms containing α'' as that from the direct process, since α' and α'' are associated with resonances of 2-3 transition and 1-3 transition, respectively.

Equations (6.29)–(6.39) represent the general form of the transition amplitude under the conditions of case J. They have been compared with the results of direct numerical integration of Eqs. (5.5) using attractive van der Waals potentials of constants $C_{VDW}=-1.2\times10^{18}$ Å^{6}sec^{-1}, $C'_{VDW}=-1.5\times10^{18}$ Å^{6}sec^{-1}, and several detunings of the order of 10^{13} sec^{-1}. For impact parameters smaller than the smallest of R_0, R_0', and R_0'', Eqs. (6.29)–(6.39) give very accurate results (see Fig. 4); for impact parameters outside this region, which contribute little to the total cross section, Eqs. (6.29)–(6.39) are not applicable as discussed above. There are two cases (a and b) of special interest in which Eqs. (6.29)–(6.39) can be very much simplified.

a. Exactly coinciding times of instantaneous resonance, $\tau_0=\tau_0'=\tau_0''$. All the times of instantaneous resonance coincide. In this case, $z_i=0$, $f_i=g_i=\frac{1}{2}$, and $\theta_i=\frac{1}{4}\pi$ so we obtain from Eqs. (6.29)–(6.39),

$$A_1=(\pi/\alpha')^{1/2}e^{-i(\phi+\phi'+3\pi/4+s'\pi/4)},\tag{6.40}$$

$$A_2=(\pi/\alpha')^{1/2}e^{i(\phi+\phi'+3\pi/4+s'\pi/4)},\tag{6.41}$$

$$A_3=2(\pi/\alpha')^{1/2}e^{-i(\phi-\phi'+3\pi/4-s'\pi/4)}.\tag{6.42}$$

The amplitude is given by Eqs. (6.40), (6.41), (6.42), and (6.29). The contributions from the

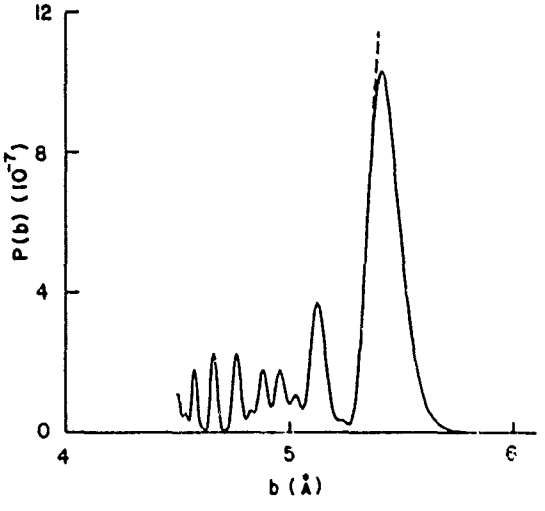

FIG. 4. Comparison of $P(b)$ vs b curves from the analytic expression [Eqs. (6.29)–(6.39)] and the numerical calculation [integration of Eqs. (5.5)] for an attractive van der Waals potential with $\chi_0=\chi_0'=10^{11}$ sec^{-1}, $\Delta=-4.0\times10^{13}$ sec^{-1}, and $\Delta'=-5.05\times10^{13}$ sec^{-1}. Other parameters are the same as those in Fig. 3. The analytic expression, which is singular at $b=5.57$ Å, was cut off at $b=5.40$ Å, where it begins to diverge. The agreement at smaller impact parameters is near perfect. —— numerical integration of Eqs. (5.5); ----- analytic expression [Eqs. (6.29)–(6.39)].

direct process are *absent*, leaving a very simple form involving only the stepwise contributions.

For given interatomic potential and Δ, the condition $\tau_0=\tau_0'=\tau_0''$ corresponds to a particular value of Δ' (e.g., $\Delta'=(C_{VDW}'/C_{VDW})\Delta$, for van der Waals potentials). Near this value of Δ', according to Eqs. (6.41)–(6.42), one would expect that the direct process would be less important than the stepwise process, which should be reflected in the line shape. We find this result when we numerically evaluate Eqs. (6.29)–(6.39) to obtain the total cross section, as will be shown later.

b. Well-separated times of instantaneous resonance. In this case, the arguments of f_i and g_i in Eq. (6.36) become large, and since f_i and g_i are rapidly decreasing functions with maximum values $f_i(0)=g_i(0)=\frac{1}{2}$, we can, to a good approximation, neglect terms containing factors $\sqrt{2}\,(f_i^2+g_i^2)^{1/2}$, as compared with 1 in Eqs. (6.30) and (6.31). We obtain

$$A_1=(\pi/\alpha')^{1/2}e^{-i(\phi+\phi'+s\pi/4+s'\pi/4)}(1-s_1)$$
$$-i\sqrt{2}\,ss_2(\pi/\alpha'')^{1/2}(f_0^2+g_0^2)^{1/2}e^{is\theta_0-i(\phi''+s''\pi/4)}, \tag{6.43}$$

$$A_2=(\pi/\alpha')^{1/2}e^{i(\phi+\phi'+s\pi/4+s'\pi/4)}(1+s_1)$$
$$-i\sqrt{2}\,ss_2(\pi/\alpha'')^{1/2}(f_0^2+g_0^2)^{1/2}e^{-is\theta_0+i(\phi''+s''\pi/4)}. \tag{6.44}$$

The amplitude as given by Eqs. (6.43), (6.44), (6.32)–(6.39), and (6.29) contains contributions from the stepwise and the direct process that interfere with each other.

It is not difficult to understand the physical meaning of each term in Eqs. (6.32), (6.43), and (6.44) by tracing back the calculations leading to them in Appendix A. Term A_1 [Eq. (6.43)] contains the contributions from the instantaneous resonance points before $t=0$; term A_2 [Eq. (6.44)] contains the contributions from the instantaneous resonance points after $t=0$; and term A_3 [Eq. (6.32)] contains the contribution from the *stepwise process* in which 1-2 resonance occurs before $t=0$ and 2-3 resonance occurs after $t=0$. Terms A_1 and A_2 contain both stepwise and direct contributions. For a given ordering of τ_0, τ_0', and τ_0'' some stepwise contributions will be absent. For example, when $\tau_0<\tau_0'$, $s_1=1$ and the first term in Eq. (6.43) vanishes, indicating that no stepwise process is occuring before $t=0$, since the 1-2 resonance happens at a later time than the 2-3 transition ($-\tau_0>-\tau_0'$). The first term in Eq. (6.44) does not vanish because $\tau_0<\tau_0'$ and the stepwise process can occur after $t=0$. The situation is reversed when $\tau_0>\tau_0'$ ($s_1=-1$). However, A_3 always survives since the 1-2 transition occurs before $t=0$ and the 2-3 transition occurs after $t=0$. In any case, there are *four* terms in the amplitude corresponding to the *four* excitation channels discussed in Sec. IV.

2. The total cross section

It is straightforward to obtain the excitation probability by taking the modulus of Eq. (6.29). The resulting expressions are lengthy and are given in Appendix B. Only for the two special cases ($\tau_0=\tau_0'=\tau_0''$ and $\tau_0, \tau_0', \tau_0''$ far apart) are the analytic expressions given in this subsection.

To demonstrate the success of the stationary-phase method used in Appendix A, we compare in Fig. 4 two $|\bar{C}_3(t=\infty)|^2$ vs b curves, one from numerically integrating Eqs. (5.5), the other from squaring Eq. (6.29) for an attractive van der Waals potential with $C_{VDW}=-1.2\times10^{18}$ Å^6 sec^{-1}, $C_{VDW}'=-1.5\times10^{18}$ Å^6 sec^{-1}, $\Delta=-4.0\times10^{13}$ sec^{-1}, and $\Delta'=-5.05\times10^{13}$ sec^{-1}. The agreement is near perfect except for $b\gtrsim5.40$ Å, which is close to $R_0=(C_{VDW}/\Delta)^{1/6}=5.57$ Å, at which Eqs. (6.29)–(6.39) become singular. The values of detunings used are large ($|\Delta|\tau_c\gg1$, $|\Delta'|\tau_c\gg1$); however, for smaller values of detunings ($\sim10^{12}$ sec^{-1}), good agreement (to within 10%) is still obtained.

To obtain accurate cross sections, we have to do numerical integrations of Eqs. (5.5) for impact parameters b near and larger than the smallest of R_0, R_0', and R_0'' and to use Eqs. (6.29)–(6.39) for smaller impact parameters. This procedure is used to obtain the total cross section as a function of Δ' in a range including the point $\Delta'=(C_{VDW}'/C_{VDW})\Delta$ at which all the times of instantaneous resonance coincide, for the attractive van der Waals potential used in Fig. 4, and for $\Delta=-2.0\times10^{13}$ sec^{-1}. The results are shown in Fig. 5 along with two curves, one with a $(\Delta+\Delta')^{3/2}$ dependence, the other with a $\Delta'^{-3/2}$ dependence. The calculated cross section lies between the two curves, which are normalized to the same value as the calculated one at $\Delta'=(C_{VDW}'/C_{VDW})\Delta$ ($=-2.5\times10^{13}$ sec^{-1} in this case).

From the discussion earlier, the contributions from the $(1\to3)$ direct process disappear at this point, since $\tau_0=\tau_0'=\tau_0''$. The calculated line shape shows no marked structure due to this "interference" effect; the line profile is a smooth curve exhibiting the influence of both the stepwise and the direct processes. If the stepwise process is the only contributing one, the line shape would have followed the $\Delta'^{-3/2}$ curve; if, on the other hand, the direct process is the predominant one, the line shape should go as $(\Delta+\Delta')^{-3/2}$. Since the calculated curve on Fig. 5 tends to follow more closely the $\Delta'^{-3/2}$ curve, it suggests that at the

vicinity of $\Delta' = (C'_{\rm VDW}/C_{\rm VDW})\Delta$, the stepwise process is more important than the direct process, as previously discussed.

Simple analytic results can be obtained for the following two special cases (*i* and *ii*)

i. Exactly coinciding times of instantaneous resonance, $\tau_0 = \tau'_0 = \tau''_0$. Using Eqs. (6.29), (6.40), (6.41), and (6.42), we obtain

$$|\bar{C}_3(t=\infty)|^2 = (\pi^2\chi_0^2\chi_0'^2/\alpha\alpha')[\cos^2(\phi+\phi'+s\pi/4+s'\pi/4)+1 + 2\cos(\phi+\phi'+s\pi/4+s'\pi/4)\cos(\phi-\phi'+s\pi/4-s'\pi/4)]. \quad (6.45)$$

Although this is a simple expression, it cannot be used to obtain an accurate value for the total cross section for reasons to be discussed below. The time derivatives of the interatomic potentials α and α' can be expressed in terms of the internuclear distance and the impact parameter,

$$\alpha = (v/2R_0)(R_0^2 - b^2)^{1/2}\left|\left(\frac{dV}{dR}\right)_{R_0}\right|, \quad (6.46)$$

$$\alpha' = (v/2R'_0)(R_0'^2 - b^2)^{1/2}\left|\left(\frac{dV'}{dR}\right)_{R'_0}\right|. \quad (6.47)$$

When $R_0 = R'_0$ (as in this case), both α and α' approach 0 as b approaches $R_0(=R'_0)$, and Eq. (6.45) is singular, varying as $(R_0^2 - b^2)^{-1}$. An approximate formula for obtaining the total cross section, such as Eq. (6.10), is not applicable since it leads to a logarithmic divergence. Therefore, for a certain range of impact parameter b near R_0, numerical integration of Eqs. (5.5) and of $\int|\bar{C}_3(t=\infty)|^2 2\pi b\,db$ are required to obtain an accurate value for the total cross section. The result for a specific van der Waals potential and a given Δ is represented by a point on the line-shape curve, such as the one in Fig. 5 [the point $\Delta' = \Delta(C'_{\rm VDW}/C_{\rm VDW})$].

ii. Well-separated times of instantaneous resonance. The probability can be obtained from Eqs. (6.43), (6.44), (6.32)–(6.39), and (6.29). Since the amplitude contains contributions from both the stepwise and the direct processes, there will be interference terms in the probability. The interference effect is best illustrated using a specific order of instantaneous resonances (e.g., $\tau'_0 > \tau''_0 > \tau_0$). For this order ($\tau'_0 > \tau''_0 > \tau_0$), the excitation probability is obtained as

$$|\bar{C}_3(t=\infty)|^2 = (\pi\chi_0\chi'_0)^2(P_S + P_D + P_{\rm INT}), \quad (6.48)$$

with

$$P_S = 2(1 - s\sin2\phi)/\alpha\alpha', \quad (6.49)$$

$$P_D = (f_0^2+g_0^2)[1 - s''\sin2(\phi'' - s\theta_0)]/\alpha\alpha'', \quad (6.50)$$

$$P_{\rm INT} = -s\left(\frac{2(f_0^2+g_0^2)}{\alpha^2\alpha'\alpha''}\right)^{1/2}\{\sin[\phi+\phi'-\phi''+(s+s'-s'')\pi/4+s\theta_0] + \sin[\phi+\phi'+\phi''+(s+s'+s'')\pi/4-s\theta_0] + \sin[\phi'+\phi''-\phi+(s'+s''-s)\pi/4-s\theta_0] + \sin[\phi'-\phi''-\phi+(s'-s''-s)\pi/4+s\theta_0]\}, \quad (6.51)$$

where all the quantities have been defined in Eqs. (6.29)–(6.39). Equations (6.48)–(6.51) clearly show the contributions to the total cross section from the stepwise process, the direct process, and the interference between the two. This result has been obtained and discussed in a recent paper,[7] and we summarize only the essential features.

All the sine functions in Eqs. (6.48)–(6.51) oscillate rapidly as functions of impact parameter b, except the one varying as

$$\sin[\phi+\phi'-\phi''+(s+s'-s'')\pi/4+s\theta_0]$$

(the first term in $P_{\rm INT}$), which is a slowly varying function of b. On integrating over b to obtain the total cross section, only this term survives to yield a term representing the interference of the stepwise and the direct processes which oscillates as a function of inverse active-atom-perturber relative speed $1/v$.

An approximation such as Eq. (6.10) is used to calculate the total cross section, yielding

$$\sigma=\frac{(\pi\chi_0\chi_0')^2R_0}{v^2\left|\left(\frac{dV}{dR}\right)_{R_0}\right|}\left[\frac{4R_0'}{\left|\left(\frac{dV'}{dR}\right)_{R_0'}\right|}\ln\frac{R_0'+R_0}{R_0'-R_0}+\frac{2R_0''(f_0^2+g_0^2)}{\left|\left(\frac{d(V+V')}{dR}\right)_{R_0''}\right|}\ln\frac{R_0''+R_0}{R_0''-R_0}\right.$$
$$\left.-2s\left[\frac{2R_0'R_0''(f_0^2+g_0^2)}{\left|\left(\frac{dV'}{dR}\right)_{R_0'}\left(\frac{d(V+V')}{dR}\right)_{R_0''}\right|}\right]^{1/2}\ln\frac{R_0'+R_0''+2R_0}{R_0'+R_0''-2R_0''}\sin\left(\frac{A}{v}+\phi_0\right)\right], \tag{6.52}$$

where A is the area enclosed by the three crossings on the interatomic potential curves in a dressed-atom picture, and

$$\phi_0=(s+s'-s'')\pi/4+s\theta_0$$

is a constant phase.

Equation (6.52) is not restricted to any specific type of potential, and the calculation of total excitation cross section using it is remarkably simple. For given interatomic potential curves and detunings, one can graphically obtain the slopes at the crossing points and the area A enclosed by them. Substitution of these values into Eq. (6.52) yields σ. A comparison of this cross section with the corresponding one obtained from computer solutions indicates that Eq. (6.52) is accurate to within 15%.

The third term in Eq. (6.52), which represents the interference between the stepwise and the direct processes, contains a sine function which will oscillate as the relative speed v is varied. It is clear from Eq. (6.52) that the area A determines the oscillation frequency, while the slopes at the crossing points determine the amplitudes of the oscillations. For given interatomic potential curves, these quantities (A and slopes) can be changed by varying the detunings, and hence the frequency and the amplitude of the oscillation in the total cross section.

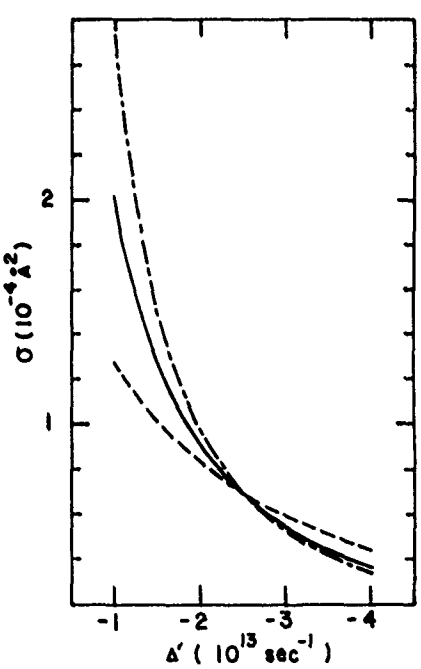

FIG. 5. The total excitation cross section as a function of Δ' near $\Delta'=(C_{VDW}'/C_{VDW})\Delta$ for a fixed $\Delta=-2.0\times10^{13}$ sec^{-1}. The interatomic potential and other parameters used are the same as those in Fig. 4. —— this calculation; ------ $\propto(\Delta+\Delta')^{-3/2}$; - · - · - $\propto\Delta'^{-3/2}$. The three curves are normalized to the same value at $\Delta'=\Delta(C_{VDW}/C_{VDW})$.

The restriction to a specific ordering of the crossing times (i.e., $\tau_0'>\tau_0''>\tau_0$) corresponds to confining the detunings in certain regions depending on the given interatomic potential. For detunings in different regions, the ordering will be different. However, it would be just as easy to obtain the excitation probability and the total cross section from Eqs. (6.43), (6.44), (6.32)-(6.39), and (6.29).

To illustrate this interference effect and to investigate the feasibility of its experimental observation, we use a specific potential, as shown in Figs. 6(a) and 6(b), instead of van-der-Waals-type potentials for detunings $\Delta=-8.0\times10^{13}$ sec^{-1} and $\Delta'=-3.0\times10^{13}$ sec^{-1}. The resulting total excitation cross section as a function of inverse relative speed $1/v$ is shown in Fig. 7, with $\chi_0=\chi_0'=10^{11}$ sec^{-1}. The curve rises as $(1/v)^2$ with equally spaced peaks when the speed is varied from 10^5 to 4×10^5 cm sec^{-1}. In terms of the laser power, the excitation cross sections are of the order of $(10^{-34}I_0I_0')$ cm^2, with I_0, I_0' the peak power density in W/cm^2. Thus, the interference effect should be observable with moderate laser power. Although a specific potential [Figs. 6(a) and 6(b)] is used to demonstrate this effect, we emphasize that the oscillatory feature occurs regardless of the form of the potential as long as three conditions are satisfied. First, there must be three crossings, as shown in Fig. 6(b). Second, the area enclosed by the crossings must be large enough to produce a phase change of order π when the speed is varied in a convenient range. Third, the stepwise and the direct excitation contributions must be comparable. The first condition is required for there to be four excitation channels interfering with each other. This condition allows for a phase factor that is nearly independent of

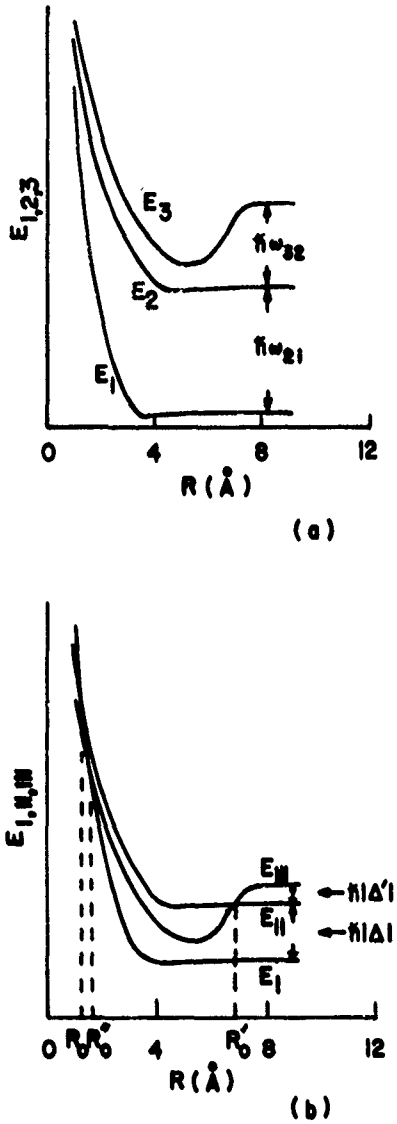

FIG. 6. Interatomic potential used to demonstrate the interference effect discussed in case J. (a) Bare-state-classical-field picture. (b) Dressed-atom picture. The dressed-state energies $E_{I,II,III}$ are related to the bare-state energies $E_{1,2,3}$ by Eqs. (4.2). In (a), the level separations are not drawn to scale; in (b), the energies $\hbar|\Delta|$ and $\hbar|\Delta'|$ set the energy scale. $\Delta = -8.0\times10^{13}$ sec^{-1}, $\Delta' = -3.0\times10^{13}$ sec^{-1}.

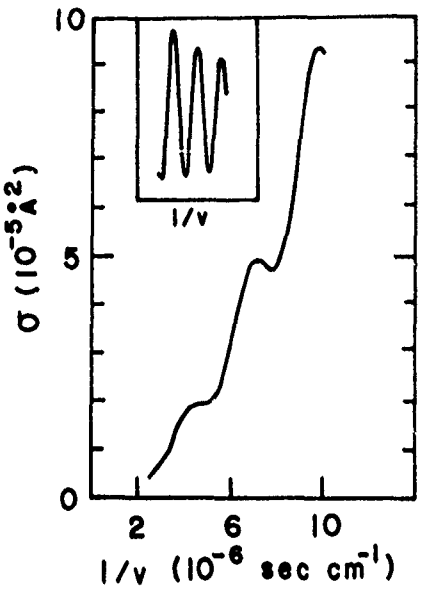

FIG. 7. Total excitation cross section as a function of inverse relative speed $1/v$ for a potential shown in Fig. 6, with $\chi_0 = \chi_0' = 10^{11}$ sec^{-1}, $\Delta = -8.0\times10^{13}$ sec^{-1}, and $\Delta' = -3.0\times10^{13}$ sec^{-1}. The curve rises as $(1/v)^2$. As the speed varies from 10^5 to 4×10^5 cm sec^{-1}, equally spaced peaks are clearly seen. In the inset, the product of the total cross section and v^2 as a function of $1/v$ is shown.

impact parameter b. The second and third conditions determine the frequency and amplitude of the oscillatory term.

VII. DISCUSSION

CARE, as presented in the dressed-atom picture, is similar to radiationless inelastic collisions. However, there is an important difference between the two. In the radiationless inelastic atomic collision, the process, and hence the cross section, is determined by the interatomic potential of the atom-atom system, which cannot be controlled once the system is chosen. In CARE, on the other hand, the corresponding interatomic potential (in the dressed-atom picture) depends not only on the atom-atom system, but also on the atom-field detunings as well as the field intensities. In the weak-field limit, one can vary the detunings to change the level spacings of the dressed states and the positions of, and the slopes at, the potential curve crossings (if any) which are the essential parameters determining the CARE cross section. Hence, the interaction between the two colliding atoms can be probed in a controlled fashion by using CARE, a great advantage over the ordinary radiationless atomic collisions. The three-level problem discussed in this paper provides a good example of the relationship between CARE and inelastic collisions. The oscillatory features obtained in case J of the previous section for the total CARE cross section as a function of active-atom-perturber relative speed are of similar nature to those obtained by Rosenthal and Foley[8] for He-He$^+$ charge-exchange inelastic collisions. The He-He$^+$ atom-ion interatomic potential curves are analogous to those of the three-level CARE in the dressed-atom picture [Fig. 6(b)]. The frequency and amplitude of oscillation in CARE can be varied by changing the detunings and thus the

potential-curve crossing properties (positions and slopes); such a variation is not possible in charge-exchange inelastic collisions. Although oscillation of this type continue to be discovered[18,19] for charge-exchange inelastic collisions in alkali-ion-noble-gas systems such as Na^+-Ne, K^+-Ar, Cs^+-Ar, they are confined in systems with atom-ion interatomic potentials bearing a resemblance to Fig. 6(b), and thus have limited value in investigating the atom-atom or atom-ion interactions. With CARE, the scope of such studies can be extended.

In case J of the previous section, we mentioned that the interference effect should be observable with moderate laser powers, without referring to any specific experimental setup. The experiment can be performed using crossed atomic beams or a beam interacting with a gas sample. The beam-gas sample method works only if the active-atom-perturber relative velocity is approximately equal to the beam velocity. In cases when better detection efficiency is required, one can use a third laser to ionize the active atom from the upper excited state (state 3) and thus detect the ions instead of the fluorescence.

Finally, let us mention another type of oscillation which can occur in a two-level system and should be distinguished from the present one. The modulation in the absorption coefficient as a function of *detuning* for atoms in a collisional environment was discussed by Mies,[20] Carrington *et al.*,[21] Shlyapnikov and Shmatov,[22] and observed by Scheps *et al.*[23] and Bergeman and Liao.[24] This has been attributed to the oscillatory structure of the vibrational wave function of the quasimolecule formed by the colliding atoms. Such an effect does not involve interference of different channels of excitation, and is due to oscillation in the transition matrix elements.

VIII. CONCLUSION

We have presented a theory of collisionally aided radiative excitation for three-level systems in the weak-fields limit. Attempts are made to cover as many cases as possible and to be as general as possible, although results are given for some specific potentials only. Because of the complexity of a three-level system and the distinct physical features and mathematical treatments in different limiting cases, we classified the problem into thirteen cases according to the sizes and the signs of the detunings. These cases were treated in detail, except the last three cases (K, L, M) which give rise to exponentially small excitation cross sections for which reliable analytic approximations are lacking at the present time.

A dressed-atom picture was also given which brought the CARE problem into complete parallel with the problem of radiationless inelastic atomic (or molecular) collisions. In this picture, the collision-induced instantaneous resonances between the atomic transitions and the external fields are transformed into interatomic potential curve crossings. Such curve crossings enhance the excitation, especially in the large detuning cases, and interfere with each other, leading to effects reflecting the crossing configurations. Some special crossing configurations yield particularly interesting interference effects (e.g., the modulation of the total excitation cross section discussed in case J). A quantitative examination indicates that experimental observations of such effects are feasible.

The theory does not include the cases of strong fields which are of increasing importance and interest with the advent of high-power lasers. The dressed-atom approach seems to be most suitable for attacking such cases, and numerical calculations may be inevitably needed. The established numerical method used in two-level CARE problems and the analytic methods presented in this paper can be combined to form useful tools in the investigation of these cases.

ACKNOWLEDGMENTS

This work was supported by the U. S. ONR through contract number N00014-77-C-0553. The authors thank Professor E. J. Robinson for many discussions during the course of the work.

APPENDIX A

In this appendix we give the details of calculations leading to Eqs. (6.29)–(6.39) from Eq. (6.1). Assuming that the collision trajectories are symmetric about $t=0$, the time of closest approach between the active atom and the perturber, we break the t integral of Eq. (6.1) into two parts, $t>0$ and $t<0$,

$$\tilde{C}_3(t=\infty) = -\int_{-\infty}^{0} \chi'(t) \exp\left[-i\left(\Delta' t - \int_0^t V'(t')dt'\right)\right] Q(t)\,dt - \int_0^{\infty} \chi'(t) \exp\left[-i\left(\Delta' t - \int_0^t V'(t')dt'\right)\right] Q(t)\,dt, \tag{A1}$$

where

$$Q(t)=\int_{-\infty}^{t}\chi(t_1)\exp\left[-i\left(\Delta t_1-\int_0^{t_1}V(t')dt'\right)\right]dt_1.$$

Because of the condition $|\Delta|\tau_c\gg 1$, the contributions to Q are from the neighborhood of the crossing points $\pm\tau_0$, satisfying $\Delta=V(t)$ only. Thus, for the first term (restricted to $t<0$), we expand the exponent of the integrand in Q in Taylor series about $t_1=-\tau_0$, and for the second term (restricted to $t>0$), we break the Q integral into two parts, from $-\infty$ to 0 and from 0 to t, and expand the exponent about $t_1=-\tau_0$ and $t_1=\tau_0$ for each region, respectively. The factor $\chi(t_1)$ is evaluated at $\chi(\pm\tau_0)\equiv\chi_0$. The Taylor series is terminated at terms $\propto(t_1\pm\tau_0)^2$, and the integrals obtained are evaluated exactly to yield

$$Q(t)=\chi_0 e^{-i(\phi+s\pi/4)}\tfrac{1}{2}(\pi/\alpha)^{1/2}\{1+\mathrm{erf}[\alpha^{1/2}(t+\tau_0)e^{is\pi/4}]\}\quad\text{for } t<0 \tag{A2}$$

and

$$\begin{aligned}Q(t)=\chi_0 e^{-i(\phi+s\pi/4)}\tfrac{1}{2}(\pi/\alpha)^{1/2}&[1+\mathrm{erf}(\alpha^{1/2}\tau_0 e^{is\pi/4})]\\&+\chi_0 e^{i(\phi+s\pi/4)}\tfrac{1}{2}(\pi/\alpha)^{1/2}\{\mathrm{erf}[\alpha^{1/2}(t-\tau_0)e^{-is\pi/4}]-\mathrm{erf}(-\alpha^{1/2}\tau_0 e^{-is\pi/4})\}\quad\text{for } t>0\end{aligned} \tag{A3}$$

where erf is the error function and ϕ, s, α are defined in Eqs. (6.29)–(6.39). Putting Eqs. (A2) and (A3) into Eq. (A1), using the relation $\mathrm{erf}(z)=1-\mathrm{erfc}(z)$, and combining terms, we can write $\tilde{C}_3(t=\infty)$ as a sum of four terms. Under the assumption that the crossing points are far from $t=0$ ($\alpha^{1/2}\tau_0\gg 1$), one of the four terms, which contains a factor $\mathrm{erfc}[\alpha^{1/2}\tau_0 e^{-is\pi/4}]$, can be neglected. Thus,

$$\begin{aligned}\tilde{C}_3(t=\infty)=-\frac{\chi_0}{2}(\pi/\alpha)^{1/2}\Bigg\{&e^{-i(\phi+s\pi/4)}\int_{-\infty}^{0}\chi'(t)\exp\left[-i\left(\Delta' t-\int_0^t V'(t')dt'\right)\right]\mathrm{erfc}[-\alpha^{1/2}(t+\tau_0)e^{is\pi/4}]dt\\&+e^{i(\phi+s\pi/4)}\int_0^{\infty}\chi'(t)\exp\left[-i\left(\Delta' t-\int_0^t V'(t')dt'\right)\right]\mathrm{erfc}[-\alpha^{1/2}(t-\tau_0)e^{-is\pi/4}]dt\\&+e^{-i(\phi+s\pi/4)}\mathrm{erfc}[-\alpha^{1/2}\tau_0 e^{is\pi/4}]\int_0^{\infty}\chi'(t)\exp\left[-i\left(\Delta' t-\int_0^t V'(t')dt'\right)\right]dt\Bigg\}.\end{aligned} \tag{A4}$$

This again, is to be evaluated using the stationary-phase method. Since the error functions with complex arguments are oscillatory functions, their presence in the integrands of the first two terms in Eq. (A4) will modify the stationary-phase positions of these integrals. To cope with this, we use Eqs. 7.1.2, 7.1.9, 7.1.10, 7.3.9, 7.3.10, and 7.3.22 of Abramowitz and Stegun[25] to express the error functions in terms of an exponential (oscillating) part and the auxiliary functions f,g of the Fresnel's integrals, which are slowly varying functions. By doing this, the integrals are written in a form suitable for the stationary-phase method. We shall now demonstrate the method by evaluating the first term in the curly bracket of Eq. (A4), to be called W. The evaluation of the second term follows exactly the same procedure.

In terms of f,g and the exponential function, W can be written as a sum of three terms. In two of these terms a phase of the form $\phi+s\alpha(t+\tau_0)^2$ appears which is simply the Taylor-series expansion of $\Delta t-\int_0^t V(t')dt'$ at $t=-\tau_0$. We transform this term back to its original form and find

$$\begin{aligned}W=2e^{-i(\phi+s\pi/4)}&\int_{-\tau_0}^{0}\chi'(t)\exp\left[-i\left(\Delta' t-\int_0^t V'(t')dt'\right)\right]dt\\&+is\sqrt{2}\int_{-\tau_0}^{0}\chi'(t)(f^2+g^2)^{1/2}e^{is\theta}\exp\left[-i\left((\Delta+\Delta')t-\int_0^t[V(t')+V'(t')]dt'\right)\right]dt\\&-is\sqrt{2}\int_{-\infty}^{-\tau_0}\chi'(t)(f^2+g^2)^{1/2}e^{is\theta}\exp\left[-i\left((\Delta+\Delta')t-\int_0^t[V(t')+V'(t')]dt'\right)\right]dt,\end{aligned} \tag{A5}$$

where $\theta=\tan^{-1}g/f$ and the argument of f,g is

$$\left|(2\alpha/\pi)^{1/2}(t+\tau_0)\right|.$$

Other parameters are defined in Eqs. (6.29)–(6.39). The integrals in Eq. (A5) can be evaluated using the stationary-phase method. Since $\chi'=\chi_0'$, a constant during the collision, and f,g,θ are slowly varying functions compared with the rapidly oscillating exponential part, we can evaluate them at the stationary-phase points, $-\tau_0'$ for the first term, $-\tau_0''$ for the second and the third term, and take them out of the integrals. The remaining integrals are evaluated using the same method as that leading to Eqs. (A2) and (A3) for Q. Then, the error functions can again be written in terms of f,g functions, which leads to Eq. (6.30).

The same procedure applied to the second term in Eq. (A4) yields Eq. (6.31). The evaluation of the

third term in Eq. (A4) is particularly simple. For stationary-phase point τ_0 far from 0, the erfc function can be approximated by 2, and the integral is done by the stationary-phase method. This method yields Eq. (6.32).

APPENDIX B

The excitation probability can always be written as a sum of three terms, P_S, D_D, and P_{INT} representing the stepwise, the direct, and the interference contributions, respectively. In the most general case, they are

$$P_S=\frac{(\chi_0\chi_0'\pi)^2}{\alpha\alpha'}\{2-(1+s_1)s\sin2\phi-(1-s_1)s'\sin2\phi'$$
$$+(f_1^2+g_1^2)[1-s\sin2(\phi+\phi'_{\tau_0}-s'\theta_1)]$$
$$+[2(f_1^2+g_1^2)]^{1/2}[s\sin(2\phi+\phi'+\phi'_{\tau_0}-s'\pi/4-s'\theta_1)-\cos(\phi'-\phi'_{\tau_0}-s'\pi/4+s'\theta_1)]$$
$$+s_1[2(f_1^2+g_1^2)]^{1/2}[s\sin(2\phi-\phi'+\phi'_{\tau_0}+s'\pi/4-s'\theta_1)-\cos(\phi'+\phi'_{\tau_0}-s'\pi/4-s'\theta_1)]\}, \tag{B1}$$

$$P_D=[(\chi_0\chi_0'\pi)^2/\alpha\alpha'](f_0^2+g_0^2)\{1-s''\sin2(\phi''-s\theta_0)+2(f_2^2+g_2^2)[1-\cos2(\phi''_{\tau_0}-s\theta_0-s''\theta_2)]$$
$$+2[2(f_2^2+g_2^2)]^{1/2}[\cos(\phi''+\phi''_{\tau_0}-2s\theta_0-s''\theta_2-s''\pi/4)-\cos(\phi''_{\tau_0}-\phi''-s''\theta_2+s''\pi/4)]\}, \tag{B2}$$

$$P_{INT}=\frac{(\chi_0\chi_0'\pi)^2}{\alpha}\left(\frac{2(f_0^2+g_0^2)}{\alpha'\alpha''}\right)^{1/2}$$
$$\times(-s_1s_2\{\cos[\phi+\phi'+\phi''-(s-s'-s'')\pi/4-s\theta_0]+\cos[\phi+\phi'-\phi''-(s-s'+s'')\pi/4+s\theta_0]\}$$
$$+s_2\{\cos[\phi-\phi'+\phi''-(s+s'-s'')\pi/4-s\theta_0]$$
$$+\cos[\phi-\phi'-\phi''-(s+s'+s'')\pi/4+s\theta_0]\}$$
$$+s_1s_2s''[2(f_2^2+g_2^2)]^{1/2}\{\sin[\phi+\phi'-\phi''_{\tau_0}-(s-s')\pi/4+s\theta_0+s''\theta_2]$$
$$-\sin[\phi+\phi'+\phi''_{\tau_0}-(s-s')\pi/4-s\theta_0-s''\theta_2]\}$$
$$-s_2s''[2(f_2^2+g_2^2)]^{1/2}\{\sin[\phi-\phi'-\phi''_{\tau_0}-(s+s')\pi/4+s\theta_0+s''\theta_2]$$
$$-\sin[\phi-\phi'+\phi''_{\tau_0}-(s+s')\pi/4-s\theta_0-s''\theta_2]\}$$
$$-s_1s_2s'[2(f_1^2+g_1^2)]^{1/2}\{\sin[\phi+\phi''+\phi'_{\tau_0}-(s-s'')\pi/4-s\theta_0-s'\theta_1]$$
$$+\sin[\phi-\phi''+\phi'_{\tau_0}-(s+s'')\pi/4)+s\theta_0-s'\theta_1]\}$$
$$+2s_1s_2s's''[(f_1^2+g_1^2)(f_2^2+g_2^2)]^{1/2}[\cos(\phi+\phi'_{\tau_0}+\phi''_{\tau_0}-s\pi/4-s\theta_0-s'\theta_1-s''\theta_2)$$
$$-\cos(\phi+\phi'_{\tau_0}-\phi''_{\tau_0}-s\pi/4+s\theta_0-s'\theta_1+s''\theta_2)]), \tag{B3}$$

where

$$\phi'_{\tau_0}=-\Delta'\tau_0+\int_0^{\tau_0}V'(t')dt',\quad \phi''_{\tau_0}=-(\Delta+\Delta')\tau_0+\int_0^{\tau_0}[V(t')+V'(t')]dt',$$

and all the other quantities have been defined in Eqs. (6.29)–(6.39).

---

*Present address: Systems and Applied Sciences Corp., 17 Research Dr., Hampton, Va. 23606.

[1]An extensive list of papers, books, and reviews regarding radiative collisions and optical collisions (CARE) in two-level systems for all limits, including impact and nonimpact regions, can be found in a recent review. See S. I. Yakovlenko, Sov. J. Quantum Electron. 8, 151 (1978).

[2]S. Yeh and P. R. Berman, Phys. Rev. A 19, 1106 (1979) and references therein.

[3]M. H. Nayfeh, Phys. Rev. A 20, 1927 (1979).

[4]We follow the terminology used in some pressure-broadening theories; for example, J. Szudy and W. E. Baylis, J. Quant. Spectrosc. Radiat. Transfer, 15, 641 (1975).

[5]C. Cohen-Tannoudji, *Cargèse Lecture in Physics* (Gordon and Breach, New York, 1968), Vol. 2, p. 347.

[6]See, for example, J. M. Yuan and T. F. George, J. Chem. Phys. 68, 3040 (1978).

[7]S. Yeh and P. R. Berman, Phys. Rev. Lett. 43, 848 (1979).

[8]H. Rosenthal and H. M. Foley, Phys. Rev. Lett. 23, 1480 (1969); H. Rosenthal, Phys. Rev. A 4, 1030 (1971).

[9]S. H. Dworetsky and R. Novick, Phys. Rev. Lett. 23,

1484 (1969).
[10]See, for example, S.-Y. Chen and M. Takeo, Rev. Mod. Phys. 29, 20 (1957); R. G. Breene, Jr., *ibid.* 29, 94 (1957).
[11]See, for example, J. D. Murray, *Asymptotic Analysis* (Clarendon, Oxford, 1974).
[12]These are the standard results of pressure-broadened line shape for a van der Waals potential. See, for example, Ref. 10.
[13]The approximation has been used in connection with semiclassical atomic-collision theory, especially in two-level model calculation. See, for example, W. Fritsch and U. Wille, J. Phys. B 11, L43 (1978). For a detailed account, see M. S. Child, *Molecular Collision Theory* (Academic, London, 1974), pp. 191–194.
[14]S. D. Tvorogov and V. V. Fomin, Opt. Spectrosc. (USSR) 30, 228 (1971); V. V. Fomin and S. D. Tvorogov, Appl. Opt. 12, 584 (1973).
[15]J. Szudy and W. E. Baylis, J. Quant. Spectrosc. Radiat. Transfer 15, 641 (1975).
[16]See Ref. 11 or Ref. 14.
[17]This radius was originally defined by V. V. Weisskopf as the impact parameter at which $\int_{-\infty}^{\infty}[\omega_{31}(t)-\omega_{31}]dt = 1$.
[18]R. Odom, J. Caddick, and J. Weiner, Phys. Rev. A 15, 1414 (1977).
[19]J. Østgaard Olsen *et al.*, Phys. Rev. A 19, 1457 (1979).
[20]F. H. Mies, J. Chem. Phys. 48, 482 (1967).
[21]C. G. Carrington, D. Drummond, A. Gallagher, and A. V. Phelps, Chem. Phys. Lett. 22, 511 (1973).
[22]G. V. Shlyapnikov and I. P. Shmatov, Opt. Spectrosk. 45, 209 (1978) [Opt. Spectrosc. (USSR) 45, 117 (1978)].
[23]R. Scheps, Ch. Ottinger, G. York, and A. Gallagher, J. Chem. Phys. 63, 2581 (1975); G. York, R. Scheps, and A. Gallagher, *ibid.* 63, 1052 (1975).
[24]T. Bergeman and P. F. Liao (unpublished).
[25]M. Abramowitz and I. A. Stegun, *Handbook of Mathematical Functions* (Dover, New York, 1972).

J. Phys. B: At. Mol. Phys. 14 (1981) 1741–1759. Printed in Great Britain

Supported by the U.S. Office of Naval Research under Contract No. N00014-77-C-0553.

Multiphoton scattering processes

S Yeh† and P Stehle‡

† Systems and Applied Science Corporation, Hampton, VA 23666, USA
‡ Department of Physics and Astronomy, University of Pittsburgh, Pittsburgh, PA 15260, USA

Received 30 June 1980, in final form 7 January 1981

Abstract. A direct, completely quantum mechanical method of calculating transition probabilities involved in multiphoton scattering processes is described. It is applied to the often treated problem of resonance fluorescence of a two-level atom and is used to give a completely general description of the resonance scattering from an atom with two nearly degenerate excited states coupled to a ground state. Other applications of the method are indicated.

1. Introduction

A very direct method of calculating multiphoton scattering amplitudes and probabilities is described. It is a non-perturbative method which permits one to select the information desired in the sense that no information is discarded in the formulation of the calculation, but undesired information may be integrated out at later stages. The method is based on a continued fraction development of the diagonal Green's function or propagator of an interacting system given in an earlier paper (Yeh and Stehle 1977, to be referred to as I). The method is then applied here to the old problem of the resonance fluorescence of a two-level atom, and to the problem of the resonance fluorescence of an atom with two excited states coupled to a ground state. In the two-level case termination of the continued fraction at an early stage reproduces the well known result of a three-peaked spectrum. The continued fraction is carried one step further and the result shows that the natural line width Γ is not affected by the power in the optical regime. This result does not conflict with the existence of power broadening and lends support to the truncation of the continued fraction. For the three-level case the treatment yields results for the most general case including unequal couplings and arbitrary detunings of the two excited states. An application to photon–photon frequency–time correlations is also described.

2. The continued fraction development

The results of I needed here are briefly stated. The derivation may be found in I.

The system contemplated consists of an atom interacting with the radiation field. The interaction is assumed to be of the electric dipole form, linear in the field and therefore involving the emission or absorption of photons one at a time. Let the system

0022-3700/81/111741+19$01.50

be specified by the time-independent Hamiltonian

$$H = H_0 + V.$$

Let P_N be a projection operator onto a subspace of the state space of H_0, so that

$$P_N^2 = P_N \qquad [P_N, H_0] = 0 \qquad P_N V P_N = 0. \tag{1}$$

The last of these equations is satisfied if the subspace defined by P_N contains a definite number N of photons of whatever modes, as V acts to change the photon number by unity. Under these conditions it was shown in I that the Green's function

$$G(E, V) = \frac{1}{E - H_0 - V} \tag{2}$$

satisfies the equation

$$P_N G(E, V) P_N \equiv G_N(E, V)$$

$$= \frac{P_N}{E - H_0 - P_N V G_{N+1}(E, V_N) V P_N - P_N V G_{N-1}(E, V_N) V P_N} \tag{3}$$

where

$$V_N = (1 - P_N) V (1 - P_N) \tag{4}$$

does not couple any state within the subspace defined by P_N to any other state inside or outside the subspace.

The form of (3) does not allow a continued fraction development by iteration because of the presence of processes both increasing and decreasing the number of photons present. However, on writing the analogue of (3) for $G_{N+1}(E, V_N)$, only those processes increasing the photon number occur in the denominator because the interaction V_N cannot return the system to an N-photon state. Thus

$$G_{N+1}(E, V_N) = \frac{P_{N+1}}{E - H_0 - P_{N+1} V_N G_{N+2}(E, V_{N+1}) V_N P_{N+1}}$$

$$= P_{N+1}\left(E - H_0 - P_{N+1} V_N \frac{P_{N+2}}{E - H_0 - P_{N+2} V_{N+1} G_{N+3}(E, V_{N+2}) V_{N+1} P_{N+2}} \times V_N P_{N+1}\right)^{-1} \tag{5}$$

etc does yield a continued fraction development. A similar development exists for $G_{N-1}(E, V_N)$.

Off-diagonal Green's functions or transition amplitudes can be expressed in terms of these diagonal ones or propagators as is shown in I

$$P_{N+1} G(E, V) P_N = P_{N+1} G(E, V_N) P_{N+1} V G_N(E, V). \tag{6}$$

This may be iterated to give higher degrees of being off-diagonal, connecting states with different photon number. Equation (6) is not an expansion in power of V but is exact. It does, however, describe a transition in terms of a sequence of steps, none of which is retraced later in the transition, leading from the initial to the final state.

3. Forward scattering and virtual processes

Consider the atom to have a set of states $|e_i\rangle$ which are fairly close to each other in energy, all of which are coupled to another state $|g\rangle$ through the electric dipole coupling V and which are not, therefore, coupled directly to one another by V. The projection operator P_e is defined to project onto the subspace of the state space of H_0 spanned by the n states $|e_i\rangle$ together with a state of the radiation field in which one mode ω, the 'laser mode', contains $N-1$ photons and all other modes are empty. If ξ_i' is the dipole coupling matrix element coupling states $|g\rangle$ and $|e_i\rangle$, the effective coupling ξ_i with the laser mode is $N^{1/2}\xi_i'$, where the distinction between N and $N\pm1$ is neglected because N is assumed large. The transitions of concern here are in the optical frequency range, so the rotating-wave approximation may be made. This states that photon emission is associated only with downward atomic transitions, and photon absorption only with upward ones. The projection operator P_g projects onto the state with the atom in $|g\rangle$ and N photons in the laser mode.

Under the circumstances just given, the above expression for the propagator $G_g(E, V)$ becomes

$$G_g(E, V)=\frac{P_g}{E-H_0-P_gVG_e(E, V_g)VP_g}. \tag{7}$$

The processes included are transitions to an excited state by photon absorption, propagation in this state, and then a return to the original state by photon emission. The only absorption process possible is the absorption of a laser photon, which must subsequently be re-emitted, so the process is one of forward scattering of laser photons. The fact that VG_eV is present in the denominator of (7) indicates that the propagator $G_g(E, V)$ contains absorption–re-emission of laser photons to all orders.

The propagator $G_e(E, V_g)$ becomes

$$G_e(E, V)=\frac{P_e}{E-H_0-P_eV_gG_{\bar{g}}(E, V_e)V_gP_e} \tag{8}$$

$\bar{g}$ specifies a state distinct from g because V_g cannot cause a transition to g. Therefore the processes included in (8) are the emission of a non-laser photon, propagation with the atom in its ground state, $N-1$ laser photons, and a non-laser photon in the field, and reabsorption of the non-laser photon. The propagation of the system in $|\bar{g}\rangle$ can involve forward scattering. It is shown in appendix 1 that this has only a small effect in cases of interest and it will be neglected. What is left is exactly the set of virtual processes leading to the existence of a finite width of the excited states, or to a mean lifetime for these states against spontaneous radiation (Low 1952). Thus (8) can be written as

$$G_e(E, V_g)=\frac{P_e}{E-(H_0-i\Gamma)}. \tag{9}$$

Insertion of (9) into (7) yields the propagator for the atom in its ground state initially and finally, in the presence of the laser beam.

4. Resonance fluorescence

Resonance fluorescence consists of the scattering by an atom of light whose frequency ω is close to a resonance frequency ω_0 of the atoms. When the incident intensity is low this

can be treated as a single-photon process (Heitler 1954), and then energy conservation requires the scattered photon to have the same frequency as the incident one except for the extremely small effect produced by the recoil of the scatterer. This can be expressed in terms of the Rabi frequency (Allen and Eberly 1975) of the atom in the field of the incident radiation. When that radiation is weak, the Rabi period is much longer than the mean lieftime of the excited atom, so successive scatterings are mutually independent. When the intensity is increased so that the Rabi period becomes comparable with the mean lifetime, the process becomes a multiphoton one because at any instant the state of the system in the Schrödinger or interaction picture is a superposition of states containing different numbers of incident and scattered photons. Under these circumstances energy conservation imposes only a condition on the sum of the energies of all the scattered photons. Also, various scattering processes lead to the same final state, so quantum mechanical interferences affect the fluorescence spectrum.

The spectrum of resonance fluorescence of a two-level atom has been found by many authors using many methods of calculation (Mollow 1969, 1975, Carmichael and Walls 1975, Smithers and Freedhoff 1975, Swain 1975, Renaud *et al* 1976). When the excited state is not unique but is multiple, the problem becomes more complicated, but has been treated in a special case by Sobolewska (1976) and more generally by Kornblith and Eberly (1978). What is presented here is a formulation of this problem in completely orthodox quantum mechanical terms; a transition amplitude from a prepared initial state to a possible final state is calculated, and the corresponding transition probability is summed over all observables not used in specifying the final state of interest experimentally. It differs from methods involving the direct calculation of correlation functions (Renaud *et al* 1976) in that the transition amplitude contains all the information about the system that exists in the specification of the system, while a formulation which calculates the evolution of a correlation operator does not automatically contain any information about higher order correlations.

The system at time $t = 0$ contains an atom in its ground state $|g\rangle$ and a radiation field with a single mode, the laser mode, excited to its N-photon state, all other modes being in their ground or vacuum state. At time $t > 0$, a number of photons may be missing from the laser mode and some other modes may be occupied. Neither the number of laser photons missing nor the number of scattered photons present has a definite value at a specified time, but under the rotating-wave approximation (which will be made) the two numbers will be the same if the initial and the final atomic states are the same. In the method to be described, the coupling system of atom and field is allowed to develop until m scattered photons have been emitted, and then the atom is removed from the laser beam. This does not correspond exactly to a common experimental situation (Schuda *et al* 1974, Hartig *et al* 1976, Grove *et al* 1977) where the atom is illuminated for a definite time by the laser, but the difference is small if m is at all large, and the resulting simplification is great.

A Feynman diagram representing the process is seen in figure 1. The atom, initially in its ground state, alternately absorbs laser photons of mode ω and emits scattered photons of modes $\nu_1, \nu_2, \ldots, \nu_m$. The alternation is a consequence of the use of the rotating-wave approximation in which photon absorption necessarily accompanies an upward atomic transition and photon emission a downward one. Not shown in the diagram are the forward scattering processes that also occur or the virtual emission and absorption processes that account for the existence of spontaneous emission into the non-laser modes with mean lifetime $1/\Gamma$. These are contained in the propagators. The propagator $G_g(E, V)$ is denoted by a broken line, $G_e(E, V)$ is denoted by a dotted line.

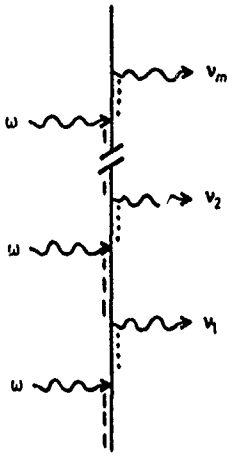

Figure 1. Feynman diagram representing the successive emissions of scattered photons by an atom illuminated with single-mode light. Propagation with forward scattering is shown by broken lines, with emission and reabsorption of non-laser photons by dotted lines. The single line represents a free propagator.

After the emission of the mth scattered photon the atom leaves the laser beam so the last propagator is $G_0(E)$ denoted by a single line.

The strength of the coupling between the atom and a mode of the field is given by

$$\xi' = \left(\frac{e^2\omega_0}{2L^3}\right)^{1/2} \langle e|\hat{d}|g\rangle \tag{10}$$

if the mode is unoccupied (emission only possible) or contains one photon (reabsorption of a virtual photon). If the mode is highly populated, the coupling ξ is given by

$$\xi = N^{1/2}\xi' \tag{11}$$

where the difference between N and $N \pm 1$ is neglected. Here L^3 is the volume of the space in which the field is quantised, and $\hat{d}$ is the dipole moment of the atom. Polarisation effects can be included in the calculation by suitably specifying this dipole coupling, but this is not done here.

As stated above, virtual emission and reabsorption of non-laser photons are included in the propagators. It is possible for a virtual emission and reabsorption process to straddle other processes such as forward scattering or non-forward scattering. The effect of the former is shown to be small in appendix 1, and the latter is also assumed to be negligible. This means that the propagators occurring in later segments of the Feynman diagram depend on the earlier segments only through the eigenvalues of H_0 that occur in them, i.e. on the energies of previously scattered photons.

The propagator $G_g(E, V)$ occurring after the emission of the rth scattered photon contains the eigenvalue of H_0

$$E_g + N\omega + \sum_{i=1}^{r} x_i \tag{12}$$

if $x_i = \nu_i - \omega$ is the inelasticity of the ith scattered photon. If the atom has p excited states coupled to the ground state, the free Hamiltonian H_0 appearing in the next

following propagator $G_e(E, V)$ is diagonal and has the form of a $p \times p$ matrix

$$\begin{pmatrix} E_1-(N-1)\omega+\Sigma'_{i=1}x_i & & 0 \\ & E_2-(N-1)\omega+\Sigma'_{i=1}x_i & \\ 0 & & E_p-(N-1)\omega+\Sigma'_{i=1}x_i \end{pmatrix}. \tag{13}$$

The couplings of the ground atomic state to the excited states are all of the form

$$P_eVP_g = \begin{pmatrix} \xi_1 \\ \xi_2 \\ \vdots \\ \xi_p \end{pmatrix}$$

$$P_gVP_e = (\xi'_1, \xi'_2, \ldots, \xi'_p) \tag{14}$$

the former describing the absorption of laser photons, the latter the emission of scattered photons. The emission of laser photons occurs only in connection with forward scattering, and the absorption of non-laser photons in connection with virtual processes.

The amplitude for the successive emission of scattered photons $\nu_1, \nu_2, \ldots, \nu_m$ in that order is

$$\mathscr{C}^{(\nu_i)}(t) = \frac{-1}{2\pi i}\int_{-\infty}^{\infty} dE\, F(E)\, e^{-iEt} \tag{15}$$

with

$$\begin{aligned} F(E) = {} & G_0(E; x_m+\ldots+x_1)[VG_e(E; x_{m-1}+\ldots+x_1)VG_g(E; x_{m-1}+\ldots+x_1)] \\ & \times\ldots\times[VG_e(E;0)VG_g(E;0)] \end{aligned} \tag{16}$$

G_e, G_g and G_0 are here no longer operators.

The second argument indicates the value of H_0 appearing there. All of the poles of $F(E)$ lie in the lower half of the complex E plane for reasons of causality, and they all lie a finite distance below the real axis except for the one coming from G_0, which is only infinitesimally below. At large times, therefore, only the contribution from this one pole need be retained. It occurs at

$$E = E_g + N\omega + \sum_{i=1}^{m} x_i \tag{17}$$

therefore

$$\begin{aligned} \mathscr{C}^{(\nu_i)}(t) \underset{t\to\infty}{=} {} & g(x_m)g(x_m+x_{m-1})\ldots g(x_m+x_{m-1}+\ldots+x_1) \\ & \times\exp[-i(E_g+N\omega+x_1+\ldots+x_m)t] \end{aligned} \tag{18}$$

where $g(x)$ is the content of a pair of square brackets in (16) evaluated at the pole of G_0.

The amplitude $\mathscr{C}^{(\nu_i)}(t)$ corresponds to a specified order of emission of the m scattered photons. The final state is the same for any order of emission, so this amplitude must be symmetrised by summing over the $m!$ different orders of emission. There is a continuum of modes present in the limit $L^3 \to \infty$ so that double occupancy of modes does not occur. The transition probability is the absolute square of the symmetrised amplitude, and will contain 'direct' terms in which the order of vertices in the two complex conjugate factors is the same and 'cross' terms in which it is different.

The cross terms will be shown to be responsible for the 'coherent' part of the spectrum and for the modification of the side bands coming from the direct part.

The transition probability just found relates to an observation made on the system after m photons have been scattered. It is possible to make observations of a different kind involving, for example, the sequential emission of two photons of different prescribed frequency in a specified order (Aspect *et al* 1980). In this situation the amplitude $\mathscr{C}^{(r_1)}(t)$ must not be symmetrised in these two photons. Such a situation is discussed in § 7. The summation over unobserved photons is converted to an integration over the wavevectors in the customary way, namely

$$\sum_{k} \to L^3 \int \frac{d^3k}{(2\pi)^3}.$$

The frequency dependencies of the quantities of interest here are all peaked in the neighbourhood of the atomic resonance, so the above integration can be reduced to

$$\frac{L^3}{(2\pi)^3} \int d\Omega_k \omega_0^2 \int dk = K \int dk$$

with ω_0 either the resonance frequency or the laser frequency. x_1 is chosen as the observed frequency and is denoted by x.

A major simplification is provided by the vanishing of all integrals in which the order of the variables integrated over in the two complex conjugate factors entering the absolute square is not the same. This is shown in appendix 2. In evaluating the spectrum, therefore, the only ordering of significance is provided by the location of the observed photon's emission vertex; in the direct terms this is the same in the two factors, in the cross term it differs in the two factors.

A typical direct term in the spectrum is

$$K^{m-1} \int dx_2 \ldots dx_m g^*(x_m) g^*(x_m + x_{m-1}) \ldots g^*(x_m + \ldots + x + x_2)$$

$$\times g(x_m) g(x_m + x_{m-1}) \ldots g(x_m + \ldots + x + x_2) \tag{19}$$

where x replaces x_1 and the observed photon is emitted at the second vertex. x_2 occurs in only two factors, and on integrating over the interval $(-\infty, \infty)$ one obtains

$$K \int dx' g^*(x') g(x') = 1 \tag{20}$$

because this is simply the probability that the atom will absorb a laser photon and emit a scattered photon sometime during the process of scattering m laser photons, which it is certain to do. After this, integration over x_3 leads to

$$A(x) = K \int dx' g^*(x') g^*(x' + x) g(x') g(x' + x). \tag{21}$$

Subsequent integrations lead to further factors of unity. Because the observed photon can be emitted at any vertex, the total contribution of the direct terms is

$$mA(x) \tag{22}$$

neglecting the anomaly of the contribution when x is the mth photon emitted when instead of $A(x)$ one obtains $g^*(x)g(x)$.

A typical cross term in the spectrum is

$$K^{m-1}\int dx_2 \ldots dx_m g^*(x_m)g^*(x_m+x)g^*(x_m+x+x_{m-1})\ldots g^*(x_m+x+\ldots+x_2)$$
$$\times g(x_m)g(x_m+x_{m-1})\ldots g(x_m+\ldots+x_{m-l}+x)\ldots g(x_m+\ldots+x_2). \quad (23)$$

Here x appears l places later in the sequence of g^* than in the sequence of g. Integrations over x_2 up to x_{m-l-1} lead to factors of unity. Integration over x_{m-l} leads to

$$E(x)=K\int dx'\, g^*(x'+x)g(x')g(x'+x). \quad (24)$$

After this, integration over x_{m-l+1} leads to

$$H(x)=K\int dx'\, g^*(x'+x)g(x'). \quad (25)$$

Note that $H(0)=1$, and $H^*(x)=H(-x)$. Altogether $l-1$ such factors occur followed by

$$E'(x)=K\int dx'\, g^*(x')g^*(x'+x)g(x')$$
$$=E^*(-x) \quad (26)$$

unless x occurs in the left-most factor g^* when $E'(x)$ is replaced by $H(x)g^*(x)$. For large m this makes little difference and is not taken into account.

For a given separation l of the occurrences of x in the factors g^* and g there are $m-l$ positions of x, and l can range from 1 to $m-1$. The total contribution of the cross terms is, therefore,

$$2\,\mathrm{Re}\left(E(x)E^*(-x)\sum_{l=1}^{m-1}(m-l)(H(x))^{l-1}\right). \quad (27)$$

The factor 2 includes the contributions from terms in which x occurs later in the sequence of g than in that of g^*.

The spectrum $P(x)$ of a scattered photon observed without regard to the frequencies of any other scattered photons can now be written as

$$P(x)=A(x)+E(x)E^*(-x)\frac{1}{m}\sum_{l=1}^{m-1}(m-l)(H(x))^{l-1}$$
$$+E(-x)E^*(x)\frac{1}{m}\sum_{l=1}^{m-1}(m-l)(H(-x))^{l-1}. \quad (28)$$

This depends on m only through the sums. These sums contribute, for small x, a very sharp peak whose height is proportional to m and whose width is proportional to $1/m$, as shown in appendix 3. For $m\to\infty$ this approaches a delta function, and is the 'coherent' part of the fluorescence. It is satisfactory to obtain a finite peak for a finite m. As $m\to\infty$, the duration of the experiment becomes long without limit and then an infinitely sharply defined frequency first becomes physically possible. The spectrum is symmetric about $x=0$ or $\nu=\omega$.

5. Two-level atom

This case is very familiar, so it will be discussed only to the extent that it clarifies the application of the method of calculation. The projection operators are one dimensional. Defining the detuning δ by

$$\delta = \omega - \omega_0 = \omega - (E_e - E_g) \tag{29}$$

the function $g(y)$ becomes, setting $E_g + N\omega = 0$,

$$g(y) = \frac{\xi'\xi}{(y + \delta + i\Gamma)y - \xi^2}. \tag{30}$$

The denominator is quadratic in y so the poles are readily located analytically and the integrations carried out. From (21) one finds

$$K = \Gamma/\pi\xi'^2 \tag{31}$$

which is the result to be expected if ξ' is the coupling responsible for the decay characterised by Γ. Introducing the quantities

$$\begin{aligned} X^2 &= \tfrac{1}{2}(\delta^2 + 4\xi^2 - \Gamma^2) + \tfrac{1}{2}[(\delta^2 + 4\xi^2 - \Gamma^2)^2 + 4\delta^2\Gamma^2]^{1/2} \\ Y &= \delta\Gamma/X \end{aligned} \tag{32}$$

it is found that

$$A(x) = \frac{4\Gamma^2\xi'^2\xi^4}{(X^2+Y^2)(X^2+\Gamma^2)(\Gamma^2-Y^2)}\left[\frac{(\Gamma-Y)/\Gamma}{x^2+(\Gamma+Y)^2} + \frac{(\Gamma+Y)/\Gamma}{x^2+(\Gamma-Y)^2}\right.$$
$$\left. + \frac{1}{X^2+\Gamma^2}\left(\frac{X^2-\Gamma^2-2X(x-X)}{(x-X)^2+\Gamma^2} + \frac{X^2-\Gamma^2+2X(x+X)}{(x+X)^2+\Gamma^2}\right)\right] \tag{33}$$

$$H(x) = \frac{4i\xi^2\Gamma(x - i\Gamma)}{[(x-i\Gamma)^2 - X^2][(x-i\Gamma)^2 + Y^2]} \tag{34}$$

$$E(x) = 4\Gamma^2\xi'\xi^3\frac{x^2 + (\delta - 3i\Gamma)x - 2\Gamma(\Gamma + i\delta)}{[(x-i\Gamma)^2 - X^2][(x-i\Gamma)^2 + Y^2](x^2+\Gamma^2)(\Gamma^2-Y^2)}. \tag{35}$$

Inserted into (28) these yield the familiar three-peaked spectrum. The contribution of the direct terms, $A(x)$, consists of four Lorentzians, two centred on the laser frequency ω, which reduce to three at exact resonance, $\delta = 0$. In this case the central peak is twice as high as the side peaks and of the same width. The peaks are separated by X which is the Rabi frequency 2ξ corrected for detuning δ and damping Γ. This is the spectrum obtained by Smithers and Freedhoff (1975) and Smithers (1975) and later corrected by them to include the contribution coming from the cross terms. These add the coherent peak and modify the side peaks to one third the central peak height and three halves the central peak width. This can be seen in the high-intensity limit. When $\xi \gg \delta$ and Γ, the direct term becomes

$$A = \frac{\xi'^2}{4}\left(\frac{2}{x^2+\Gamma^2} + \frac{1}{(x-2\xi)^2+\Gamma^2} + \frac{1}{(x+2\xi)^2+\Gamma^2}\right) \tag{36}$$

and the cross terms in (29) yield, except at $x = 0$,

$$\frac{\xi'^2}{4}\left(\frac{-1}{(x-2\xi)^2+\Gamma^2}+\frac{-1}{(x+2\xi)^2+\Gamma^2}+\frac{\frac{3}{2}}{(x-2\xi)^2+(\frac{3}{2}\Gamma)^2}+\frac{\frac{3}{2}}{(x+2\xi)^2+(\frac{3}{2}\Gamma)^2}\right). \tag{37}$$

Thus the cross terms replace the sidebands given by the direct term $A(x)$ with wider, lower ones and supply the coherent part at $x = 0$ consisting of a sharp peak whose limiting form is a delta function, as shown in appendix 3.

6. Three-level atom

The level scheme is shown in figure 2. The detuning δ is measured from the lower level E_1 which is Δ below E_2. The coupling of the excited states to the ground state is measured by ξ'_1, ξ'_2. The matrix $H_0 - i\Gamma$ is two dimensional and the couplings are

$$P_e V P_g = \begin{pmatrix}\xi_1\\ \xi_2\end{pmatrix} \qquad P_g V P_e = (\xi'_1, \xi'_2). \tag{38}$$

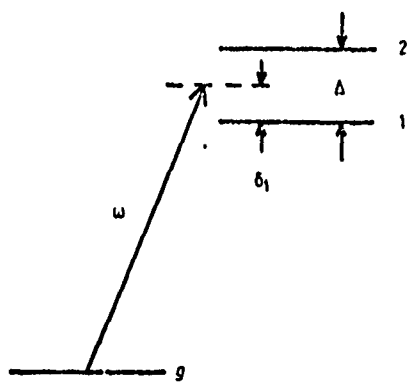

Figure 2. Level scheme of an atom with two levels coupled to a single ground level.

The propagator $G_e(E, V_g)$ depends on $H_0 - i\Gamma$. For Γ to be non-diagonal in the two-dimensional subspace of the excited states these states would have to be coupled by the emission and reabsorption of photons. They would have to have the same angular momentum and parity quantum numbers. Within the electric dipole approximation they could differ only in principal quantum number which would make them widely separated. It is natural, therefore, to assume that Γ is also diagonal in this subspace. From (9), then,

$$\begin{aligned} G_e(E, V_g) &= P_e\begin{pmatrix}E-E_g-N\omega+\delta+i\Gamma_1 & 0\\ 0 & E-E_g-N\omega+\delta-\Delta+i\Gamma_2\end{pmatrix}^{-1} P_e \\ &= \frac{P_e\begin{pmatrix}E-E_g-N\omega+\delta-\Delta+i\Gamma_2 & 0\\ 0 & E-E_g-N\omega+\delta+i\Gamma_1\end{pmatrix} P_e}{(E-E_g-N\omega+\delta+i\Gamma_1)(E-E_g-N\omega+\delta-\Delta+i\Gamma_2)} \end{aligned} \tag{39}$$

for the leg before the emission of the first scattered photon. Later legs are different in including the inelasticities of previously emitted photons. The function $g(y)$ now has the form,

$$g(y)=\frac{\xi_1'\xi_1(y+\delta-\Delta+i\Gamma_2)+\xi_2'\xi_2(y+\delta+i\Gamma_1)}{(y+\delta+i\Gamma_1)(y+\delta-\Delta+i\Gamma_2)}$$
$$\times\left(y-\frac{\xi_1^2(y+\delta-\Delta+i\Gamma_2)+\xi_2^2(y+\delta+i\Gamma_1)}{(y+\delta+i\Gamma_1)(y+\delta-\Delta+i\Gamma_2)}\right)^{-1}$$
$$=\frac{\xi_1'\xi_1(y+\delta-\Delta+i\Gamma_2)+\xi_2'\xi_2(y+\delta+i\Gamma_1)}{y(y+\delta+i\Gamma_1)(y+\delta-\Delta+i\Gamma_2)-[\xi_1^2(y+\delta-\Delta+i\Gamma_2)+\xi_2^2(y+\delta+i\Gamma_1)]}. \tag{40}$$

The denominator is cubic in y and it is not practical to locate the poles analytically. As $\xi_2'\to 0$ this approaches the expression (30) for the two-level atom.

Some results for the spectrum resulting from using expression (40) for $g(y)$ in evaluating (28) are shown in figures 3, 4 and 5. The poles needed for this evaluation are located numerically. This spectrum has also been calculated for a non-diagonal Γ matrix (Yeh 1977), for one with all elements equal. The result is a single sideband spectrum for tuning midway between the levels, a result quite distinct from figure 3 and from that of Sobolewska (1976). This suggests that observation of resonance fluorescence from a three-level atom of the kind considered would provide a way of determining any off-diagonal character of Γ.

For unequal couplings the spectrum is more complicated, showing three sidebands. These can be interpreted as sidebands separated by the Rabi frequency $2\xi_1$, prominent when the laser is tuned near the lower excited state, as sidebands separated by the Rabi

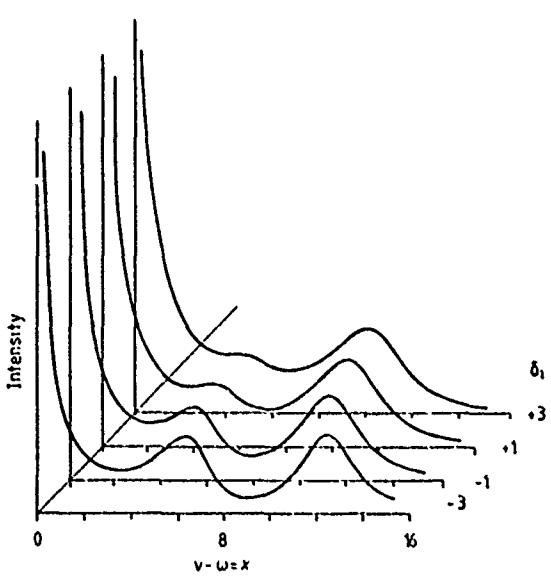

Figure 3. Three-level atom fluorescence, with variation of detuning δ_1 when $\xi_1=\xi_2=3$, $\Delta=6$, $\Gamma_1=\Gamma_2=1$, $m=15$. All spectra are symmetric about $x=0$.

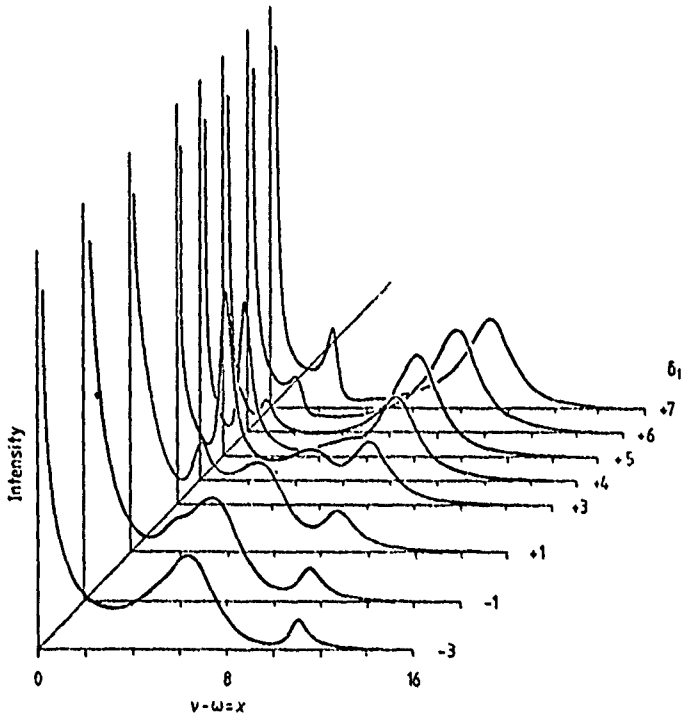

Figure 4. Three-level atom fluorescence, with variation of detuning δ_1 when $\xi_1 = 3$, $\xi_2 = 1$, $\Delta = 6$, $\Gamma_1 = 1$, $\Gamma_2 = 0.11$ and $m = 15$.

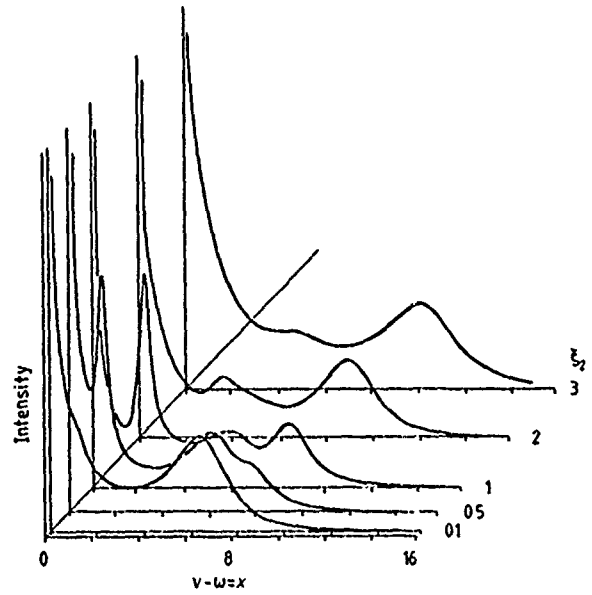

Figure 5. Three-level atom fluorescence, with variation of coupling ξ_2, when $\xi_1 = 3$, $\Delta = 6$, $\delta_1 = 3$, $\Gamma_1 = 1$, $\Gamma_2 = (\xi_2/\xi_1)^2$, $m = 15$.

frequency $2\xi_2$, prominent when the laser is tuned near the after excited state, and as interferences between the amplitudes for these two kinds of scattering. In general, the number of sidebands agrees with a dressed-atom picture (Cohen-Tannoudji and Reynaud 1977), and the details of the spectrum depend on the detunings and couplings involved.

The resonance fluorescence from a three-level atom has been studied by Kornblith and Eberly (1978) using a very different method which seems to use the diagonal character of Γ in an essential way. They also consider polarisation of the scattered light, which could be done here but has not been. Their results for equal couplings show two sidebands above and below the central peak, just like the present results. They report a disagreement with the present authors, a disagreement arising from a comparison of their results with results calculated with a non-diagonal Γ and presented at the 1977 International Conference on Multiphoton Processes at Rochester. The source of the disagreement was not known until recently.

7. Two-photon frequency and time correlations

Two-photon correlation experiments have been done in connection with resonance fluorescence. One was the 'antibunching' experiment of Kimble *et al* (1977) showing that a single atom which has just emitted a scattered photon cannot immediately emit another. This had been predicted by Kimble and Mandel (1976) and by Carmichael and Walls (1976). Another is a correlation experiment involving detecting photons occurring in the two sidebands of two-level resonance fluorescence with a delayed coincidence (Aspect *et al* 1980). Aspect *et al* show that photons corresponding to the two sidebands tend to come out in pairs with a small time-delay, and that the photon corresponding to one side band preferentially precedes the one from the other sideband. They give a theoretical account of this in terms of perturbation theory.

This particular experiment has a remarkably simple description in the formulation of resonance fluorescence given here. The transition detected is one in which a photon of frequency $\nu_A = \omega + x_A$ is emitted, and then a photon of frequency $\nu_B = \omega + x_B$. ν_A and ν_B are chosen to be the two sideband frequencies, and the laser is detuned by an amount large compared with the Rabi frequency 2ξ and with the natural linewidth Γ. Consider the two photons ν_A and ν_B to be emitted successively, say after ν_1. Then the amplitude (18) contains the sequence

$$g(x)_m \ldots g(x_m + \ldots + x_2) g(x_m + \ldots + x_2 + x_B) \times g(x_m + \ldots + x_2 + x_B + x_A) g(x_m + \ldots + x_2 + x_B + x_A + x_1) \tag{41}$$

which must be symmetrised in all photon variables except x_B and x_A, which must retain their relative order, and it is assumed for simplicity that they are always successive. On squaring there will be direct and cross terms.

The analogue of $P(x)$ in (28) is now

$$\tilde{P}(x_A, x_B) = \tilde{A}(x_A, x_B) + \tilde{E}(x_A, x_B)\tilde{E}^*(-x_B, -x_A)\frac{1}{m}\sum_{l=1}^{m-2}(m-l)(H(x_A + x_B))^{l-1} + \tilde{E}(-x_B, -x_A)\tilde{E}^*(x_A, x_B)\frac{1}{m}\sum_{l=1}^{m-2}(m-l)(H(-x_B - x_A))^{l-1}. \tag{42}$$

For a two-level atom one finds that

$$\tilde{A}(x_A, x_B) = K\int dx'\, g^*(x')g^*(x'+x_B)g^*(x'+x_B+x_A)g(x')g(x'+x_B)g(x'+x_B+x_A)$$

$$= \frac{2i\Gamma\xi'^4\xi^6}{(X-iY)(X+i\Gamma)i(\Gamma-Y)}\left(\frac{1}{(x_B+X-iY)x_B(x_B+X+i\Gamma)(x_B+i(\Gamma-Y))}\right.$$

$$\times\frac{1}{(x_B+x_A+X-iY)(x_B+x_A)(x_B+x_A+X+i\Gamma)[x_B+x_A+i(\Gamma-Y)]}$$

$$+\frac{1}{(-x_B+X-iY)(-x_B)(-x_B+X+i\Gamma)[-x_B+i(\Gamma-Y)]}$$

$$\times\frac{1}{(x_A+X-iY)x_A(x_A+X+i\Gamma)[x_A+i(\Gamma-Y)]}$$

$$+\frac{1}{(-x_B-x_A+X-iY)(-x_B-x_A)(-x_B-x_A+X+i\Gamma)[-x_B-x_A+i(\Gamma-Y)]}$$

$$\left.\times\frac{1}{(-x_A+X-iY)(-x_A)(-x_A+X+i\Gamma)[-x_A+i(\Gamma-Y)]}\right)$$

$$+(X, Y)\to(-X, -Y). \tag{43}$$

It is readily verified that the poles at $x_A = 0$, $x_B = 0$ and $x_A + x_B = 0$ have zero residues. There are no singularities in $\tilde{A}(x_A, x_B)$ for physical values of the variables.

$$\tilde{E}(x_A, x_B) = K\int dx' g(x')g(x'+x_B)g(x'+x_B+x_A)g^*(x'+x_B+x_A)$$

$$= 2i\Gamma\xi'^2\xi^4\frac{1}{(X-iY)(X+i\Gamma)i(\Gamma-Y)}$$

$$\times\frac{1}{(-x_A+X+i\Gamma)[-x_A+i(\Gamma-Y)](-x_A-x_B+X+i\Gamma)[-x_A-x_B+i(\Gamma-Y)]}$$

$$+(X, Y)\to(-X, -Y). \tag{44}$$

To compare with the experiment of Aspect *et al* (1980) one sets

$$x_A + x_B = \eta \qquad \eta \text{ small}$$

and

$$\delta \gg \xi \gg \Gamma$$

so that

$$X \simeq \delta$$

$$Y \simeq \Gamma(1 - 2\xi^2/\delta^2).$$

Just as in expression (28) for the single-photon spectrum, the sums in (42) lead to a coherent part of the two-photon frequency correlation at $x_A + x_B = 0$. To study this one

looks at the value of $\varepsilon_0(x_B) = |\tilde{E}(-x_B, x_B)|^2$

$$\varepsilon_0(x_B) \simeq \frac{\xi'^4\delta^2}{4\Gamma^2}\frac{1}{(x_B+\delta)^2+\Gamma^2}\frac{1}{x_B^2+\Gamma^2(2\xi^2/\delta^2)^2}. \tag{45}$$

The value of a in the expansion $H(\eta) = 1 + ia\eta + \ldots$ is given by

$$a = \frac{-1}{\Gamma}\left(1+\frac{\Gamma^2+\delta^2}{2\xi^2}\right). \tag{46}$$

From appendix 3, equation (A.12), the coherent part is now seen to be

$$\tfrac{1}{2}\varepsilon_0(x_B)(m - \tfrac{1}{12}m^3a^2\eta^2) \xrightarrow[m\to\infty]{} \frac{4}{\sqrt{3}|a|}\varepsilon_0(x_B)\delta(\eta). \tag{47}$$

The coefficient of $\delta(\eta)$ has maxima as a function of x_B at $x_B = 0$ and at $x_B = -\delta$. The value of x_A associated with the former is $x_A = 0$, and so this is just a reappearance of the coherent part of the single-photon spectrum. The value of x_A associated with the latter is $x_A = +\delta$, so that the first photon is in the upper sideband and the second photon in the lower sideband if $\delta > 0$. The maximum with the two photons in the sidebands is smaller than that with both photons in the central peak by the factor $(2\xi^2/\delta^2)^2$. This coherent part has an interpretation similar to that of the single-photon spectrum coherent part. Emission of a single photon with $x = 0$ does not disturb the energy balance and amplitudes for this emission can interfere even when widely separated along the sequence of emission vertices, which yields the coherent part of the spectrum. Emission of pairs of photons x_A and x_B with $x_A, x_B \neq 0$ but $x_A + x_B = 0$ is a process of higher order which also preserves the energy balance, and therefore interference over large intervals can occur and yield a coherent part, but a smaller one because the process is a two-photon process. These amplitudes are largest, of course, when the two photons are in the sidebands of the single photon spectrum.

The direct term $\tilde{A}(x_A, x_B)$ has a very similar behaviour, but it is less dramatic because it contains no delta function and because at large detuning the coherent part is dominant.

In the experiment of Aspect *et al* (1980)

$$\delta/\Gamma \simeq 1.2\times10^5 \qquad \xi/\Gamma \simeq 1.2\times10^3$$

so that conditions (44) are well satisfied. The time delays employed in their delayed coincidence measurements are of the order of, or less than, $1/\Gamma$ so that the restriction here to successive photons is justified. Their δ is positive so the early photon should be the high-frequency one, as is seen in their figure 2(a). The width in $x_A + x_B$ should be extremely narrow, but that of x_B separately is Γ so there is no conflict with their result shown in their figure 2(b).

For longer times the probability that the observed photons are emitted successively, will decay more or less exponentially, and on integrating over the modes of any intervening photons, the correlation will be expected to be much reduced. The lack of an observable rise time in the correlation is due to the large detuning which makes the Rabi frequency large even though the transition probability to the excited state remains small so the atom quickly becomes as excited as it ever does. Near resonance the Rabi frequency is smaller because here it depends mostly on the coupling, not the detuning, and the rise time can be detected. This is just the antibunching effect mentioned above.

8. Discussion

It has been shown how a conventional quantum mechanical approach involving only the calculation of transition probabilities can be used to find the spectrum of resonance fluorescence and other features of multiphoton scattering processes. This has the advantage over some other calculational methods of making the dynamical basis of various approximations clear. It also has the advantage of being extendible to aspects of the problem other than the spectrum without new formulations. For example, the two-photon correlation experiment just decided by Aspect *et al* (1980) in which successive fluorescence photons are shown to have inelasticities predominantly of opposite sign is seen from (18) to result from the fact that propagators contain the sum of the inelasticities of already emitted photons in the denominator, and that the amplitude for successively emitting photons with small resultant inelasticity will exceed that for the emission of successive photons with large resultant inelasticity. This experiment is a convincing demonstration of the multiphoton character of the entire effect. Another such demonstration is the existence of the coherent spike in the spectrum, which requires interference between amplitudes for the emission of many photons for its emergence.

It can also be determined how many components the fluorescent spectrum should have. If there are p excited states, here either 1 or 2, the projection operator P_e will be p dimensional, and the reciprocal of $H_0 - i\Gamma$ in (9) will have a polynomial of degree p in its denominator. The function $g(y)$ will then, in general, have a polynomial of degree $r = p+1$ in y as denominator. All the functions determining the spectrum are integrals over y of products of g and g^*, which can be evaluated using the residue theorem. The result is a sum of terms with polynomials in x containing factors of the form $(\pm x + \eta_i^* - \eta_j)$ where the η_i are the poles of $g(y)$, and similar factors with η replaced by η^*. A partial fraction decomposition leads to Lorentzian terms with denominators $\pm x + \eta_i^* - \eta_j$ etc. These terms lead to lines centred at $\pm\mathrm{Re}(\eta_i - \eta_j)$ where it now does not matter whether the η are starred or not. There are, therefore

$$2 \times \frac{r(r-1)}{2}$$

lines arising from terms $i \neq j$. When $i = j$ the line is centred at $x = 0$ and has a width which may vary with i. There are, therefore,

$$r(r-1)+1 = p(p+1)+1$$

lines to be expected in the resonance fluorescence spectrum if there are p excited states coupled to the ground state, or better, if $g(y)$ has a denominator of degree $p+1$.

In the three-level atom case, if Γ is chosen to have all its elements equal instead of being diagonal, $g(y)$ 'accidentally' acquires a quadratic denominator for tuning midway between the two resonances and, as mentioned above, this yields a three-peaked spectrum even from a three-level atom (Yeh 1977).

Acknowledgments

S Yeh thanks Paul Berman for his interest in this work and for discussions of it. His work was supported in part by the Office of Naval Research.

Appendix 1

There is an effect on the natural linewidth of an excited atomic state produced by the presence of a laser beam. In the absence of a laser beam the natural linewidth Γ (half width at half maximum) appears as the imaginary part of the sum in the denominator of (8),

$$P_e V_g G_g(E_0, V_e) V_g P_e = \sum_k \frac{\xi'^2}{E_0 - E_g - (N-1)\omega - |k|} \tag{A.1}$$

where no forward scattering is included because of the absence of the laser beam. On converting the sum into an integral through the prescription

$$\sum_k \to V \int \frac{d^3k}{(2\pi)^3}$$

and inserting the standard $i\varepsilon$ to define the treatment of the pole, one arrives at

$$\Gamma = -\mathrm{Im} \frac{V}{(2\pi)^3} \int k^2 \, dk \, d(\cos\theta) \, d\phi \frac{\xi'^2}{\omega - |k| + i\varepsilon} = \frac{2}{3}\omega^3 \frac{e^2}{4\pi} |\langle e|d|g\rangle|^2. \tag{A.2}$$

The real part, the level shift, is in this approximation formally infinite and is neglected as usual, or is absorbed into the eigenvalue E_e.

When forward scattering is included in the propagator $G_g(E_0, V_e)$, then

$$\begin{aligned}\Gamma(\xi) &= -\mathrm{Im} \frac{V}{(2\pi)^3} \int d^3k \frac{\xi'^2}{E_0 - E_g - (N-1)\omega - |k| - \xi^2 [E_0 - E_e - (N-2)\omega - |k|]^{-1}} \\ &= -\mathrm{Im} \frac{V}{(2\pi)^3} \int d^3k \frac{\xi'^2}{2\Omega} \left(\frac{\Omega + \delta}{\omega + \frac{1}{2}(\delta - \Omega) - |k|} - \frac{\Omega - \delta}{\omega + \frac{1}{2}(\delta + \Omega) - |k|} \right) \\ &= \Gamma_1 + \Gamma_2 \end{aligned} \tag{A.3}$$

where $\Omega = (\delta^2 + 4\xi^2)^{1/2}$ is the Rabi frequency. Then

$$\begin{aligned}\Gamma_1 &= \frac{\Omega + \delta}{2\Omega\omega_0^3} (\omega_0 + \tfrac{1}{2}\delta - \tfrac{1}{2}\Omega)^3 \Gamma \\ \Gamma_2 &= \frac{\Omega - \delta}{2\Omega\omega_0^3} (\omega_0 + \tfrac{1}{2}\delta + \tfrac{1}{2}\Omega)^3 \Gamma. \end{aligned} \tag{A4}$$

The intensity-dependent width is

$$\Gamma(\xi) = \Gamma \left(1 + \frac{3\xi^2}{\omega_0^2} + \frac{\xi^2 \delta}{\omega_0^3} \right). \tag{A5}$$

There is no 'first-order' effect on the width, and where the 'second-order' effects are appreciable the approximations such as the frequency independence of the matrix element which have been made are questionable.

This result does not contradict the existence of power broadening, where the width of the absorption spectrum increases with increasing laser intensity. It only shows that the parameter Γ is not itself strongly intensity dependent, so that the width of the central peak in resonance fluorescence is nearly intensity independent, as is the case experimentally. The width of the absorption spectrum does increase with increasing incident intensity.

Appendix 2

Let x_k, x_l be two photon variables to be integrated over which occur in different order in the sequence of g^* and of g in (17) or (21). If x_k appears further to the left than x_l, then x_l appears only in the combination $x_k + x_l$. Let

$$u = x_k + x_l \qquad v = x_k \qquad du\, dv = dx_k\, dx_l. \tag{A.6}$$

In the sequence of g^*, then, if x_k is to the left of x_l these two variables can be replaced by u, v. In the sequence of g, x_l appears alone rather than x_k, so these variables can be replaced by $u - v$, u. Thus in the g^*, v appears as $+v$, in the g as $-v$. The poles of $g(y)$ lie in the lower half of the y plane for reasons of causality, so all the poles in the integral here lie in the upper half of the v plane. On evaluating the integral by closing the contour in the lower half plane, zero is obtained.

Appendix 3

The coherent term in the spectrum given in (26) comes from the cross terms. From the definition of $H(x)$ in (23) it follows that the expansion of $H(x)$ about $x = 0$ has the form

$$H(x) = 1 + iax + bx^2 + \ldots \tag{A.7}$$

with real a and b. Similarly $E(x)E^*(-x)$ has the expansion

$$E(x)E^*(-x) = \varepsilon_0 + ia'x + b'x^2 + \ldots \tag{A.8}$$

with real ε_0, a', b'. The first sum in (26) becomes, up to quadratic terms in x,

$$\begin{aligned}(\varepsilon_0 + ia'x + b'x^2)\frac{1}{m}\sum_{l=1}^{m-1}(m-l)[1 + (l-1)(iax + bx^2) + \tfrac{1}{2}(l-1)(l-2)(iax^2)]\ldots \\ = (\varepsilon_0 + ia'x + b'x^2)[\tfrac{1}{2}(m-1) + \tfrac{1}{6}(m-1)(m-2)(iax + bx^2) \\ - \tfrac{1}{24}(m-1)(m-2)(m-3)a^2x^2].\end{aligned} \tag{A.9}$$

Only the real part contributes to the spectrum, and for large m the contribution becomes

$$\varepsilon_0(\tfrac{1}{2}m - \tfrac{1}{24}m^3a^2x^2). \tag{A.10}$$

This has a height at $x = 0$ proportional to m. It has a half width at half maximum determined by

$$\tfrac{1}{2}m - \tfrac{1}{24}m^3a^2x_{1/2}^2 = \tfrac{1}{4}m \qquad x_{1/2} = \sqrt{6}/ma \tag{A.11}$$

which is inversely proportional to m, so the function approaches a multiple of a delta function as $m \to \infty$, The constant of proportionality depends slightly on the higher terms in x. For example on taking (A.10) to be exact between its zeros and the contribution from beyond this to vanish one obtains

$$\lim_{m\to\infty} \tfrac{1}{2}\varepsilon_0 m\left(1 - \frac{m^2a^2x^2}{12}\right) = \frac{4}{\sqrt{3}}\frac{\varepsilon_0}{|a|}\delta(x) \simeq 2.309\frac{\varepsilon_0}{|a|}\delta(x). \tag{A.12}$$

Alternatively, fitting the left-hand side to the function $(\sin ky/y)$ whose limit for large k is $\pi\delta(y)$ one finds

$$\lim_{m\to\infty} \tfrac{1}{2}\varepsilon_0 m\left(1-\frac{ma^2x^2}{12}+\ldots\right)=\frac{\pi}{\sqrt{2}}\frac{\varepsilon_0}{|a|}\delta(x)=2.221\frac{\varepsilon_0}{|a|}\delta(x). \tag{A.13}$$

A more accurate determination of the constant would be tedious and seems unnecessary for present purposes.

References

Allen L and Eberly J H 1975 *Optical Resonance and Two-level Atoms* (New York: Wiley Interscience) p 56
Aspect A, Roger G, Reynaud S, Dalibard J and Cohen-Tannoudji C 1980 *Phys. Rev. Lett.* **45** 617
Carmichael H J and Walls D F 1975 *J. Phys. B: At. Mol. Phys.* **8** L77
—— 1976 *J. Phys. B: At. Mol. Phys.* **9** 1199
Cohen-Tannoudji C and Reynaud S 1977 *J. Phys. B: At. Mol. Phys.* **10** 345
—— 1978 *Multiphoton Processes* ed J H Eberly and P Lambropoulos (New York: Wiley) p 103
Grove R E, Wu F Y and Ezekiel S 1977 *Phys. Rev.* A **15** 227
Hartig W, Rasmussen W, Schieder R and Walther H 1976 *Z. Phys.* A **278** 205
Heitler W 1954 *The Quantum Theory of Radiation* (Oxford: Oxford University Press) p 201
Kimble H J, Dagenais M and Mandel L 1977 *Phys. Rev. Lett* **39** 695
Kimble H J and Mandel L 1976 *Phys. Rev.* A **13** 2123
Kornblith R and Eberly J H 1978 *J. Phys. B: At. Mol. Phys.* **11** 1545
Low F E 1952 *Phys. Rev.* **88** 53
Mollow B R 1969 *Phys. Rev.* **188** 1969
—— 1975 *Phys. Rev.* A **12** 1919
Renaud B, Whitley R M and Stroud C R 1976 *J. Phys. B: At. Mol. Phys.* **9** L19
Schuda F, Stroud C R and Hercher M 1974, *J. Phys. B: At Mol. Phys.* **7** L198
Smithers M E 1975, *J. Phys. B: At. Mol. Phys.* **8** 2911
Smithers M E and Freedhoff H S 1975 *J. Phys. B: At. Mol. Phys.* **8** L209
Sobolewska B 1976 *Opt. Commun.* **19** 185
Swain S 1975 *J. Phys. B: At. Mol. Phys.* **8** L437
Yeh S 1977 *PhD Thesis* University of Pittsburgh
Yeh S and Stehle P 1977 *Phys. Rev.* A **15** 213

Tiré à part de:
Reprint from:

ANNALES
DE
PHYSIQUE

Supported by the U.S. Office of Naval Research
under Contract No. N00014-77-C-0553.

APPLICATION OF LASER SPECTROSCOPY TO COLLISIONAL STUDIES

par

P. R. Berman

Supported by the U.S. Office of Naval Research
under Contract No. N00014-77-C-0553.

MASSON
PARIS NEW-YORK BARCELONE MILAN

Invited paper

Ann. Phys. Fr., 1980, *5*, pp. 199-206

Application of laser spectroscopy to collisional studies*

P.R. Berman

Physics Department, New York University, 4 Washington Place, New York, New York 10003 (U.S.A.)

Summary. The manner in which laser spectroscopic techniques can be use to probe collisional processes in atomic vapors is reviewed. A discussion of the saturation spectroscopy of three-level systems, coherent transient spectroscopy, and a beam-laser spectroscopy system is presented. It is shown that such experiments can provide useful information on both the total and differential cross sections for atom-atom scattering.

Résumé. *Application de la spectroscopie laser aux études collisionnelles.* Nous examinons la façon dont les méthodes de spectroscopie laser peuvent être utilisées pour sonder les processus collisionnels. On examine la spectroscopie de saturation dans les systèmes à trois niveaux, la spectroscopie des effets transitoires cohérents ainsi qu'une expérience de spectroscopie par jet atomique et laser. On montre que de telles expériences peuvent fournir des informations importantes concernant à la fois les sections efficaces totales *et* différentielles de diffusion atome-atome.

The traditional method for studying atomic or molecular collisions is the use of crossed atomic or molecular beams. Owing to the low beam densities one encounters, such studies have generally been restricted to atoms or molecules in ground or metastable states ; however, it is now possible to use lasers to achieve substantial excited state atomic populations so that scattering from excited states may also be studied in crossed beam experiments [1]. Typically, one obtains the differential scattering cross section as a function of center-of-mass energy in crossed beam experiments. These experiments, although often difficult to perform, provide a *direct* measure of the scattering process.

A somewhat less direct method for studying collisional processes in gases has been available for many years under the heading *pressure broadening*. Since the absorptive properties of a vapor are affected by collisions occuring within the vapor, collisional information is implicitly contained in the absorption or emission profiles associated with various atomic transitions in the vapor. Using linear spectroscopy, one can measure the broadening (or narrowing) of the spectral profile associated with a given transition of *active* atoms as a function of perturber gas pressure. From such data, one can reach some conclusion regarding the total cross section for scattering between active atoms (in the states involved in the transition) and ground state perturbers. Using saturation spectroscopy or coherent transient techniques, one can also obtain information about differential scattering cross sections involving excited-state active atoms (*see* below), albeit of a somewhat different nature than that obtained in beam experiments.

Owing to time limitations, I shall not discuss linear spectroscopy [2], and shall, instead, concentrate on the saturation spectroscopy of three-level systems. I shall also mention some coherent transient experiments that are particularly well-suited to collisional studies and a recent experiment employing a combination of atomic beam and laser spectroscopic techniques.

(*) Supported by the *U.S. Office of Naval Research.*

Before beginning to discuss three-level systems, it is perhaps useful to describe the type of collisional data one can hope to obtain from laser spectroscopic studies involving cells rather than beams. In a typical experiment, one uses a laser to excite active atoms having a specific longitudinal velocity and then probes the manner in which collisions with perturber atoms cause this velocity distribution to return towards equilibrium. Thus, in such an experiment, one measures the differential scattering cross section averaged over the perturber velocity distribution and the transverse active-atom velocity distribution. I have referred to this as a *poor man's* differential scattering cross section, since it contains less information than the corresponding cross sections obtained in beam experiments. Still, the *poor man's* differential cross section is rich enough to draw conclusions concerning the interatomic potential giving rise to the scattering. Moreover, the variety of cross-sections (elastic, inelastic, exchange, magnetic relaxation, etc.) that are easily probed using laser spectroscopic techniques guarantees, in my opinion, a promising future for this mode of collisional study.

Three-level systems

Three-level systems have received considerable attention [3-18] for both high resolution and collisional studies. *Figure 1* illustrates three types of three-level systems. The quantities β and β' label the different level schemes so that all may be treated by a single formalism ; $\beta = \beta' = 1$ in *Figure 1a* (upward cascade) ; $\beta = 1, \beta' = -1$ in *Figure 1b* (inverse V) ; $\beta = -1, \beta' = 1$ in *Figure 1c* (V). The three levels are incoherently pumped at some rate density $\lambda_i(\vec{v})$ $(i = 1, 2, 3)$ and each level decays at some rate γ_i. External fields having frequency Ω and Ω' drive the 1 - 2 transition (frequency ω) and 2 - 3 transition (frequency ω'), respectively. The field propagation vectors are kz and $\epsilon k'z$ ($k = \Omega/c$, $k' = \Omega'/c$) with ϵ equal to either + 1 (copropagating) or - 1 (counterpropagating). Spontaneous emission between level 2 and 1 is allowed at rate γ_2'. The Rabi frequencies associated with the 1 - 2 and 2 - 3 transitions are denoted by χ and χ', respectively. I shall limit the discussion to the upward cascade (*Fig. 1a*) and take $\lambda_2 = \lambda_3 = 0$; $\lambda_1 \sim 0$; $\gamma_1 \sim 0$, $\lambda_1/\gamma_1 =$ constant, to simulate level 1 being the ground state. The field at frequency Ω (pump) is of arbitrary strength and that at frequency Ω' (probe) is assumed to be weak.

The binary, elastic collisions between active atoms and ground state foreign gas perturbers are treated in the impact approximation [2]. Collisions are assumed to be *phase-*

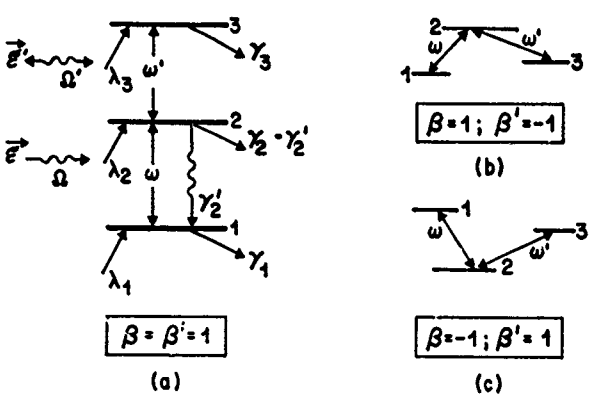

FIG. 1. – *Three-level systems : (a) upward cascade, (b) inverted V, (c) V.*

interrupting in their effect on level coherences (giving rise to broadening and shift parameters) and velocity-changing in their effect on population densities (*i.e.* collisions result in the relaxation of any velocity-selected population excited by the pump field). This rather simple collision model is generally valid for electronic transitions.

The pump field is detuned a fixed amount Δ from the 1-2 transition and the probe absorption is monitored as a function of its detuning Δ' from the 2-3 transition. If u is the most probable active atom speed, then two cases of interest are $|\Delta| \gg ku$, $|\Delta| < ku$.

$|\Delta| \gg ku$

If the pump detuning is equal to several Doppler widths, the only resonance in the absence of collisions occurs at $\Delta' = -\Delta + (k + \epsilon k')\, v_z$. When averaged over the active atom velocity distribution, the resulting line shape is a Voigt profile centered at $\Delta' = -\Delta$ with a width obtained form the convolution of a Lorentzian of width (HWHM) $\gamma_3/2$ and a Gaussian of width $0.83\,(k + \epsilon k')\,u$, if $k \approx k'$ and $\epsilon = -1$, this two-photon resonance can be very narrow.

With collisions present, a *new* resonance centered at $\Delta' = 0$ can result from a collisionally-aided radiative excitation [19] of level two, via the reaction.

$$A_1 + P + \hbar\Omega \rightarrow A_2 + P$$

where A_i is the active-atom in state i and P is the perturber. The difference in energy between $\hbar\Omega$ and $\hbar\omega$ is now compensated by a corresponding change in the atoms' kinetic energy following a collision. With collisionally-aided excitation of level 2, probe absorption on the 2-3 transition centered at $\Delta' = 0$ can occur.

Thus, in the absence of collisions, there is only one resonance centered at $\Delta' = -\Delta$. In the presence of foreign gas perturbers, a new resonance appears at $\Delta' = 0$ which grows with increasing pressure. The width and shift of the $\Delta' = -\Delta$ resonance can be used to obtain the 1-3 broadening and shift coefficients, that of the $\Delta' = 0$ resonance to obtain the 2-3 broadening and shift coefficients. Moreover, the amplitude of the $\Delta' = 0$ resonance is proportional to the 1-2 broadening coefficient. Recent experimental data [20] on $Na(3S_{1/2} \rightarrow 3P_{1/2} \rightarrow 4D_{3/2})$ perturbed by Ne is shown in *Figure 2*. The effects of collisions for this large detuning case ($\Delta = -4.0\,ku$, $k'/k = 1.0375$, $\epsilon = -1$) are clearly seen (the second narrow resonance centered at $\Delta' = 5.77\,ku$ arises from ground state hyperfine structure).

$|\Delta| < ku$

The above type of experiment can provide total cross section data (total cross sections may be extracted from the broadening coefficients). However, to obtain information concerning differential cross sections, one must tune within the Doppler width. In this case, the pump laser selects a specific longitudinal velocity group having $v_z = \Delta/k$, leading to a resonance condition $\Delta' = -\Delta + (k + \epsilon k')\, v_z = \epsilon\,(k'/k)\,\Delta$. The resonance width is on the order of the natural widths of the transition levels, owing to the fact that only a small longitudinal velocity class of atoms is being used. The resonance is broadened and may even be split in strong pump fields, reflecting power broadening and the ac Stark effect, respectively. Probe absorption in the absence of collisions is shown in *Figure 3* for $k'/k = 0.4$. There is ac Stark splitting for counterpropagating waves in strong fields. For the case shown of complete branching to the ground state ($\gamma_2' = \gamma_2$) there is also some splitting for the copropagating case.

In the presence of collisions, the following interactions can occur :

$$A_1 + P + \hbar\Omega \rightarrow A_2(v_z' = \Delta'k) + P$$

$$A_2(v_z' = \Delta/k) + P \rightarrow A_2(v_z) + P$$

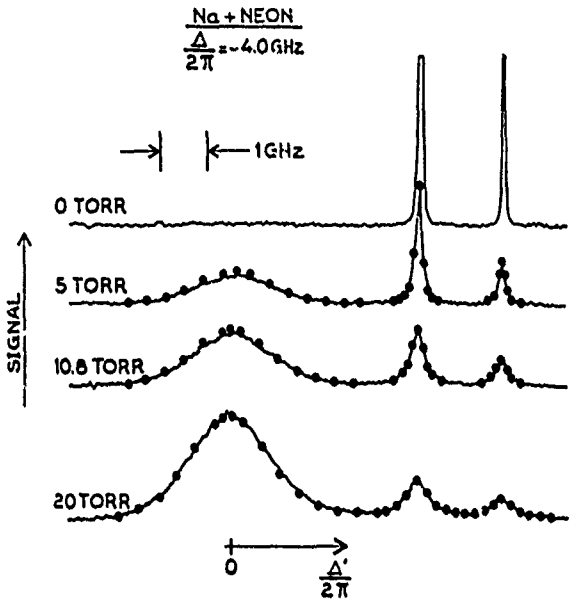

FIG. 2. – *Experimental excitation spectra for Na (3S → 3P → 4D) perturber by various pressures of Ne for a pump detuning* $\Delta/2\pi = -4.0$ *GHz. (Doppler width* $= 1.66\ ku/2\pi = 1.66$ *GHz.). Dots represent theoretical fit with no free parameters.*

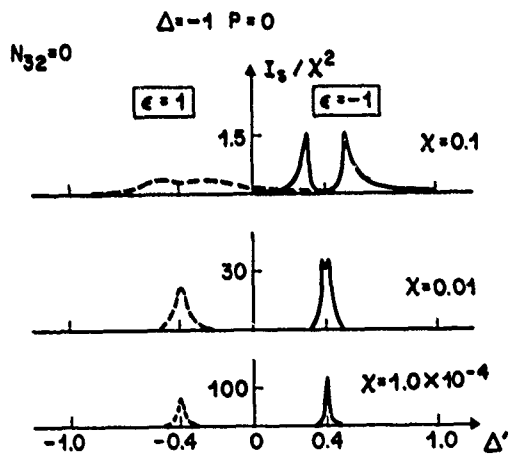

FIG. 3. – *Probe absorption* I_s *in the absence of collisions.* I_s *is normalized to* χ^2*, but is in arbitrary units. All frequencies are in units of ku, P is the pressure in Torr, and* N_{32} *(population difference of levels 3 and 2 in the absence of any applied fields) equals zero. The broken curve is for copropagating fields* ($\epsilon = 1$) *and the solid curve for counterpropagating ones* ($\epsilon = -1$)*. Profiles are drawn for* $\gamma_1 = 0$, $\gamma_2 = .02$, $\gamma_2' = .02$, $\gamma_3 = .01$, $k'/k = .4$, $\beta = \beta' = 1$, $\Delta = -1$, *and several values of* χ.

Collisions result in an excitation of level 2 and a partial thermalization of the velocity distribution from the initial value $v_z' = \Delta/k$ selected by the pump field to values describing a thermal distribution. The degree of thermalization is determined by the number of collisions $n = \Gamma_2/\gamma_2$ (Γ_2 = collision rate) occuring within the lifetime of level 2 and the rms change in velocity per collision Δu. In addition, the structure of the velocity redistribution may be used to infer something about the interatomic potential giving rise to the scattering.

Theoretical probe absorption profiles for weak and strong pump fields are shown in *Figures 4* and *5*, respectively, using the Keilson-Storer [21] collision kernel. One may note the gradual thermalization with increasing perturber pressure. In the strong field case

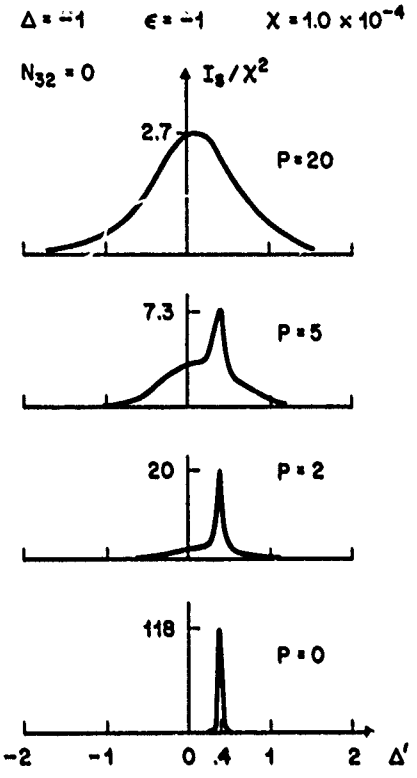

FIG. 4. – *Probe absorption in the weak pump field limit for various perturber pressures. Parameters not explicitly displayed are the same as in Figure 3. Collision parameters (in units of ku) are as follows : phase-interrupting broadening rates* $\Gamma_{12} = .007P$, $\Gamma_{23} = .015P$, $\Gamma_{13} = .016P$; *velocity-changing collision rates* $\Gamma_1 = .004P$, $\Gamma_2 = .006P$. *A Keilson-Storer kernel with* $\Delta u = .66u$ *is used to describe velocity-changing collisions.*

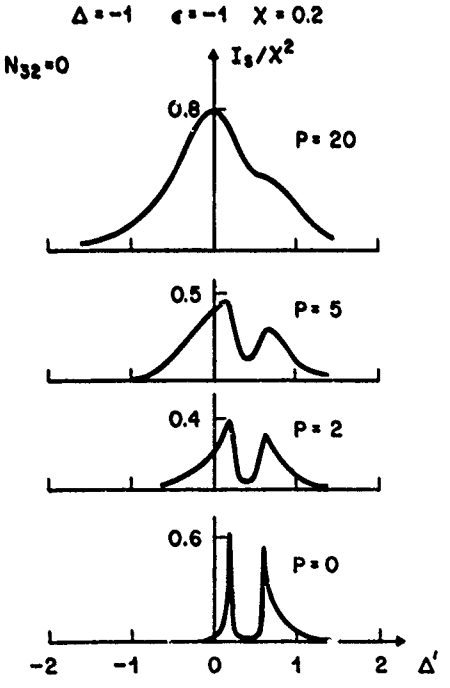

FIG. 5. – *Probe absorption for a strong pump field* ($\chi = .2$). *Other parameters are as in Figure 4.*

both the integrated and peak probe absorption can increase with increasing pressure whereas, in the weak field case, the areas under the curves are constant.

Systematic experiments of this nature were recently carried out by Bréchignac *et al.* [22] in Kr perturbed by rare gases and by Liao *et al.* [23] for Na perturbed by rare gases. The data for Na($3S_{1/2} \rightarrow 3P_{1/2} \rightarrow 4D_{3/2}$) perturbed by Ne is shown in *Figure 6* for a detuning $\Delta/ku = -1.6$. The overall qualitative features are similar to those shown in *Figure 4* (for the three-level Na system chosen, $k'/k = 1.0375$ so that ac Stark splitting is suppressed). One can see the thermalization of the $3P_{1/2}$ level of Na with increasing Ne pressure.

The data of Liao *et al.* [23] could also be used to test different collision kernels that are used to describe scattering in level 2. It was found that both the Keilson-Storer and classical Hard-Sphere kernels correctly characterized Na-He collisions, that the hard-sphere kernel was superior to Keilson-Storer for Na-Ne and Na-Kr collisions, and that neither kernel adequately described the entire profile for Na-Ne and Na-Kr collisions. These results imply that large-angle scattering of Na($3P_{1/2}$) with heavy foreign gases can not be characterized as totally hard-sphere in nature ; it would not be surprising if some large-angle scattering could be attributed to attractive wells in the interatomic potentials. It appears to me that this type of experiment reflects an increased interest in both the experimental and theoretical [24] determination of atomic collision kernels.

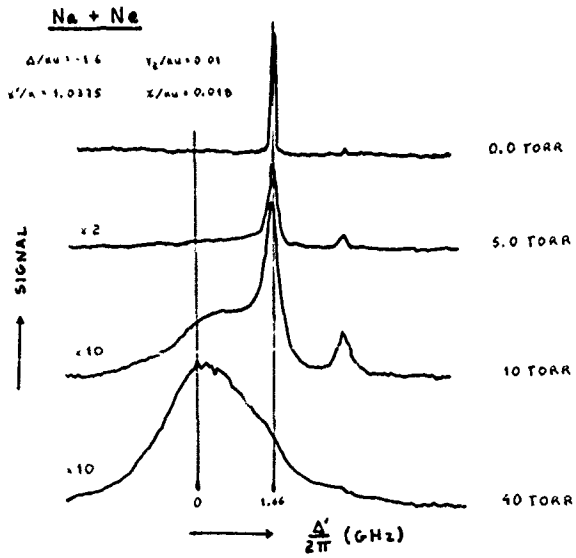

FIG. 6. – *Experimental excitation spectra for Na (3S → 3P → 4D) perturbed by various pressures of Ne with a pump detuning of – 1.6 GHz.*

Coherent transients

It is also possible to carry out laser spectroscopic collisional studies using time resolved techniques. Some of these methods are particularly well suited to collisional studies. I shall mention two such types of experiments.

In time-delayed saturation spectroscopy, one uses a narrow band, pulsed laser to excite atoms having a given longitudinal velocity. A second laser, time delayed from

the first, is then applied to the same or a coupled transition in order to monitor the velocity relaxation as a function of either time delay or perturber pressure. An advantage of this technique to steady-state methods is that two-photon processes do not occur in the time-resolved experiment since the fields are applied at different times. Thus, the probe absorption occurs only from *stepwise* excitation, greatly simplifying the analysis. A limited number of experiments of this type have been performed [25].

A second class of experiments which holds promise for collisional studies may be broadly characterized as photon echo experiments. In these experiments, a system is exposed to two or more pulses. The pulses lead to a dephasing and rephasing of atomic dipoles in the sample such that, at some time following the last applied pulse, the dipoles rephase and emit an *echo*. Collisions disturb this dephasing-rephasing process and cause a decrease in echo amplitude. Thus, the echo amplitude can be used to monitor collisional processes in gases. This method is especially useful in determining whether collisions are *phase-interrupting* or *velocity-changing* in their effect on level coherences [13, 14, 26].

By using standing waves as the excitation pulses, one excites higher-order harmonics in both populations and level coherences. The photon echoes following such excitation can reflect collisional effects on both population densities and level coherences [27]. Moreover, one can also observe population echoes as various population spatial harmonics rephase following the second pulse [28]. Studies of velocity-changing collisions on level populations can also be made using *stimulated* echoes [29], which is simply a variation of the standing-wave echo method. Photon echo experiments offer an interesting possibility for future collisional investigations [28, 29].

Beam-laser experiment

Finally, I should like to mention the experiment of Phillips *et al.* [30]. This experiment employed crossed atomic beams and a laser excitation-detection scheme. As in the steady-state experiment, a pump laser excites a particular velocity class of atoms to some intermediate state. A second laser, directed along the active atom-perturber relative velocity axis, is then scanned to probe a coupled transition. At each probe laser frequency, only those active atoms which have been scattered through a particular scattering angle θ (these atoms form a cone of angle θ about the laser axis) in the center-of-mass system resonantly interact with the probe. Thus, measuring the probe absorption is equivalent to measuring the differential scattering cross section. This method has high sensitivity and can be used for short-lived excited states; it was used to determine the differential cross section for $3P_{1/2} \rightarrow 3P_{3/2}$ fine structure state changing collisions in Na undergoing collisions with Ar perturbers [30].

References

[1] See, *for example*, Hertel (I.V.), Stoll (W.), *in* Advances in Atomic and Molecular Physics, (D.R. Bates, B. Bederson, eds.) *Academic Press*, New York, 1977, vol. *13*, p. 113.

[2] For discussions of linear spectroscopy with many additional references, see Berman (P.R.). – *Appl. Phys. (Germ.)*, 1975, *6*, 283., and Shimoda (K.), in High Resolution Laser Spectroscopy (K. Shimoda, ed.), *Springer-Verlag*, New York, 1976, p. 11.

[3] Notkin (G.E.), Rautian (S.F.), Feoktistov (A.A.). – *Zh. Eksp. Teor. Fiz*, 1967, *52*, 1673, [*Sov. Phys.-JETP*, 1967, *25*, 1112].

[4] Feld (M.S.), Javan (A.). – *Phys. Rev.*, 1969, *177*, 540.

[5] Hansch (T.W.), Toschek (P.E.). – *Z. Phys.*, 1970, *236*, 213.

[6] Popova (T.Y.), Popov (A.K.), Rautian (S.G.), Sokolovskii (R.I.). – *Zh. Eksp. Teor. Fiz.*, 1969, *57*, 850, [*sov. Phys.-JETP*, 1970, *30*, 466, 1208].

[7] Feldman (B.J.), Feld (M.S.). – *Phys. Rev.*, 1972, *A5*, 899; Skribanowitz (N.), Kelly (M.J.), Feld (M.S.), *Phys. Rev.*, 1972, *A6*, 2302.

[8] Beterov (I.M.), Chebotaev (V.P.). – *Prog. Quantum Elec.*, 1974, *3*, 1, and references therein.
[9] Salomaa (R.), Stenholm (S.). – *J. Phys.*, 1975, *B8*, 1795; 1976, *9*, 1221; Salomaa (R.), *ibid*, 1977, *10*, 3005.
[10] Additional references may be found *in* Laser Spectroscopy III (éd. J.L. Hall, J.L. Carlsten) *Springer-Verlag*, New York, 1977; Letokhov (V.S.), Chebotaev (V.P.), non-linear Laser Spectroscopy, *Springer-Verlag*, New York, 1977; High Resolution Laser Spectroscopy (ed. K. Shimoda) *Springer-Verlag*, New York, 1976; Laser Spectroscopy of Atoms and Molecules (ed. H. Walther) *Springer-Verlag*, New York, 1976; Frontiers in Laser Spectroscopy (ed. R. Balian, S. Haroche, S. Liberman) *North-Holland*, Amsterdam, 1977.
[11] Stenholm (S.). – *J. Phys.*, 1977, *B10*, 761.
[12] Borde (C.J.), – *in* Laser Spectroscopy III (J. Hall, J.L. Carlsten, eds.), *Springer-Verlag*, New York, 1977, p. 121.
[13] Berman (P.R.). – *in* Advances in Atomic and Molecular Physics (ed. D.R. Bates, B. Bederson) *Academic Press Inc.*, New York, 1977, Vol. *13*, p. 57.
[14] Berman (P.R.). – *Phys. Rep.*, 1978, *43*, 101.
[15] Kolchenko (A.P.), Pukhov (A.A.), Rautian (S.G.), Shalagin (A.M.). – *Zh. Eksp. Teor. Fiz.*, 1972, *63*, 1173, [*Sov. Phys.-JETP*, 1973, *36*, 619].
[16] Kochanov (V.P.), Rautian (S.G.), Shalagin (A.M.). – *Zh. Eksp. Teor. Fiz.*, 1977, *72*, 1358, [*Sov. Phys.-JETP*, 1977, *45*, 714].
[17] Klein (L.), Giraud (M.), Ben-Reuven (A.). – *Phys. Rev.*, 1977, *A16*, 289.
[18] Extensive additional references may be found in Refs. [2] and [13].
[19] Yeh (S.), Berman (P.R.). – *Phys. Rev.*, 1979, *A19*, 1106, and references therein.
[20] Liao (P.F.), Bjorkholm (J.E.), Berman (P.R.). – *Phys. Rev. A*, 1979, *120*, 1489.
[21] Kellson (J.), Storer (K.E.), – *Q. Appl. Math.*, 1952, *10*, 243.
[22] Bréchignac (C.), Vetter (R.), Berman (P.R.). – *Phys. Rev.*, 1978, *A17*, 1609, *J. Phys. Lett.*, 1978, *39*, L231.
[23] Liao (P.F.), Bjorkholm (J.E.), Berman (P.R.). – *Phys. Rev.*, 1980, *A21*, 1927.
[24] Avrillier (S.). – *Thesis*, Paris, 1978.
[25] Hansch (T.W.), Shahin (I.S.), Schawlow (A.L.). – *Phys. Rev. Lett.* 1971, *27*, 707; (J.) Brochard, (P.) Cahuzac. – *J. Phys.*, 1976, *B9*, 2027; (P.) Cahuzac, (X.) Drago, *Opt. Comm.*, 1978, *24*, 63.
[26] Three-level systems in which the 1-2 population difference vanishes in the absence of applied fields are also ideal for studying this aspect of collisions. *See* (P.) Cahuzac, (J.L.) LeGouet, (P.E.), Toschek, (R.) Vetter. *Appl. Phys.* (Germany), 1979, *20*, 83.
[27] LeGouet (J.L.), Berman (P.R.). – *Phys. Rev.* A, 1979, *A20*, 1105, and references therein.
[28] Kachru (R.), Mossberg (T.W.), Whittaker (E.), Hartmann (S.R.). – Opt Comm., 1979, *31*, 223; Kachru (R.), Whittaker (E.), Hartmann (S.R.). – *Phys. Rev. Lett.*, 1979, *43*, 851.
[29] Mossberg (T.), Flusberg (A.), Kachru (R.), Hartmann (S.R.). – *Phys Rev. Lett.*, 1979, *42*, 1665.
[30] Phillips (W.D.). Serri (J.A.), Ely (D.J.), Pritchard (D.E.), Way (K.R.), Kinsey (J.L.). – *Phys. Rev. Lett.*, 1978, *41*, 937.

Line Shapes in Laser Experiments

A brief review of recent developments in line-shape studies using laser spectroscopy is presented. Experiments are discussed in which the absorption- or emission-line profiles associated with various transitions in a vapor can be used to provide useful information concerning the atomic sample being tested. In particular, ways in which collisional effects manifest themselves in line shapes are described and the manner in which collision cross sections can be extracted from these line shapes is discussed. Illustrative experiments using methods of linear spectroscopy, two-photon spectroscopy and saturation spectroscopy are presented.

1. *Introduction*

With the rapid development of tunable lasers, there has been a renewed interest in the field of atomic spectroscopy. Not only has traditional spectroscopy been carried out with increased precision using laser sources, but also new spectroscopic techniques for probing atomic systems have been developed. Historically, absorption or emission line shapes have been studied to determine atomic transition frequencies, lifetimes and oscillator strengths. Moreover, line-shape studies have been used to provide information pertaining to collisional processes occurring in *vapors*. With the laser revolution, new and valuable data concerning both atomic structure and collisional effects can be expected from the study of laser-spectroscopic line shapes.

In this brief review it is not possible to discuss all the recent developments in laser spectroscopy. Therefore, we limit the discussion to a few cases of current interest. In particular, we emphasize the experimental aspects of linear and saturation spectroscopy using weak laser fields (Rabi frequency much less than homogeneous widths) in which collisional processes are probed. We assume that collisions can be described by relatively simple models. The collisions are taken to be thermal and describable by the impact theory of pressure broadening – we consider only binary collisions between atoms and detunings between laser and atomic transition frequencies which are small compared with the inverse duration of a collision.

Several reviews of collisional studies using laser spectroscopy have recently appeared,[1-6] but these reviews did not emphasize the experimental aspects of the problem as we shall do here. Section II is devoted to a study of linear spectro-

Comments Atom. Mol. Phys.
1981, Vol. 10, No. 2-3, pp. 69-86
0010-2687/81/1002-0069 $06.50/0

Supported by the U.S. Office of Naval Research under Contract No. N00014-77-C-0553.

scopy, Section III to two-photon spectroscopy, Section IV to saturated absorption and Section V to the saturation spectroscopy of three-level systems.

II. Linear Absorption

Linear spectroscopy is a classic technique for studying atomic systems that can be easily carried out using laser sources. The absorption of a given transition is monitored as a function of the frequency of the applied laser field. The laser field is assumed to be weak enough so as not to alter atomic state populations significantly. Profiles in linear absorption are characterized by the following features.

(1) Profile intensities are proportional to the difference of populations in the two levels involved in the transition.

(2) The line shape is given by the convolution of a Doppler-shifted Lorentzian representing the absorption profile of a given longitudinal velocity subclass of atoms with the velocity distribution of these atoms.

(3) With laser sources, the apparatus function is negligible compared with other sources of broadening.

(4) High signal-to-noise ratios are easily obtained.

Collisions within the vapor add new features to the line shapes. The most common effect of collisions is to introduce a pressure- and speed-dependent width and shift into the Lorentzian component of the profile. The width can be related to the total cross section for scattering of the active atoms in the states of the transition by ground-state perturbers. It is also possible, in certain cases, to observe a narrowing of the total profile (Dicke narrowing) with increasing perturber pressure, provided that the collisional interaction for the two states of the transition is nearly identical.[2] We do not consider this narrowing effect in this Comment since it rarely occurs for electronic transitions. We therefore take line shapes of the form

$$\frac{\gamma(v)}{\gamma^2(v) + (\Delta + S(v) - k \cdot v)^2}\, G(v)\, dv \qquad (1)$$

where $2\gamma(v)$ is the speed-dependent homogeneous width (FWHM, natural plus collisional width), $S(v)$ is the speed-dependent collisional shift, Δ the detuning of the laser frequency from the absorption transition frequency, k the laser propagation vector and $G(v)$ the velocity distribution of the active atoms.

If the speed dependence of γ and S is neglected, and if $G(v)$ is Gaussian, the resultant line shape is termed a Voigt profile.

As an example of linear spectroscopy with lasers, we describe an absorption experiment on the 3.51-μ line of Xe I.[7] A xenon laser oscillating at 3.51 μ and finely tunable across its gain curve provides a weak laser beam which propagates inside a discharge tube filled with ^{136}Xe. The absorbed or amplified part of the laser flux is recorded as its frequency is scanned. Background signal is eliminated by using a square-wave excitation of the discharge and phase-sensitive detection.[8] The line profile is analyzed at several pressures according to Eq. (1), where $G(v)$ is assumed Gaussian and the speed dependence of γ and S is neglected. The shift is determined by the position of the symmetry axis of the line profile relative to that of the same transition measured using a reference tube. Fitting the profile of the line shape involves two free parameters, the homogeneous and Doppler widths. Although the deconvolution procedure is not unique, consistent results are obtained by assuming profiles of the form (1). The width of the Lorentzian component is shown in Figure 1 as a function of pressure of either the He, Ne or Ar perturbers. The width of the Gaussian remains constant with pressure, slightly above the temperature of the bath. The different widths plotted in Figure 1 are linear functions of pressure, and converge to the value 4.7 MHz as the pressure approaches zero, in agreement with the expected value of 4.6 MHz.[7] Data taken from Ref. 7 indicate that shifts are also linear functions of pressure and converge to zero as the pressure approaches zero.

The situation is somewhat more complicated with Xe atoms as perturbers. Figure 2 shows the width of the Voigt profile, of the Gaussian component and of the Lorentzian obtained after profile analysis.[7] The data clearly show that

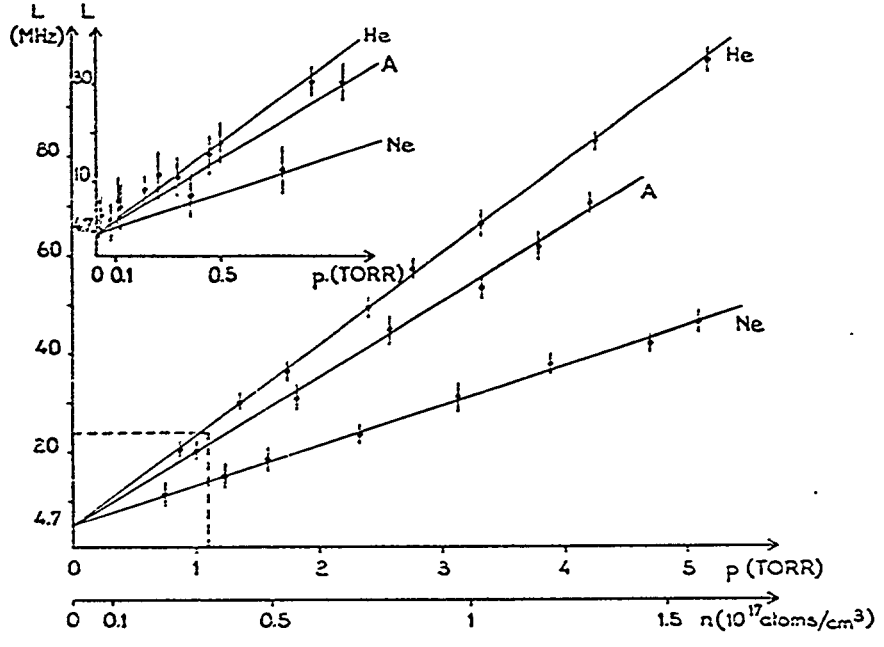

FIGURE 1. Width L of the Lorentzian component of the 3.51-μ Line of Xe I as a function of perturber pressure obtained in linear spectroscopy. The insert shows the low-pressure domain.[7]

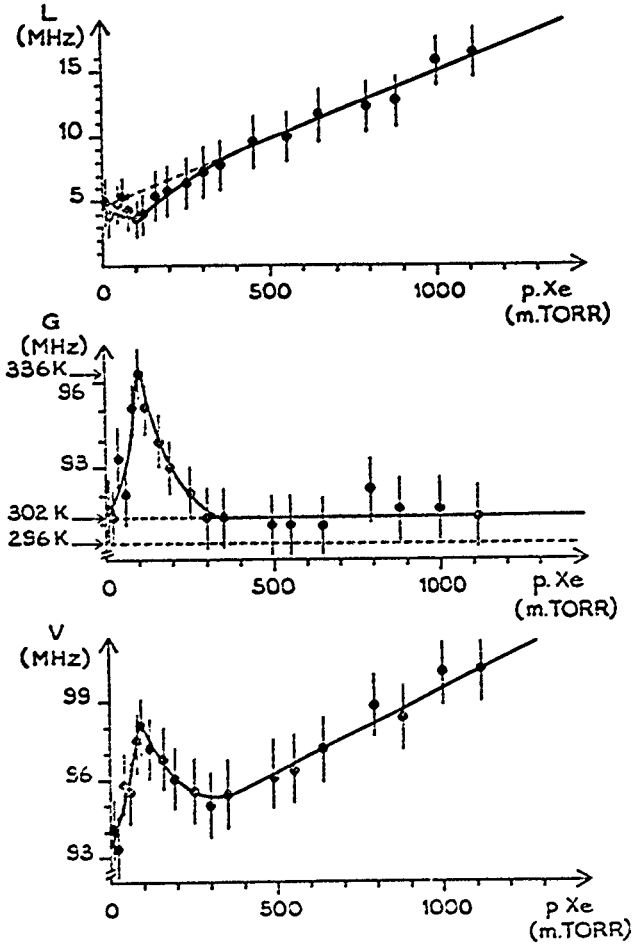

FIGURE 2. FWHM of the Lorentzian component L, the Gaussian component G, and the total Voigt profile V of the 3.51-μ Xe I line as a function of pressure. One notices a marked variation of the Gaussian width at low pressure; the corresponding temperatures associated with the widths are indicated on the ordinate of the G–P curve. The variation of the Lorentzian width is nearly linear with a slope of (10.9 ± 1.3) MHz/torr.[7]

the Gaussian width no longer remains constant with pressure, and that there is a corresponding effect on the width of the Voigt profile. However, the width of the Lorentzian remains a linear function of pressure within experimental accuracy. The cause of the deviation of the Gaussian may be due to a nonresonant transfer of excitation.[7] With Kr atoms as perturbers, a nonresonant excitation transfer leads to severely distorted profiles.[9] Similar experiments have been performed with He and Ne as active atoms.[10,11]

The creation of non-Maxwellian initial state velocity distributions occurs in certain of the above discharge tube experiments and can be strictly avoided only in absorption experiments on transitions originating from the atomic ground state. Although the existence of non-Maxwellian distributions complicates the analysis, there are certain transitions in the rare gases that can be readily studied spectroscopically only by using discharges. It may be noted that one can readily vary the temperature of discharges to study the temperature dependence of collision rates and shifts.[12] The data shown in Figures 1 and 2 are restricted to the core of the line (frequency range on the order of several Doppler widths). In this range observation is sensitive mainly to collisions with large impact parameters, typically greater than 5 Å. In order to probe the short-range part of the interatomic potential one must study the far wings of the line.[13,14]

III. Two-photon Absorption

In linear spectroscopy, one is always faced with the problem of deconvoluting a profile into its components. Over the past few years great emphasis has been placed on the development of spectroscopic techniques which are essentially Doppler-free; that is, profiles in which the Doppler component is suppressed. One such method that has been developed is that of two-photon Doppler-free spectroscopy.[15-19] The principle involved is easily understood if one writes the condition for absorption of two photons in the atomic rest frame. If the separation of the two levels of the same parity is 2ω and the excitation photons of frequency Ω are provided by copropagating ($\epsilon = 1$) or counterpropagating ($\epsilon = -1$) laser beams, the resonance condition is: $\Omega(1 - v_z/c) + \Omega(1 - \epsilon v_z/c) = 2\omega$. One sees immediately that for $\epsilon = -1$ the Doppler shifts cancel. As Ω is varied, an absorption profile characterized by the natural width of the initial and final states of the transition is obtained. In this method each atom contributes to the signal, regardless of its velocity. The Doppler-free nature of this signal is provided by a *cancellation* of Doppler shifts. The profile also may contain a broad background signal arising from absorption of two copropagating photons from one of the laser beams. It can be eliminated by suitable polarization of the beam. It should be noted that, by "two-photon" spectroscopy, we are referring to the absorption of two photons of the same frequency between two levels of the same parity with a nonresonant intermediate level.

In the absence of collisions, the two-photon absorption operator determines the line shape. It has been shown that this operator is the sum of a scalar operator and a quadrupolar one, leading to two contributions to the line shape. However, in most cases of interest, only one operator couples the two levels and the line shape reduces to a single Lorentzian[20] having the homogeneous width of the two transition levels. In principle, it is possible to obtain extremely narrow lines, especially if the initial and final states are metastable. There have been many high-resolution experiments carried out using this technique.[21]

As in the case of linear spectroscopy, collisions can be incorporated by using a speed-dependent width and shift in the line profile. The line is no longer a true Lorentzian and can be asymmetric. If one neglects the speed dependence of width and shift, one recovers a Lorentzian line shape that is collision-broadened and shifted.

Experiments specifically designed to study collisional effects have been carried out initially by Cagnac's group,[22] and subsequently by others.[23,24] In particular, in Ref. 22, one is able to find the variation of the width and shift of two-photon excitation of Na (3S–5S and 3S–4D) transitions as a function of the pressure of various noble gases. The lines have a similar appearance to those of Figure 1, with typical broadening coefficients on the order of 25 MHz/torr (of the same order as that observed in linear spectroscopy). A similar experiment has been carried out with Ne as active atoms.[25] In this case, absorption takes place from a metastable level. More recently, two-photon absorption has also been used to study collisional processes in Rydberg states.[23,24]

Although two-photon absorption offers unique possibilities for high-precision spectroscopic studies, the signal strengths are limited by the small excitation probability one generally encounters. The excitation probability can be enhanced if there is a nearly-resonant intermediate state.

IV. Saturated Absorption

As a more versatile alternative, one can use saturation spectroscopy to obtain Doppler-free line shapes.[21] The principle involved is quite simple, and differs from that of two-photon spectroscopy. In saturation spectroscopy, one uses a laser beam ("pump") to excite a given longitudinal velocity subclass of atoms and probes these atoms with a second laser beam ("probe"). Since atoms having only a narrow range of axial velocities contribute to the signal in the absence of collisions, the width of the line shape can be on the order of the natural width. The Doppler-free nature of the response arises from the *selection* of a narrow Lorentzian velocity class, whereas in two-photon spectroscopy it is due to a cancellation of Doppler phase.

The resonance condition for saturated absorption is easily understood. The pump excites only those atoms having velocities $kv_z = \Delta$, where Δ is the atom-field detuning. On the other hand the probe (counterpropagating with the pump) interacts only with those atoms having $kv_z = -\Delta$, and hence the saturated absorption signal is nonzero only for $\Delta = 0$ (within limits of plus or minus the natural width). A linear absorption background can be eliminated by suitable experimental techniques. The term "saturation spectroscopy" is used to indicate that the signal one observes is proportional to the cube of the applied field amplitude; this cubic power is composed of a quadratic term E^2 representing the change of population induced by the pump field and a factor E representing the linear absorption of the probe. One can still speak of a "weak-field" limit, since one

is obtaining a term corresponding to the lowest nonvanishing contribution to the signal. Narrow profiles of this type have been obtained in many atomic systems.[21]

In the presence of collisions the line shapes are modified.[26,27] The process can be viewed as follows: the pump field excites a particular velocity subclass of atoms, collisions cause this narrow distribution to relax towards thermal equilibrium and the probe absorption from these partially thermalized atoms gives rise to the overall line shape. Collisions enter the line shape in two ways. First, there is the effect of collisions on optical coherence (off-diagonal density-matrix elements). These effects manifest themselves as a broadening and a shift of the Lorentzian component of the absorption profile, just as in linear absorption. However, in saturated absorption there is a second effect. Collisions result in a relaxation of the nonthermal velocity distribution of the populations (diagonal density-matrix elements) created by the pump field. The saturated absorption profile reflects the various collisional processes occurring in the vapor and may be used to gain information about the interatomic potential giving rise to scattering within the vapor.

In order to describe velocity changes in collisions, one generally uses a collision kernel $W(v' \to v)$ giving the probability density per unit time for an active atom to undergo a change from v' to v, as a result of collisions with the perturber bath. Although the precise form of the line shape is dependent on the specific nature of the collision kernel, general comments can be made without reference to a particular kernel. However, one must introduce the parameter Δu, which is the rms velocity change per collision, and also $\Gamma = \int W(v' \to v)dv$, the rate of velocity-changing collisions (vcc). The amount of thermalization is then determined by the number of collisions $\bar{n}$ occurring within the lifetime of the transition levels and the strength of the collision, which is characterized by Δu. Two cases of interest occur.

(1) If $k\Delta u > \gamma$, where γ is the homogeneous width (FWHM) associated with the transition, collisions are strong enough to remove atoms from the velocity "holes" or "bumps" created by the pump field. In this case, collisions lead to a broad background in the saturated absorption profile and the line shape can be used to monitor these vcc. As the perturber pressure is increased, the line shape tends towards a Voigt profile, whose Gaussian component is provided by collisionally thermalized active atoms.

(2) If $k\Delta u < \gamma$, vcc are so weak that they do not significantly alter the line shape. An interesting effect can arise at low pressures. At such pressures, γ is determined by the natural width and one can have $k\Delta u > \gamma$ for relatively small Δu. This condition leads to distorted profiles which nevertheless may appear Lorentzian in nature. As the process is increased, γ is determined by the collision-broadened homogeneous width and the limit $k\Delta u < \gamma$ is achieved. At these pressures, the line *is* a Lorentzian with FWHM γ. A nonlinear variation of the line width with pressure can occur for these relatively weak collisions.

All these effects can be seen in the data shown in Figures 2 and 4. In Figure 3, the saturated absorption profile of the 557-nm Kr I line is shown, for Kr active atoms perturbed by He.[28] One can identify three components in the profile: (1) a narrow Lorentzian arising from atoms not having undergone vcc; (2) a component arising from Kr*-Kr collisions leading to a broad, completely thermalized Gaussian background; (3) a background arising from Kr*-He collisions having $k\Delta u > \gamma$. Also,

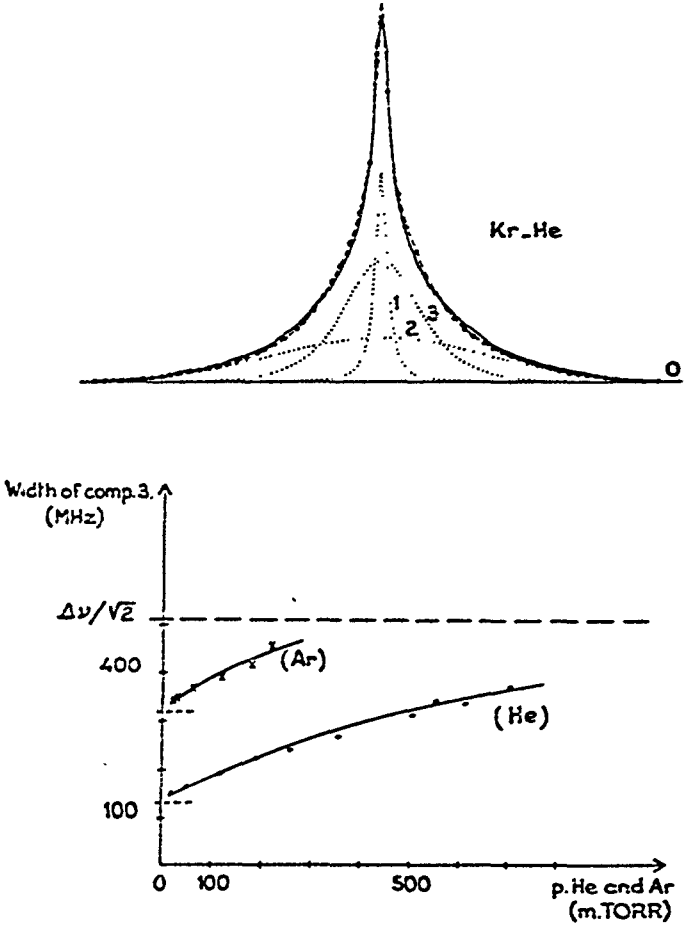

FIGURE 3. Saturated absorption of the 557-nm line of Kr I. The upper curve shows the experimental profile (solid line) for a perturber pressure of 110 mtorr of He and curves 1, 2 and 3 represent, respectively, the components of this line arising from Kr* atoms that have not experienced vcc, from Kr* atoms that have undergone vcc with Kr and from Kr* atoms that have undergone vcc with He atoms. The lower graph represents the width of the vcc component 3 perturbed by He (dots) or Ar (crosses) perturbers. The dashed line is the thermal equilibrium value.[28]

in Figure 3, the variation with pressure of the width of the components arising from vcc with He and Ar atoms, respectively, is shown. Note that both widths approach the thermal one with increasing pressure, and that Δu for Ar perturbers is greater than Δu for He perturbers.

In Figure 4, the variation with pressure of the "Lorentzian" component width 2γ for saturated absorption in the 3.51-μ Xe I line is shown, for Xe active atoms perturbed by Xe.[29] For comparison, the corresponding width $2\gamma_0$ of linear absorption is also displayed.[7] The saturated absorption data are strongly suggestive of the presence of the weak vcc described above. Similar nonlinear variations have been obtained in other systems.[30-36]

Experimental values for cross sections and rates of vcc having $k\Delta u > \gamma$ are generally in agreement with calculations based on hard-sphere models.[37,38] On the other hand, rates for weaker vcc (representing collisions with larger impact parameters) can be orders of magnitude larger than hard-sphere values.

It should be noted that saturated absorption can also be performed using two independent counterpropagating laser beams, the pump having a fixed frequency and the probe a variable one. The line shape in this case is similar to that

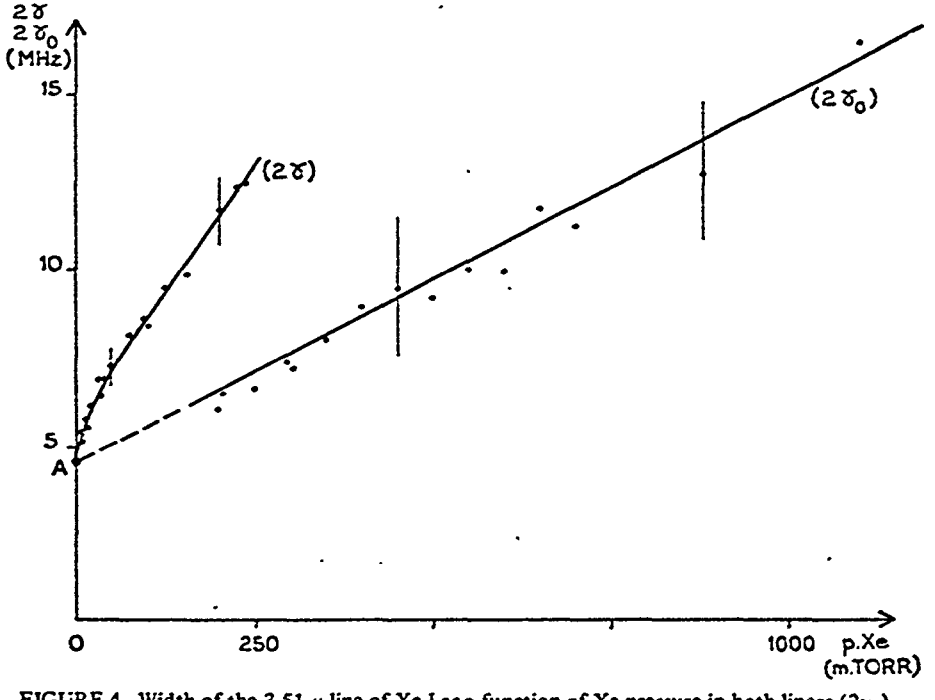

FIGURE 4. Width of the 3.51-μ line of Xe I as a function of Xe pressure in both linear ($2\gamma_0$) and saturation (2γ) spectroscopy. Point A is the natural line width of 4.6 MHz. Note the marked nonlinear variation of the width, owing to vcc.[29]

encountered in three-level systems, discussed in the next section. Modifications of saturated absorption experiments that have the potential of yielding higher signal-to-noise ratios may be used; the most popular is polarization spectroscopy.[21,39]

V. *Three-level Systems*

One slight disadvantage of saturated absorption collisional studies is that the vcc effects occur in the populations of both states of the transition, and it is sometimes difficult to isolate the effect on a given level. This situation can be rectified if one studies collisions using three-level systems,[40-42,21] although many of these experiments require an additional laser. In a typical experiment, one starts with a population in level 1 (Figure 5), applies a field of frequency Ω, amplitude $\mathscr{E}$ to drive the 1–2 transition which has a frequency ω and, in addition, applies a second field of frequency Ω', amplitude $\mathscr{E}'$ to complete transitions to level 3 (the 2–3 transition frequency being ω'). The λ_i represent incoherent pumping rates for the various levels, while the γ_i represent decay rates from those levels. In general, the pump detuning $\Delta = (\Omega - \omega)$ is fixed, and the population of level 3 is monitored as a function of the probe detuning $\Delta' = (\Omega' - \omega')$. There are many variations of this three-level system (TLS) but, to be specific, we shall consider the case of the upward cascade in Figure 5a with $\lambda_2 = \lambda_3 = 0, \lambda_1 \sim 0$, $\gamma_1 \sim 0, \lambda_1/\gamma_1$ = constant to simulate the case where level 1 is the ground state. Note, however, that high-resolution line shapes can also be obtained when levels other than level 1 are incoherently pumped.[6]

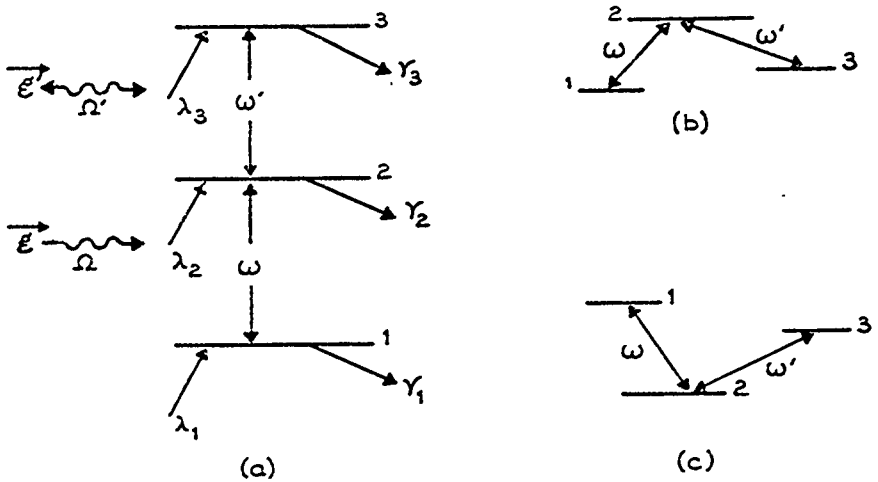

FIGURE 5. Three-level systems used in saturation spectroscopy: (a) upward cascade; (b) inverted V; (c) V. The λ_i are values for incoherent pumping and γ_i the decay rates for the states i. We consider case (a) in the limit $\lambda_2 = \lambda_3 = 0, \lambda_1 \sim 0, \gamma_1 \sim 0$ and $\lambda/\gamma \sim$ constant, simulating a system in which level 1 is the ground state.

In the absence of collisions, there is only one resonance condition for excitation to level 3 for each velocity subclass of atoms. This condition is simply a "two-photon" resonance requirement, $\Delta' = -\Delta + (k + k'\epsilon)v_z$, where $\epsilon = 1$ for copropagating and -1 for counterpropagating fields.

There remains some freedom in satisfying this resonance condition by the choice of the velocity subclass v_z. If $|\Delta| >> ku$ (large detunings), one obtains maximum excitation by choosing v_z at the center of the Doppler profile ($v_z = 0$). This leads to the resonance condition $\Delta' = -\Delta$. In this case the line shape is the convolution of a Lorentzian of width $2\gamma_{13}$, where $\gamma_{ij} = (\gamma_i + \gamma_j)/2$, and a Gaussian of width $1.66(k + \epsilon k')u$, where u is the most probably active atom velocity. Note that, if $\epsilon = -1$ and $k \approx k'$, the width of the resonance is approximately equal to the natural width $2\gamma_{13}$ associated with the two-photon transition. This width can be extremely narrow, especially if level 3 is metastable. The Doppler-free nature of the line under such conditions arises from the cancellation of the Doppler phases associated with the 1–2 and 2–3 transitions.

If $|\Delta| < ku$ (small detunings) one obtains a maximum excitation by choosing those atoms having velocity $v_z = \Delta/k$ such that they are resonant with the pump field Ω. Substituting this value of v_z into the resonance condition one obtains $\Delta' = (\epsilon k'/k)\Delta$ as the position for maximum probe absorption. The line width is always on the order of the natural width of the states involved in the transitions. The Doppler-free nature of this line, however, arises from the fact that only atoms having a narrow range of longitudinal velocities are contributing to the signal (there can be an additional narrowing of the line if counterpropagating waves are used owing to Doppler-phase cancellation). For either small or large detunings the probe absorption is proportional to $\mathscr{E}^2\,\mathscr{E}'$. For the case of intermediate detunings it is possible to observe resonances at both $\Delta' = -\Delta$ and $\Delta' = (\epsilon k'/k)\Delta$.[43]

To include collisional effects it is more convenient to look at large and small detunings separately.

1. $|\Delta| >> ku$. With collisions present, a *new* resonance[44-50] centered at $\Delta' = 0$ can result from a collisionally aided radiative excitation of level 2 by means of the reaction $A_i + P + \hbar\Omega \rightarrow A_2 + P$, where A_i is the active atom in state i and P is the perturber. The difference in energy between $\hbar\Omega$ and $\hbar\omega$ is now compensated by a corresponding change in the atoms' kinetic energy following a collision. With collisionally aided excitation of level 2, probe absorption in the 2–3 transition centered at $\Delta' = 0$ can occur. In the absence of collisions, there is only one resonance centered at $\Delta' = -\Delta$ and, in the presence of foreign-gas perturbers, there appears a new resonance at $\Delta' = 0$, which grows with increasing pressure. The width and shift of the $\Delta' = -\Delta$ resonance can be used to obtain the 2–3 broadening and shift coefficients. Moreover, the amplitude of the $\Delta' = 0$ resonance is proportional to the 1–2 broadening coefficient. Recent experimental data[50] on Na ($3^2S_{1/2}$–$3^2P_{1/2}$–$4^2D_{3/2}$) perturbed by the Ne are shown in Figure 6. The

effects of collisions for this large-detuning case ($\Delta = -4.0ku$, $k/k' = 1.0375$, $\epsilon = -1$) are clearly seen (the second narrow resonance centered at $\Delta' = 5.77ku$ arises from ground-state hyperfine structure).

2. $|\Delta| \lesssim ku$. The pump laser excites a given velocity subclass of level-2 population, which collisions tend to thermalize. By studying the profiles as a function of pressure, it is possible to obtain information on the interatomic potential giving rise to the relaxation.[51-56] The following interactions occur when collisions are present

$$A_1 + P + \hbar\Omega \rightarrow A_2(v_z' = \Delta/k) + P$$

$$A_2(v_z' = \Delta/k) + P \rightarrow A(v_z) + P.$$

Collisions result in an excitation of level 2 and a partial thermalization of the velocity distribution. The degree of thermalization is determined by the number of collisions $\bar{n} = \Gamma_2/\gamma_2$ (Γ_2 is the collision rate) occurring within the lifetime of level 2 and the rms change in velocity per collision Δu. In addition, the structure

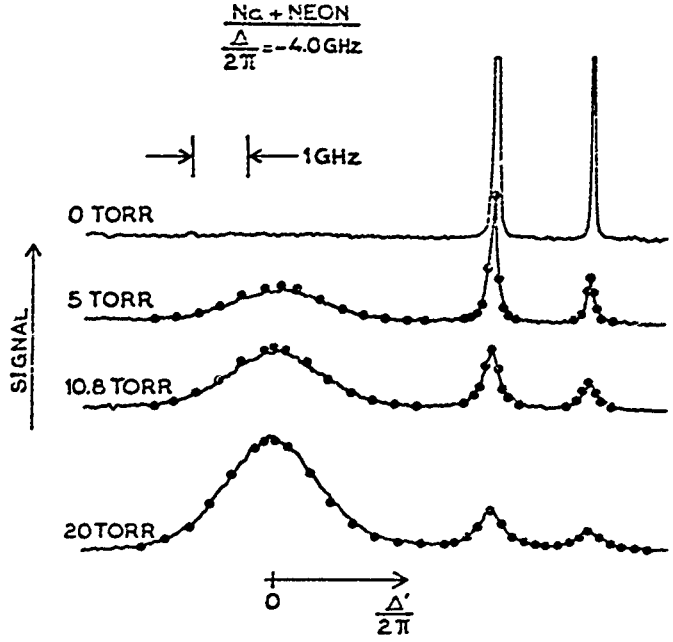

FIGURE 6. Experimental profiles of probe absorption for the excitation of the $3^2S_{1/2}$–$3^2P_{1/2}$–$4^2D_{3/2}$ transition in Na for various pressures of Ne perturbers. The pump detuning is $\Delta/2\pi = -4$ GHz $= -4ku/2\pi$. The two narrow resonances represent "direct" two-photon excitation of the 4^2D state from the two hyperfine components of the ground state. The collision-induced broad resonance is centered at the $3^2P_{1/2}$–$4^2D_{3/2}$ transition frequency. The solid lines correspond to experiment and the points to a theoretical fit.[50]

of the velocity redistribution may be used to infer something about the interatomic potential giving rise to scattering within the sample.

Theoretical probe-absorption profiles for a weak pump field are shown in Figure 7 for several pressures using the Keilson–Storer collision kernel.[57] Note the gradual thermalization with increasing perturber pressure. The area under the curve remains constant. Systematic experiments of this nature were recently carried out by Bréchignac *et al.*[58] in Kr perturbed by He (Figure 8), and by Liao *et al.*[59] in Na perturbed by noble gases (Figure 9). In both figures, one can see a collision-induced partial thermalization of the sample.

A complementary experiment performed using Kr and Xe was published recently.[60] In that system, transfer from an excited state of Kr to an excited state of Xe can be achieved by quasiresonant collisional excitation transfer. The Kr excited state is pumped in a velocity-selective manner and the excited state is probed. Results show that the Xe atoms retain some memory of the Kr velocity, despite the fact that the Xe atoms were characterized by a Gaussian distribution before the transfer.

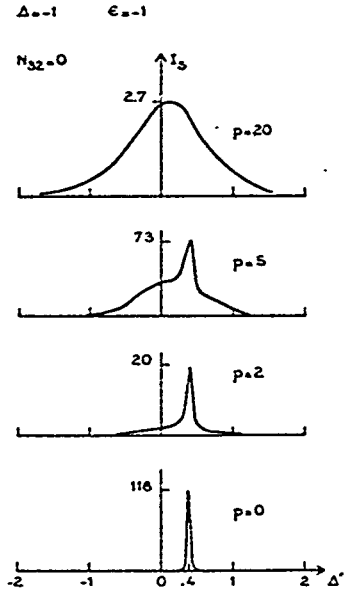

FIGURE 7 Theoretical profiles for probe absorption I_5 (in arbitrary units) in a TLS with $k'/k = 0.4$, counterpropagating waves ($\epsilon = -1$), a detuning $\Delta/ku = -1$ and a weak pump field. The population inversion N_{32} between levels 3 and 2 in the absence of collisions is taken to be zero. The abcissa is the probe detuning Δ' in units of ku. The curves are calculated for different perturbers using a Keilson–Storer collision kernel with $\Delta u = 0.66u$ and a vcc rate $\Gamma_2/ku = 0.006P$, where P is the perturber pressure in torr. The lifetime of the intermediate state is $\gamma_2/ku = 0.02$. These curves show the thermalization of the intermediate-state population velocity distribution with increasing P.

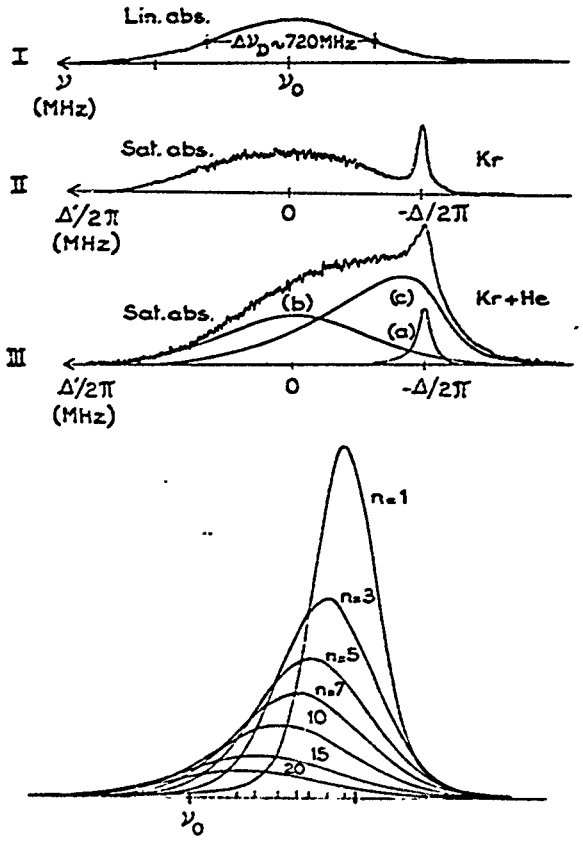

FIGURE 8. Profiles for linear and saturation spectroscopy of the 557-nm line of Kr I. Curve I shows the linear absorption profile in pure Kr, centered at ν_0. Curves II and II represent saturated absorption profiles obtained with two counterpropagating laser beams, the pump being detuned by Δ/π = 600 MHz from ν_0. Curve II is recorded for pure Kr at a pressure of 10 mtorr and curve III for a mixture of Kr (10 mtorr) and He (450 mtorr). Curve III is analyzed in terms of components arising from Kr* atoms which have not experienced vcc (a), Kr* atoms that have undergone thermalizing events with Kr atoms (b) and Kr* atoms that have undergone vcc with He atoms (c). The lower graph shows the contribution to curve c from Kr* atoms that have undergone 1, 3, 5, . . . collisions with He, indicating the gradual thermalization of Kr* as a function of the number of Kr*–He collisions.[58]

By careful studies of the line shapes associated with TLS, one ultimately hopes to be able to test various models for the interatomic potentials. There is some evidence from the data of Liao *et al.*[59] for example, that suggests a hard-sphere model is not sufficient to explain large-angle scattering between Na(3P) and Kr or Ne perturbers. Future studies involving TLS may be expected to provide additional insights into the collisional processes occurring in atomic systems.

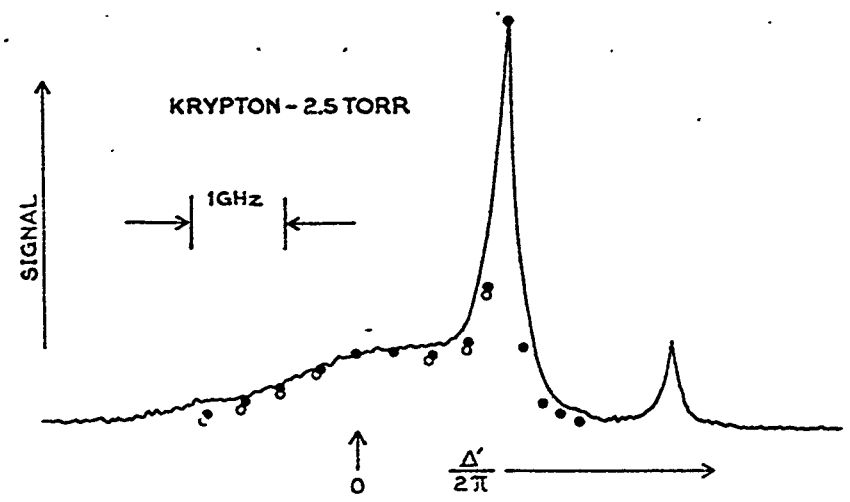

FIGURE 9. Experimental probe absorption as a function of $\Delta'/2\pi$ for the same transition in Na shown in Figure 6, but for a pump detuning $\Delta/2\pi = -1.6ku/2\pi = -1.6$ GHz. The partial thermalization resulting from vcc is evident. The solid circles represent a theoretical fit using a hard-sphere collision kernel, and the open circles a fit using the Keilson–Storer collision kernel.[59]

VI. Conclusion

We have briefly discussed some of the ways in which the study of laser-spectroscopic line shapes associated with atomic states can be used to provide collisional data. Of necessity, many interesting aspects of collisional processes and line-shape formations have not been discussed at all. Among these are inelastic collisions, resonant exchange collisions, collision-induced magnetic relaxation, polarization spectroscopy, laser-assisted collisional excitation, collisionally aided radiative excitation, resonance fluorescence, strong-field effects (ac Stark splitting), coherent transient methods and laser spectroscopy using atomic beams. Nevertheless, we hope to have conveyed a sense of the type of information that can in principle be obtained from the experimental line shapes of laser spectroscopy.

R. VETTER
and P.R. BERMAN†
Laboratoire Aimé Cotton, CNRS II
Bâtiment 505, 91405 Orsay, France

Acknowledgements

One of the authors (PRB) was supported by the US Naval Research Office, Fulbright Research Scholar Fund for the period October-November, 1979.

† Permanent address: Physics Department, New York University, New York, N.Y. 10003